Hindered diffusion of nanoparticles
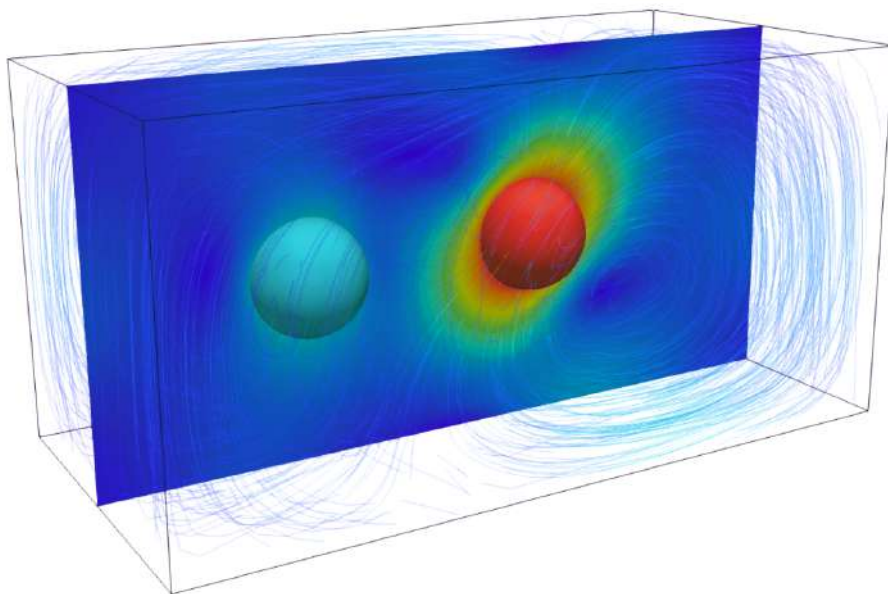
Investigations at molecular and continuum scales

ANANDA SUBRAMANI KANNAN

Hindered diffusion of nanoparticles

Investigations at molecular and continuum scales

ANANDA SUBRAMANI KANNAN

Cover:
Streamlines of velocity magnitude around two spherical Brownian particles (400 nm in diameter) diffusing in a square micro-channel.

Hindered diffusion of nanoparticles
Investigations at molecular and continuum scales
ANANDA SUBRAMANI KANNAN
Department of Mechanics and Maritime Sciences
Division of Fluid Dynamics
Chalmers University of Technology

Abstract

Brownian theory provides us with a powerful tool which can be used to delve into a microscopic world of molecules, cells and nanoparticles, that was originally presumed to be beyond our reach. Consequently, modeling the inherent dynamics of a system through a Brownian transport equation is of relevance to several real-word problems that involve nanoparticles including, the transport and mitigation of particulate matter (PM) generated though fossil fuel combustion and nanocarrier mediated drug delivery. Experimentally forecasting these systems is challenging due to the simultaneous prevalence of disparate length and time scales in them. Correspondingly, an *in-silico* driven assessment at such nanoscales can complement existing experimental techniques.

Hence, in this thesis, a novel multiphase direct numerical simulation (DNS) framework is proposed to address the transport at these nanoscales. A coupled Langevin-immersed boundary method ($LaIBM$), that solves the fluid as an Eulerian field and the particle in a Lagrangian basis, is developed in this thesis. This framework is unique in its capability to include the resolved instantaneous hydrodynamics around the Brownian nanoparticle (without the need for an *a priori* determination of the relevant mobility tensors) into the particle (Langevin) equation of motion. The performance of this technique is established and validated using well-established theoretical bases including the well-known theories for unbounded and hindered diffusion (wherein hydrodynamic interactions mediated by the fluid such as particle-particle or particle-wall influence the governing dynamics) of Brownian particles in a liquid. Correspondingly, it is shown that directional variations in mean-squared displacements, velocity auto-correlation functions and diffusivities of the Brownian nanoparticle correspond well with these standard theoretical bases. Moreover, since the resolved flow around the particle is inherently available in the proposed DNS method, the nature of the hydrodynamic resistances (on the particle) including the inherent anisotropies and correlated inter-particle interactions (mediated by the fluid) are further identified and shown to influence particle mobility. Furthermore, this framework is also extended towards Brownian transport in a rarefied gas using first order models to account for the non-continuum effects. Thus, the utility of this novel method is established in both colloids and aerosols, thereby aiding in modeling the transport of a fractal shaped PM (in the latter) and a spherical nanocarrier in a micro-channel (in the former).

Keywords: Aerosols; Brownian motion; Colloids; Hydrodynamic interactions; Langevin-immersed boundary method; Mobility; Multiphase DNS; Nanoscale and Rarefied gas.

i

To my son... My lucky charm...
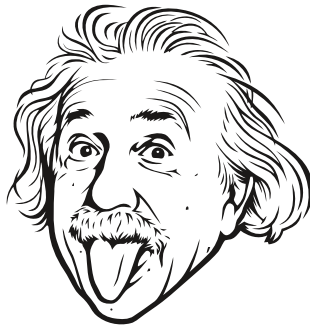
"Logical thinking cannot yield us any knowledge of the empirical world; all knowledge of reality starts from experience and ends in it."

- Albert Einstein, 1933

Acknowledgements

ABBREVIATIONS

AmgX	–	Algebraic Multi-Grid solvers
BGK	–	BhatnagarGrossKrook
CFD	–	Computational fluid dynamics
DNS	–	Direct numerical simulation
DPD	–	Dissipative particle dynamics
DSMC	–	Direct simulation Monte-Carlo
DPF	–	Diesel particulate filters
EC	–	European commission
FLBM	–	Fluctuating lattice Boltzmann method
GLE	–	Generalized Langevin Equation
IBM	–	Immersed boundary method
IBOFlow	–	Immersed Boundary Octree Flow Solver
LaIBM	–	Langevin immersed boundary method
LBM	–	Lattice Boltzmann method
LLNS	–	Landau and Lifshitz Navier-Stokes
OpenFOAM	–	Open-source Field Operation And Manipulation
FH	–	Fluctuating hydrodynamics
FLBM	–	Fluctuating lattice Boltzmann method
LGA	–	Lattice gas automata
LTI	–	Linear time invariant
MD	–	Molecular dynamics
MSD	–	Mean squared displacement
NS	–	Navier-Stokes equations
ODE	–	Ordinary differential equation
PDF	–	Probability distribution function
PM	–	Particulate matter
SDE	–	Stochastic differential equation
TIRFM	–	Total internal reflection fluorescence microscopy
VACF	–	Velocity auto-correlation function

NOMENCLATURE

Greek letters

α	Friction coefficient at the solid-fluid interface	
β_{St}^{corr}	Corrected Stokes mobility for hindered diffusion	$\mathrm{s\,kg^{-1}}$
β_{St}	Stokes mobility	$\mathrm{s\,kg^{-1}}$
$\delta(x)$	Dirac delta function	
$\Delta x(t)$	is the displacement $x(t) - x(0)$	m
Δt	Time step in the numerical simulation	
γ_{St}	Stokes friction factor	$\mathrm{kg\,s^{-1}}$
λ	Reduction in particle mobility	
λ_{gas}	mean free path of the gas	m
μ_f	Dynamic fluid viscosity	$\mathrm{kg\,m^{-1}\,s^{-1}}$
ν_f	Kinematic fluid viscosity	$\mathrm{m^2\,s^{-1}}$
ρ_f	Fluid density	$\mathrm{kg\,m^{-3}}$
$\boldsymbol{\omega_p^i}$	Angular velocity of the particle	
$\boldsymbol{\sigma}$	Total fluid stress tensor	
τ_B	Ballistic time scale of a Brownian particle	s
τ_D	Smoluchowski or diffusion time scale of a Brownian particle	s
τ_p	Particle response time	s
$\upsilon(r,t)$	Standard Gaussian white noise tensor field with uncorrelated components δ-correlated in space and time	
ζ	Magnitude of Brownian fluctuations	

Roman letters

A	Function of Kn that is determined based on empirical data	
b	Slip length in liquids	m
C_c	Cunningham correction	
$C(t)$	Auto-correlation function	
ΔV	Volume of a control element	$\mathrm{m^3}$
D_∞	Diffusivity of a free particle	$\mathrm{m^2\,s^{-1}}$
d_p	Particle diameter	m
F_f	Fluid force on a single Brownian particle in the control volume	N
$\mathbf{F_{IB}}$	Total force on the IB	
F_p	Pressure force on a single Brownian particle in the control volume	N
$f(x,t)$	Probability density function of a free Brownian particle	
h	Distance from the particle center to the wall surface	m
$\mathbf{I}$	Moment of inertia of the particle	
$\mathbf{J}$	Identity tensor	

k_B	Boltzmann constant	$\mathrm{m^2\,kg\,s^{-2}\,K^{-1}}$
Kn	Knudsen number	
L	Characteristic system scale	m
m_p	Particle mass	kg
$\mathbf{n}$	Normal at the surface over which the fluid stress is computed	
n	Number of moles of fluid in the equation of state	mol
N_1	Number of Brownian particles in a control volume	
N_{av}	Avogadro's number	$\mathrm{mol^{-1}}$
p	Pressure on a Brownian particle	$\mathrm{kg\,m^{-1}\,s^{-2}}$
Q	Mass-flow rate of a molecular gas in micro-channels	$\mathrm{kg\,s^{-1}}$
R	Universal gas constant	$\mathrm{J\,K^{-1}\,mol^{-1}}$
$r(x,y,z)$	Particle position vector	
r_p	Particle radius	m
R_f	Stochastic forcing of the fluid stress tensor FH	
$r(t)$	Impulse response of a stationary stochastic process	
$R(\omega)$	Fourier transform of the impulse response of a stationary stochastic process	
S	Surface over which the fluid stress is computed	
S_1, S_2	Cross-sectional surface area of a control volume	$\mathrm{m^2}$
Sc	Schmidt number	
$S(t)$	Stochastic forcing term in the Langevin equation	N
$S(\omega)$	Fourier transform of the stochastic forcing	
$\tilde{S}_{uu}(\omega)$	Velocity power spectral density	
T	Temperature	K
t	Time	s
$\mathbf{F_{IB}}$	Total torque on the IB	
$\mathbf{u_p}$	Particle velocity vector	
u_{rms}	Particle root mean squared velocity	$\mathrm{m\,s^{-1}}$
v	Fluid velocity vector	
x	Particle x-position	m
$\mathbf{x_p}(t)$	Particle position	m
$x(t), y(t)$	Linear signals in time domain	
$X(\omega), Y(\omega)$	Linear signals in frequency domain	

Superscripts and subscripts

$\langle\square\rangle^2$	Mean squared value
$\langle\square\rangle_\perp$	Wall-normal component
$\langle\square\rangle_\infty$	Free-diffusion
$\langle\square\rangle_\parallel$	Co-axial component

LIST OF PUBLICATIONS

This thesis is based on the following appended papers:

Paper A A. S. Kannan, V. Naserentin, A. Mark, D. Maggiolo, G. Sardina, S. Sasic, and H. Ström. A continuum-based multiphase DNS method for studying the Brownian dynamics of soot particles in a rarefied gas. *Chemical Engineering Science* **210** (2019), 115229. ISSN: 0009-2509. DOI: `10.1016/j.ces.2019.115229`

Paper B A. S. Kannan, A. Mark, D. Maggiolo, G. Sardina, S. Sasic, and H. Ström. Assessment of hindered diffusion in arbitrary geometries using a multiphase DNS framework. *Chemical Engineering Science* **230** (2021), 116074. ISSN: 0009-2509. DOI: `10.1016/j.ces.2020.116074`

Paper C A. S. Kannan, A. Mark, D. Maggiolo, G. Sardina, S. Sasic, and H. Ström. A hydrodynamic basis for off-axis Brownian diffusion under intermediate confinements in micro-channels. *International Journal of Multiphase Flow* (Submitted December 2020)

Paper D A. S. Kannan, A. Mark, D. Maggiolo, G. Sardina, S. Sasic, and H. Ström. Hindered diffusion of nanoparticles in a liquid re-visited with a continuum based direct numerical simulation framework. *To be submitted to a journal* (2021)

Paper E A. S. Kannan, T. S. B. Narahari, Y. Bharadhwaj, A. Mark, D. Maggiolo, G. Sardina, S. Sasic, and H. Ström. The Knudsen paradox in micro-channel Poiseuille flows with a symmetric particle. *Applied sciences* (Submitted November 2020)

ADDITIONAL RELEVANT PUBLICATIONS

Paper 1 A. S. Kannan, A. Mark, D. Maggiolo, G. Sardina, S. Sasic, and H. Ström. "A novel multiphase DNS method for the resolution of Brownian motion in a weakly rarefied gas using a continuum framework". *Proceedings of the 10th International Conference on Multiphase Flow (ICMF19)*. Rio de Janeiro, Brazil, May 2019

Paper 2 H. Ström, J. Sjöblom, A. S. Kannan, H. Ojagh, O. Sundborg, and J. Koegler. Near-wall dispersion, deposition and transformation of particles in automotive exhaust gas aftertreatment systems. *International Journal of Heat and Fluid Flow* **70** (2018), 171–180. ISSN: 0142-727X. DOI: 10.1016/j.ijheatfluidflow.2018.02.013

Paper 3 A. S. Kannan, A. Mark, D. Maggiolo, G. Sardina, S. Sasic, and H. Ström. "Assessment of pore diffusion in a micro-channel using an immersed boundary method". *Proceedings of the 14th International Conference on Multiphase Flow in Industrial Plant (MFIP17)*. Desenzano del Garda, Italy, 2017

Paper 4 A. S. Kannan, K. Jareteg, N. C. K. Lassen, J. M. Carstensen, M. A. E. Hansen, F. Dam, and S. Sasic. Design and performance optimization of gravity tables using a combined CFD-DEM framework. *Powder Technology* **318** (2017), 423–440. ISSN: 0032-5910. DOI: 10.1016/j.powtec.2017.05.046

Paper 5 A. S. Kannan, N. C. K. Lassen, J. M. Carstensen, J. Lund, and S. Sasic. Segregation phenomena in gravity separators: A combined numerical and experimental study. *Powder Technology* **301** (2016), 679–693. ISSN: 0032-5910. DOI: 10.1016/j.powtec.2016.07.003

Paper 6 J. Sjöblom, H. Ström, A. S. Kannan, and H. Ojagh. Experimental Validation of Particulate Matter (PM) Capture in Open Substrates. *Industrial & Engineering Chemistry Research* **53**.9 (2014), 3749–3752. DOI: 10.1021/ie404046y

Paper 7 J. Sjöblom, A. S. Kannan, H. Ojagh, and H. Ström. Modelling of particulate matter transformations and capture efficiency. *The Canadian Journal of Chemical Engineering* **92**.9 (2014), 1542–1551. DOI: 10.1002/cjce.22004

Contents

Part I

Extended Summary

1

Introduction

Brownian motion: a macroscopic window to the microscopic world

"These motions were such as to satisfy me, after frequently repeated observation, that they arose neither from currents in the fluid, nor from its gradual evaporation, but belonged to the particle itself."

- Robert Brown, 1828

Brownian motion, or the chaotic dance of molecules/nanoparticles due to incessant collisions with the constituent elements of a fluid, has been an integral part of modern day science ever since it was serendipitously noticed by Dutch scientist Jan Ingenhousz (in 1785) while observing finely ground charcoal under a microscope. This characteristic random behavior, named after Robert Brown (a British botanist) who noticed these irregular motions in a great variety of materials suspended in a liquid ranging from pollen to fragments of an Egyptian sphinx [13], has been the subject of extensive research since the 17th century. From understanding the complex behavior of micro-organisms, to forecasting the next stock market crash, to studying the dynamics of super-massive black holes and to modern day artificial intelligence – understanding chaos through the lens of Brownian theory has been the approach of choice for a generation's worth of research. In fact, the significance of Brownian theory in modern day science is unmistakable, as this core idea is the subject of Einstein's famed dissertation [14] and many would argue that it is his biggest contribution (to science) along with the theory of relativity. Thus, Brownian theory is touted to be that elusive window into a microscopic world of molecules, cells and nanoparticles that was presumed to be beyond our reach.

The simplistic representation of systematic chaos as a mathematical abstraction of a random process, in a scale independent framework (i.e. applicable in the same form to both micro-organisms as well as spinning galaxies), has been the unique feature of modern day Brownian theory that makes it an appealing modeling technique across several research fronts. To limit the scope of the ensuing discussions, the developed ideas in this thesis are positioned with two potential overarching applications:

1. Cleaner emissions from combustion processes

3

2. Nanocarrier mediated drug delivery

These are explained in this chapter in order to establish the necessary context for the theoretical and numerical developments presented in this thesis.

1.1 Clean air: a basic requirement for society?

Urban air quality has been on the decline since the industrial revolution particularly due to the increasing energy demands from the modernization of our society. With the increasing dependence on energy from fossil fuels, the corresponding levels of particulate matter (PM) such as PM10 (less than 10 microns in diameter) and PM2.5 (less than 2.5 microns in diameter), that contain pollutants such as sulfates and nitrates rise [15]. These PM aerosols, which are usually formed due to incomplete combustion of hydrocarbon-based fuels during a variety of common combustion processes in power generation, vehicular propulsion etc., are hazardous to human health. This is due to their widespread dispersion in the atmosphere, particularly PM2.5, as its microscopic size allows the pollutant particles to enter the blood stream via the respiratory tract and travel throughout the body. Such an intravenous transport of PM can cause far-reaching health effects including asthma, lung cancer and heart disease [15]. This chronic issue with poor air quality is highlighted in Fig. 1.1, indicating that a significant portion of the global population breathes PM2.5 contaminated air at concentrations* exceeding the limits set by the World Health Organization (WHO).

A more local survey in Europe, further, identified that emissions from households, industrial plants and road transport accounted for a majority of the fine aerosols (PM2.5 and PM10) emitted in the region [16]. Hence, the European commission (EC) has implemented a series of directives that establishes the health based standards and objectives for these pollutants (Directive 2008/50/EC of the European Parliament [17]). Stringent PM emission control needs to be adopted if these demands from the EC are to be met, indicating a palpable need for novel strategies to mitigate the same. The most generic mitigation strategy is some form of after-treatment of the gases emitted as a result of the combustion of hydrocarbon-based fuels using a particulate filter. For vehicular emissions, which account for 10-15 % of the total PM emissions in Europe, a combination of the diesel oxidation catalyst (DOC), diesel particulate filter (DPF) and diesel NOx reduction catalyst (DeNOx) are employed downstream from the tail pipe to regulate the exhaust. Among these, the DPF (see Fig. 1.2), a dedicated unit that is commonly made from cordierite or silicon carbide extruded monoliths, is used to purge the exhaust gas of PM by trapping them in its constituent monolith channels. In a typical DPF, every second channel is plugged at either end, creating a chessboard-like appearance of the

---

*The US AQI is among the most widely recognized index for communicating air quality. This index converts pollutant concentrations into a color-coded scale between 0-500, where higher values indicate increased health risk.
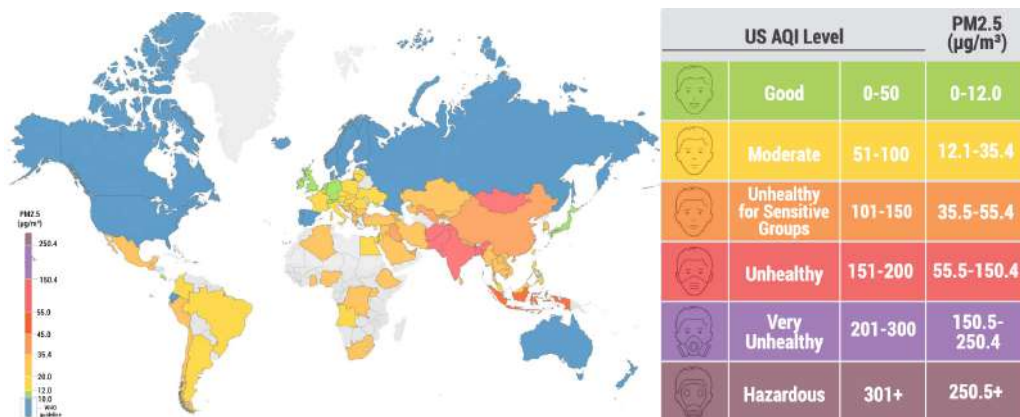
Figure 1.1: *This map presents average PM2.5 exposure by country for 2019, as calculated from available city data and weighted by population. Grey countries and regions indicate that these locations had insufficient data available. This figure is adapted from the report published by IQAir, a Swiss air quality technology company [15].*

monolith front and back. Further, the flow in these channels is laminar, meaning that PM accumulates in the channel through Brownian or molecular deposition/diffusion and interception. Although effective at PM capture, these DPF's are associated with a significant fuel penalty, mainly because of the pressure build up due to deposition. Hence, smarter technologies to circumvent the deficiencies of these traditional monolith filters are desirable, consequently, creating a niche requirement for advanced experimental and modeling techniques to better design and further improve these existing systems.

1.2 Nanocarriers: a new tool to combat cancer?

While the industrial revolution has had a detrimental impact on the environment, it has simultaneously benefited mankind by improving the overall standard of living, catering to better hygiene and sanitation. These improved conditions for living coupled with the modern advancements in medical science have brought about dramatic declines in the mortality rate from infectious diseases. These improvements, however, come at the cost of changing demographics and exposure to a wider class of risk factors, increasing the incidence of another dangerous disease, i.e. cancer, in the human population (with more than 10 million new cases reported every year) [20]. Current cancer treatments include surgical intervention, radiation and chemotherapeutic drugs, which often also kill healthy cells and generate a toxic response in the patient. It would, therefore, be desirable to develop strategies that can either passively or actively target cancerous cells [21]. The aim of such smart drug-delivery systems is to administer smaller drug doses to patients while offering improved therapeutic efficiency and fewer side effects when compared with conventional drug delivery methods [22].
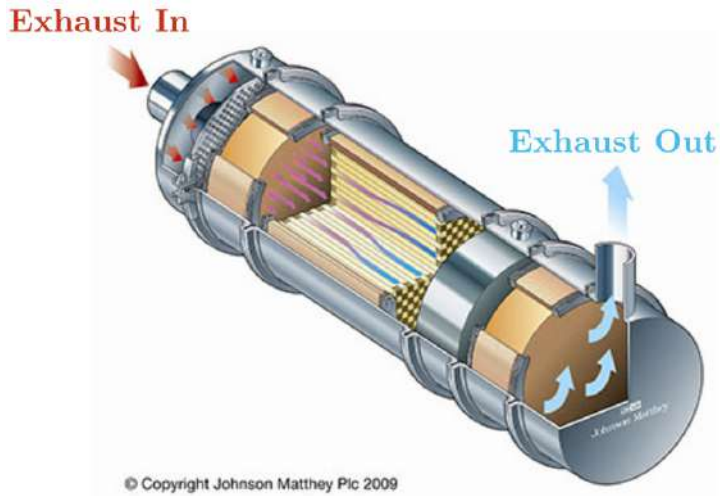
Figure 1.2: *An example of a PM emission mitigation device: diesel particulate filter (DPF) employed in diesel powered drives. This figure is adapted from [18].*
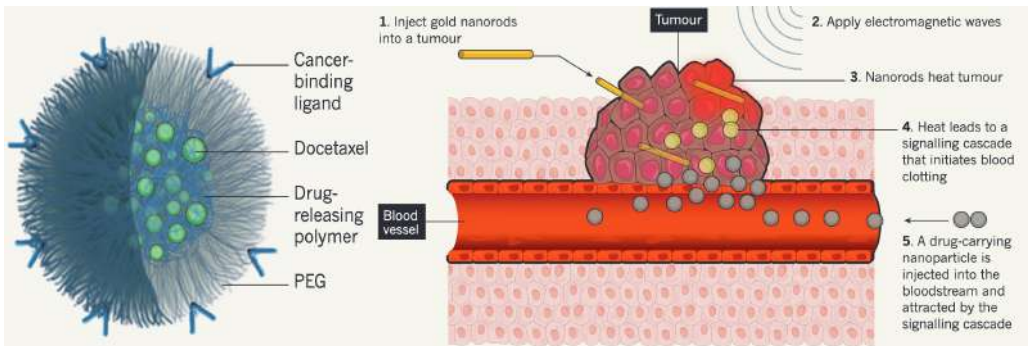
Figure 1.3: *An example of nanocarrier mediated drug delivery targeting tumor cells. The carrier is a 100 nm polymer sphere (poly-ethylene glycol or PEG) loaded with docetaxel, a drug that kills malignant cells. This figure has been adapted from Bourzac [19].*

Recent research in nanomedicine [22, 23], or the application of nanotechnology to achieve innovation in healthcare, has catapulted the technological advancements in both active and passive targeting of a cancerous cells to new heights. These recent advances are also resulting in therapies that were previously thought impossible, such as drugs that change their properties depending on where they are in the body or targeting tumor cells at inaccessible regions. Some labs are even testing ideas inspired by robotics, such as nanoparticles that communicate with each other to increase accumulation at a tumor site [19]. Correspondingly, Fig. 1.3 depicts a plausible way to actively target cancerous cells. The tumor site is injected with gold nanoparticles and is subsequently heated to warm the site up, thereby bringing about a signaling cascade that initiates blood clotting. The drug carrying nanoparticle (termed as a nanocarrier), which is injected in the blood, is attracted to this signaling cascade due to the unique markers it possesses, binding selectively only with the tumor cells. In this case, the nanocarrier (which is 100 nm in diameter) consists of a hydrophobic biodegradable polymeric core (made of polyethylene glycol or PEG) that encapsulates the active substance (the drug docetaxel) and enables its controlled release. Moreover, this coating also provides the needed mobility to transport the nanocarrier in the blood stream. It follows that the targeted delivery of a nanocarrier is governed by a complex interplay of hydrodynamic and multivalent interactions with the biomolecules (such as red blood corpuscles) in blood. Hence, novel insights into the dynamics of a nanocarrier in such a system can enable advanced, personalized and targeted nanomedical services by delivering the next level of cancer treatments to clinicians and patients. A numerical model of this system would definitely accelerate such a development as experimental assessments are both cumbersome and time-consuming.

1.3 Brownian behavior: the connecting link

Two disparate applications that target some of the most pressing concerns of today are introduced in this chapter. Although these use cases seem uncorrelated, they are united by a common thread that correlates behavior at the smallest scales to the observed system-wide phenomena. This brings us back to the title of this chapter - 'Brownian motion: a macroscopic window to the microscopic world', meaning, the Brownian perspective can provide the missing link in these challenging problems. This is particularly relevant here as we deal with nanoparticle (with a size range 1 nm to 1 μm) transport in a fluid, where multiple effects (both molecular and hydrodynamic in nature) compete for dominance in governing the inherent particle dynamics. Moreover, in these cases, the particles diffuse in the vicinity of a wall and/or other particles, thereby increasing the complexity of the transport process. Thus, a comprehensive insight into the complex interplay between the micro- and macro scale phenomena mediated (in-part) by the hydrodynamic fields developed (in the surrounding fluid) is crucial to improving our understanding of the underlying transport phenomena in these systems. Moreover, as the aforementioned systems involve fine particles, experimentally forecasting the hydrodynamics is challenging due to the simultaneous prevalence of disparate length and time scales. This necessitates the parallel development of numerical approaches that complement existing experimental

techniques. Hence, the development of a general numerical technique that can handle both the complex hydrodynamics as well as the accompanying Brownian behavior in such systems, is the overarching objective of this thesis. The corresponding developments in this regard are detailed in the subsequent chapters and in the appended papers.

1.4   Document structure

This thesis is organized as follows. In Chapter 2 the aims and objectives of this work are established. Next, in Chapter 3 the relevant theoretical background on Brownian theory in a fluid (i.e. both unbounded and bounded flows) is presented. This chapter establishes the basis that is needed to interpret the results presented in the appended papers. This is followed by Chapter 4 which provides an overview of the numerical methods typically used in Brownian modeling, including a detailed account of a novel continuum based direct numerical simulation (DNS) framework (which is one of the primary contributions of this thesis) and positions its relevance with respect to the available methods. In Chapter 5 some essential highlights from this thesis are listed within the context of the appended papers. Finally, Chapter 6 consists of the concluding remarks within the context of the overarching goals of this thesis (as established in Chapter 2) along with a brief description on the future scope of this research effort.

2

Aim

The transport of nanoparticles (in the size range 1 nm to 1 μm) in a fluid presents a challenging problem that couples both molecular and hydrodynamic (or continuum) phenomena. Consequently, it is governed by disparate length and time scales. Thus, the main objective of the current work is to develop various strategies to numerically resolve phenomena at these relevant scales within the context of the applications introduced in Chapter 1. These overarching objectives are listed as follows:

1. To develop a general numerical method that can handle nanoparticle dynamics in a fluid, including the accompanying macro-scale and micro-scale effects, using a continuum based framework (multiphase DNS) i.e. projecting down from the continuum to the molecular scales.

   - Extend the ideas from traditional Langevin based treatments to include the fully resolved hydrodynamics around the particle.
   - Derive a generalized method that extends the applicability of well established resolved-surface multiphase DNS techniques (such as the immersed boundary method, for instance).
   - Demonstrate the capability of this method by validating it against existing analytical theories for Brownian motion in both unbounded as well as bounded domains (i.e. for both free and hindered diffusion.)

2. Establish a hydrodynamic basis, using numerical simulations for diffusive transport of nanoparticles, within the context of the two use cases briefly described in Chapter 1 (i.e. hindered diffusion).

   - Probe the hydrodynamic fields around a Brownian particle (uniform and fractal shaped) in a rarefied gas (i.e. micro-channel flows).
   - Identify the relevant nature of the hydrodynamic stresses on the particle, i.e. the directional bias of the hydrodynamic resistance (along the wall-normal and co-axial directions) on a particle transported along the co-axial centerline of a micro-channel and the corresponding implications on its diffusive behavior.
   - Identify anomalies in the directional bias of the hydrodynamic resistance in non-symmetric scenarios such as off-axis (i.e. a position that is displaced from the co-axial centerline of the channel) diffusion in micro-channels.

3

Nanoparticle dynamics

Brownian transport in a fluid

In the context of this thesis, *nanoparticle dynamics* predominantly refers to the incessant and irregular motion of a nanoparticle in a liquid or gas. The surrounding fluid mediates the complex interactions between the nanoparticles and the surrounding environment (for instance bounding walls or other particles). The physical Brownian motion of nanoparticles (investigated in this thesis) is undertaken in a Newtonian fluid with a non-porous and inert nanoparticle. These investigations are carried out numerically in a dilute fluid (whose density is much lower than that of a particle) using theory and methods that probe both the short and long time-scale aspects of the Brownian behavior. A continuum based hydrodynamic approach to describing Brownian systems is adopted in this thesis. Correspondingly, a brief survey of Brownian theory along with the necessary theoretical basis required to interpret the reported results (appended in the papers) is elaborated in this chapter.

3.1   Overview of Brownian theory

The fundamentals of modern Brownian theory were established in the 1900's by Albert Einstein [14], William Sutherland [24], Marian von Smoluchowski [25] and Paul Langevin [26]. It is surprising that this Brownian perspective played almost no role in physics until 1905 and was generally ignored even by the physicists who developed the kinetic theory of gases, though it is now frequently remarked that Brownian movement is the best illustration of the existence of random molecular motion [27]. It was Einstein who first attempted to establish the relevance of Brownian behavior by combining statistical mechanics and Stokes' result [28] for the friction around a spherical particle due to a steady flow [14]. Einstein's theory neglects the inertia of the particle, implying that an infinite force is required to change its velocity to achieve a random displacement at each step. Von Smoluchowski, shortly afterwards, published a more comprehensible derivation of a similar result (in terms of a random walk – or discrete straight trajectories), using a theoretical model taken over from gas theory [25]. He clarified that each (apparently) straight segment of the Brownian trajectory is a consequence of multiple collisions with

the fluid particles which gives rise to a net displacement along that direction. Langevin used this random walk theory and coupled it with a continuum assumption of the fluid to recover Einstein's result through the use of a stochastic differential equation: the Langevin equation* [26]. The particle inertia was inherently accounted for within this description. Although Langevin employed a continuum description of the fluid (at the scale of the particle), the fluid is perceived through its constituent molecules. These constantly collide with the Brownian particle, accelerating and decelerating it perpetually. Thus, the random displacements can be estimated from the balance between the viscous damping from the fluid and thermal fluctuations due to molecular collisions. This molecular basis of Brownian theory was confirmed by Jean Baptiste Perrin consequently proving the existence of molecules [30]. A chronological account of these early developments in Brownian theory is available in the review by Brush [27].

Langevin's theory neglected fluid inertia as it used the steady state Stokes' drag for damping the thermal fluctuations from molecular collisions (i.e. the Brownian particle is significantly heavier than the molecules it is interacting with). Consequently, Ornstein and Uhlenbeck generalized the original Langevin description to include non-Stokes behavior (i.e. fluid inertia) as well [31]. They achieved this by deriving the frequency distribution function for the velocity and displacement of a free (unbounded) particle undergoing Brownian motion [31]. The resulting random process is commonly referred to as the Ornstein-Uhlenbeck process. Using this treatment, they showed that the velocity auto-correlation function (VACF) of the particle decays exponentially. However, Kubo [32] (another prominent name in the field) noted that this description is not valid at the shortest time-scales, in which the Brownian particle suffers only a few or no impacts (i.e. the particle has a well-defined velocity). These observations are also applicable in systems where the Brownian particle is not necessarily heavier than the molecules interacting with it. Computer simulations of the atoms in liquid argon by Rahman [33], further, corroborated these observations by demonstrating a power law dependence for the VACF at long time-scales (as opposed to the exponential decay). Thus, a generalized form of the Langevin equation (GLE) was proposed by Kubo [32] to account for dynamical coherence in Brownian displacements at short times. Additionally, hydrodynamic models for the fluid (to generalize Stokes' law for the frictional force), can also be used to describe Brownian motion inclusive of fluid inertia, as shown by Alder and Wainwright [34], Zwanzig and Bixon [35], Widom [36] and Hinch [37], to name a few. All these developments culminated into the modern hydrodynamic theory of Brownian motion for a free particle, which has been further validated with exhaustive experimental evidence, recently, by Blum et al. [38], Huang et al. [39] and Kheifets et al. [40]. A more detailed overview of these theories is also available in the reviews by Chandrasekhar [41], Bian et al. [42], Radhakrishnan et al. [43] and Mo and Raizen [44].

Correspondingly, the rest of this chapter establishes the needed mathematical bases which are derived from these popular hydrodynamic theories for both bounded and unbounded Brownian diffusion in a fluid (either liquid or gas). Note that the continuum assumption

---

*A translation of Langevin's original work is available at [29]

§§ needs to be satisfied for these bases to hold since, it is assumed that the momentum of a Brownian particle relaxes to an equilibrium through its interaction with the immediately surrounding fluid (i.e. the system is strongly overdamped by the viscous friction forces). This limit in a fluid, where the Brownian particle interacts through continuum-level forces, permits these macro-scale abstractions of molecular level phenomena.

3.2 Mathematical basis for free diffusion

In this thesis, we are concerned with the transport of nanoparticles in the size range 1 nm to 1 μm, which would mean that both macro- and molecular scale effects compete for dominance. Physically, this results in two primary consequences – firstly, the molecular effects manifest as a random driving force on the particle maintaining its incessant irregular motion and secondly, the ensuing hydrodynamic effects give rise to a frictional force (or drag) for a forced motion. Thus, in mathematical terms, a superposition of these two opposing effects gives rise to the meandering Brownian displacements, which when averaged over long times yields a net diffusivity (a measure of the rate at which particles diffuse) for the Brownian particle. Such a Brownian behavior is typically represented within the Stokes-Einstein or (alternately) Langevin bases for a freely (unbounded) diffusing particle. These representations are followed in this thesis as well and are described below.

3.2.1 Stokes-Einstein description

Einstein's seminal work [14] provided two major contributions: (i) it relates the mass diffusion to the mean squared dispacement (MSD) of the particle and (ii) connects two transport processes – the mass diffusion of the particle and the momentum diffusion of the fluid. These contributions are contained in the equations that describe the long-term statistical behavior of a Brownian particle. Correspondingly, the MSD of a particle with position vector $r(x, y, z)$ is given as:

$$< \Delta r(t)^2 > = 6 D_\infty t. \tag{3.1}$$

Eq. (3.1) can be used for directly estimating diffusivity from a measurement of the particle MSD (in a general random-walk like process). Further, the diffusivity, D_∞, of a freely diffusing particle is given by the Stokes-Einstein relation as:

---

§§The continuum assumption considers the fluid as a continuous collection of macroscopic volumes (which are orders of magnitude greater than the distance between two adjacent molecules of fluid) within which the molecular details of the system are smoothed out. This concept of a continuous medium permits the definition of averaged quantities that reflect the underlying molecular nature such as temperature, density, pressure, velocity etc. at each point in the fluid domain (these quantities are assumed to have a continuous distribution in space and time) [45, 46]

$$D_\infty = \beta_{St} k_B T, \tag{3.2}$$

where, β_{St} is the Stokes' mobility (reciprocal of the friction coefficient γ_{St} [47]) of the particle, which for a sphere in an incompressible fluid at steady state is:

$$\beta_{St} = \gamma_{St}^{-1} = \frac{1}{6\pi\mu_f r_p}, \tag{3.3}$$

with, μ_f as the dynamic viscosity of the fluid and r_p as the particle radius, respectively. Note that Eq. (3.3) is applicable when the no-slip (i.e. fluid velocity at the particle surface is zero) condition is valid at the particle. The particle response time, τ_p, or the time scale of a particle slowing down owing to friction from the fluid (after an initial impulse) is estimated from the mobility as:

$$\tau_p = m_p \beta_{St}. \tag{3.4}$$

The Eq. (3.2) balances the mass transport of the particle with the momentum transport of the fluid. Consequently, the drag on the particle is steady and the thermal kicks (due to collisions with the fluid molecules) average to zero over a long period, leaving the drag on the particle as that in a deterministic fluid. It follows that, the particle inertia is neglected in this description, meaning an infinite force is required to change the velocity of the particle at each instance in the trajectory. Thus, the particle velocities cannot be defined, leading to a fractal trajectory or random walk as shown in Fig. 3.1. A mathematical model corresponding to this case is a Gaussian white noise process for the velocity. Meaning, the instantaneous position $x_p(t)$ corresponds to a Wiener process[¶¶], which is continuous but nowhere differentiable in time. Note that the velocity can still be determined from consecutive positions along the random walk, if the observations are time-resolved sufficiently. Consequently, the chosen temporal resolution should capture the relevant mass-diffusion process as given by the diffusion or Smoluchowski time-scale:

$$\tau_D = \frac{r_P^2}{D_\infty}, \tag{3.5}$$

Another inherent assumption in the Stokes-Einstein treatment is that the Schmidt number (Sc), given as the ratio ν_f/D_∞, is $\ll 1$, where ν_f is the kinematic viscosity (μ_f/ρ_f) of the fluid. Physically, this means that momentum diffuses much faster than does the particle and this motion is viscous-dominated. In particular, the fluid velocity quickly relaxes to the solution of the steady Stokes' equation as the particle barely moves [49].

[¶¶]A continuous-time stochastic process $W(t)$ for $t \geq 0$ with $W(0) = 0$ and such that the increment $W(t) - W(s)$ is Gaussian with mean 0 and variance $t - s$ for any $0 \leq s < t$, and increments for non-overlapping time intervals are independent [48].

Thus, the Eq. (3.2) captures the long term behavior of a free Brownian particle in a viscous fluid well, however it disallows a definition of an instantaneous particle velocity. This is particularly relevant at the shortest time scales of motion ($\ll \tau_D$), when the Brownian particle moves in a straight line with a constant velocity before collisions with fluid molecules slow it down and randomize its motion (as shown in experiments by Huang et al. [50]). At this scale, known as the ballistic regime, the particle's inertia becomes significant and its motion is highly correlated. The ballistic time-scale (τ_B) can be deduced from the collisional time scale of the molecules (i.e. the duration between successive random bombardments). This is resolved using Langevin's treatment [26]. Finally, and most importantly, the Brownian process is assumed to be a Markovian, i.e. the future states of the system are independent of the present and past states. This assumption is usually valid, when it is assumed that the fluid is inertia-less (as is the case in the Stokes-Einstein description).
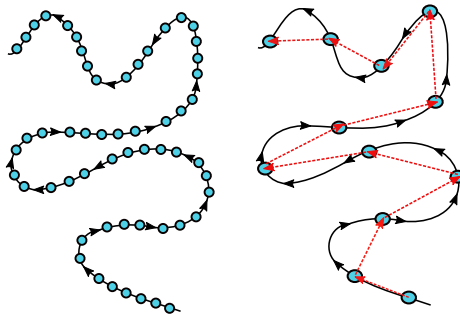
Figure 3.1: *Concept of random-walk: On the left is the actual trajectory of a Brownian particle, while on the right are the observed locations of the particle as extracted from a Stokes-Einstein description (Eq. (3.2)) at the diffusive time scale (τ_D in Eq. (3.5)). The red arrows indicate the fractal trajectory (random walk) that is usually identified from this description.*

3.2.2 Langevin description

The fundamental theory of Einstein and Smoluchowski is restricted to time scales at which the decay of the velocity of the Brownian particle is negligible (i.e much larger than the particle response time). Hence, a more complete description of the Brownian motion of a free particle was proposed by Langevin [26, 41]. Although Langevin's approach, like Einstein's, is from a mathematical point-of-view rather simple, there is a very subtle conceptual point at the basis of his theory for Brownian motion. This is the validity of Stokes' law (which has a macroscopic nature) together with the assumption that the Brownian particle is in statistical equilibrium with the molecules in the liquid. In other words, despite the mass of the colloidal particle being (exceedingly) larger than the mass of the molecules, energy equipartition is assumed to hold. This equation of motion[†] for

---

[†]Brownian motion occurs in 3D and Eq. (3.6) applies only to the x-component of this motion.

the Brownian particle, with mass m_p, is formally based on Newton's second law as:

$$m_p \frac{\mathrm{d}u_p}{\mathrm{d}t} = -\gamma_{St} u_p + \chi(t), \tag{3.6}$$

where, u_p denotes the velocity of the particle and $\chi(t)$ is the stochastic forcing (in the attached papers this is referred to as $\mathbf{F_{Brownian}}$) that denotes the fluctuating part of the Brownian motion. It should be noted that both these parts are related as they are a result of the same fundamental phenomenon, i.e. random collisions with the surrounding molecules. The frictional term γ_{St} is given by Eq. (3.3). Hence, the Langevin equation (3.6) is the momentum equation for the particle with a random forcing for the non-equilibrium behavior and with a friction force that is linear in instantaneous velocity. The fluctuating component $\chi(t)$ is assumed to be independent of the velocity u_p and further fluctuate rapidly in comparison with variations in velocity. Consequently, in this description, the particle velocity is well defined and is subject to both the viscous dissipation (friction force) from the fluid and the random stochastic forcing. Uhlenbeck [31] further showed that Eq. (3.6) is constrained by certain restrictions on the fluctuating component $\chi(t)$, i.e. it follows a Markovian Gaussian white noise process. Hence, the stochastic forcing satisfies:

$$\langle \chi(t) \rangle = 0, \quad \langle \chi(t) \chi(t') \rangle = \tilde{S}_{uu} \delta(t - t')$$

$$\langle \chi(t) x(t') \rangle = 0, \quad \langle \chi(t) u_p(t') \rangle = 0. \tag{3.7}$$

Here, $\langle ... \rangle$ denotes an ensemble average in thermal equilibrium and $\tilde{S}_{uu}$ is the strength of the Gaussian noise (which will be determined below). In the Langevin Eq. (3.6), u_p is continuous and differentiable under the constraints of a stochastic differential equation (provided $\chi(t)$ is an additive and independent noise). Thus, the MSD and velocity auto-correlation function (VACF) can be extracted from this equation as shown below.

MSD and VACF

The MSD can be derived by re-writing Eq. (3.6) in terms of the position $x(t)$ and averaging the same using the $\langle ... \rangle$ operator under the constraints presented in Eq. (3.7), followed by the application of the equipartition theorem $m_p \langle u_p^2 \rangle = k_B T$[‡]. Correspondingly, we obtain the expression for the MSD at all time scales as:

$$\langle \Delta x^2(t) \rangle = \frac{2k_B T}{\gamma_{St}} \left(t - \frac{m_p}{\gamma_{St}} + \frac{m_p}{\gamma_{St}} \mathrm{e}^{\frac{-\gamma_{St} t}{m_p}} \right). \tag{3.8}$$

[‡]A colloidal particle suspended in a liquid at temperature T is assimilated to a particle of the liquid, so that it possesses an average kinetic energy $\frac{2RT}{N_{av}}$. Accordingly we get: $\frac{1}{2} m_p \langle u_p^2 \rangle = \frac{2RT}{N_{av}}$

In Eq. (3.8), when $t \gg \tau_B$, the exponential term is negligible, leading to the Einstein's result for long-term or over-damped behavior i.e. Eq. (3.1) (in 1D). However, when $t \ll \tau_B$ or as $t \to 0$, the ballistic or under-damped result can be obtained:

$$< \Delta x(t)^2 > = \frac{k_B T}{m_p} t^2 = u_{rms}^2 t^2. \tag{3.9}$$

Here, u_{rms} is the root-mean-squared velocity of the particle. The corresponding time scale (i.e. lesser than the relaxation time for the Brownian particle) in the ballistic regime, τ_B, is given as:

$$\tau_B \ll \frac{m_p}{\gamma_{St}}. \tag{3.10}$$

The VACF of the Brownian particle can be derived by evaluating the solution of the first-order inhomogeneous stochastic differential equation i.e. Eq. (3.6). Ornstein-Uhlenbeck showed that the VACF of a freely diffusing Brownian particle is:

$$C(t) \equiv \langle u_p(0) u_p(t) \rangle = \langle u_p^2(0) \rangle \, \mathrm{e}^{\frac{-\gamma_{St} t}{m_p}} = \frac{k_B T}{m_p} \mathrm{e}^{\frac{-\gamma_{St} t}{m_p}}. \tag{3.11}$$

The detailed derivation of both the MSD and VACF is available in Appendix 7.2.

3.2.3 Linear response theory and the Langevin equation
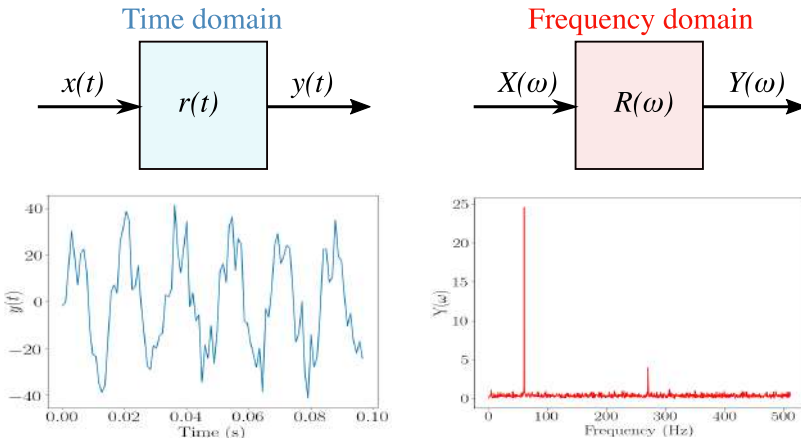
Figure 3.2: *Schematic of an output from a linear time invariant (LTI) system in the time (left) and frequency (right) domains.*

Linear response theory describes how an (small) external perturbation affects the macroscopic properties of a system. In this context, a Brownian process can be regarded as a system which is regularly perturbed by thermal kicks (from the fluid molecules) and can correspondingly be modeled using linear response theory (as shown by Ounis and Ahmadi [51–53]). Since the magnitude of these applied stochastic forces are small, the response of the system has a linear dependence on it. Moreover, this response does not depend on the time when the stochastic forcing is applied, meaning it is a linear time-invariant (LTI) system. Consequently, the Brownian system is perturbed by a Gaussian white noise with zero mean ($\mathbb{E}[\chi(t)] = 0$) and a co-variance given by the Dirac-delta function ($\mathbb{E}[\chi(t)\chi(\tau)] = \delta(t - \tau)$). This forcing appears at a time-scale lesser than the particle response time (τ_p). Consequently, such a strategy is adopted to model Brownian behavior in this thesis.

The correlation functions, derived previously (see Eq. (3.11)) represents a stationary[¶] stochastic process in the time domain, which satisfies the Wiener-Khinchin theorem[‖]. It follows that, such time signals can be represented in the frequency space using the corresponding Fourier transforms. Correspondingly, the power spectral density, $\tilde{S}_{uu}(\omega)$, of the random process (based on the velocity), which is needed in order to describe the Gaussian white noise signal, can be deduced as:

$$\tilde{S}_{uu}(\omega) = \frac{k_B T \gamma_{St}}{\pi m_p} = \frac{2\gamma_{St}^2}{\pi} D_\infty, \tag{3.12}$$

Thus, the stochastic forcing term, $\chi(t)$, is modeled as a Gaussian white noise process with the vector of spectral intensity S_{ij}^n given as:

$$S_{ij}^n = \tilde{S}_{uu}(\omega)\delta_{ij}. \tag{3.13}$$

A detailed derivation of this power spectrum (i.e. Eq. (3.13)) is provided in Appendix 7.3.

To summarize, in this thesis, the Langevin behavior is studied as an LTI system, i.e. a Gaussian white noise perturbed Brownian particle that is immersed in a fluid is studied. This approach is chosen as it is easy to implement in a Lagrangian form within the numerical framework developed in this thesis. Moreover, this approach accurately reproduces the necessary dynamics of the system (see Fig. 3.3) as well. Additionally, hindered diffusion can easily be included in such a Langevin description by accounting

---

[¶]A continuous-time random process, $X(t), t \in \mathbb{R}$ is wide sense stationary if:

1. $\mu_X(t) = \mu_X$, for all $t \in \mathbb{R}$, where μ_X is the mean.

2. $C_X(t_1, t_2) = C_X(t_1 - t_2)$, for all $t_1, t_2 \in \mathbb{R}$, where C_X is the correlation function.

[‖]The power spectrum $S(\omega)$ of a stationary random process and its auto-correlation function are Fourier transform pairs

for the relevant particle mobility in Eq. (3.3), as will be elaborated in the subsequent section.
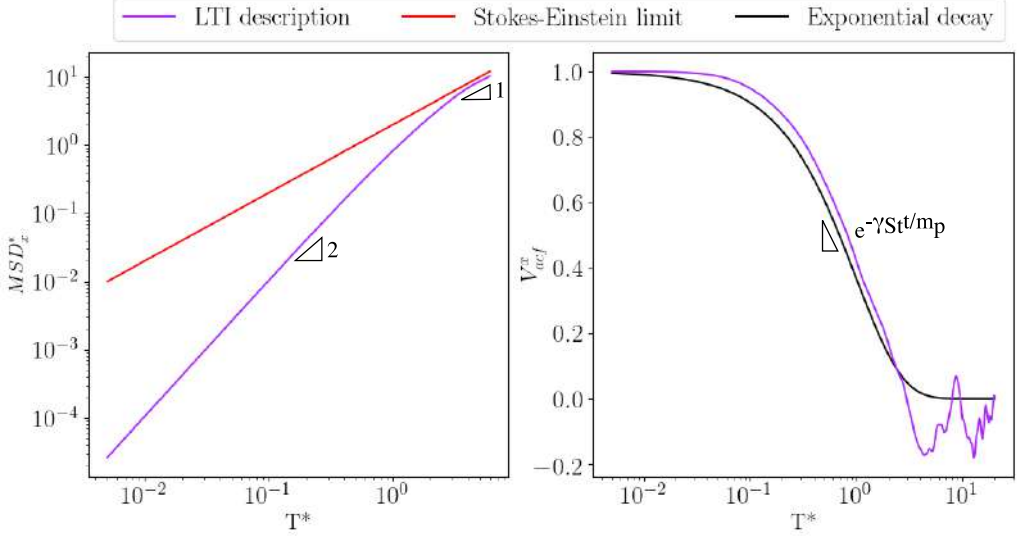
Figure 3.3: *1D Brownian behavior modeled as an LTI system (stochastic forcing done using a Gaussian white noise signal): Particle mean-squared behavior (represented as $MSD_x^* = MSD_x/D_\infty \tau_p$) in the left panel and VACF in the right panel. Note that the Langevin Eq. (3.6) is integrated using a forward Euler explicit time marching scheme. The mean-squared behavior shows the clear transition from the correlated ballistic regime (indicated with slope 2) to an un-correlated and linear Stokes-Einstein regime. Further, V_{acf}^x decays exponentially.*

Note, however, that this approach is valid only under the following conditions:

1. The random forcing appears as a white noise at a scale lesser than the particle response (or ballistic) time scale τ_p.

2. The hydrodynamic coupling between the particle and the fluid (i.e. the fluid friction) is given by the steady Stokes' drag [47].

3. There is equipartition of kinetic energy among the degrees of freedom of the system, i.e. between the molecules of the fluid and the particle performing Brownian motion.

The white-noise assumption is satisfied when the particles are much larger than the surrounding fluid molecules without being much less dense [37]. The validity of the steady drag has been a source of debate for several applications of the Langevin treatment, especially when the particle-fluid density ratios are lower (i.e unsteady effects such as Basset history and added mass forces begin to play a role) [33, 34, 37]. However, for

the typical cases studied in this thesis, the particle-fluid density ratios are significantly higher, meaning that the hydrodynamic coupling can be given by steady hydrodynamic forces. Moreover, the particle Reynolds number[††] is $\ll 1$, for the nanoparticles studied in this thesis, meaning, the fluid inertia is negligible.

3.3   Hindered diffusion

In the previous section, a detailed mathematical basis for describing free (or unbounded) diffusion is established. In particular, the Langevin approach, which is central to this thesis, has been described in detail. However, not all real systems are so ideally behaved. In many cases, the Brownian particle diffuses in an environment where other interactions mediated by the fluid (such as particle-particle, particle-wall or non-continuum effects), assume a governing role in dictating the dynamics of the system. Within the context of this thesis, nanoparticle transport in such altered environments is referred to as hindered diffusion (i.e. the free diffusion of a Brownian particle is 'hindered' by additional effects mediated by the fluid). It is well established that the mobility of the particle is altered and in most cases reduced when diffusing in the vicinity of a wall or another particle. This was confirmed by direct measurements in Brownian systems, first by MacKay and Mason [54] and later by others [50, 55–70] using advanced particle tracking techniques. This reduction in particle mobility is attributed to the associated increase in the hydrodynamic resistance on the particle when diffusing in the vicinity of a wall or another particle. A detailed account of related hindered diffusion theories for Brownian motion is available in the reviews by Deen [71], Burada et al. [72] and Mo and Raizen [44]. The details on these theoretical developments are omitted from this section for brevity (but are briefly discussed in the appended papers, see Papers *B* and *D*).

A similar reduction in the hydrodynamic resistance is also noticed for a particle suspended in a rarefied gas, as first reported by Epstein [73] and later by Cercignani and Pagani [74, 75]. The reduction in this case is, however, due to the existence of non-continuum effects in the gas. These are attributed to the longer mean free paths (or distance between successive molecular collisions) in air when compared with a corresponding liquid (where the molecules are more tightly packed). Thus, a new transport scale defined by the Knudsen number (*Kn*):

$$Kn = \frac{\lambda_{gas}}{L},\tag{3.14}$$

with λ_{gas} as the mean free path of the gas and L as a characteristic system length scale, is introduced in these systems. This scale identifies the relative importance between (microscopic) molecular and (macroscopic) hydrodynamic interactions (or the degree of

---

[††]Ratio between inertial and viscous forces given as $\frac{d_p \rho_f u_p}{\mu_f}$

rarefaction). When $Kn > 0.001$, the particle does not perceive the gas as a continuum any longer and begins directly interacting with its constituent molecules, particularly as the particle sizes are very close to the mean free path (molecular length scales) of the surrounding gas. Thus, the overall resistance to motion is also reduced.

In this thesis, hindered diffusion is modeled by correcting the Stokes' mobility (in Eq. (3.3)) used in the Langevin basis to adequately represent the actual mobility of the particle. Correspondingly, the respective treatments adopted for this mobility correction (in liquids and gases) are described in this section.

3.3.1 Wall-bounded diffusion

The dynamics of Brownian particles close to a rigid wall are significantly affected by wall interactions. When a rigid particle approaches within a few radii from the wall, its mobility is altered. Usually, this mobility is discussed along two principal directions relative to the motion between the particle and the wall, a co-axial (or parallel) and wall normal (or perpendicular) mobility, respectively. Independent measurements of the mobility and diffusion coefficient (D) of Brownian particles diffusing near a wall have indicated that they are each to be corrected by the same factor [50, 57, 61, 63–65, 76, 77]. This implies that these quantities are functions of the radial position of the Brownian particle in relation to the boundary walls. This is due to the increased hydrodynamic resistances in the vicinity of a wall, leading to a reduction in particle mobility. Further, the wall-normal motion is impeded more strongly than the co-axial one. This is expected as, for wall-normal motion, the fluid between the particle and the wall needs to be squeezed out, correspondingly, increasing the resistance. This basis was first established by Faxén and later improved upon by the analytical theories of Brenner [78, 79] for longitudinally bounded flows.

The correction to the particle mobility in a liquid is represented as λ throughout this thesis. This is done by multiplying the Stokes' mobility (see Eq. (3.3)) for a free particle with this factor as:

$$\beta_{St}^{corr} = \frac{1}{6\pi\mu_f r_p \lambda},$$
(3.15)

where β_{St}^{corr} is the corrected Stokes' mobility. Most recently, Kihm and co-workers [63, 80] further validated with experiments that the reduction in mobility (by the factor λ) is indeed described by the analytical theories of Brenner [78, 79]. Moreover, λ can represent any other effect such as a slip-wall [81, 82] or even other neighboring particles (multi-particle diffusion) [60, 78, 83, 84], provided the appropriate correlation is used. An overview of most analytical/theoretical developments including the appropriate expressions for λ can be found in the classical books of Happel and Brenner [85] and Kim and Karilla [86].

3.3.2   Diffusion in a rarefied gas

Diffusion of a nanoparticle in a rarefied gas is usually not classified under hindered diffusion, however, within the context of this thesis, this is also included within this broad classification. The motivation behind this inclusion is that these systems are also modeled in a similar way as hindered diffusion in liquids, i.e. the particle mobility is corrected to incorporate the necessary deviations from the Stokes' mobility (Eq. (3.3)). For rarefied gases, these deviations are due to the breakdown of the continuum assumption when the characteristic dimensions of the flow are comparable to the mean free path of the gas (in this case air has a mean free path of approximately 67 nm at 20°C and standard atmospheric pressure). Thus, for the range of Brownian particles considered in this thesis (1 nm to 1 μm), rarefaction effects of the gas are also relevant. Under such conditions, the fluid can no longer be regarded as being in thermodynamic equilibrium (with the particle) and a variety of non-continuum or rarefaction effects are likely to be exhibited [87]. This necessitates an additional correction factor in the Langevin equation, Eq. (3.6) (in a similar manner as that of λ) while modeling the relevant Brownian behavior. Note that in a rarefied gas the no-slip boundary condition, traditionally employed at the particle surface, is no longer applicable and a sub-layer (known as the Knudsen layer) of the order of one mean free path starts to affect the fluid interaction between the bulk flow and the particle.
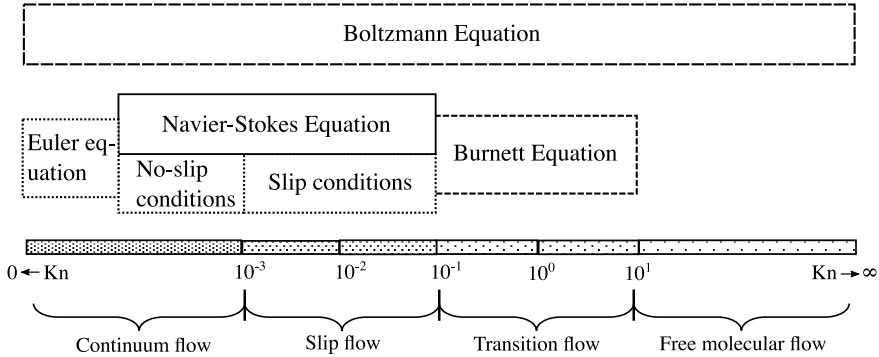
Figure 3.4: *Flow regimes classified based on the Knudsen number (figure adapted from Bird [88]).*

Rarefied flows are characterized by Kn into the following four regimes: continuum flows ($Kn < 0.001$), slip flows ($0.001 \leq Kn < 0.1$), transition flows ($0.1 \leq Kn < 10$), and free-molecular flows ($Kn \geq 10$) [87, 89–94]. The applicability of the continuum hypothesis is determined on the basis of these regimes, as shown in Fig. 3.4. Systems which are strongly rarefied or at the limit of free molecular flow are characterized by a Kn greater than unity while those which are at the continuum flow limit are characterized by a Kn much lower than unity. As Kn increases, the rarefaction effects become more pronounced and eventually the continuum assumption breaks down. Hence, the particle-fluid interaction has to be resolved by solving the Boltzmann equation (will be discussed

in Section 4.1.2). Nevertheless, conventional continuum descriptions of the forces can be extended to describe weakly rarefied or slip flows ($10^{-3} < Kn < 10^{-1}$) by imposing the appropriate slip and temperature jump boundary conditions on the surface [87].

Early attempts at understanding such rarefied flow regimes at low densities began with Maxwell [95], when he derived a slip boundary condition for a dilute gas using kinetic theory. This idea was extended by Cunningham [96], who derived an empirical first-order slip velocity correction factor from hydrodynamic theory for small Kn. Further, Millikan [97] confirmed that the drag reduction (due to hindered momentum transfer between the particle and fluid) at higher Kn can be deduced using the Cunningham correction (C_c) when formulated as a function of Kn as:

$$C_c(Kn) = 1 + AKn, \tag{3.16}$$

where, A is a function of Kn that is determined based on empirical data. The Cunningham correction produces results that are in excellent agreement with the available experimental data as shown by Alan and Raabe [98]. Mosfegh et al. [99] summarize the Cunningham-based slip correction factors (and corresponding A values) that have been proposed and commonly used (based on extensive experimental trials) for air with mean free path of 67.3 nm at 101.3 kPa and 23°C. Among these, the most commonly used correlation is the one proposed by Davis [100] and is given as -

$$C_c = 1 + Kn \left(1.257 + e^{\frac{-1.1}{Kn}} \right). \tag{3.17}$$

Correspondingly, the correction to Stokes' mobility (i.e. Eq. (3.3)) for diffusion in rarefied gases is given as:

$$\beta_{St}^{corr} = \frac{1}{6\pi \mu_f r_p (\frac{1}{C_c})}. \tag{3.18}$$

The Eq. (3.18) shows that C_c is always used in conjunction with the steady Stokes' drag, which is by definition obtained using a no-slip condition at the particle surface. The continuum hypothesis could also be extended for moderate Kn by exchanging the no-slip condition for a slip condition (at the particle surface) [101]. This approach can be used with some success in the slip flow regime (up to $Kn \approx 0.15$). Nevertheless, in this thesis, we limit ourselves only to the empirical first-order Cunningham slip correction due–in–part to its relative ease of implementation (within the developed framework) and demonstrated capability to adequately represent non-continuum effects in weakly rarefied gases [98]. Moreover, these higher-order slip conditions are highly geometry dependent [102], further adding to the complexity of the problem. Consequently, there is not yet a consensus in open literature neither on the best choice for a higher-order slip formulation, nor on their advantages in complex geometries [103].

4

Numerical modeling approaches

Molecular and continuum based methods

The primary objective of this thesis is to present a novel continuum based framework to assess the (Brownian) dynamics of a nanoparticle under any given condition (either free or hindered diffusion). Traditionally, the modeling of Brownian behavior has been approached from two perspectives – building up from micro-scales or projecting down from the macro-scale. This dichotomy consequently leads towards assessments at varying levels of detail. The former are generally at a high level of detail but at a microscopic scale of abstraction, while the latter are lacking in the molecular details but are, however, at a relevant macroscopic scale. In this thesis, a continuum based abstraction is preferred (as elaborated in Chapter 3). Furthermore, these continuum based projections are additionally improved by consistently incorporating the missing molecular details, thereby extending their applicability. Note also that molecular methods are used as well in order to investigate certain complex dynamics in rarefied particulate flows where a continuum based abstraction fails. Thus, in this chapter, these numerical treatments are described in relation to the theoretical bases introduced in the previous chapter. Furthermore, a brief review of the current state-of-the art in the numerical modeling of Brownian motion is also presented here.

4.1 Current state-of-the-art

Early analytical developments within Brownian theory were derived with both first principles based approaches using kinetic theory (i.e. Langevin, Fokker-Planck[§§] and

---

[§§]The Fokker-Planck equation for the distribution function f of the Brownian particles (derived from the Langevin Eq. (3.6)) is given as:

$$\frac{\partial f}{\partial t} = \frac{\partial}{\partial x_p} \cdot (\gamma_{St} u_p f) + q \frac{\partial^2 f}{\partial x_p^2},$$

Boltzmann equations [31, 41]) and hydrodynamic approaches using the linearized Stokes' equations¶¶ [86, 104]. Most modern techniques heavily borrow from these classical approaches and further improve upon them. Correspondingly, these modeling techniques are classified into three overarching categories based on the corresponding level of computational abstraction (as shown in Fig. 4.1). These are: micro-scale, meso-scale and macro-scale methods, in decreasing level of spatial resolution (i.e. moving from meter-scales to pico/nano-scales), respectively. Due to the large scale-separations, the dynamics of the Brownian particles are largely dependent on the detailed mechanics of the suspending fluid. Thus, the wide spectrum of available methods are generally applicable (efficiently) based on the governing length scales of the system as represented in terms of Kn. Correspondingly, micro-scale methods are more relevant when directly describing molecular-scale interactions ($Kn \geq 10$) and macro-scale methods when the continuum theory holds ($Kn \to 0$). The meso-scale methods are applicable when the continuum theory begins to fail and when micro-scale methods are too expensive. The relevant developments within these three categories of numerical methods are described below.

4.1.1 Micro-scale methods

Dynamic simulations of Brownian systems at a molecular level of abstraction (using kinetic theory) were pioneered by Alder and Wainwright [105]. The aim of such a method was to obtain the spatial and temporal evolution of the relevant macroscopic properties of the system on the basis of the mechanical laws governing the molecular motion. This method, referred to as molecular dynamics (MD), solves the Newton's equation of motion for the simulated molecules/particles interacting through Lennard-Jones, hard-sphere, electrostatic, etc. types of inter-particle forces. This was first successfully used by Rahman [33] to demonstrate the non-exponential decay of the VACF in liquids and has since been used for several applications, including studying bio-molecules [106]. The MD technique evaluates the time-dependent behavior and evolution of a molecular system, from which the thermodynamic and kinetic properties are evaluated. Although such an approach works reasonably efficiently in liquids (where the molecules directly interact with only a few neighboring molecules), it gets computationally expensive in dilute gases where a molecule could have potentially thousands of collision partners. This could make the problem completely intractable for certain applications, as the computational burden of the method scales with the square of the number of simulated molecules. This is because the computation for any single molecule requires the consideration that all other molecules are possible collision partners [88]. This inherent limitation of the MD method, led to the development of the most widely used molecular method for dilute gas flows, the direct simulation Monte Carlo (DSMC). This method, pioneered by Bird [88, 107], is also similar to the MD approach with one crucial difference: the inter-molecular collisions are dealt with on a probabilistic rather than a deterministic basis (hence the

---

where $q = \frac{k_B T \gamma_{St}}{m_p}$

¶¶The continuum Navier-Stokes equations can be linearized by neglecting the non-linear convective terms, meaning the Brownian particle is diffusing in a quiescent fluid.

name Monte-Carlo). DSMC has been shown in principle to be an exact solution of the Boltzmann equation*** [108], meaning the necessary molecular nature of the system can be obtained without the need for any additional models or fitting. The DSMC method can in principle be used across the regimes indicated in Fig. 3.4. However, it is best applicable to describe flows with $Kn \geq 10$, as it can get computationally expensive when $Kn \to 0$. Moreover, Michaelides recently used this method to assess nanoparticle diffusivity in an isothermal fluid within narrow cylindrical pores [109], further demonstrating the usefulness of the method in assessing the micro-scale dynamics of a Brownian system. Thus, Bird's DSMC framework is used in this thesis to describe rarefied gas dynamics in the transition regime. More specifically, the effect of a symmetric nanoparticle in rarefied micro-channel flows is investigated using a DSMC solver (*dsmcFoamPlus*), details of which are discussed in the succeeding sections.
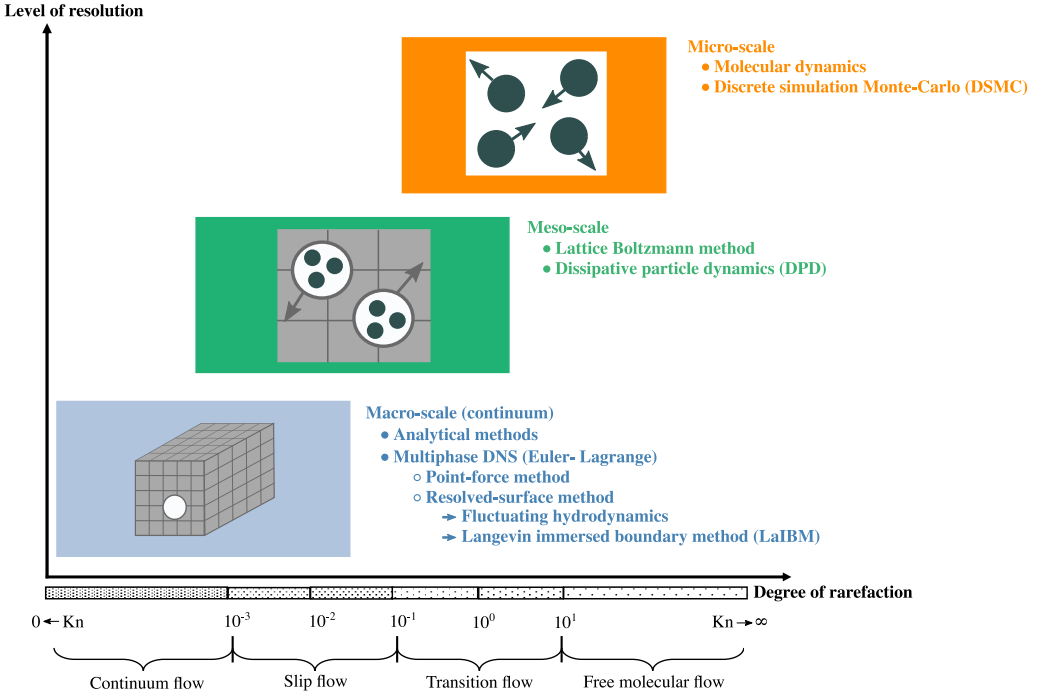
Figure 4.1: *Classification of numerical methods based on their corresponding scales of abstraction in terms of level of detail.*

***The Boltzmann transport equation is given as:

$$\frac{\partial f}{\partial t} + u_p^i \frac{\partial f}{\partial x^i} + a_p^i \frac{\partial f}{\partial u_p^i} = \left(\frac{Df}{Dt}\right)_{\text{coll}} ,$$

where, u_p^i and a_p^i represents the velocity and acceleration of a distribution of molecules/particles. Note that f is a one-particle distribution function, i.e. it is assumed that the probability of finding a particle at a particular point in phase space is independent of the coordinates of all other particles in that phase space. Such a description is only valid for a dilute gas.

4.1.2 Meso-scale methods

Simulating every aspect of a system at a molecular level of detail can not only be very expensive but also unnecessary. Under conditions where Kn is sufficiently low that a detailed molecular basis is intractable, while still being sufficiently high enough that the continuum based approaches are reaching their limit (i.e. usually in the slip and transition flow regimes), a meso-scale approach is more preferred. Methods at this level of abstraction are based on microscopic models and meso-scopic kinetic equations. The basic premise for using these simplified kinetic-type methods for macroscopic fluid flows is that the macroscopic dynamics of a fluid is the result of the collective behavior of many microscopic particles in the system and that the macroscopic dynamics is not sensitive to the underlying details in the microscopic physics [110]. Consequently, in mesoscopic kinetic theory, the distribution of particles in a gas is the quantity which evolves on timescales around the mean collision time between the molecules (i.e. at a scale where the system relaxes to local equilibrium through collision events).

Some of the most widely used mesoscopic methods for modeling Brownian behavior are the lattice Boltzmann method (LBM) and dissipative particle dynamics (DPD). These are briefly described below.

Lattice Boltzmann method

The LBM framework originated from lattice gas automata (LGA), which was proposed as a new technique to solve the continuum averaged Navier-Stokes equations (described later in Eq. (4.1)). Consequently, these equations were solved using a simulation where particles of the same mass are allowed to move on a regular lattice and local collision rules are introduced at the nodes which conserve the number of particles and momentum (discrete particle kinetics utilizing a discrete lattice over discrete time) [111–113]. The lattice gas automata was extended to solve the Boltzmann equation (for a distribution of particles/molecules) with a linear BGK collision operator, that directly captures the relaxation of the distribution function towards the equilibrium Maxwellian distribution. This is achieved by discretising the Boltzmann equation in velocity space, physical space and time[†††]. Thus, the particles in the LGA method are replaced by distribution functions in the LBM approach. A more detailed account of the LBM framework is beyond the scope of this thesis and the reader is referred to detailed reviews on the same by Chen and Doolen [114] and the book by Kruger et al. [115].

[†††]Discretized Boltzmann equation:

$$f_i \left(x + c_i \Delta t, t + \Delta t \right) = f_i(x,t) - \frac{\Delta t}{\tau} \left(f_i(x,t) - f_i^{eq}(x,t) \right),$$

where, $f_i(x,t)$ moves with velocity c_i to a neighboring point on the lattice $x + c_i \Delta t$ at the time step $t + \Delta t$ and τ is a velocity-dependent collision time that relaxes the system to the equilibrium distribution f_i^{eq}.

LBM has been used in conjunction with existing MD methods, for studying Brownian behavior in finite size suspensions. Ladd [116, 117] proposed one such hybrid method that solved the particle dynamics using Newton's equations of motion (MD) and the surrounding fluid using the LBM framework. Since the molecular fluctuations are inherently absent in the Boltzmann equation, these are additionally included in the fluid description using the fluctuating hydrodynamics approach of Landau and Lifshitz [118], leading to a stochastic term in the the time evolution of the velocity distribution function. This approach, also known as the fluctuating lattice Boltzmann method (FLBM), was extended to polymer solutions by coupling it to a Langevin evolution of the particle dynamics, by Ahlrichs and Dunweg [119] and later by Mynam et al. [120]. Despite being highly paralellizable, LBM is memory-intensive. Consequently, propagating populations requires a large number of memory access events. Moreover, FLBM has a few bottlenecks associated with the choice of the discretization scheme for the stochastic differential equation, primarily due to the correlation between the form of the required fluctuation-dissipation relations and the choice of scheme [121].

Dissipative particle dynamics

DPD, on the other hand, can be considered as a coarse-grained MD method that allows for the simulation of larger length and time scales than molecular dynamics and avoids the lattice-related artefacts of LBM. This model consists of a set of point particles that move off-lattice, interacting with each other through three types of forces: a conservative force derived from a potential, a dissipative force that tries to reduce radial velocity differences between the particles and a stochastic force directed along the line joining the center of the particles. The last two forces can be termed as a pair-wise Brownian dashpot which represents the viscous forces and thermal noise between the groups of atoms represented by the dissipative particles. All these forces describe additive pair-interactions between particles (obeying Newton's third law). Hence, DPD conserves momentum. Due to this, the behavior of the system is hydrodynamic at sufficiently large scales [122]. Note that all interactions have a finite radial range. For a more detailed description of this method, the reader is referred to the review by Espanol [122].

DPD is particularly suited for evaluating the hydrodynamics of complex fluids at the mesoscale with finite Kn. Typical applications are suspensions of polymers. This method has also been used in conjunction with the Langevin equation to assess Brownian systems. Gubbioti and co-workers used DPD to account for a spatially dependent mobility field determined *a priori*. This field was solved in conjunction with a rigid body Langevin equation [123] to assess hindered diffusion in micro-channels. This method is perfectly suited for studying pore scale diffusion in symmetric channels, however, the *a priori* determination of the mobility field gets progressively harder in heterogeneous pores, thereby limiting its applicability. Another disadvantage of DPD is that it contains a large number of parameters that have to be selected carefully. For instance, the choice of the radial cut-off limits is delicate and affects the emergent hydrodynamic behavior. Finally, as with other mesocale methods, these can also be memory intensive as the dynamics of

individual particles have time scales significantly shorter than the hydrodynamic time scales.

4.1.3 Macroscopic methods

The Macroscopic or continuum based methods are in essence coarse-grained abstractions of micro- and meso-scale descriptions that rely on two fundamental assumptions: (i) the continuum limit, i.e. the point in space where the field is defined is a volume element containing a large number of atoms and (ii) the local equilibrium assumption, i.e. these volumes are large enough to reproduce the thermodynamic behavior of the whole system. This concept of a continuum fluid is fundamental to the viscous damping being described in the Langevin equation, which models the total fluid resistance (in the over damped limit) as the continuum Stokes' drag on the particle (as elaborated in Chapter 3). Hence, the original Langevin equation (i.e. Eq. (3.6)) can be considered to model Brownian behavior at a continuum level of abstraction, consequently requiring the molecular fluctuations to be added additionally (as these have been averaged out in a continuum description) through the stochastic forcing term.

This continuum assumption permits the governing equation system to be simplified into non-linear partial differential equations, i.e. the Navier-Stokes (NS) equations [28, 47, 124][***]. This equation, for an incompressible (divergence free) fluid is given by the following continuity and momentum equations:

$$\boldsymbol{\nabla} \cdot \boldsymbol{v} = 0,$$
$$\rho_f \left(\frac{\partial}{\partial t} \boldsymbol{v} + \boldsymbol{v} \cdot \boldsymbol{\nabla} \boldsymbol{v} \right) = -\boldsymbol{\nabla} P + \mu_f \boldsymbol{\nabla}^2 \boldsymbol{v}, \tag{4.1}$$

where, $\mathbf{v}$ and P are the velocity vector and pressures in the fluid, respectively[‡‡].

The NS equations are strongly non-linear, meaning they require advanced iterative techniques such as computational fluid dynamics (CFD) for obtaining the desired solution. Alternately, these equations can also be linearized by neglecting the non-linear convective terms, giving an equation system that can be determined by semi-analytical solutions. This means that the solution to the governing hydrodynamic fields (obtained from the NS equations) coupled with the integration of the Langevin equation for the particle yields

---

[***]A concise history of the conceptual foundations of fluid mechanics from the time of Newton's Principia in 1687 up to the definitive work of Stokes in 1845, can be found in [125]

[‡‡]The operators are given as:

$$\boldsymbol{\nabla} = \left(\frac{\partial}{\partial x}, \frac{\partial}{\partial y}, \frac{\partial}{\partial z} \right), \boldsymbol{\nabla}^2 = \left(\frac{\partial^2}{\partial x^2} + \frac{\partial^2}{\partial y^2} + \frac{\partial^2}{\partial z^2} \right)$$

a reasonable description of Brownian behavior. Note that within the context of this thesis, the former CFD based approaches are grouped under multiphase direct numerical simulation or DNS methods while the latter are grouped as analytical methods. These are described below.

Analytical methods

Analytical approximations of the NS equations, obtained by linearizing Eq. (4.1) or neglecting the non-linear convective terms when $Re_p \ll 1$ (meaning the particle is diffusing in a quiescent fluid) is given as:

$$\boldsymbol{\nabla} \cdot \boldsymbol{v} = 0,$$

$$\rho_f \frac{\partial}{\partial t}\boldsymbol{v} = -\boldsymbol{\nabla}P + \mu_f \boldsymbol{\nabla}^2 \boldsymbol{v}, \tag{4.2}$$

are used to estimate the hydrodynamic resistance γ_{St} used in the Langevin Eq. (3.6). A variety of methods have been reported in literature to solve the linearized (unsteady) Stokes' Eq. (4.2), as listed in the classical books by Happel and Brenner [85] and Kim and Karilla [86]. Among these, the method of reflections pioneered by Smoluchowski [25] and later extensively used by Brenner [78] has been popular in solving the steady Stokes' equations (i.e. without the time derivatives in Eq. (4.2)). This technique has since been extended to Brownian motion by Ermak and McCammon [126] through the Brownian dynamics (BD) approach. The BD approach was further extended towards a colloidal system of N-particles in a viscous, incompressible fluid under creeping flow conditions by Brady and Bossis [127] through the Stokesian dynamics (SD) approach. Despite being successful at simulating the rheology of spherical particles in a suspension, both BD and SD neglect unsteady particle inertia to accommodate for computational efficiency, thus, limiting their applicability to only particle-fluid systems at high density ratios.

In most real systems of interest, the net force on the particle from the fluid includes both reactive (e.g. added mass or Basset history forces) and resistive (e.g. viscous dissipation) components. These can be included by solving the unsteady Stokes' equation for the fluid given in Eq. (4.2). Consequently, the method of reflections for steady Stokes' flows was extended by Ardekani and Rangel [128] and later by Simha et al. [129] to account for these unsteady effects within the mobility estimates. Felderhof [130, 131] further simplified this problem using a point-particle approximation to determine the dynamics of sufficiently small spherical particles (i.e. approximating the spherical particle by a point force, reducing this to a Green's function problem). All these approaches may not be analytically tractable in a closed-form without approximations (despite the linearity) particularly in situations with reduced symmetry. Moreover, the solution procedure gets progressively elaborate (in a mathematical sense) when describing asymmetrical particles (such as nanofibers, nanorods, nanosheets, nanowires or nanotubes) and/or channels such

as an arbitrary pore. This is due to the direct dependence of the morphology (including shape, size and structure/composition) of the particle on its corresponding hydrodynamic interaction [85, 86]. Note that detailed descriptions of these aforementioned analytical methods are beyond the scope of this thesis. For a broader perspective on these methods, the reader is referred to the classical books by Happel and Brenner [85] and Kim and Karilla [86]. Additionally, papers on the subject by Felderhof [130], Simha et al. [129], Mo and Raizen [44] and Brady and Bossis [127], are also a relevant resource.

Multiphase direct numerical simulation (DNS)

The NS equations can also be solved numerically using computational fluid dynamics (CFD). This solution procedure discretizes the equation system both temporally and spatially in the domain of interest. The chosen discretization reduces the partial differential equations into a linear algebraic equation system that can be solved directly using efficient sparse-matrix solvers. In this thesis, a finite volume discretization is used to solve the NS equations [132]. Moreover, this solution is coupled to the Brownian description of the particle through the Langevin equation. Such a method that can simultaneously account for both the particle dynamics via a solution to the particle transport equation and the fluid hydrodynamics via a solution to the governing fluid equations (using CFD), along with the accompanying interactions is referred to as a multiphase CFD technique. Note that in this method the fluid and the particle are treated individually and the coupling is achieved through both the hydrodynamic drag and the fluctuation-dissipation relation in the Langevin description (see Appendix 7.1).

Within the context of multiphase CFD, direct numerical simulations (or DNS) refers to a class of methods that directly solve the coupled equation system describing the various phases [133]. Thus any macro-scale description of Brownian motion can inherently be considered a multiphase DNS method when, the Brownian particle and the surrounding fluid are accounted-for individually. Moreover, the two phases under consideration can be coupled with each other to varying degrees. These are given as 2-way and 4-way coupling, respectively. The 2-way coupled system represents both particle-fluid and fluid-particle coupling, implying that each phase is affected by the presence of the other. While, a 4-way coupled system is a 2-way coupled system with additional interaction between the constituent particulate phase entities (i.e. particle-particle interactions such as collisions) also included. The continuum based methods discussed in this thesis are 2-way coupled since we deal with single or (at the most) pairwise hydrodynamic behavior. It follows that, the two phases can be adequately represented as an Eulerian-Lagrangian combination. Consequently, in this thesis, the fluid is solved as an Eulerian field (using CFD) and the particle Langevin equation is solved in the Lagrangian frame of reference. This Lagrangian representation (or inertial frame of reference) is further classified as point-force (or point-particle) or surface-resolved treatments [133], based on how the particulate phase is resolved (see Fig. 4.2).

As the name suggests, the point-force approach (shown in the left panel of Fig. 4.2)
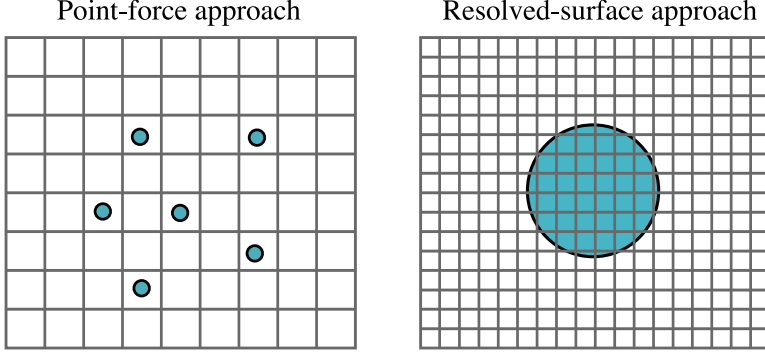
Figure 4.2: *Different types of Lagrangian representations where the shaded area represents the particle (with effective diameter d_p) and the grid represents the spatial resolution for the continuous phase solution (where Δx is the effective cell resolution): Left panel – point-force representation ($d_p < \Delta x$). Right panel – Resolved surface representation ($\Delta x \ll d_p$). This figure is adapted from Michaelides et al. [133].*

includes the Lagrangian particulate phase as point masses (or sources) i.e. the particles have negligible volume but a finite mass or inertia and move at their own (independent) velocity. Usually, this approach is referred to as a pseudo-DNS method, since the relevant hydrodynamic forces on the particle are modeled (and not resolved). Despite this, since the solution from the NS equations governing the fluid at the point where the particle is located is used in the hydrodynamic models, it is an improvement over the analytical methods listed earlier. The point-particle assumption is central to this Lagrangian representation with an ordinary differential equation (ODE) based on the changing particle position. Such an equation, which was provided by Maxey and Riley [134], also includes unsteady fluid effects such as the added mass (due to fluid acceleration caused by the particle acceleration) and Basset history forces (due to acceleration between the phases and the development of a boundary layer near the interfacial surface) [135]. The corresponding equation of motion for a Brownian particle is given as:

$$m_p \frac{d\mathbf{u_p}}{dt} = -\gamma \mathbf{v_{rel}} + F_{am} + F_{history} + \chi(t),\qquad(4.3)$$

where, F_{am} and $F_{history}$ represent the added mass and Basset history forces, written as:

$$F_{am} = -\frac{1}{2}\rho_f V_p \left(\frac{d\mathbf{u_p}}{dt} - \frac{D\mathbf{v_{rel}}}{Dt} \right),\qquad(4.4)$$

$$F_{history} = -\frac{3}{2}d_p^2 \sqrt{(\pi \rho_f \mu)} \int_0^t \frac{\frac{d\mathbf{v_{rel}}}{d\tau}}{\sqrt{t-\tau}} d\tau,\qquad(4.5)$$

with, $\mathbf{v_{rel}}$ as the relative velocity between the particle and the fluid (at the location of the particle) i.e. $\mathbf{u_p} - \mathbf{v}$, τ as the time period for the integration and the material

derivative as $\frac{D}{Dt} \equiv \frac{\partial}{\partial t} + u_j \frac{\partial}{\partial x_j}$. This Eq. (4.3) is integrated over the duration of the simulation (i.e. t). Consequently, in this approach, the hydrodynamic interactions with the fluid are modeled as point forces (i.e. for e.g. the steady state Stokes' drag is used to describe the particle-fluid coupling). Thus, for this to work, these point-particles have to be sufficiently smaller than the spatial discretization or resolution (Δx) of the surrounding fluid ($d_p < \Delta x$). Note that the flow between the particles and the particle and flow boundaries is actually resolved and is further used within the particle equation of motion. Consequently, this approach has been widely used to study Brownian transport (including their turbulent dispersion) in a gas, as first shown by Ounis and Ahmadi [51, 52]. Despite being a popular method, these point-force based methods inherently fail when the particles have a definite volume (i.e. the point-particle assumption is not valid), as is the case during pore diffusion wherein the particles occupy a significant portion of the flow domain. Correspondingly, the applicability of these point-force methods is limited to studying dilute particulate flows in channels where the particles are significantly smaller than the characteristic channel dimension.

Thus, due to the inherent limitations of the point-force treatment, the resolved surface approach (shown in the right panel of Fig. 4.2) is the preferred choice in this thesis (since we deal with particles that are significant when compared with a relevant system length scale). In this approach, the detailed flow around each particle must be solved to a high degree of resolution. This permits the flow solution to be numerically integrated over the particle surface in order to obtain the net momentum exchange with the surrounding fluid [133]. Thus, the Lagrangian method updates the particle position based on this integrated interaction. If particle rotation is permitted, a torque equation can be used to determine its angular velocity. Consequently, the resolved surface approach has found increasing incidence in some of the most recent studies on Brownian hydrodynamics, overcoming some of the major drawbacks of the point-forcing approach. Note that in this approach, the spatial grid resolution Δx, in the vicinity of the particle, must be fine enough to allow for a detailed resolution of the fluid stresses around it ($\Delta x \ll d_p$). Thus, the resolved-surface approach is computationally intensive, such that simulation of many (e.g. hundreds or thousands of) particles will generally be impractical on even the most advanced computers [133].

It is reiterated that the continuum based multiphase DNS frameworks available do not contain the relevant molecular details (thermal fluctuations), as these have been averaged out during the derivation of the NS equations (Eq. (4.1)). Thus, when these methods are used in Brownian hydrodynamics simulations, the corresponding micro-scale effects have to be consistently incorporated within the continuum description of the system. Traditionally, this can be accomplished by either adding the relevant fluctuations to the fluid phase or on the Brownian particle (as in the Langevin description). While the Gaussian forcing of the particle has been well explored, since the original assessments of Langevin [26], the stochastic forcing of the fluid or the fluctuating hydrodynamics approach is a relatively newer idea. This is described in brief below.

Fluctuating hydrodynamics

The fundamental concept behind this approach is that at intermediate length and time scales between the molecular and the hydrodynamic levels of abstraction, thermally induced fluctuations can be reduced to random fluctuations in the fluxes of the conserved variables, i.e. the momentum, heat and mass fluxes. Correspondingly, the fluctuations are included only within the deterministic fluid description, thereby ensuring that the microscopic conservation laws and thermodynamic principles are obeyed, while also maintaining the fluctuation-dissipation balance. These constitute a group of methods referred to as the fluctuating hydrodynamics (*FH*) approach of Landau and Lifshitz [118] which is derived using the fluctuation-dissipation theorem of statistical mechanics applicable at mesoscopic scales [136, 137]. Correspondingly, the Landau and Lifshitz Navier-Stokes (LLNS) equations is given as:

$$\nabla \cdot \mathbf{v} = 0,$$
$$\rho_f \left(\mathbf{v}_t + (\mathbf{v} \cdot \nabla)\mathbf{v} \right) = \nabla \cdot \sigma,$$
$$\sigma = -P\delta_{\mathbf{ij}} + \mu \left[\nabla\mathbf{v} + (\nabla\mathbf{v})^T \right] + R_f, \tag{4.6}$$

where, $\delta_{\mathbf{ij}}$ is the identity tensor and R_f is the random fluctuations in the total fluid stress tensor σ, respectively. These non-equilibrium fluctuations, which are captured through the random stresses (stochastic momentum flux), are modeled as:

$$R_f = \sqrt{\mu_f k_B T}[v(r,t) + v(r,t)^T]. \tag{4.7}$$

Here, $v(r,t)$ is a standard Gaussian white noise tensor field with uncorrelated components, that is δ-correlated [¶¶¶] in space and time. The particle motion is solved using Newton's equation of motion (velocity u_p is directly estimated from the hydrodynamic force on the particle). Note that the LLNS equations are stochastic partial differential equations that reduce to the NS equations (Eq. (4.1)) in the limit of large volumes. The validity of the LLNS equations (see eq. (4.6)) for non-equilibrium systems has been extensively assessed by Espanol et al. [138] and verified using molecular dynamics simulations by Mansour et al. [139]. Further, the LLNS based methods have been used predominantly in liquid-solid systems, wherein the breakdown of continuity (i.e. the traditional NS equations) occurs at considerably smaller scales [140]. Hence, this approach has successfully been incorporated in several numerical methods that describe Brownian dynamics in dilute fluids and in modeling reactive multi-species fluid mixtures [141–145]. These numerical simulations have been carried out either using the finite volume method [142, 143, 146–148], finite difference method [149], finite element method [150] or the immersed boundary method [151–154] (an alternate approach to solving the NS equations). All these techniques represent a surface-resolved approach to solving Brownian diffusion using *FH*. A detailed insight into these *FH* based methods is beyond the scope of this thesis and the reader is

---

[¶¶¶] $\langle v(r,t)v(r,\tau)\rangle = \delta(t-\tau)$. Thus, $v(r,t)$ is correlated with itself only when $t = \tau$.

referred to the papers by Donev et al. [143, 144] , Uma et al. [142], Atzberger et al. [151, 152], Balboa et al. [153] and to the reviews by Radhakrishnan et al. [43] and Griffith and Patankar [148] for the same.

Although the fluctuating hydrodynamic approach has found utility in Brownian particle dynamics studies, there are still some bottlenecks associated with its implementation in general finite volume or finite element based DNS frameworks. The main difficulty is in devising a discretization scheme for the stochastic differential equations primarily because of the correlation between the form of the required fluctuation-dissipation relations and the choice of scheme [121]. Further, finite-volume discretizations naturally impose a grid-scale regularization (smoothing) of the stochastic forcing. Moreover, the non-linear LLNS equations are ill-behaved stochastic partial differential equations that are challenging to integrate [155]. This is because, the stability properties of the available numerical schemes for the nonlinear LLNS system are not well understood and the whole notion of stability is different from those in regular deterministic schemes [144]. Finally, and most crucially, employing the LLNS equations to describe gas-solid flows is still heavily debated particularly due to the higher Kn encountered in these systems.

Since the overarching objective of this thesis is to develop a general numerical method (for Brownian transport) which is applicable in both liquids and gases, the *FH* based methods are not preferable. Consequently, an alternate approach is proposed where the particle motion is modeled using a stochastic differential equation (in the spirit of the Langevin Eq. (3.6)) while employing the resolved-surface Lagrangian treatment, thereby leaving the fluid equations unaltered. This idea is described in detail in the subsequent sections (see Section 4.3). However, prior to this discussion, some desirable features of such a framework are first listed in order to establish the minimum requirements for the ensuing numerical development.

4.2 Desired features of a DNS framework

The brief overview of the current state-of-the-art in the numerical modeling of Brownian systems identified a noticeable requirement for a general method that can easily be implemented within the confines of a multiphase DNS framework at a reasonable computational load. It is possible to envisage a DNS scheme where the NS equations for the fluid are solved coupled with the Langevin equation (which includes a random forcing term) for particle motion. Since the flow around the Brownian particle is fully resolved, hydrodynamic interactions mediated by the fluid (such as particle-particle or particle-wall effects) are inherently accounted for in such a description. The only noticeable challenge is to consistently account for the random forcing of the particle. Moreover, since the continuum formulation of the fluid is untouched in this approach, existing discretization schemes used in CFD can be applied effectively. The Langevin equation can also be integrated using elementary temporal integration strategies that obey the Itô interpretation [156]. In summary, the development of such a Langevin based resolved-surface

Euler-Lagrangian method seems feasible and is the primary objective of this thesis. Consequently, we can establish some desirable features for such a framework:

1. *General DNS methodology:* applicability is not restricted by the choice of the solver (i.e. can be applied across a variety of resolved-surface DNS frameworks such as the immersed boundary method, arbitrary-Lagrangian-Eulerian technique etc.)

2. *Sound theoretical basis:* the stochastic forcing is consistently incorporated within the validity of the fluctuation-dissipation theorem, so that the statistical behavior is accurately reproduced.

3. *Reasonable computational overhead:* effectively utilize the current generation of advanced sparse matrix GPU solvers to further make simulations tractable.

4. *Capability to handle both gas-particle and liquid-particle systems:* adequately resolve the varying particle diffusion dynamics in liquids and gases.

5. *Capability to handle hindered diffusion:* simulate challenging theoretical problems involving hydrodynamic interactions mediated by the fluid (such as particle-boundary, particle-particle interactions).

6. *Capability to handle asymmetric systems:* simulate non-symmetric particles and/or geometries with ease.

In the remainder of this chapter, the fundamental aspects of the numerical tools used and developed in this thesis are elaborated. First, a detailed account of the novel Langevin based multiphase DNS method developed is presented (used in **Papers A**, **B**, **C** and **D**) followed by a brief account of the utilized DSMC solver (in **Paper E**).

4.3   *Langevin* immersed boundary method (*LaIBM*)

One of the primary objectives of this thesis is to develop a multiphase DNS method that can overcome the limitations of the available continuum based multiphase CFD methods and further extend their applicability towards assessing nanoparticle transport in a fluid. Consequently, as motivated in the earlier sections, an Euler-Lagrange resolved surface approach is chosen as a basis for such a development. Such an approach is also favorable since it is simpler to formulate and easier to implement. However, the available methods need to be extended to also include both non-equilibrium (rarefied) as well as molecular-scale details, in order to accurately represent the Brownian diffusion of a nanoparticle. Hence, an improved multiphase DNS framework that can simultaneously handle particle-fluid and fluid-particle coupling (i.e. at least 2-way coupled) as well as the accompanying Brownian dispersion of the nanoparticle at high solid volume fractions would be ideally suited to describe the nanoparticle dynamics discussed in Chapter 3. Since this method

leverages both the Lagrangian Langevin description and an immersed boundary method, it is henceforth referred to as the Langevin-Immersed boundary method or $LaIBM$. Note that the immersed boundary method solves the Eulerian fluid field using discretizations of the governing NS equations similar to those applied in conventional CFD [132].

In this section, the necessary numerical details of the $LaIBM$ framework are provided within the context of the resolved-surface Euler-Lagrangian multiphase DNS class of methods discussed in Section 4.1.3. Further, a general overview of immersed boundary methods is also provided to establish the needed context.

4.3.1   Immersed boundary methods: A general overview

Immersed boundary methods are a class of numerical techniques employed in the CFD (i.e. numerical solutions to the NS equations Eq. (4.1) using for e.g. finite volume discretization) of complex flow systems that greatly simplify the spatial discretization demands. This method, originally proposed by Peskin [157] to simulate cardiac mechanics and the associated blood flow, solves the governing equations in a Cartesian grid that does not conform with the complex geometries of the simulated system. In essence, the object around which the flow is to be assessed is *immersed* in a standard Cartesian flow grid and its presence is accounted for by slightly modifying the governing NS equations. Note that a surface grid still has to be generated for the immersed body (IB), however, the volume grid on which the actual governing equations are solved for can be generated with no-regard to this surface grid [158] i.e. regular boxy domains can be used over which the IB object (included as an external *.stl* geometry file) is triangulated. The main advantages of such a treatment are as follows:

1. Using a Cartesian grid can significantly reduce the per-grid-point operation count due to the absence of additional terms associated with grid transformations.

2. On a non-body conforming grid, complexity and quality are not significantly affected by the complexity of the geometry.

3. Including body motion in IB methods is relatively simple due to the use of a stationary and non-deforming Cartesian grid.

4. Dynamic refinement around the immersed object is permissible, meaning, the accuracy is increased at a minimal computational overhead.

Incorporating the presence of the IB in the NS equations is the primary challenge in setting up this framework. Usually this modification takes the form of a source term (or forcing function) in the governing equations that reproduces the effect of the boundary. This is usually done in one of the following ways:
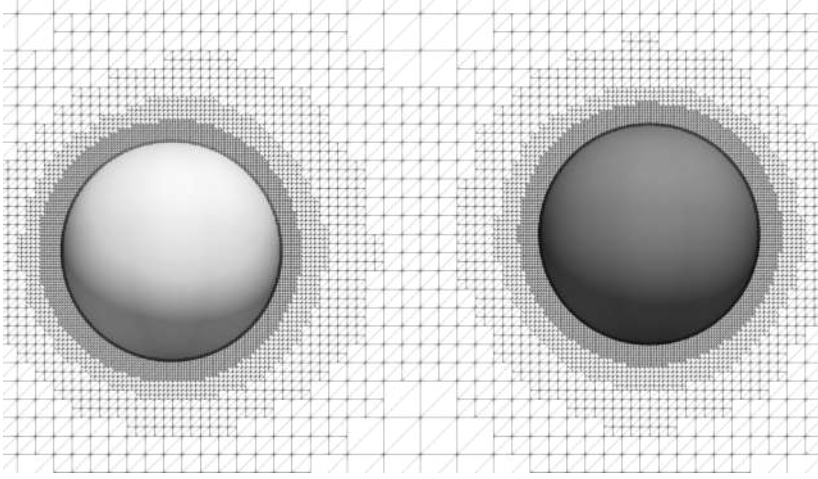
Figure 4.3: *Example of an immersed Cartesian octree grid around a pair of spherical Brownian particles with a diameter of 400 nm each (x-z plane): Note that there is no need for a body conforming mesh as the spheres cut through an adaptive Cartesian octree background grid on which the discretized NS equations are solved.*

1. Continuous forcing: the source term is introduced into the continuous equations (i.e. prior to the discretization) around the vicinity of the IB.

2. Discrete forcing: the source term is only introduced in the discretized equations around the vicinity of the IB (typically within the IB).

3. Implicit forcing: there is no source term introduced into the equations. Instead, a boundary condition is used to constrain the velocity at the IB surface so that the correct behavior is reproduced.

The continuous forcing approach is very attractive for flows with immersed elastic boundaries and was originally envisioned by Peskin for the coupled simulation of blood flow and muscle contraction [157]. In this method, the IB is represented as a set of elastic springs whose locations are tracked in a Lagrangian framework by a collection of mass-less points that move with the local fluid velocity. The effect of the IB on the surrounding fluid is essentially captured by transmitting the elastic stress (calculated using Hooke's law) to the fluid through a localized forcing term in the momentum equations [158]. This forcing is, however, distributed over a band of cells around each Lagrangian point (based on the discrete Dirac delta function). Consequently, this approach poses challenges for rigid bodies as the forcing terms are not easy to implement at the rigid limit. Moreover, due to the smoothing of the forcing term, a sharp representation of the IB is not available. Consequently, this method is explicit, first-order accurate and unstable.

Hence, for dealing with sharply defined rigid bodies (as we do in this thesis), a better forcing alternative is desired. This can be fulfilled by employing a discrete (or non-

distributive) direct forcing approach that adds the requisite source terms in the vicinity of the IB. Despite being second order accurate, this approach is only explicitly formulated and can be unstable for unsteady flows. Alternately, the implicit forcing approach can also be used to treat bodies with sharply defined edges. In this method, the velocity at the IB is constrained by an implicitly formulated immersed boundary condition (IBC) that is second-order accurate. This unique and stable treatment is central to the efficiency and accuracy of the multiphase DNS framework used in the thesis and is elaborated in the following section.

4.3.2 Immersed Boundary Octree Flow Solver: IPS IBOFlow®

In this thesis, we use the multiphase flow solver `IPS IBOFlow`®, developed by the Fraunhoffer-Chalmers Research Centre (FCC), Sweden [159]. This solver employs a unique mirroring immersed boundary method (MIBM) to efficiently handle the particle-fluid coupling (resolved-surface DNS). The MIBM discretizes the NS equations over a Cartesian octree grid¶¶¶ that can be dynamically coarsened and refined. Further, it is coupled with a finite-element (FEM) rigid body solver to resolve the particle short range dynamics (i.e. handle the particle motion in a Lagrangian basis). This coupling between the Eulerian and Lagrangian descriptions is elucidated in Fig 4.4. Details on these two core-components of the solver are further presented below beginning with the MIBM used.
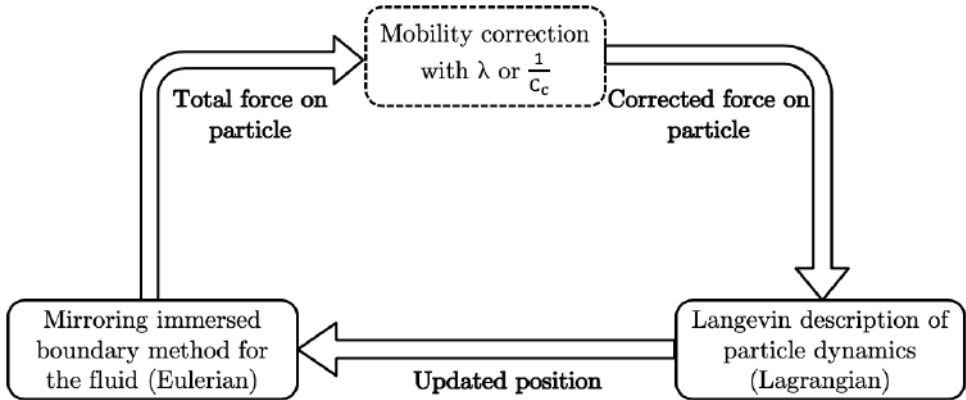
Figure 4.4: *Overview of the LaIBM framework: the particle dynamics are handled in a Lagrangian basis while the surrounding fluid is resolved in an Eulerian one. Note that the Lagrangian basis utilizes the resolved fluid stresses on the particle (from the Eulerian solution) to compute/correct the particle mobility. This framework is 2-way coupled. This figure is adapted from **Paper C** [3].*

¶¶¶This is a recursive decomposition of the spatial domain into blocks (not necessarily rectangular) in which each internal node has exactly eight children. Octrees are most often used to partition a three-dimensional space by recursively subdividing them it into eight octants.

Eulerian description of the fluid: mirroring immersed boundary method

The governing equations for the flow around the immersed boundaries are given by the continuity and momentum equations for incompressible flows i.e. the NS equations (see Eq. (4.1)). This set of equations are solved together with the implicit Dirichlet IB condition:

$$u_i = u_i^{ib},\tag{4.8}$$

which sets the velocity of the fluid to the local IB velocity. In MIBM, the velocity is set by an implicitly formulated second-order accurate immersed boundary condition. In this method, the interior cells and the cells close to the surface are identified as shown in Fig. 4.5.
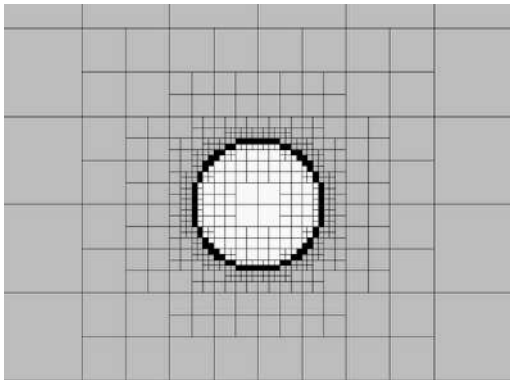
Figure 4.5: *2D view of the adaptive dynamic grid refinement around an immersed spherical particle (with diameter 400 nm). Cell types shown are exterior (grey), interior (white) and mirror or IB cells (black). This figure is adapted from* **Paper A** *[1].*

For the mirroring cells that lie close to the surface, their centers (mi) are geometrically mirrored over the local IB to the exterior points (e) as:

$$u_i^{ib} = \frac{u_{mi} + u_e}{2}.\tag{4.9}$$

By mirroring the velocity field over the IB second order accuracy is achieved. Typically, the exterior points do not coincide with a grid point, hence, implicit tri-linear interpolation is adopted to accomplish this. When the velocity is mirrored over the IB, a fictitious (velocity) field is generated within it. To fulfill the continuity equation, this field needs to be replaced by the IB velocity in all flux calculations (note that the velocity within the IB is not used). A more detailed description of this method is available in [160–162].

It should be noted that in the current method the total force acting on the IB is given by the surface integral of the total stress tensor over the IB as:

$$\mathbf{F_{IB}^i} = \int_{IB} \boldsymbol{\sigma} \cdot \mathbf{n} dS = \int_{IB} \left(-P\delta_{ij} + \tau\right) \cdot \mathbf{n} dS = \int_{IB} \left(-P\delta_{ij} + \mu_f \boldsymbol{\nabla}^2 \boldsymbol{v}\right) \cdot \mathbf{n} dS, \quad (4.10)$$

where, δ_{ij} is the Dirac delta and σ is the total fluid stress tensor with $P\delta_{ij}$ and τ as the pressure and viscous contributions for a surface S with normal $\boldsymbol{n}$, respectively. The index i represents the degrees of freedom for the IB in a Cartesian basis. The corresponding torque on the IB with a position vector $\mathbf{r}$ is calculated using:

$$\mathbf{T_{IB}} = \int_{IB} \mathbf{r} \times \boldsymbol{\sigma} \cdot \mathbf{n} dS. \quad (4.11)$$

The pressure-velocity coupling in Eq. (4.1) is handled using the segregated SIMPLEC method, [163] which first approximates the momentum equation with an estimated pressure field and then corrects the pressure by employing the continuity equation. All variables are stored in a co-located grid arrangement (meaning the variables such as pressure, velocity etc. are stored at the cell centers). Further, the Rhie-Chow [164] flux interpolation is used to suppress pressure oscillations. A partitioned approach is employed to solve the coupled problem. Correspondingly, the grid and assembly are fully parallelized on the CPU and the resulting large sparse-matrices are solved on the GPU with Algebraic Multi-Grid solvers (AmgX) [165]. The IB method described above has been extensively validated and used for the DNS of complex multiphase flow phenomena [162, 166–172]. More recently, it has also been extended towards non-Newtonian flows as well [173, 174].

Lagrangian Langevin description of the particle

The particulate phase in the *LaIBM* framework is governed by the Lagrangian Langevin equation of motion (see Eq. (3.6)). This equation balances the macro-scale hydrodynamic drag on the particle with the molecular-scale Brownian fluctuations. For the diffusion of a particle (represented by an IB) with mass m_p, translational velocity $\mathbf{u_p^i}$, angular velocity $\boldsymbol{\omega}_p^i$ and moment of inertia $\boldsymbol{I}$, the corresponding Lagrangian Langevin basis is rewritten as:

$$m_p \frac{d\mathbf{u_p^i}}{dt} = \mathbf{F_{IB}^i} + \mathbf{F_{Brownian}^i}, \quad (4.12)$$

$$\mathbf{I}\frac{d\omega_\mathbf{p}^\mathbf{i}}{dt} = \mathbf{T_{IB}^i} - \boldsymbol{\omega}_p^i \times \mathbf{J} \cdot \boldsymbol{\omega}_p^i. \quad (4.13)$$

In Eqs. (4.12) and (4.13), note that the continuum resolved translational ($\mathbf{F^i_{IB}}$) and rotational ($\mathbf{T^i_{IB}}$) hydrodynamic fields are directly used in the Langevin equation, thus, enforcing a direct coupling of the Eulerian solution with the corresponding Langevin equation of motion (resolved-surface DNS). Thus, these Eqs. (4.12) and (4.13) are modeled as an LTI system as established in Section 3.2.2. Note that the hindered diffusion of the Brownian nanoparticle is included through the correction factors to the particle mobility used in the stochastic forcing term $\mathbf{F^i_{Brownian}}$ (synonymous with $\chi(t)$ used in Eq. (3.6)) i.e. either λ or $1/C_c$ based on if hindered diffusion or rarefied hydrodynamics are being evaluated, respectively. The essential descriptors of this representation in terms of the mobility correction λ (i.e. in a liquid) are given below.

The directional reduction in mobility, λ^i, which is required in the stochastic forcing term used in $\mathbf{F^i_{Brownian}}$, is estimated by normalizing the magnitude of the hydrodynamic force on the confined Brownian particle ($\mathbf{F^i_{IB}}$) with the corresponding Stokes' drag (along the ith direction) on the same particle. This is given as:

$$\lambda^i = \frac{\|\mathbf{F^i_{IB}}\|}{\gamma\|\mathbf{u^i_p}\|}. \tag{4.14}$$

Here, the Stokes' friction factor γ_{St} has the form as defined in Eq. (3.3) and a representative particle time scale , τ_p, is given as:

$$\tau_p = \frac{m_p}{\gamma_{St}\lambda^i} \tag{4.15}$$

The force $\mathbf{F^i_{Brownian}}$, which represents the Brownian fluctuations in the particle motion, is modeled as a Gaussian white noise process (an LTI system as described in Section 3.2.3) as given by:

$$\mathbf{F^i_{Brownian}(t)} = m_p\mathbf{G}\sqrt{\frac{\pi\mathbf{S^i_{uu}}}{\Delta t}}. \tag{4.16}$$

Here, $\mathbf{G}$ is a vector of normally distributed independent random numbers of zero mean and unit variance (Gaussian distribution) and Δt is the time step length during which the Brownian force is active. The vector of spectral intensity $\mathbf{S^i_{uu}}$ (as given in Eq. (3.12)), is a function of the directional Brownian diffusivity D^i, which is in-turn given by the Stokes-Einstein relation with the corrected mobilities as:

$$D^i = \frac{D_\infty}{\lambda^i} = \frac{k_B T}{\gamma_{St}\lambda^i}, \tag{4.17}$$

where, D_∞ (or bulk diffusivity) is given by Eq. (3.2) with a further reduction by λ^i (in accordance with [175–177]) to account for confinement effects. Note that unbounded

Brownian diffusion is simulated by setting λ as unity. Moreover, a rarefied gas-solid system is modeled by using $1/C_c$ (as given in Eq. (3.17)) in place of λ.

These linear and angular momentum conservation equations (Eqs. (4.12) and (4.13)) are integrated using the Newmark time-marching scheme [178]. In this method, acceleration, velocity and displacement at time $t = t^{n+1}$ are obtained as functions of the values at $t = t^n$ by assuming a linear acceleration during that small time step. This one-step semi-implicit method can be represented by the following set of equations:

$$\dot{u}_p{}^{n+1} = \dot{u}_p{}^n + \frac{\Delta t}{2}\left(\ddot{u}_p{}^n + \ddot{u}_p{}^{n+1}\right) \tag{4.18}$$

$$u_p^{n+1} = u_p^n + \Delta t \dot{u}_p{}^n + \frac{1-2\kappa}{2}\Delta t^2 \ddot{u}_p{}^n + \kappa \Delta t^2 \ddot{u}_p{}^{n+1} \tag{4.19}$$

The scheme is unconditionally stable with κ as a tuning parameter that has a default value of 0.25 (the constant average acceleration method) [178]. It is stressed that this solution (or solution process) to Eq. (4.12), a stochastic differential equation (SDE), is not synonymous with the commonly encountered ordinary differential equations (ODE's). The integration of these SDE's are constrained by certain properties of the stochastic time integral as first defined by Itô [156]. To understand these constraints let us split the integral time interval into a number of small time steps which are then summed to give the final solution. This limit result is not independent of the choice of the intermediate time interval, which is used while splitting the solution into smaller time steps, as one would expect from classical Riemann integration laws [179][§§§]. This is because the solution would change depending on the time point at which the integration is started, as these are random time evolving systems (the trajectories have infinite variation). Hence, it is very important to decide on the sense (or form) of the integral which should be solved. The Itô sense, which has a clear probabilistic interpretation and is most often used to describe Brownian processes, assumes that the integral is solved from the beginning of the time interval. This interpretation is most convenient for numerical simulations because the increment of the stochastic process is uncorrelated with the variables at the same time. This would mean that, forward stepping explicit schemes are preferred while solving SDE's in an Itô sense. More generally, higher order schemes (such as higher order Runge-Kutta schemes) can introduce spurious drifts in the solution and should be avoided [180].

[§§§]A bounded function $f : [a, b] \to \mathbb{R}$, is said to be Riemann integrable over $[a, b]$ if there is a number $A \in \mathbb{R}$, such that for every $\varepsilon > 0$, there is a $\delta > 0$; implying that any partition $P = \{a = x_0 < x_1 < ... < x_n = b\}$ of the interval $[a, b]$, with lengths $|x_i - x_{i-1}| < \delta$ for all $i = 1, ..., n$. Further, if there exists $t_i \in [x_{i-1}, x_i]$, then:

$$\left|\sum_{i=1}^{n} f\left(t_i\right)\left(x_i - x_{i-1}\right) - A\right| < \varepsilon \implies \int_R^b f(x)dx = A$$

4.3.3 Some unique capabilities of *LaIBM*

LaIBM is developed with the ambition of satisfying the requirements listed in Section 4.2. Thus, this framework has some unique features which are derived from the existing capabilities of the resolved-surface multiphase DNS method (described in Section 4.3.2). These are:

1. *Contains the resolved hydrodynamics around the Brownian particle:* the framework leverages a resolved solution of the hydrodynamics around the Brownian particle to estimate the relevant reduction in mobility λ.

2. *Mobility estimation on-the-fly:* closely coupled with the previous point, since the resolved hydrodynamics are used to compute mobility, the instantaneous hydrodynamic fields around the particle are directly reflected in the estimated diffusive behavior.

3. *Multi-particle dynamics:* diffusion of several particles and the accompanying hydrodynamic interactions mediated by the fluid can be assessed simultaneously (each particle's motion is individually solved for and the accompanying inter-particle hydrodynamic interactions are included in the respective λ's).

4. *Not limited by symmetry considerations:* the framework is derived for any shape or form (singular or aggregates) of the particle and the accompanying domain (straight or arbitrary tortuous channels) and is, hence, not limited by the availability of uniform solutions to the hydrodynamic resistances nor symmetry considerations, such as other methods reported in literature [68, 104, 130, 175].

4.3.4 Some limitations of the framework

As with any method development, the over-arching objectives are made realizable (primarily to demonstrate a proof-of-concept) for the derived DNS method, by simplifying the system under investigation. The corresponding assumptions that currently limit the developed framework are:

1. *Validity of the Langevin equation:* the early iterations of this new DNS method are derived based on the fundamental assumption that the steady Langevin equation (i.e. Eq. (3.6)) is valid. This means that the framework is limited to handling high particle-fluid density ratios (where unsteady effects such as history and added mass forces are negligible). The main issue with handling lower density ratios is that the unsteady effects would be included in F_{IB} and T_{IB}, but not in the Brownian forcing modeled using Eq. (4.16). Hence, the stochastic forcing term would have to be re-derived.

2. *Gaussian white noise assumption:* closely coupled with the previous point, the Brownian fluctuations are assumed to be a Gaussian white noise that is delta correlated in time (i.e. Markovian in nature). This means that the VACF of the Brownian particle decays exponentially (as given in Eq. (3.11)), whereas in real liquids it is shown to have a long time tail [33, 34, 181]. This is attributed to the unsteady hydrodynamic effects on the particle (fluid inertia mediated).

3. *Negligible fluid inertia:* although, the framework can inherently handle the convective fields in the fluid, the numerical studies chosen in this thesis mimic low Reynolds number hydrodynamics i.e. primarily creeping flows ($Re_p \ll 1$), where the fluid inertia is negligible, are simulated. This choice is made to maintain the validity of the steady Langevin Eq. (3.6) and the analytical bases discussed in Chapter 3.

4. *Rarefaction effects are modeled and not resolved:* gas-particle systems modeled in this DNS framework are limited by the first-order Cunningham correction, which is based on a theoretical ansatz that is not necessarily always valid. Nevertheless, the corresponding parameters (in the expression for C_c) are fitted to experimental data and the agreement is good for all Kn. Thus, the non-continuum diffusion dynamics are being modeled and not resolved.

5. *Numerical instabilities in the IBM:* the inherent length and time scales in the Brownian transport problem (of a nanoparticle) are very close to the machine precision of most modern computing platforms, meaning, these problems push existing sparse matrix solvers to the limit. Thus, a scaling up of the problem (using the Reynolds and Schmidt number's) is needed in the current iteration of the DNS method to circumvent these issues without a loss of generality.

4.4   Direct simulation Monte-Carlo

The direct simulation Monte-Carlo (DSMC), developed by Bird [88, 107, 182], is a stochastic particle-based technique for modeling dilute real gases in which the molecular diameter is much smaller than the mean free path (λ_g). This method leverages three physical characteristics of a dilute gas:

1. Molecules move in free flight without interaction at time scales in the order of the local mean collision time.

2. The impact parameters and initial orientation of colliding molecules are random.

3. There are an enormous number of molecules per cubic mean free path and only a small fraction need be simulated to obtain an accurate molecular description of the flow.

These three assumptions are highly accurate for dilute gases and combined they enable the DSMC method to simulate macroscopic non-equilibrium flows [183]. It is reiterated that the defining characteristic of a non-equilibrium flow is the local departure (within a volume) from the Maxwell-Boltzmann equilibrium distribution functions for molecular velocity and internal energy. The continuum based methods (including the multiphase CFD techniques developed in this thesis) inherently assume only small departures from this equilibrium distribution, while the DSMC method is able to predict the distribution functions (within each small gas volume) with no such assumptions or restrictions on the shape of the distribution.
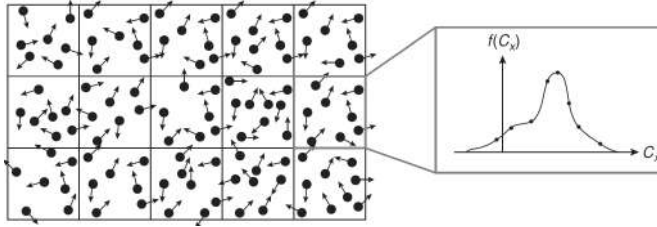
Figure 4.6: *Schematic of a DSMC simulation domain with simulator particles that represent a large number of identical real molecules within discretized collision cells. An example of a sampled distribution function from a single DSMC cell is also shown. This figure is adapted from Boyd and Schwartzentruber [183].*

The primary objective of the DSMC method is to decouple molecular motion (modeled deterministically) and inter-molecular collision (modeled probabilistically) over small time intervals. The time interval over which the solution is sought is subdivided into smaller sub-intervals over which the particle motion and collisions are decoupled. Consequently, the trajectories are computed over a time interval which is lesser than the mean collision time in discretized collision cells (see Fig. 4.6). Further, DSMC relies on discrete parcels, which each contain a collection of molecules, to represent the total molecular number density (N) of the real gas. This enables collisions between pairs of simulated particles to be modeled with precisely the same physical considerations as collisions between pairs of real molecules. Consequently, the deterministic nature of molecular movement and collisions (as simulated with MD, for example) is lost. A DSMC simulation cannot determine precisely which real molecules actually collide and what impact parameters characterize the initial conditions of such collisions. This loss of determinism is also a result of moving simulated particles in straight lines for a fraction of their mean collision time. In effect, although the distribution functions are accurately resolved at spatial and temporal scales of the mean free path and mean collision time, the precise locations of the real molecules comprising those distributions are no longer known below these scales (positions of simulated particles within a DSMC cell significantly below the mean free path is irrelevant to the method) [183].

In this thesis, the open-source solver *dsmcFoam+* developed by White and co-workers [184–186] is used for carrying out the relevant assessments. This code-base, which is built within the OpenFOAM (or Open-source Field Operation And Manipulation) suite

of libraries [187], is licensed under the GNU general public license with a publicly available software repository [188]. Further, it has been extensively validated against experimental and theoretical data across a wide variety of rarefied flows [184, 186, 189–194]. A brief overview of this solver is provided in Fig. 4.7. For a more comprehensive outlook of this method, the reader is referred to Bird's monograph [182] and to the papers by White et al. [184, 185].
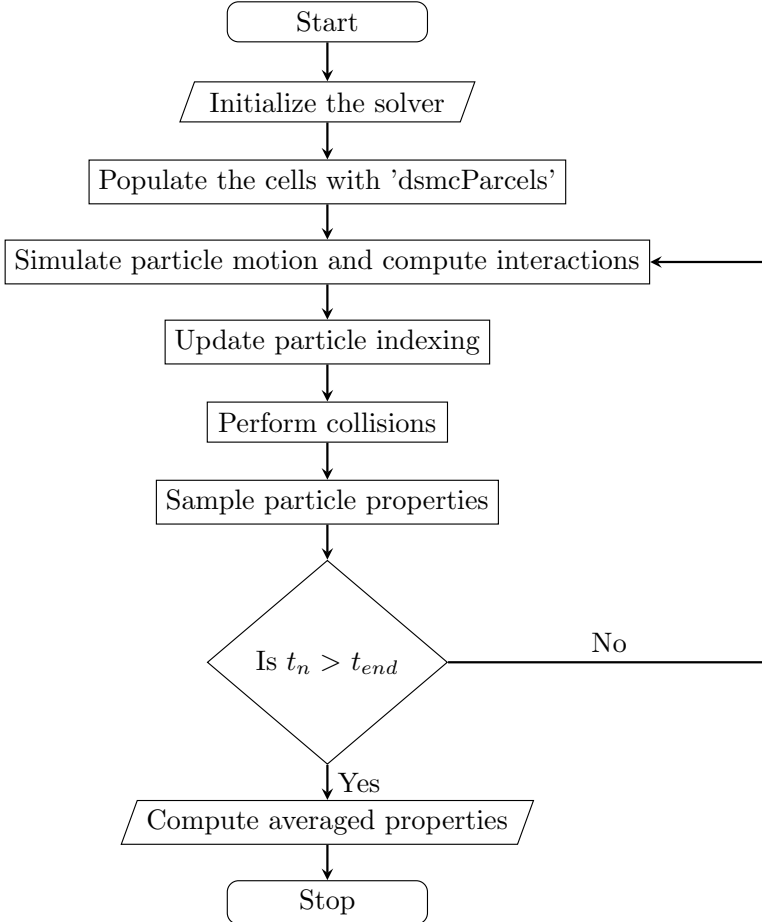
Figure 4.7: *Overview of the dsmcFoam+ solver (adapted from White et al. [185]).*

5

Highlights

Summary of the key scientific contributions and papers

The primary objective of this thesis is to develop an *in-silico* based evaluation strategy for the transport of Brownian nanoparticles in a fluid (a gas or liquid). Correspondingly, these contributions (from this thesis), as reflected in the appended papers, are briefly highlighted in this chapter. These papers represent a chronological development of the original research questions identified in Chapter 2. Correspondingly, in **Paper A** the fundamentals of the novel multiphase DNS method are established by demonstrating that the Langevin description of the Brownian particle can be combined with a resolved-surface DNS of the Eulerian fluid fields around the particle for a gas-particle system. Subsequently, in **Paper B** the developed framework is extended towards liquid-particle systems, particularly to investigate the hindered diffusion of a spherical particle in arbitrary geometries (including micro-channels and pores). Further, in this paper a directional bias (anisotropy) in the hydrodynamic resistances on the particle is identified, with a pronounced co-axial resistance noted when compared with a wall-normal one. This hydrodynamic bias is further examined in **Paper C** by evaluating the off-axis hindered diffusion dynamics (i.e. at a location displaced from the co-axial axis along the center-line) in micro-channels. Next, in **Paper D** the liquid-particle investigations are extended towards pair-wise transport and diffusion near a soft-boundary (formed at the interface of two liquids), thereby demonstrating the capabilities of *LaIBM* in handling multi-particle dynamics (in the former) as well as complex diffusive behavior (in the latter), which are beyond the scope of the traditional analytical methods (as discussed in Section 4.1.3). Finally, in **Paper E** the gas-particle system is revisited at a molecular level of abstraction using the DSMC method to better understand the non-equilibrium effects around a symmetric particle in a micro-channel. In summary, the main scientific contributions from this thesis (which are summarized in Table 5.1) address some of the challenges encountered while studying the transport of Brownian nanoparticles (such as a nanocarrier or soot particles) under hydrodynamic confinement and further establishes the foundations for an *in-silico* assessment of such complex transport of nanoparticles. The rest of this chapter contains a summary of each appended paper.

Table 5.1: Key scientific contributions in the appended papers.

	Highlights
Paper A	• Derived and validated a multiphase DNS framework for Brownian motion in a gas-particle system. • Extended the DNS method to include non-equilibrium (rarefied) particle dynamics. • Modeled the diffusion dynamics of a fractal shaped soot particle.
Paper B	• Derived and validated the multiphase DNS framework for Brownian motion in a liquid-particle system. • Extracted the reduction in particle mobility, λ, from the resolved hydrodynamic field around the particle (λ estimation on-the-fly), for a Brownian particle under hydrodynamic confinement (wall-bounded diffusion). • Incorporated the resolved instantaneous hydrodynamics around the Brownian particle (without the need for an *a priori* determination of the relevant mobility tensors) into the particle Langevin equation of motion. • Identified anisotropies in the hydrodynamic resistances on the Brownian particle in the wall-normal and co-axial directions. • Modeled the diffusion dynamics in an arbitrary pore.
Paper C	• Established a hydrodynamic basis for off-axis Brownian diffusion in micro-channels (i.e. at a location off-set from the co-axial axis of the channel). • Identified an enhancement in co-axial diffusivity during off-axis hindered diffusion under intermediate confinements.
Paper D	• Extended the applicability of the validated multiphase DNS framework towards multi-particle systems (i.e. pairwise diffusion) and diffusion near a soft-boundary (a 3-phase system). • Demonstrated that the inter-particle interactions (mediated by the fluid) leads to a correlated motion between the pair of particles as a result of being accelerated by each other's wakes. • Demonstrated that particle mobility is enhanced near a soft-boundary due to a significant reduction in the hydrodynamic resistances near such an interface (accomplished by incorporating the dynamics of the evolving interface with *LaIBM* through a volume of fluid coupling).
Paper E	• Demonstrated the impact of a particle on the Knudsen paradox in micro-channel Poiseuille flows. • Identified that the Knudsen minimum is shifted towards higher Kn and that the mass-flow rate changes (in the channel) become less pronounced towards the free molecular flow regime (due to a shift towards relatively more ballistic molecular motion at shorter geometrical distances).

Paper A

Motivation and division of work

The main objective of this paper is to derive and validate a novel multiphase DNS technique based on the immersed boundary method (that satisfies some of the requirements listed in Section 4.2) to study the diffusion dynamics of a nanoparticle in a gas-particle system. Besides being the main author, my contribution consisted of setting-up/conceptualizing the simulations and post-processing/analyzing the results. The other co-authors supervised, reviewed and provided valuable feedback on the analyzed results and on the drafted manuscript.

Results and discussion

In this paper, the fundamentals of the novel multi-phase DNS method are established by showing that the Langevin description of the Brownian particle can be combined with a resolved-surface DNS of the Eulerian fluid fields around the particle. The developed general framework is validated using a gas-particle quiescent aerosol inclusive of non-continuum effects (modeled with the Cunningham correction i.e. Eq. 3.16). It is shown that this framework can capture the diffusion dynamics of a spherical Brownian particle (with a 400 nm diameter) in an unbounded domain, including its transition from a particle-inertia dominated (correlated ballistic regime) to a non-correlated diffusive one. Further, the exponential decay (due to creeping flow conditions) of the velocity auto-correlation function (as given in Eq. 3.11) is also captured.

Vectors of velocity magnitude around a fractal aggregate (with diameter 348 nm).

The assessment is carried out over a range of particle-fluid density ratios relevant to soot aerosol applications, mimicking the conditions established in the analytical basis described in Chapter 3. Furthermore, the proposed DNS method is extended to model the diffusion dynamics of a real fractal soot aggregate. The reported results show that the proposed framework can reproduce the meandering motion of soot particles under rarefied conditions.

Paper B

Motivation and division of work

The main objective of this paper is to extend the applicability of the developed multiphase DNS framework towards liquid-particle systems, particularly to investigate the hindered diffusion of a spherical particle in arbitrary geometries (including micro-channels and pores). Besides being the main author, my contribution consisted of setting-up/conceptualizing the simulations and post-processing/analyzing the results. The other co-authors supervised, reviewed and provided valuable feedback on the analyzed results and on the drafted manuscript.

Results and discussion

In this paper, the hindered diffusion of a spherical particle in arbitrary geometries is investigated. The correction factor for Stokes mobility (given by Eq. 3.3) of the particle, λ (given by Eq. 4.14), is directly estimated from the Eulerian solution of the surrounding fluid. This estimated value is further used to adjust the stochastic forcing (given by Eq. 4.16) on the Brownian particle to accurately represent the relevant diffusive behavior. As a proof-of-concept, the Brownian diffusion of a spherical nanoparticle (with a 400 nm diameter) under creeping flow conditions is assessed at varying degrees of confinement (i.e across progressively narrower micro-channels). Correspondingly, the fundamental form of the Langevin equation (i.e. Eq. 3.6), with the additional correction (λ) for the increased hydrodynamic wall resistances, is employed. The relevant dynamics of the Brownian particle are reproduced including, the transition from a ballistic to a diffusive regime and the exponential decay of the velocity auto-correlation function (due to creeping flow conditions). Further, a directional bias (anisotropy) in the hydrodynamic resistances on the particle is identified, with a pronounced co-axial resistance noted when compared with a wall-normal one. These observations are also corroborated with relevant analytical [195, 196] and experimental [197] studies from literature. Additionally, the qualitative capabilities of the DNS framework in resolving the hydrodynamics around a Brownian particle diffusing in an arbitrary pore are also demonstrated.
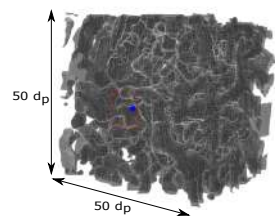
Spherical particle diffusing in an arbitrary pore.

Paper C

A. S. Kannan, A. Mark, D. Maggiolo, G. Sardina, S. Sasic, and H. Ström. A hydrodynamic basis for off-axis Brownian diffusion under intermediate confinements in micro-channels. *International Journal of Multiphase Flow* (Submitted December 2020)

Motivation and division of work

The main objective of this paper is to further examine the hydrodynamic ansiotropies reported in **Paper B** by evaluating off-axis hindered diffusion dynamics (i.e. at a location displaced from the co-axial axis along the center-line) in micro-channels. Besides being the main author, my contribution consisted of setting-up/conceptualizing the simulations and post-processing/analyzing the results. The other co-authors supervised, reviewed and provided valuable feedback on the analyzed results and on the drafted manuscript.

Results and discussion

In this paper, the directionally varying diffusive behavior of a spherical nanoparticle (with a 400 nm diameter) diffusing at a location off-set from the center-line (co-axial axis) of a square micro-channel (over varying degrees of intermediate hydrodynamic confinements) is investigated using the DNS framework proposed in the earlier papers. It is showed that the co-axial diffusivity of a particle diffusing off-axis is enhanced when compared with a corresponding center-line diffusion. Further, this

Hydrodynamic fields around a spherical particle: contours of non-dimensional velocity overlaid with flow vectors (from the CFD simulations).

effect is augmented as the particle confinement increases (or as the micro-channel gets narrower). This increased particle diffusivity is attributed to the reduced co-axial fluid resistance on the particle when it is displaced off-center. A hydrodynamic basis is established for the noted anisotropies in the resistances by further supporting the hydrodynamic fields around the diffusing particle with CFD simulations around a similar moving non-Brownian particle (the general hydrodynamic behavior is similar in both cases). More specifically, the direction of fluid motion in the narrow region between the particle and the wall changes with the particle-wall distance at tighter confinements, creating a position of minimum hydrodynamic resistance for co-axial motion at an off-axis location (which in turn is a function of the effective confinement). Such a minimum was noted in both multiphase DNS and steady-state CFD results, as well as in the results reported in literature (the dissipative particle dynamics results of Gubbiotti et al. [123]).

Paper D

A. S. Kannan, A. Mark, D. Maggiolo, G. Sardina, S. Sasic, and H. Ström. Hindered diffusion of nanoparticles in a liquid re-visited with a continuum based direct numerical simulation framework. *To be submitted to a journal* (2021)

Motivation and division of work

The main objective of this paper is to extend the applicability of the validated DNS framework from the earlier papers towards multi-particle systems (i.e. pairwise diffusion) and diffusion near a soft-boundary (a 3-phase system). Besides being the main author, my contribution consisted of setting-up/conceptualizing the simulations and post-processing/analyzing the results. The other co-authors supervised, reviewed and provided valuable feedback on the analyzed results and on the drafted manuscript.

Results and discussion

In this paper, the hindered diffusion problem in a liquid – wherein hydrodynamic interactions mediated by the fluid (such as particle-particle or particle-boundary effects) influence the governing particle dynamics, is revisited using the DNS framework derived in the earlier papers. It is shown that the expected hindered diffusion behavior near a no-slip boundary is captured, with both the directional mean squared displacement and velocity autocorrelation functions reflecting the increased hydrodynamic resistance. This discussion is

Single particle diffusion   Pair-wise diffusion

Comparison between single and pairwise diffusion: contours of velocity magnitude overlayed with flow streamlines around the particle.

further extended towards diffusion near a soft-boundary (formed at the interface of two liquids) by incorporating the dynamics of the evolving interface with the motion of the nearby Brownian particle, through a volume of fluid coupling. It is shown that the particle mobility is enhanced near such a soft-boundary due to significant reduction in the hydrodynamic resistances that result from the lowered fluid shear near this interface. Furthermore, the pairwise diffusion of Brownian particles is also assessed in this paper. It is demonstrated that the inter-particle interactions (mediated by the fluid) leads to a correlated motion between the pair of particles as a result of being accelerated by each other's wakes. This discussion further establishes the applicability of the proposed DNS framework in evaluating hindered diffusion phenomena over a wide range of applications including (but not limited to) nano-carrier mediated drug delivery and particulate emission dispersion and mitigation.

Paper E

A. S. Kannan, T. S. B. Narahari, Y. Bharadhwaj, A. Mark, D. Maggiolo, G. Sardina, S. Sasic, and H. Ström. The Knudsen paradox in micro-channel Poiseuille flows with a symmetric particle. *Applied sciences* (Submitted November 2020)

Motivation and division of work

The main objective of this paper is to revisit the gas-particle aerosol at a molecular level of abstraction, by investigating the effects of a stationary particle on a micro-channel Poiseuille flow, using a DSMC framework. Besides being the main author, my contribution consisted of conceptualizing the simulations and post-processing/analyzing the results. Tejas Sharma Bangalore Narahari and Yashas Bharadhwaj set-up the simulations and performed the initial post-processing of the data. The other co-authors supervised, reviewed and provided valuable feedback on the analyzed results and on the drafted manuscript.

Results and discussion

In this paper, the effects of a stationary particle on a micro-channel Poiseuille flow (from continuum to free-molecular conditions) are investigated using the DSMC method. Correspondingly, the non-equilibrium Knudsen paradox (a unique and well-established signature of micro-channel rarefied flows), which is the non-monotonous variation of channel mass-flow rate with the *Kn*, is evaluated in such micro-channel rarefied flows. These assessments show that with the presence of a particle, the Knudsen minimum is shifted towards higher *Kn* and

Contours of Mach number (Ma) around a square nanoparticle (in the transition regime), overlaid with velocity streamlines along an xy plane.

the accompanying mass-flow rate changes becomes less pronounced towards the free molecular flow regime. This effect is more significant as the particle becomes large (in relation to the channel) and results from a shift towards relatively more ballistic molecular motion at shorter geometrical distances. Further, an increase in the local hydrodynamic resistances in the flow (due to the presence of the particle), leads to noticeable deviations from the numerical basis derived for straight micro-channel Poiseuille flows by Cercignani et al. [198]. Thus, this paper addresses a perceived knowledge gap in rarefied flows, along with a relevant challenge while modeling reactive gas-solid flows in confined geometries at the nanoscale, where simultaneous handling of local and non-local transport mechanisms over the particle surfaces must be realized.

6

Final word

Conclusion and future outlook

The primary objective of this thesis was to facilitate an *in-silico* evaluation of nanoparticle transport in a confined environment (such as a micro-channel or a blood vessel), by developing novel strategies to study these complex phenomena at both molecular and continuum scales of abstraction. In this process, the existing collection of numerical tools (routinely used for this purpose) are improved and further extended, thereby complementing and in some cases replacing experimental based efforts. This is increasingly the trend, as assessments in such highly confined Brownian systems are challenging to undertake due to the inherent difficulties with accurate measurements at these scales. Furthermore, there are additional difficulties in ensuring proper access for the measurement techniques under such confinements as well. Thus, the next generation of technologies which are needed to tackle some of the common problems that plague our society today (as highlighted in Chapter 1) can be developed and optimized by employing the novel *in-silico* based strategies discussed (see Section 4.1) and developed (see Section 4.3) in this thesis.

Consequently, the two over-arching objectives of this thesis (as listed in Chapter 2), which were:

1. To develop a general numerical method that can handle nanoparticle dynamics in a fluid, including the accompanying macro-scale and micro-scale effects, using a continuum based framework (multiphase direct numerical simulation) i.e. projecting down from the continuum to the molecular scales and,

2. To establish a hydrodynamic basis, using numerical simulations for diffusive transport of nanoparticles, within the context of the two use cases briefly described in Chapter 1 (i.e. hindered diffusion),

have been achieved. This was accomplished by developing a DNS framework ($LaIBM$) that leverages a resolved solution of the hydrodynamics around the Brownian particle and couples this with a Lagrangian Langevin description. This approach is preferred over the alternative fluctuating hydrodynamics based method [43, 142–144, 148, 151–153], due

57

to the relative ease of implementation and the accompanying avoidance of the issues related to the discretization of the LLNS equations (see Eq. 4.6). To our best knowledge, this is the first continuum-based framework that directly includes the resolved instantaneous hydrodynamics around the Brownian particle into the particle Langevin equation of motion. Consequently, the framework is used to evaluate both gas-particle and liquid-particle systems, probing certain aspects of the Brownian transport problem relevant to the use cases introduced in Chapter 1 (i.e. soot aerosols and nanocarrier mediated drug delivery). In addition, a molecular DSMC method is also used to further probe the non-continuum phenomena (such as the Knudsen paradox) around a symmetrical particle in a rarefied gas (i.e. under conditions where continuum based methods fail). All these assessments combined provide a description that spans across molecular and continuum scales, thereby resolving the Brownian transport problem from two opposing perspectives i.e. building up from kinetic theory or alternately projecting down from continuum theory. The results achieved during the course of this thesis are still in their nascent stages as evidenced by the limitations of the current iteration of the method (as listed in Section 4.3.4). However, a lot of the future potential is already built into the framework, which makes it equipped to handle the complex transport phenomena encountered in both aerosols and colloids.

Future outlook

This thesis is primarily positioned to encourage a multiphase DNS based assessment of nanoparticle transport, hence, much of the future outlook will be focused on this aspect. Further, although the current form of the framework is based on the steady Langevin equation (see Eq. 3.6), it could be extended towards the generalized Langevin equation [32, 199] including unsteady effects (such as Basset history, added mass force etc), provided the stochastic forcing has the right form (the Gaussian noise is replaced by a colored noise instead). As stated earlier, the developed $LaIBM$ framework has the in-built capability to account for multi-particle dynamics including collisions. Moreover, as an IB method is used, complex fractal-shapes as well as any other type of particle including (but not limited to) nanofibers or droplets can be included. Since the framework relies on a continuum-based solution to the surrounding flow field, additional transport of temperature and/or species can be directly incorporated by solving the relevant transport equations. Hence, it has the inherent capability to provide a detailed insight into reactive pore-scale phenomena as well. Furthermore, this framework can also resolve particle deformation if needed (coupling between hydrodynamics and structural mechanics), which is very useful while evaluating the interactions of a nanocarrier with the constituent entities (such as red blood corpuscles) in blood. More recently, the IBM method has also been demonstrated to handle non-Newtonian fluids [173, 174], another feature that can support the *in-silico* modeling of nanocarrier transport. In summary, this framework has the necessary infrastructure to simulate the complex Brownian phenomena of nanoparticles in a fluid by taking into account both the hydrodynamic and molecular interactions that govern such flows.

7

Appendix

7.1 Derivation of the Stokes-Einstein relation

A detailed derivation of the closed-form expression for the diffusion coefficient D_∞ in Eq. (3.2). This derivation is done in accordance to Peskir's [200] ideas, by establishing a dynamic equilibrium between the pressure and viscous forces acting on the particle, thereby aiding in a simplified representation of Einstein's [14] original derivation.
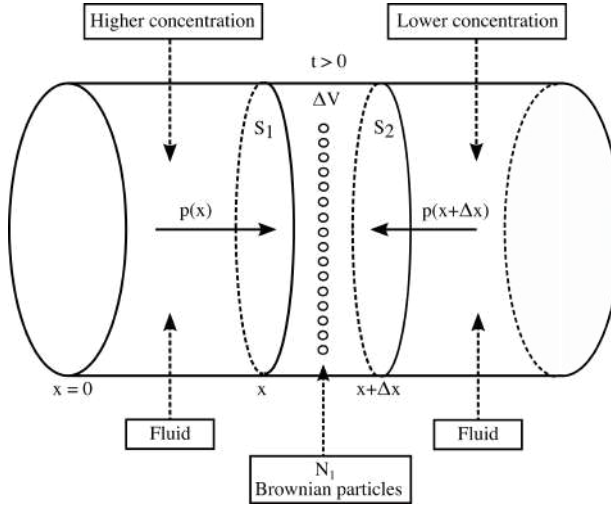
Figure 7.1: *A schematic of a cylindrical vessel filled with a fluid, containing N suspended Brownian particles. Due to the impacts by fluid molecules, Brownian particles will begin the process of diffusion.*

Consider a cylindrical vessel as shown in Fig. 7.1 filled with a fluid containing N suspended Brownian particles at $t = 0$. The diffusion of the Brownian particles is initiated from $x = 0$ due to collisions with the fluid molecules. Thus, at an instant $t > 0$, a concentration gradient for the Brownian particles is established across the cylinder, with a higher number of particles on the left side as opposed to the right (assuming diffusion

is from left to right), as shown in the Fig. 7.1. Consequently, the pressure on imaginary cross-sections S_1 and S_2 (with area A) of a fluid control volume, at locations x and $x+\Delta x$ is:

$$\frac{p(x) - p(x + \Delta x)}{\Delta x} = \frac{F(x) - F(x + \Delta x)}{A\Delta x} = \frac{N_1 F_p}{A\Delta x}, \tag{7.1}$$

where $p(x) > p(x + \Delta x)$ and N_1 is the number of Brownian particles in the fluid element with volume ΔV. F_p is the force exerted on every Brownian particle that passes through this control volume. Taking $\lim_{\Delta x \to 0}$ in Eq. (7.1):

$$\frac{\partial p}{\partial x} = -\nu F_p, \tag{7.2}$$

where, $\nu = \nu(t, x)$ is the average number of Brownian particles in the control volume. This force on the particle will impose a velocity on each particle given as:

$$F_p = \frac{v_p}{\beta_{St}} = -F_f, \tag{7.3}$$

with $1/\beta_{St}$ as the fluid friction. This equation demonstrates a dynamic equilibrium between the forces of pressure and friction i.e. F_p is retarded by the fluid force F_f. Further, Einstein concluded with statistical mechanical arguments that N Brownian particles suspended in a liquid satisfy the equation of state given by:

$$pV = nRT, \tag{7.4}$$

where, n is the number of moles and R is the gas constant (one mole of the gas contains N_{av} molecules). Thus, with $N_1 = nN_{av}$:

$$p = \frac{nN_{av}}{\Delta V}\frac{R}{N_{av}}T = \nu k_B T. \tag{7.5}$$

Differentiating Eq. (7.5) and using Eqs. (7.2) and (7.3), we get:

$$\frac{\partial p}{\partial x} = k_B T \frac{\partial \nu}{\partial x} = -\nu F_p = -\frac{v_p \nu}{\beta_{St}}. \tag{7.6}$$

The number of Brownian particles (ΔN) passing through an area ΔA under an interval Δt is given by Fick's law as:

$$\Delta N = -D_\infty \frac{\partial \nu}{\partial n} \Delta A \Delta t. \tag{7.7}$$

Thus, it follows that:

$$\nu v = \frac{N_1}{A \Delta x} \frac{\Delta x}{\Delta t} = \frac{N_1}{A \Delta t} = -D_\infty \frac{\partial \nu}{\partial x} \tag{7.8}$$

Inserting Eq. (7.8) into Eq. (7.6), we get the Stokes-Einstein relation:

$$D_\infty = \frac{k_B T}{6 \pi \mu_f r_p} \tag{7.9}$$

when, the Stokes mobility of the particle is:

$$\beta_{St} = \frac{1}{6 \pi \mu_f r_p}. \tag{7.10}$$

7.2 Derivation of the MSD, VACF and fluctuation-dissipation relation from the Langevin equation

The equation of motion for a Brownian particle, with mass m_p, is formally based on Newton's second law as:

$$m_p \frac{\mathrm{d}u_p}{\mathrm{d}t} = -\gamma_{St} u_p + \chi(t), \tag{7.1}$$

The fluctuating component $\chi(t)$ is assumed to be independent of the velocity u_p and further fluctuate rapidly in comparison with variations in velocity. Consequently, in this description, the particle velocity is well defined and is subject to both the viscous dissipation (friction force) from the fluid and the random stochastic forcing. Uhlenbeck [31] further showed that Eq. (7.1) is constrained by certain restrictions on the fluctuating component $\chi(t)$, i.e. it follows a Gaussian white noise process. Hence, the stochastic forcing (with an intensity S_{uu}) satisfies:

$$\langle \chi(t) \rangle = 0, \quad \langle \chi(t)\chi(t') \rangle = S_{uu}\delta(t - t')$$

$$\langle \chi(t)x(t') \rangle = 0, \quad \langle \chi(t)u_p(t') \rangle = 0. \tag{7.2}$$

The MSD can be derived by re-writing Eq. (7.1) in terms of the position $x(t)$ as:

$$m_p \frac{\mathrm{d}^2 x}{\mathrm{d}t^2} = -\gamma_{St} \frac{\mathrm{d}x}{\mathrm{d}t} + \chi(t), \tag{7.3}$$

Multiplying Eq. (7.3) with x and by further using:

$$\frac{\mathrm{d}x^2}{\mathrm{d}t} = 2x \frac{\mathrm{d}x}{\mathrm{d}t} \quad \text{and}$$

$$\frac{\mathrm{d}^2 x^2}{\mathrm{d}t^2} = 2(\frac{\mathrm{d}x}{\mathrm{d}t})^2 + 2x \frac{\mathrm{d}^2 x}{\mathrm{d}t^2}, \tag{7.4}$$

we get:

$$\frac{m_p}{2} \frac{\mathrm{d}^2 x^2}{\mathrm{d}t^2} - m_p u_p^2 = -\frac{\gamma_{St}}{2} \frac{\mathrm{d}x^2}{\mathrm{d}t} + x\chi(t). \tag{7.5}$$

Averaging Eq. (7.5) (or using the $\langle...\rangle$ operator) under the constraints presented in Eq. (7.2) and by applying the equipartition theorem $m_p \langle u_p^2 \rangle = k_B T$ [‡], we obtain the differential equation:

$$\frac{m_p}{2} \frac{\mathrm{d}\mathbf{z}}{\mathrm{d}t} + \frac{\gamma_{St}}{2} \mathbf{z} = k_B T, \tag{7.6}$$

where, $\mathbf{z} = \frac{d}{dt} \langle x^2 \rangle$.

Since $\langle \mathbf{z} \rangle = 2 \langle x(0) u_p(0) \rangle = 0$, the solution of Eq. (7.6) is given as:

$$\mathbf{z}(t) = \frac{2k_B T}{\gamma_{St}} (1 - \mathrm{e}^{\frac{-\gamma_{St} t}{m_p}}). \tag{7.7}$$

Eq. (7.7) is integrated to yield the expression for MSD at all time scales as:

$$\langle \Delta x^2(t) \rangle = \frac{2k_B T}{\gamma_{St}} \left(t - \frac{m_p}{\gamma_{St}} + \frac{m_p}{\gamma_{St}} \mathrm{e}^{\frac{-\gamma_{St} t}{m_p}} \right). \tag{7.8}$$

In Eq. (7.8), when $t \gg \tau_B$, the exponential term is negligible, leading to the Einstein's result for long-term or over-damped behavior in 1D. Correspondingly, the MSD of the particle increases linearly in time as:

$$< \Delta x(t)^2 > = 2Dt. \tag{7.9}$$

When $t \ll \tau_B$ or as $t \to 0$, the ballistic or under-damped result can be obtained. This is done by using the power series:

$$\mathrm{e}^{-t} = 1 - t + \frac{t^2}{2!} + O(t^3), \tag{7.10}$$

in Eq. (7.8). We then obtain the result (consistent with the equipartition theorem):

$$< \Delta x(t)^2 > = \frac{k_B T}{m_p} t^2 = u_{rms}^2 t^2. \tag{7.11}$$

Here, u_{rms} is the root-mean-squared velocity of the particle. The corresponding time scale (i.e. the relaxation time for the Brownian particle) in the ballistic regime, τ_B, is given as:

[‡] A colloidal particle suspended in a liquid at temperature T is assimilated to a particle of the liquid, so that it possesses an average kinetic energy $\frac{2RT}{N_{av}}$. Accordingly we get: $\frac{1}{2} m_p \langle u_p^2 \rangle = \frac{2RT}{N_{av}}$

$$\tau_B = \frac{m_p}{\gamma_{St}}. \tag{7.12}$$

The VACF of the Brownian particle can be derived by evaluating the solution of the first-order inhomogeneous stochastic differential equation i.e. Eq. (7.1). Ornstein-Uhlenbeck showed that a formal solution to this equation is:

$$u_p(t) = u_p(0)\mathrm{e}^{\frac{-\gamma_{St}t}{m_p}} + \frac{1}{m_p} \int_0^t \mathrm{e}^{\frac{-\gamma_{St}(t-\xi)}{m_p}} \chi(\xi)\mathrm{d}\xi. \tag{7.13}$$

Using the $\langle ... \rangle$ operator in Eq. (7.13), under the constraints in Eq. (7.2) and assuming that all particles start at $t = 0$ with the same velocity $u_p(0)$, we get:

$$\langle u_p \rangle = u_p(0)\mathrm{e}^{\frac{-\gamma_{St}t}{m_p}}. \tag{7.14}$$

This equation shows that velocity goes down exponentially due to the fluid friction. This exponential decay is further visible in the VACF, which is obtained by multiplying Eq. (7.13) with $u_p(0)$ and using the $\langle ... \rangle$ operator under the corresponding constraints. This simplification leads to:

$$C(t) \equiv \langle u_p(0)u_p(t) \rangle = \left\langle u_p^2(0) \right\rangle \mathrm{e}^{\frac{-\gamma_{St}t}{m_p}} = \frac{k_B T}{m_p} \mathrm{e}^{\frac{-\gamma_{St}t}{m_p}}. \tag{7.15}$$

Fluctuation-dissipation theorem

Furthermore, squaring Eq. (7.14) and using the $\langle ... \rangle$ operator again, we obtain:

$$\langle u_p^2 \rangle = \langle u_p^2(0) \rangle \mathrm{e}^{\frac{-2\gamma_{St}t}{m_p}} + \mathrm{e}^{\frac{-2\gamma_{St}t}{m_p}} \int_0^t \int_0^t \mathrm{e}^{\frac{t(\xi+\eta)}{m_p}} \langle \chi(\xi)\chi(\eta) \rangle \mathrm{d}\xi \mathrm{d}\eta. \tag{7.16}$$

Ornstein-Uhlenbeck further showed that the integral in Eq. (7.16) can be written as:

$$\int_0^t \int_0^t \mathrm{e}^{\frac{t(\xi+\eta)}{m_p}} \langle \chi(\xi)\chi(\eta) \rangle \mathrm{d}\xi \mathrm{d}\eta = \frac{\zeta}{2\gamma_{St}m_p}(1 - \mathrm{e}^{\frac{-2\gamma_{St}t}{m_p}}). \tag{7.17}$$

Hence, the mean-squared velocity is given as:

$$\langle u_p^2 \rangle = \langle u_p^2(0) \rangle \mathrm{e}^{\frac{-2\gamma_{St}t}{m_p}} + \frac{\zeta}{2\gamma_{St}m_p}(1 - \mathrm{e}^{\frac{-2\gamma_{St}t}{m_p}}). \tag{7.18}$$

Over long times, the equipartition theorem is valid, meaning:

$$\zeta = 2\gamma_{St}k_B T. \tag{7.19}$$

This represents a fundamental relation named as the fluctuation-dissipation theorem, which shows that the magnitude of the fluctuation ζ must be balanced by the strength of the dissipation γ_{St} so that the temperature is well defined in Langevin's model. Therefore, the pair of friction and random forces acts as a thermostat for a Langevin system. This relationship between the friction and random forcing on the particle is physically reasonable since they have a common origin i.e. interactions between the particle and the surrounding fluid molecules.

Additionally, by taking the integral of the VACF of the Brownian particle i.e. Eq. (7.15), we can observe that:

$$\int_0^\infty \langle u_p(0)u_p(t) \rangle \mathrm{d}t = \frac{k_\mathrm{B}T}{m_p} \int_0^\infty \mathrm{e}^{\frac{-\gamma_{St}t}{m_p}} \mathrm{d}t = \frac{k_\mathrm{B}T}{\gamma_{St}} = D_\infty, \tag{7.20}$$

which is the Stoke-Einstein relation for a free particle. This Eq. (7.20) is a fundamental relation, known in statistical mechanics as the Green-Kubo relation [32], that relates the macroscopic transport coefficients to the correlation functions of the variables fluctuating due to said microscopic processes. Similarly, the time-dependent diffusion co-efficient is obtained from the VACF as:

$$D_\infty(t) \equiv \int_0^t \langle u_p(0)u_p(t) \rangle \mathrm{d}\tau = \frac{1}{2}\frac{d}{dt}\langle \Delta x^2(t) \rangle = \frac{k_B T}{\gamma_{St}}(1 - \mathrm{e}^{\frac{-\gamma_{St}t}{m_p}}). \tag{7.21}$$

This equivalence of the two definitions for the VACF and the MSD is because the VACF can be calculated from the second derivative of the MSD[§].

[§] $\frac{d}{dt}\langle \Delta x^2(t) \rangle = 2\int_0^t C(\tau)d\tau$

7.3 Power spectrum of an Ornstein-Uhlenback process

The correlation functions, derived previously (Eq. (3.11)) represents the stochastic processes in the time domain, provided it is stationary ¶ and the Wiener-Khinchin theorem ‖ is satisfied. It follows that, such time signals can be represented in the frequency space using the corresponding Fourier transforms. The output, $y(t)$ of a LTI system can be obtained by the convolution of the input signal $(x(t))$ and its impulse response $(r(t))$, as:

$$y(t) = \int_{-\infty}^{\infty} x(\tau)r(t - \tau)d\tau. \tag{7.1}$$

The corresponding output, $Y(\omega)$, in the frequency domain can be written based on the convolution theorem ** as:

$$Y(\omega) = X(\omega)R(\omega), \tag{7.2}$$

where, $R(\omega)$ and $X(\omega)$ are the Fourier transform of the impulse response $r(t)$ and the time domain input $x(t)$, respectively. In the context of a Brownian particle being excited by a stochastic noise, this response, $R(\omega)$, is nothing but the mobility (Eq. (3.3)) of the particle. The fluctuation-dissipation relation or Green-Kubo formula (see Eq. (7.20) in Appendix 7.2) has a corresponding form in the frequency space by relating the mobility $R(\omega)$ to the Fourier-Laplace transform of the velocity auto-correlation, as:

$$Y(\omega) = \frac{1}{k_B T} \int_0^{\infty} e^{i\omega t} C(t)dt. \tag{7.3}$$

Correspondingly, the Fourier transform of the Langevin equation (see Eq. (3.6)) is given as:

$$-i\omega m_p u_p(\omega) + \gamma_{St} u_p(\omega) = S(\omega). \tag{7.4}$$

¶A continuous-time random process, $X(t), t \in \mathbb{R}$ is wide sense stationary if:

1. $\mu_X(t) = \mu_X$, for all $t \in \mathbb{R}$, where μ_X is the mean.

2. $C_X(t_1, t_2) = C_X(t_1 - t_2)$, for all $t_1, t_2 \in \mathbb{R}$, where C_X is the correlation function.

‖The power spectrum $S(\omega)$ of a stationary random process and its auto-correlation function are Fourier transform pairs

**The Fourier transform of a convolution in the time domain equals the product of the Fourier transforms of each function in the frequency domain

The response $R(\omega)$, of the system (based on Eq. (7.2)) can be written as:

$$R(\omega) = \frac{1}{-i\omega m_p + \gamma_{St}}. \tag{7.5}$$

Thus, the power spectrum density, $\tilde{S}_u(\omega)$, of the random process output (based on the velocity), which is needed in order to describe the Gaussian white noise signal, can be deduced using the Wiener-Kinchin theorem as:

$$\tilde{S}_{uu}(\omega) = \frac{1}{2\pi} \int_{-\infty}^{\infty} e^{-i\omega t} \langle u_p(0)u_p(t) \rangle dt. \tag{7.6}$$

Using Eq. (7.3) in Eq. (7.6), we obtain:

$$\tilde{S}_{uu}(\omega) = 2k_B T \mathbb{R}[R(\omega)] = \frac{k_B T \gamma_{St}}{\pi m_p} = \frac{2\gamma_{St}^2}{\pi} D_{\infty}, \tag{7.7}$$

where, $\mathbb{R}[R(\omega)$ is the real part of the mobility given in Eq. (7.4). This is obtained by summing Eq. (7.3) and its complex conjugate and use the fact that the VACF is an even function. The position power spectrum density is obtained from Eq. (7.7) as:

$$\tilde{S}_x(\omega) = \frac{\tilde{S}_u(\omega)}{\omega^2} = \frac{2k_B T \mathbb{R}[R(\omega)]}{\omega^2}. \tag{7.8}$$

Thus, the stochastic forcing term, $\chi(t)$, in the Langevin equation (see Eq. (7.1)) is modeled as a Gaussian white noise process with the vector of spectral intensity S_{ij}^n given as:

$$S_{ij}^n = \tilde{S}_{uu}(\omega)\delta_{ij}. \tag{7.9}$$

References

[1] A. S. Kannan, V. Naserentin, A. Mark, D. Maggiolo, G. Sardina, S. Sasic, and H. Ström. A continuum-based multiphase DNS method for studying the Brownian dynamics of soot particles in a rarefied gas. *Chemical Engineering Science* **210** (2019), 115229. ISSN: 0009-2509. DOI: `10.1016/j.ces.2019.115229`.

[2] A. S. Kannan, A. Mark, D. Maggiolo, G. Sardina, S. Sasic, and H. Ström. Assessment of hindered diffusion in arbitrary geometries using a multiphase DNS framework. *Chemical Engineering Science* **230** (2021), 116074. ISSN: 0009-2509. DOI: `10.1016/j.ces.2020.116074`.

[3] A. S. Kannan, A. Mark, D. Maggiolo, G. Sardina, S. Sasic, and H. Ström. A hydrodynamic basis for off-axis Brownian diffusion under intermediate confinements in micro-channels. *International Journal of Multiphase Flow* (Submitted December 2020).

[4] A. S. Kannan, A. Mark, D. Maggiolo, G. Sardina, S. Sasic, and H. Ström. Hindered diffusion of nanoparticles in a liquid re-visited with a continuum based direct numerical simulation framework. *To be submitted to a journal* (2021).

[5] A. S. Kannan, T. S. B. Narahari, Y. Bharadhwaj, A. Mark, D. Maggiolo, G. Sardina, S. Sasic, and H. Ström. The Knudsen paradox in micro-channel Poiseuille flows with a symmetric particle. *Applied sciences* (Submitted November 2020).

[6] A. S. Kannan, A. Mark, D. Maggiolo, G. Sardina, S. Sasic, and H. Ström. "A novel multiphase DNS method for the resolution of Brownian motion in a weakly rarefied gas using a continuum framework". *Proceedings of the 10th International Conference on Multiphase Flow (ICMF19)*. Rio de Janeiro, Brazil, May 2019.

[7] H. Ström, J. Sjöblom, A. S. Kannan, H. Ojagh, O. Sundborg, and J. Koegler. Near-wall dispersion, deposition and transformation of particles in automotive exhaust gas aftertreatment systems. *International Journal of Heat and Fluid Flow* **70** (2018), 171–180. ISSN: 0142-727X. DOI: `10.1016/j.ijheatfluidflow.2018.02.013`.

[8] A. S. Kannan, A. Mark, D. Maggiolo, G. Sardina, S. Sasic, and H. Ström. "Assessment of pore diffusion in a micro-channel using an immersed boundary method". *Proceedings of the 14th International Conference on Multiphase Flow in Industrial Plant (MFIP17)*. Desenzano del Garda, Italy, 2017.

[9] A. S. Kannan, K. Jareteg, N. C. K. Lassen, J. M. Carstensen, M. A. E. Hansen, F. Dam, and S. Sasic. Design and performance optimization of gravity tables using a combined CFD-DEM framework. *Powder Technology* **318** (2017), 423–440. ISSN: 0032-5910. DOI: `10.1016/j.powtec.2017.05.046`.

[10] A. S. Kannan, N. C. K. Lassen, J. M. Carstensen, J. Lund, and S. Sasic. Segregation phenomena in gravity separators: A combined numerical and experimental study. *Powder Technology* **301** (2016), 679–693. ISSN: 0032-5910. DOI: `10.1016/j.powtec.2016.07.003`.

[11] J. Sjöblom, H. Ström, A. S. Kannan, and H. Ojagh. Experimental Validation of Particulate Matter (PM) Capture in Open Substrates. *Industrial & Engineering Chemistry Research* **53**.9 (2014), 3749–3752. DOI: `10.1021/ie404046y`.

[12] J. Sjöblom, A. S. Kannan, H. Ojagh, and H. Ström. Modelling of particulate matter transformations and capture efficiency. *The Canadian Journal of Chemical Engineering* **92**.9 (2014), 1542–1551. DOI: `10.1002/cjce.22004`.

[13] J. Renn. Einstein's invention of Brownian motion. *Annalen der Physik* **14**.S1 (2005), 23–37. DOI: `10.1002/andp.200410131`.

[14] A. Einstein. Über die von der molekularkinetischen Theorie der Wärme geforderte Bewegung von in ruhenden Flüssigkeiten suspendierten Teilchen. *Annalen der Physik* **322**.8 (1905), 549–560. DOI: `10.1002/andp.19053220806`.

[15] IQAir. *2019 World Air Quality Report*. Report. 2020. URL: `https://www.iqair.com/world-most-polluted-cities/world-air-quality-report-2019-vi.pdf`.

[16] N. Osseiran and K. Chriscaden. Press Release. 2016. URL: `http://www.who.int/news-room/detail/12-05-2016-air-pollution-levels-rising-in-many-of-the-world-s-poorest-cities`.

[17] Directive 2008/50/EC of the European Parliament and of the Council of 21 May 2008 on ambient air quality and cleaner air for Europe. *OJ* **L 152** (2008), 1–44.

[18] J. Matthey. *Diesel particulate filter*. 2020. URL: `http://www.jmdpf.com/diesel-particulate-filter-DPF-passive-systems-johnson-matthey`.

[19] K. Bourzac. Nanotechnology: Carrying drugs. *Nature* 7425 (2012), S58–S60. DOI: `10.1038/491S58a`.

[20] C. Wild, E. Weiderpass, and B. Stewart. *World Cancer Report: Cancer Research for Cancer Prevention*. Report. 2020. URL: `http://publications.iarc.fr/586`.

[21] D. Peer, J. M. Karp, S. Hong, O. C. Farokhzad, R. Margalit, and R. Langer. Nanocarriers as an emerging platform for cancer therapy. *Nature Nanotechnology* **2**.12 (2007), 751–760. DOI: `10.1038/nnano.2007.387`.

[22] J. Fu and H. Yan. Controlled drug release by a nanorobot. *Nature Biotechnology* **30**.5 (2012), 407–408. DOI: `10.1038/nbt.2206`.

[23] J. Hrkach, D. Von Hoff, M. M. Ali, E. Andrianova, J. Auer, T. Campbell, D. De Witt, M. Figa, et al. Preclinical Development and Clinical Translation of a PSMA-Targeted Docetaxel Nanoparticle with a Differentiated Pharmacological Profile. *Science Translational Medicine* **4**.128 (2012), 128ra39–128ra39. DOI: `10.1126/scitranslmed.3003651`.

[24] W. Sutherland. LXXV. A dynamical theory of diffusion for non-electrolytes and the molecular mass of albumin. *The London, Edinburgh, and Dublin Philosophical Magazine and Journal of Science* **9**.54 (1905), 781–785. DOI: `10.1080/14786440509463331`.

[25] M. von Smoluchowski. Zur kinetischen Theorie der Brownschen Molekularbewegung und der Suspensionen. *Annalen der Physik* **326**.14 (1906), 756–780. ISSN: 0003-3804. DOI: `10.1002/andp.19063261405`.

[26] P. Langevin. Sur la théorie du mouvement brownien. *C. R. Acad. Sci. (Paris)* **146** (1908), 530–533. DOI: `10.1119/1.18725`.

[27] S. G. Brush. A History of Random Processes: I. Brownian Movement from Brown to Perrin. *Archive for History of Exact Sciences* **5**.1 (1968), 1–36. ISSN: 00039519, 14320657. DOI: 10.2307/41133279.

[28] G. G. Stokes. "On the Effect of the Internal Friction of Fluids on the Motion of Pendulums". *Mathematical and Physical Papers*. Vol. 3. Cambridge Library Collection - Mathematics. Cambridge University Press, 1901, pp. 1–10. DOI: 10.1017/CBO9780511702266.002.

[29] D. S. Lemons and A. Gythiel. Paul Langevins 1908 paper On the Theory of Brownian Motion [Sur la théorie du mouvement brownien, C. R. Acad. Sci. (Paris) 146, 530533 (1908)]. *American Journal of Physics* **65**.11 (1997), 1079–1081. DOI: 10.1119/1.18725.

[30] Perrin, jean. Mouvement brownien et grandeurs moléculaires. *Radium (Paris)* **6**.12 (1909), 353–360. DOI: 10.1051/radium:01909006012035300.

[31] G. E. Uhlenbeck and L. S. Ornstein. On the Theory of the Brownian Motion. *Physical Review* **36**.5 (1930), 823–841. DOI: 10.1103/PhysRev.36.823.

[32] R. Kubo. The fluctuation-dissipation theorem. *Reports on Progress in Physics* **29**.1 (Jan. 1966), 255–284. DOI: 10.1088/0034-4885/29/1/306.

[33] A. Rahman. Correlations in the Motion of Atoms in Liquid Argon. *Phys. Rev.* **136** (2A Oct. 1964), A405–A411. DOI: 10.1103/PhysRev.136.A405.

[34] B. J. Alder and T. E. Wainwright. Decay of the Velocity Autocorrelation Function. *Phys. Rev. A* **1** (1 Jan. 1970), 18–21. DOI: 10.1103/PhysRevA.1.18.

[35] R. Zwanzig and M. Bixon. Hydrodynamic Theory of the Velocity Correlation Function. *Phys. Rev. A* **2** (5 Nov. 1970), 2005–2012. DOI: 10.1103/PhysRevA.2.2005.

[36] A. Widom. Velocity Fluctuations of a Hard-Core Brownian Particle. *Phys. Rev. A* **3** (4 Apr. 1971), 1394–1396. DOI: 10.1103/PhysRevA.3.1394.

[37] E. J. Hinch. Application of the Langevin equation to fluid suspensions. *Journal of Fluid Mechanics* **72**.3 (1975), 499–511. DOI: 10.1017/S0022112075003102.

[38] J. Blum, S. Bruns, D. Rademacher, A. Voss, B. Willenberg, and M. Krause. Measurement of the Translational and Rotational Brownian Motion of Individual Particles in a Rarefied Gas. *Phys. Rev. Lett.* **97** (23 Dec. 2006), 230601. DOI: 10.1103/PhysRevLett.97.230601.

[39] R. Huang, I. Chavez, K. M. Taute, B. Luki, S. Jeney, M. G. Raizen, and E.-L. Florin. Direct observation of the full transition from ballistic to diffusive Brownian motion in a liquid. *Nature Physics* **7** (2011), 576. DOI: 10.1038/nphys1953.

[40] S. Kheifets, A. Simha, K. Melin, T. Li, and M. G. Raizen. Observation of Brownian Motion in Liquids at Short Times: Instantaneous Velocity and Memory Loss. *Science* **343**.6178 (2014), 1493–1496. ISSN: 0036-8075. DOI: 10.1126/science.1248091.

[41] S. Chandrasekhar. Stochastic Problems in Physics and Astronomy. *Reviews of Modern Physics* **15**.1 (1943), 1–89. DOI: 10.1103/RevModPhys.15.1.

[42] X. Bian, C. Kim, and G. E. Karniadakis. 111 years of Brownian motion. *Soft Matter* **12**.30 (2016), 6331–6346. DOI: 10.1039/c6sm01153e.

[43] R. Radhakrishnan, S. Farokhirad, D. M. Eckmann, and P. S. Ayyaswamy. "Chapter Two - Nanoparticle transport phenomena in confined flows". *Advances in*

Heat Transfer. Ed. by E. M. Sparrow, J. P. Abraham, J. M. Gorman, and W. Minkowycz. Vol. 51. Advances in Heat Transfer. Elsevier, 2019, pp. 55–129. DOI: `10.1016/bs.aiht.2019.08.002`.

[44] J. Mo and M. G. Raizen. Highly Resolved Brownian Motion in Space and in Time. *Annual Review of Fluid Mechanics* **51**.1 (2019), 403–428. DOI: `10.1146/annurev-fluid-010518-040527`.

[45] C. Truesdell. *A First Course in Rational Continuum Mechanics: General concepts.* A First Course in Rational Continuum Mechanics. Academic Press, 1977. ISBN: 9780127013015.

[46] S. Colin. "Chapter 2 - Single-Phase Gas Flow in Microchannels". *Heat Transfer and Fluid Flow in Minichannels and Microchannels (Second Edition)*. Ed. by S. G. Kandlikar, S. Garimella, D. Li, S. Colin, and M. R. King. Second Edition. Oxford: Butterworth-Heinemann, 2014, pp. 11–102. ISBN: 978-0-08-098346-2. DOI: `10.1016/B978-0-08-098346-2.00002-8`.

[47] G. G. Stokes. On the Steady Motion of Incompressible Fluids. *Transactions of the Cambridge Philosophical Society* **7** (1848), 439. DOI: `10.1017/CBO9780511702242.002`.

[48] I. Karatzas and S. E. Shreve. *Brownian Motion and Stochastic Calculus.* Graduate Texts in Mathematics (113). Springer New York, 1991. ISBN: 9780387976556. DOI: `10.1007/978-1-4612-0949-2`.

[49] F. Balboa Usabiaga, X. Xie, R. Delgado-Buscalioni, and A. Donev. The Stokes-Einstein relation at moderate Schmidt number. *The Journal of Chemical Physics* **139**.21 (2013), 214113. DOI: `10.1063/1.4834696`.

[50] P. Huang and K. S. Breuer. Direct measurement of anisotropic near-wall hindered diffusion using total internal reflection velocimetry. *Physical Review E - Statistical, Nonlinear, and Soft Matter Physics* **76**.4 (2007), 1–4. ISSN: 15393755. DOI: `10.1103/PhysRevE.76.046307`.

[51] H. Ounis and G. Ahmadi. Analysis of Dispersion of Small Spherical Particles in a Random Velocity Field. *Journal of Fluids Engineering* **112**.1 (1990), 114–120. ISSN: 0098-2202. DOI: `10.1115/1.2909358`.

[52] H. Ounis and G. Ahmadi. A Comparison of Brownian and Turbulent Diffusion. *Aerosol Science and Technology* **13**.1 (1990), 47–53. ISSN: 0278-6826. DOI: `10.1080/02786829008959423`.

[53] A. Li and G. Ahmadi. Dispersion and Deposition of Spherical Particles from Point Sources in a Turbulent Channel Flow. *Aerosol Science and Technology* **16**.4 (1992), 209–226. DOI: `10.1080/02786829208959550`.

[54] G. D. M. MacKay and S. G. Mason. Approach of a solid sphere to a rigid plane interface. *Journal of Colloid Science* **16**.6 (1961), 632–635. ISSN: 0095-8522. DOI: `https://doi.org/10.1016/0095-8522(61)90049-6`.

[55] S. A. Biondi and J. A. Quinn. Direct observation of hindered brownian motion. *AIChE Journal* **41**.5 (1995), 1324–1328. ISSN: 15475905. DOI: `10.1002/aic.690410528`.

[56] L. Lobry and N. Ostrowsky. Diffusion of Brownian particles trapped between two walls: Theory and dynamic-light-scattering measurements. *Physical Review*

B - Condensed Matter and Materials Physics **53**.18 (1996), 12050–12056. ISSN: 1550235X. DOI: 10.1103/PhysRevB.53.12050.

[57] M. A. Bevan and D. C. Prieve. Hindered diffusion of colloidal particles very near to a wall: revisited. *Journal of Chemical Physics* **113**.3 (2000), 1228–1236. ISSN: 00219606. DOI: 10.1063/1.481900.

[58] E. R. Dufresne, T. M. Squires, M. P. Brenner, and D. G. Grier. Hydrodynamic Coupling of Two Brownian Spheres to a Planar Surface. *Phys. Rev. Lett.* **85** (15 Oct. 2000), 3317–3320. DOI: 10.1103/PhysRevLett.85.3317.

[59] B. Lin, J. Yu, and S. A. Rice. Direct measurements of constrained Brownian motion of an isolated sphere between two walls. *Phys. Rev. E* **62** (3 Sept. 2000), 3909–3919. DOI: 10.1103/PhysRevE.62.3909.

[60] J. C. Crocker. Measurement of the hydrodynamic corrections to the Brownian motion of two colloidal spheres. *The Journal of Chemical Physics* **106**.7 (1997), 2837–2840. DOI: 10.1063/1.473381.

[61] A. Banerjee and K. D. Kihm. Experimental verification of near-wall hindered diffusion for the Brownian motion of nanoparticles using evanescent wave microscopy. *Physical Review E - Statistical, Nonlinear, and Soft Matter Physics* **72**.4 (2005), 1–4. ISSN: 15393755. DOI: 10.1103/PhysRevE.72.042101.

[62] P. Holmqvist, J. K. G. Dhont, and P. R. Lang. Colloidal dynamics near a wall studied by evanescent wave light scattering: Experimental and theoretical improvements and methodological limitations. *The Journal of Chemical Physics* **126**.4 (2007), 044707. DOI: 10.1063/1.2431175.

[63] C. K. Choi, C. H. Margraves, and K. D. Kihm. Examination of near-wall hindered Brownian diffusion of nanoparticles: Experimental comparison to theories by Brenner (1961) and Goldman et al. (1967). *Physics of Fluids* **19**.10 (2007). ISSN: 10706631. DOI: 10.1063/1.2798811.

[64] A high-precision study of hindered diffusion near a wall. *Applied Physics Letters* **97**.10 (2010), 1–4. ISSN: 00036951. DOI: 10.1063/1.3486123.

[65] H. B. Eral, J. M. Oh, D. Van Den Ende, F. Mugele, and M. H. Duits. Anisotropic and hindered diffusion of colloidal particles in a closed cylinder. *Langmuir* **26**.22 (2010), 16722–16729. ISSN: 07437463. DOI: 10.1021/la102273n.

[66] K. Ishii, T. Iwai, and H. Xia. Hydrodynamic measurement of Brownian particles at a liquid-solid interface by low-coherence dynamic light scattering. *Optics Express* **18**.7 (Mar. 2010), 7390–7396. DOI: 10.1364/OE.18.007390.

[67] C. Ha, H. Ou-Yang, and H. K. Pak. Direct measurements of colloidal hydrodynamics near flat boundaries using oscillating optical tweezers. *Physica A: Statistical Mechanics and its Applications* **392**.17 (2013), 3497–3504. ISSN: 0378-4371. DOI: https://doi.org/10.1016/j.physa.2013.04.014. URL: http://www.sciencedirect.com/science/article/pii/S0378437113003270.

[68] J. Mo, A. Simha, and M. G. Raizen. Broadband boundary effects on Brownian motion. *Phys. Rev. E* **92** (6 Dec. 2015), 062106. DOI: 10.1103/PhysRevE.92.062106.

[69] M. J. Skaug, L. Wang, Y. Ding, and D. K. Schwartz. Hindered Nanoparticle Diffusion and Void Accessibility in a Three-Dimensional Porous Medium. *ACS Nano* **9**.2 (2015), 2148–2156. DOI: 10.1021/acsnano.5b00019.

[70] K. Misiunas, S. Pagliara, E. Lauga, J. R. Lister, and U. F. Keyser. Nondecaying Hydrodynamic Interactions along Narrow Channels. *Phys. Rev. Lett.* **115** (3 July 2015), 038301. DOI: `10.1103/PhysRevLett.115.038301`.

[71] W. M. Deen. Hindered transport of large molecules in liquidfilled pores. *AIChE Journal* **33**.9 (1987), 1409–1425. ISSN: 15475905. DOI: `10.1002/aic.690330902`.

[72] P. S. Burada, P. Hänggi, F. Marchesoni, G. Schmid, and P. Talkner. Diffusion in confined geometries. *ChemPhysChem* **10**.1 (2009), 45–54. ISSN: 14397641. DOI: `10.1002/cphc.200800526`. eprint: `0808.2345`.

[73] P. S. Epstein. On the Resistance Experienced by Spheres in their Motion through Gases. *Phys. Rev.* **23** (6 June 1924), 710–733. DOI: `10.1103/PhysRev.23.710`.

[74] C. Cercignani and C. D. Pagani. Flow of a Rarefied Gas past an Axisymmetric Body. I. General Remarks. *The Physics of Fluids* **11**.7 (1968), 1395–1399. DOI: `10.1063/1.1692120`.

[75] C. Cercignani, C. D. Pagani, and P. Bassanini. Flow of a Rarefied Gas past an Axisymmetric Body. II. Case of a Sphere. *The Physics of Fluids* **11**.7 (1968), 1399–1403. DOI: `10.1063/1.1692121`.

[76] N. A. Frej and D. C. Prieve. Hindered diffusion of a single sphere very near a wall in a nonuniform force field. *The Journal of Chemical Physics* **98**.9 (1993), 7552–7564. DOI: `10.1063/1.464695`.

[77] E. S. Pagac, R. D. Tilton, and D. C. Prieve. Hindered mobility of a rigid sphere near a wall. *Chemical Engineering Communications* **148-50**.May (1996), 105–122. ISSN: 00986445. DOI: `10.1080/00986449608936511`.

[78] H. Brenner. The slow motion of a sphere through a viscous fluid towards a plane surface. *Chemical Engineering Science* **16**.3-4 (1961), 242–251. ISSN: 00092509. DOI: `10.1016/0009-2509(61)80035-3`.

[79] A. J. Goldman, R. G. Cox, and H. Brenner. Slow viscous motion of a sphere parallel to a plane wall-I Motion through a quiescent fluid. *Chemical Engineering Science* **22**.4 (1967), 637–651. ISSN: 00092509. DOI: `10.1016/0009-2509(67)80047-2`.

[80] K. D. Kihm, A. Banerjee, C. K. Choi, and T. Takagi. Near-wall hindered Brownian diffusion of nanoparticles examined by three-dimensional ratiometric total internal reflection fluorescence microscopy (3-D R-TIRFM). *Experiments in Fluids* **37**.6 (2004), 811–824. ISSN: 07234864. DOI: `10.1007/s00348-004-0865-4`.

[81] E. Lauga, M. Brenner, and H. A. Stone. "Chapter - Microfluidics: The No-Slip Boundary Condition". *Handbook of experimental fluid dynamics*. Ed. by C. Tropea, J. Foss, and A. Yarin. Springer Handbooks. Springer, Berlin, Heidelberg, 2007, pp. 1219–1235. DOI: `10.1007/978-3-540-30299-5_19`.

[82] E. Bonaccurso, H.-J. Butt, and V. S. J. Craig. Surface Roughness and Hydrodynamic Boundary Slip of a Newtonian Fluid in a Completely Wetting System. *Phys. Rev. Lett.* **90** (14 Apr. 2003), 144501. DOI: `10.1103/PhysRevLett.90.144501`.

[83] M. Stimson, G. B. Jeffery, and L. N. G. Filon. The motion of two spheres in a viscous fluid. *Proceedings of the Royal Society of London. Series A, Containing Papers of a Mathematical and Physical Character* **111**.757 (1926), 110–116. DOI: `10.1098/rspa.1926.0053`.

[84] G. K. Batchelor. Brownian diffusion of particles with hydrodynamic interaction. *Journal of Fluid Mechanics* **74**.1 (1976), 1–29. DOI: 10.1017/S0022112076001663.

[85] J. Happel and H. Brenner. *Low Reynolds number hydrodynamics*. Martinus Nijhoff publishers, 1983. ISBN: 13: 978-90-247-2877-0. DOI: 10.1007/978-94-009-8352-6.

[86] S. Kim and S. J. Karrila. *Microhydrodynamics: principles and selected applications*. Butterworth-Heinemann, 1991. ISBN: 9781483161242.

[87] R. W. Barber and D. R. Emerson. Challenges in Modeling Gas-Phase Flow in Microchannels: From Slip to Transition. *Heat Transfer Engineering* **27**.4 (2006), 3–12. DOI: 10.1080/01457630500522271.

[88] G. A. Bird. Monte Carlo Simulation of Gas Flows. *Annual Review of Fluid Mechanics* **10**.1 (1978), 11–31. DOI: 10.1146/annurev.fl.10.010178.000303.

[89] A. Beskok, G. E. Karniadakis, and W. Trimmer. Rarefaction and Compressibility Effects in Gas Microflows. *Journal of Fluids Engineering* **118**.3 (1996), 448–456. DOI: 10.1115/1.2817779.

[90] E. S. Piekos and K. S. Breuer. Numerical Modeling of Micromechanical Devices Using the Direct Simulation Monte Carlo Method. *Journal of Fluids Engineering* **118**.3 (1996), 464–469. ISSN: 0098-2202. DOI: 10.1115/1.2817781.

[91] E. B. Arkilic, M. A. Schmidt, and K. S. Breuer. Gaseous slip flow in long microchannels. *Journal of Microelectromechanical Systems* **6**.2 (1997), 167–178. DOI: https://doi.org/10.1109/84.585795.

[92] E. Oran, C. Oh, and B. Cybyk. DIRECT SIMULATION MONTE CARLO: Recent Advances and Applications. *Annual Review of Fluid Mechanics* **30**.1 (1998), 403–441. DOI: 10.1146/annurev.fluid.30.1.403.

[93] G. E. K. Ali Beskok. Report: A model for flows in channels, pipes, and ducts at micro and nano scales. *Microscale Thermophysical Engineering* **3**.1 (1999), 43–77. DOI: 10.1080/108939599199864.

[94] A. Agrawal. A Comprehensive Review on Gas Flow in Microchannels. *International Journal of Micro-Nano Scale Transport* **2**.17 (1 2007), 3411–3421. ISSN: 0017-9310. DOI: https://doi.org/10.1260/1759-3093.2.1.1.

[95] J. C. Maxwell. On Stresses in Rarefied Gases Arising from Inequalities of Temperature. *Philosophical Transactions of the Royal Society of London* **170** (1879), 231–256. DOI: 10.1098/rspl.1878.0052.

[96] E. Cunningham. On the Velocity of Steady Fall of Spherical Particles through Fluid Medium. *Proceedings of the Royal Society of London Series A* **83**.563 (1910), 357–365. DOI: 10.1098/rspa.1910.0024.

[97] R. A. Millikan. The Isolation of an Ion, a Precision Measurement of its Charge, and the Correction of Stokes's Law. *Phys. Rev. (Series I)* **32** (4 Apr. 1911), 349–397. DOI: 10.1103/PhysRevSeriesI.32.349.

[98] M. D. Allen and O. G. Raabe. Slip Correction Measurements of Spherical Solid Aerosol Particles in an Improved Millikan Apparatus. *Aerosol Science and Technology* **4**.3 (1985), 269–286. ISSN: 0278-6826. DOI: 10.1080/02786828508959055.

[99] A. Moshfegh, M. Shams, G. Ahmadi, and R. Ebrahimi. A new expression for spherical aerosol drag in slip flow regime. *Journal of Aerosol Science* **41**.4 (2010), 384–400. ISSN: 0021-8502. DOI: https://doi.org/10.1016/j.jaerosci.2010.01.010.

[100] C. N. Davies. Definitive equations for the fluid resistance of spheres. *Proceedings of the Physical Society* **57**.4 (1945), 259. DOI: 10.1088/0959-5309/57/4/301.

[101] C. Cercignani. *Rarefied gas dynamics: From basic concepts to actual calculations.* Cambridge university press, 2000. ISBN: 9780521659925.

[102] S. Colin. Rarefaction and compressibility effects on steady and transient gas flows in microchannels. *Microfluidics and Nanofluidics* **1**.3 (July 2005), 268–279. ISSN: 1613-4990. DOI: 10.1007/s10404-004-0002-y.

[103] E. Karniadakis George, A. Beskok, and N. Aluru. *Microflows and Nanoflows: Fundamentals and Simulation.* Vol. 23. Springer-Verlag New York, 2005. DOI: 10.1007/0-387-28676-4.

[104] H. Brenner and L. J. Gaydos. The constrained brownian movement of spherical particles in cylindrical pores of comparable radius. Models of the diffusive and convective transport of solute molecules in membranes and porous media. *Journal of Colloid And Interface Science* **58**.2 (1977), 312–356. ISSN: 00219797. DOI: 10.1016/0021-9797(77)90147-3.

[105] B. J. Alder and T. E. Wainwright. Studies in Molecular Dynamics. I. General Method. *The Journal of Chemical Physics* **31**.2 (1959), 459–466. DOI: 10.1063/1.1730376.

[106] D. Hamelberg, J. Mongan, and J. A. McCammon. Accelerated molecular dynamics: A promising and efficient simulation method for biomolecules. *The Journal of Chemical Physics* **120**.24 (2004), 11919–11929. DOI: 10.1063/1.1755656.

[107] G. A. Bird. *Molecular Gas Dynamics and Direct Simulation of Gas Flow.* Oxford University Press, London, 1994.

[108] W. Wagner. A convergence proof for Bird's direct simulation Monte Carlo method for the Boltzmann equation. *Journal of Statistical Physics* **66**.3 (1992), 1011–1044. DOI: 10.1007/BF01055714.

[109] E. E. Michaelides. Nanoparticle diffusivity in narrow cylindrical pores. *International Journal of Heat and Mass Transfer* **114** (2017), 607–612. ISSN: 0017-9310. DOI: 10.1016/j.ijheatmasstransfer.2017.06.098.

[110] L. Kadanoff. "On Two Levels". Physics Today, 1986. DOI: 10.1063/1.2815134.

[111] J. E. Broadwell. Shock Structure in a Simple Discrete Velocity Gas. *The Physics of Fluids* **7**.8 (1964), 1243–1247. DOI: 10.1063/1.1711368.

[112] U. Frisch, B. Hasslacher, and Y. Pomeau. Lattice-Gas Automata for the Navier-Stokes Equation. *Phys. Rev. Lett.* **56** (14 Apr. 1986), 1505–1508. DOI: 10.1103/PhysRevLett.56.1505.

[113] D. D'humières and P. Lallemand. Lattice gas automata for fluid mechanics. *Physica A: Statistical Mechanics and its Applications* **140**.1 (1986), 326–335. ISSN: 0378-4371. DOI: 10.1016/0378-4371(86)90239-6.

[114] S. Chen and G. D. Doolen. Lattice Boltzmann method for fluid flows. *Annual Review of Fluid Mechanics* **30**.1 (1998), 329–364. DOI: 10.1146/annurev.fluid.30.1.329.

[115] T. Krüger, H. Kusumaatmaja, A. Kuzmin, O. Shardt, G. Silva, and E. M. Viggen. *The Lattice Boltzmann Method: Principles and Practice.* Graduate Texts in Physics series (GTP). Springer, Cham, 2017. DOI: 10.1007/978-3-319-44649-3.

[116] A. J. C. Ladd. Numerical simulations of particulate suspensions via a discretized Boltzmann equation. Part 1. Theoretical foundation. *Journal of Fluid Mechanics* **271** (1994), 285–309. DOI: 10.1017/S0022112094001771.

[117] A. J. C. Ladd. Numerical simulations of particulate suspensions via a discretized Boltzmann equation. Part 2. Numerical results. *Journal of Fluid Mechanics* **271** (1994), 311–339. DOI: 10.1017/S0022112094001783.

[118] L. D. Landau and E. M. Lifshitz. "CHAPTER VI - Diffusion". *Fluid Mechanics (Second Edition)*. Pergamon, 1987, pp. 227–237. ISBN: 978-0-08-033933-7. DOI: 10.1016/B978-0-08-033933-7.50014-3.

[119] P. Ahlrichs and B. Dünweg. Lattice-Boltzmann Simulation of Polymer-Solvent Systems. *International Journal of Modern Physics C* **09**.08 (1998), 1429–1438. DOI: 10.1142/S0129183198001291.

[120] M. Mynam, P. Sunthar, and S. Ansumali. Efficient lattice Boltzmann algorithm for Brownian suspensions. *Philosophical Transactions of the Royal Society A: Mathematical, Physical and Engineering Sciences* **369**.1944 (2011), 2237–2245. DOI: 10.1098/rsta.2011.0047.

[121] G. De Fabritiis, M. Serrano, R. Delgado-Buscalioni, and P. V. Coveney. Fluctuating hydrodynamic modeling of fluids at the nanoscale. *Physical Review E* **75**.2 (2007), 026307. DOI: 10.1103/PhysRevE.75.026307.

[122] P. Español and P. B. Warren. Perspective: Dissipative particle dynamics. *The Journal of Chemical Physics* **146**.15 (2017), 150901. DOI: 10.1063/1.4979514.

[123] A. Gubbiotti, M. Chinappi, and C. M. Casciola. Confinement effects on the dynamics of a rigid particle in a nanochannel. *Phys. Rev. E* **100** (5 Nov. 2019), 053307. DOI: 10.1103/PhysRevE.100.053307.

[124] G. Stokes. On the theories of internal friction of fluids in motion and of the equilibrium and motion of elastic solids. *Trans. Camb. Phil. Soc.* **8** (Jan. 1845), 24–40.

[125] O. Darrigol. Between Hydrodynamics and Elasticity Theory: The First Five Births of the Navier-Stokes Equation. *Archive for History of Exact Sciences* **56**.2 (2002), 95–150. ISSN: 00039519, 14320657. DOI: 10.2307/41134138.

[126] D. L. Ermak and J. A. McCammon. Brownian dynamics with hydrodynamic interactions. *The Journal of Chemical Physics* **69**.4 (1978), 1352–1360. ISSN: 0021-9606. DOI: 10.1063/1.436761.

[127] J. F. Brady and G. Bossis. Stokesian Dynamics. *Annual Review of Fluid Mechanics* **20**.1 (1988), 111–157. DOI: 10.1146/annurev.fl.20.010188.000551.

[128] A. M. Ardekani and R. H. Rangel. Unsteady motion of two solid spheres in Stokes flow. *Physics of Fluids* **18**.10 (2006), 103306. DOI: 10.1063/1.2363351.

[129] A. Simha, J. Mo, and P. J. Morrison. Unsteady Stokes flow near boundaries: the point-particle approximation and the method of reflections. *Journal of Fluid Mechanics* **841** (2018), 883–924. DOI: 10.1017/jfm.2018.87.

[130] B. U. Felderhof. Effect of the wall on the velocity autocorrelation function and long-time tail of Brownian motion. *Journal of Physical Chemistry B* **109**.45 (2005), 21406–21412. ISSN: 15206106. DOI: 10.1021/jp051335b.

[131]   B. U. Felderhof. Diffusion and velocity relaxation of a Brownian particle immersed in a viscous compressible fluid confined between two parallel plane walls. *The Journal of Chemical Physics* **124**.5 (2006), 054111. DOI: 10.1063/1.2165199.

[132]   H. K. Versteeg and W. Malalasekera. *An introduction to computational fluid dynamics - the finite volume method.* Addison-Wesley-Longman, 1995, pp. I–X, 1–257. ISBN: 978-0-582-21884-0.

[133]   E. Michaelides, C. T. Crowe, and J. D. Schwarzkopf. "Multiphase Flow Handbook". Second. Boca Raton: CRC Press, 2016. ISBN: 9781315371924. DOI: 10.1201/9781315371924.

[134]   M. R. Maxey and J. J. Riley. Equation of motion for a small rigid sphere in a nonuniform flow. *The Physics of Fluids* **26**.4 (1983), 883–889. ISSN: 0031-9171. DOI: 10.1063/1.864230.

[135]   A. B. Basset. *A treatise on hydrodynamics: with numerous examples.* Vol. 2. Deighton, Bell and Company, 1888.

[136]   B. Noetinger. Fluctuating hydrodynamics and Brownian motion. *Physica A: Statistical Mechanics and its Applications* **163**.2 (1990), 545–558. ISSN: 0378-4371. DOI: 10.1016/0378-4371(90)90144-H.

[137]   E. H. Hauge and A. Martin-Löf. Fluctuating hydrodynamics and Brownian motion. *Journal of Statistical Physics* **7**.3 (1973), 259–281. ISSN: 1572-9613. DOI: 10.1007/BF01030307.

[138]   P. Español. Stochastic differential equations for non-linear hydrodynamics. *Physica A: Statistical Mechanics and its Applications* **248**.1 (1998), 77–96. ISSN: 0378-4371. DOI: https://doi.org/10.1016/S0378-4371(97)00461-5.

[139]   M. M. Mansour, A. L. Garcia, G. C. Lie, and E. Clementi. Fluctuating hydrodynamics in a dilute gas. *Physical Review Letters* **58**.9 (1987), 874–877. DOI: 10.1103/PhysRevLett.58.874.

[140]   M. Gad-El-Hak. Gas and Liquid Transport at the Microscale. *Heat Transfer Engineering* **27**.4 (2006), 13–29. ISSN: 0145-7632. DOI: 10.1080/01457630500522305.

[141]   A. L. Garcia, M. M. Mansour, G. C. Lie, M. Mareschal, and E. Clementi. Hydrodynamic fluctuations in a dilute gas under shear. *Phys. Rev. A* **36** (9 Nov. 1987), 4348–4355. DOI: 10.1103/PhysRevA.36.4348.

[142]   B. Uma, T. N. Swaminathan, R. Radhakrishnan, D. M. Eckmann, and P. S. Ayyaswamy. Nanoparticle Brownian motion and hydrodynamic interactions in the presence of flow fields. *Physics of Fluids* **23**.7 (2011), 073602. DOI: 10.1063/1.3611026.

[143]   A. Donev, A. Nonaka, Y. Sun, G. Fai Thomas, A. L. Garcia, and J. B. Bell. Low Mach number fluctuating hydrodynamics of diffusively mixing fluids. *Communications in Applied Mathematics and Computational Science* **9**.1 (2014), 47–105. DOI: 10.2140/camcos.2014.9.47.

[144]   A. Donev, A. Nonaka, A. K. Bhattacharjee, A. L. Garcia, and J. B. Bell. Low Mach number fluctuating hydrodynamics of multispecies liquid mixtures. *Physics of Fluids* **27**.3 (2015), 037103. DOI: 10.1063/1.4913571.

[145]   A. K. Bhattacharjee, K. Balakrishnan, A. L. Garcia, J. B. Bell, and A. Donev. Fluctuating hydrodynamics of multi-species reactive mixtures. *The Journal of Chemical Physics* **142**.22 (2015), 224107. DOI: 10.1063/1.4922308.

[146] N. Sharma and N. A. Patankar. Direct numerical simulation of the Brownian motion of particles by using fluctuating hydrodynamic equations. *Journal of Computational Physics* **201**.2 (2004), 466–486. ISSN: 0021-9991. DOI: `10.1016/j.jcp.2004.06.002`.

[147] N. Ramakrishnan, Y. Wang, D. M. Eckmann, P. S. Ayyaswamy, and R. Radhakrishnan. Motion of a nano-spheroid in a cylindrical vessel flow: Brownian and hydrodynamic interactions. *Journal of Fluid Mechanics* **821** (2017), 117–152. DOI: `10.1017/jfm.2017.182`.

[148] B. E. Griffith and N. A. Patankar. Immersed Methods for FluidStructure Interaction. *Annual Review of Fluid Mechanics* **52**.1 (2020), 421–448. DOI: `10.1146/annurev-fluid-010719-060228`.

[149] B. Delmotte and E. E. Keaveny. Simulating Brownian suspensions with fluctuating hydrodynamics. *The Journal of Chemical Physics* **143**.24 (2015), 244109. DOI: `10.1063/1.4938173`.

[150] Spatially adaptive stochastic methods for fluidstructure interactions subject to thermal fluctuations in domains with complex geometries. *Journal of Computational Physics* **277** (2014), 121–137. ISSN: 0021-9991. DOI: `10.1016/j.jcp.2014.07.051`.

[151] P. J. Atzberger, P. R. Kramer, and C. S. Peskin. A stochastic immersed boundary method for fluid-structure dynamics at microscopic length scales. *Journal of Computational Physics* **224**.2 (2007), 1255–1292. ISSN: 0021-9991. DOI: `10.1016/j.jcp.2006.11.015`.

[152] P. R. Kramer, C. S. Peskin, and P. J. Atzberger. On the foundations of the stochastic immersed boundary method. *Computer Methods in Applied Mechanics and Engineering* **197**.25 (2008). Immersed Boundary Method and Its Extensions, 2232–2249. ISSN: 0045-7825. DOI: `10.1016/j.cma.2007.11.010`.

[153] Inertial coupling method for particles in an incompressible fluctuating fluid. *Computer Methods in Applied Mechanics and Engineering* **269** (2014), 139–172. ISSN: 0045-7825. DOI: `10.1016/j.cma.2013.10.029`.

[154] Y. Wang, H. Lei, and P. J. Atzberger. Fluctuating hydrodynamic methods for fluid-structure interactions in confined channel geometries. *Applied Mathematics and Mechanics* **39**.1 (2018), 125–152. DOI: `10.1007/s10483-018-2253-8`.

[155] J. Vom Scheidt. Kloeden, P. E.; Platen, E., Numerical Solution of Stochastic Differential Equations. Berlin etc., Springer-Verlag 1992. XXXVI, 632 pp., 85 figs., DM 118,OO. ISBN 3-540-54062-8 (Applications of Mathematics 23). *ZAMM - Journal of Applied Mathematics and Mechanics / Zeitschrift für Angewandte Mathematik und Mechanik* **74**.8 (1994), 332–332. ISSN: 0044-2267. DOI: `10.1002/zamm.19940740806`.

[156] K. Itô. "Stochastic integration". *Vector and Operator Valued Measures and Applications*. Ed. by D. H. Tucker and H. B. Maynard. Academic Press, 1973, pp. 141–148. ISBN: 978-0-12-702450-9. DOI: `10.1016/B978-0-12-702450-9.50020-8`.

[157] C. S. Peskin. The Fluid Dynamics of Heart Valves: Experimental, Theoretical, and Computational Methods. *Annual Review of Fluid Mechanics* **14**.1 (1982), 235–259. DOI: `10.1146/annurev.fl.14.010182.001315`.

[158] R. Mittal and G. Iaccarino. Immersed Boundary Methods. *Annual Review of Fluid Mechanics* **37**.1 (2005), 239–261. DOI: `10.1146/annurev.fluid.37.061903.175743`.

[159] F. C. Centre. *IPS IBOFLow*. URL: `http://www.fcc.chalmers.se/software/ips/iboflow/`.

[160] A. Mark, R. Rundqvist, and F. Edelvik. Comparison Between Different Immersed Boundary Conditions for Simulation of Complex Fluid Flows. *Fluid Dynamics and Materials Processing* **7** (Sept. 2011), 241–258. DOI: `10.3970/fdmp.2011.007.241`.

[161] A. Mark and B. G. M. van Wachem. Derivation and validation of a novel implicit second-order accurate immersed boundary method. *Journal of Computational Physics* **227**.13 (2008), 6660–6680. ISSN: 0021-9991. DOI: `10.1016/j.jcp.2008.03.031`.

[162] A. Mark, E. Svenning, and F. Edelvik. An immersed boundary method for simulation of flow with heat transfer. *International Journal of Heat and Mass Transfer* **56**.1 (2013), 424–435. ISSN: 0017-9310. DOI: `10.1016/j.ijheatmasstransfer.2012.09.010`.

[163] J. P. V. Doormaal and G. D. Raithby. Enhancements of the SIMPLE method for predicting incompressible fluid flows. *Numerical Heat Transfer* **7**.2 (1984), 147–163. DOI: `10.1080/01495728408961817`.

[164] C. M. Rhie and W. L. Chow. Numerical study of the turbulent flow past an airfoil with trailing edge separation. *AIAA Journal* **21**.11 (1983), 1525–1532. DOI: `10.2514/3.8284`.

[165] M. Naumov, M. Arsaev, P. Castonguay, J. Cohen, J. Demouth, J. Eaton, S. Layton, N. Markovskiy, I. Reguly, N. Sakharnykh, V. Sellappan, and R. Strzodka. AmgX: A Library for GPU Accelerated Algebraic Multigrid and Preconditioned Iterative Methods. *SIAM Journal on Scientific Computing* **37**.5 (2015), S602–S626. DOI: `10.1137/140980260`.

[166] R. Rundqvist, A. Mark, B. Andersson, A. Ålund, F. Edelvik, S. Tafuri, and J. S. Carlson. "Simulation of Spray Painting in Automotive Industry". *Numerical Mathematics and Advanced Applications 2009*. Ed. by G. Kreiss, P. Lötstedt, A. Målqvist, and M. Neytcheva. Berlin, Heidelberg: Springer Berlin Heidelberg, 2010, pp. 771–779. ISBN: 978-3-642-11795-4. DOI: `10.1007/978-3-642-11795-4_83`.

[167] J. Göhl, A. Mark, S. Sasic, and F. Edelvik. An immersed boundary based dynamic contact angle framework for handling complex surfaces of mixed wettabilities. *International Journal of Multiphase Flow* (2018). ISSN: 0301-9322. DOI: `10.1016/j.ijmultiphaseflow.2018.08.001`.

[168] J. Göhl, K. Markstedt, A. Mark, K. Håkansson, P. Gatenholm, and F. Edelvik. Simulations of 3D bioprinting: predicting bioprintability of nanofibrillar inks. *Biofabrication* **10**.3 (2018), 034105. URL: `http://stacks.iop.org/1758-5090/10/i=3/a=034105`.

[169] T. Johnson, S. Jakobsson, B. Wettervik, B. Andersson, A. Mark, and F. Edelvik. A finite volume method for electrostatic three species negative corona discharge simulations with application to externally charged powder bells. *Journal of Electrostatics* **74** (2015), 27–36. ISSN: 0304-3886. DOI: `10.1016/j.elstat.2014.12.009`.

[170] B. Wettervik, T. Johnson, S. Jakobsson, A. Mark, and F. Edelvik. A domain decomposition method for three species modeling of multi-electrode negative corona discharge With applications to electrostatic precipitators. *Journal of Electrostatics* **77** (2015), 139–146. ISSN: 0304-3886. DOI: `10.1016/j.elstat.2015.08.004`. URL: `http://www.sciencedirect.com/science/article/pii/S0304388615300346`.

[171] F. Edelvik, A. Mark, N. Karlsson, T. Johnson, and J. S. Carlson. "Math-Based Algorithms and Software for Virtual Product Realization Implemented in Automotive Paint Shops". *Math for the Digital Factory*. Ed. by L. Ghezzi, D. Hömberg, and C. Landry. Cham: Springer International Publishing, 2017, pp. 231–251. ISBN: 978-3-319-63957-4. DOI: `10.1007/978-3-319-63957-4_11`.

[172] T. Johnson, P. Röyttä, A. Mark, and F. Edelvik. Simulation of the spherical orientation probability distribution of paper fibers in an entire suspension using immersed boundary methods. *Journal of Non-Newtonian Fluid Mechanics* **229** (2016), 1–7. ISSN: 0377-0257. DOI: `10.1016/j.jnnfm.2016.01.001`.

[173] S. Ingelsten, A. Mark, and F. Edelvik. A Lagrangian-Eulerian framework for simulation of transient viscoelastic fluid flow. *Journal of Non-Newtonian Fluid Mechanics* **266** (2019), 20–32. ISSN: 0377-0257. DOI: `10.1016/j.jnnfm.2019.02.005`.

[174] S. Ingelsten, A. Mark, K. Jareteg, R. Kádár, and F. Edelvik. Computationally efficient viscoelastic flow simulation using a Lagrangian-Eulerian method and GPU-acceleration. *Journal of Non-Newtonian Fluid Mechanics* **279** (2020), 104264. ISSN: 0377-0257. DOI: `10.1016/j.jnnfm.2020.104264`.

[175] H. Brenner. A general theory of Taylor dispersion phenomena IV. Direct Coupling Effects. *Chemical Engineering Communications* **18**.5-6 (1982), 355–379. DOI: `10.1080/00986448208939976`.

[176] G. M. Mavrovouniotis and H. Brenner. Hindered sedimentation, diffusion, and dispersion coefficients for brownian spheres in circular cylindrical pores. *Journal of Colloid And Interface Science* **124**.1 (1988), 269–283. ISSN: 00219797. DOI: `10.1016/0021-9797(88)90348-7`.

[177] P. Dechadilok and W. M. Deen. Hindrance Factors for Diffusion and Convection in Pores. *Industrial & Engineering Chemistry Research* **45**.21 (2006), 6953–6959. DOI: `10.1021/ie051387n`.

[178] N. M. Newmark. A Method of Computation for Structural Dynamics. *Journal of the Engineering Mechanics Division* **85** (3 1959), 67–94.

[179] R. G. Bartle. Return to the Riemann Integral. *The American Mathematical Monthly* **103**.8 (1996), 625–632. ISSN: 00029890, 19300972. DOI: `10.2307/2974874`.

[180] J.-P. Minier and E. Peirano. The pdf approach to turbulent polydispersed two-phase flows. *Physics Reports* **352**.1 (2001), 1–214. ISSN: 0370-1573. DOI: `https://doi.org/10.1016/S0370-1573(01)00011-4`.

[181] B. U. Felderhof. Diffusion of interacting Brownian particles. **11**.5 (May 1978), 929–937. DOI: `10.1088/0305-4470/11/5/022`.

[182] G. A. Bird. *The DSMC method*. CreateSpace Independent Publishing Platform, 2013. ISBN: 978-1492112907.

[183] I. D. Boyd and T. E. Schwartzentruber. "Direct Simulation Monte Carlo". *Nonequilibrium Gas Dynamics and Molecular Simulation*. Cambridge Aerospace Series.

Cambridge University Press, 2017, pp. 183–251. DOI: 10.1017/9781139683494.007.

[184] C. White, M. K. Borg, T. J. Scanlon, and J. M. Reese. A DSMC investigation of gas flows in micro-channels with bends. *Computers and Fluids* **71** (2013), 261–271. ISSN: 0045-7930. DOI: 10.1016/j.compfluid.2012.10.023.

[185] C. White, M. Borg, T. Scanlon, S. Longshaw, B. John, D. Emerson, and J. Reese. dsmcFoam+: An OpenFOAM based direct simulation Monte Carlo solver. *Computer Physics Communications* **224** (2018), 22–43. ISSN: 0010-4655. DOI: 10.1016/j.cpc.2017.09.030.

[186] T. J. Scanlon, E. Roohi, C. White, M. Darbandi, and J. M. Reese. An open source, parallel DSMC code for rarefied gas flows in arbitrary geometries. *Computers and Fluids* **39**.10 (2010), 2078–2089. ISSN: 0045-7930. DOI: 10.1016/j.compfluid.2010.07.014.

[187] H. G. Weller, G. Tabor, H. Jasak, and C. Fureby. A tensorial approach to computational continuum mechanics using object-oriented techniques. *Computers in Physics* **12**.6 (1998), 620–631. DOI: 10.1063/1.168744.

[188] C. White, M. Borg, and S. Longshaw. *MicroNanoFlows: OpenFOAM-2.4.0-MNF*. https://github.com/MicroNanoFlows/OpenFOAM-2.4.0-MNF. 2018.

[189] E. Roohi, M. Darbandi, and V. Mirjalili. Direct Simulation Monte Carlo Solution of Subsonic Flow Through Micro/Nanoscale Channels. *Journal of Heat Transfer* **131**.9 (June 2009). DOI: 10.1115/1.3139105.

[190] M. Darbandi and E. Roohi. Study of subsonic–supersonic gas flow through micro/nanoscale nozzles using unstructured DSMC solver. *Microfluidics and Nanofluidics* **10**.2 (2011), 321–335. DOI: 10.1007/s10404-010-0671-7.

[191] R. C. Palharini, C. White, T. J. Scanlon, R. E. Brown, M. K. Borg, and J. M. Reese. Benchmark numerical simulations of rarefied non-reacting gas flows using an open-source DSMC code. *Computers and Fluids* **120** (2015), 140–157. ISSN: 0045-7930. DOI: 10.1016/j.compfluid.2015.07.021.

[192] A. Ebrahimi and E. Roohi. DSMC investigation of rarefied gas flow through diverging micro- and nanochannels. *Microfluidics and Nanofluidics* **21**.2 (2017), 18. DOI: 10.1007/s10404-017-1855-1.

[193] G. Yang and B. Weigand. Investigation of the Klinkenberg effect in a micro/nanoporous medium by direct simulation Monte Carlo method. *Phys. Rev. Fluids* **3** (4 Apr. 2018), 044201. DOI: 10.1103/PhysRevFluids.3.044201.

[194] M. Sabouri and M. Darbandi. Numerical study of species separation in rarefied gas mixture flow through micronozzles using DSMC. *Physics of Fluids* **31**.4 (2019), 042004. DOI: 10.1063/1.5083807.

[195] W. L. Haberman and R. M. Sayre. *Motion of rigid and fluid spheres in stationary and moving liquids inside cylindrical tubes*. Tech. rep. Department of the navy - David Taylor model basin, 1958. URL: http://hdl.handle.net/1721.3/48988.

[196] Y. Chang and H. Keh. Slow motion of a slip spherical particle perpendicular to two plane walls. *Journal of Fluids and Structures* **22**.5 (2006), 647–661. ISSN: 0889-9746. DOI: 10.1016/j.jfluidstructs.2006.02.006.

[197] F. S. Gentile, I. D. Santo, G. D'Avino, L. Rossi, G. Romeo, F. Greco, P. A. Netti, and P. L. Maffettone. Hindered Brownian diffusion in a square-shaped geometry.

Journal of Colloid and Interface Science **447** (2015), 25–32. ISSN: 10957103. DOI: 10.1016/j.jcis.2015.01.055.

[198]   C. Cercignani and A. Daneri. Flow of a Rarefied Gas between Two Parallel Plates. *Journal of Applied Physics* **34**.12 (1963), 3509–3513. DOI: 10.1063/1.1729249.

[199]   F. Mainardi, A. Mura, and F. Tampieri. Brownian motion and anomalous diffusion revisited via a fractional Langevin equation. *Modern Problems of Statistical Physics* **8** (2009), 3–23. URL: http://arxiv.org/abs/1004.3505.

[200]   G. Peskir. On the Diffusion Coefficient: The Einstein Relation and Beyond. *Stochastic Models* **19**.3 (2003), 383–405. DOI: 10.1081/STM-120023566.

Part II

Appended Papers A–E

Paper A

A continuum-based multiphase DNS method for studying the Brownian dynamics of soot particles in a rarefied gas

A continuum-based multiphase DNS method for studying the Brownian dynamics of soot particles in a rarefied gas

Ananda Subramani Kannan [a], Vasileios Naserentin [b,c,d], Andreas Mark [b], Dario Maggiolo [a], Gaetano Sardina [a], Srdjan Sasic [a], Henrik Ström [a,*]

[a] *Department of Mechanics and Maritime Sciences, Division of Fluid Dynamics, Chalmers University of Technology, Göteborg 412 96, Sweden*
[b] *Fraunhofer-Chalmers Research Centre, Göteborg 412 88, Sweden*
[c] *Division of Applied Mathematics & Statistics, Chalmers University of Technology, Göteborg 412 96, Sweden*
[d] *Department of Chemical Engineering, Aristotle University of Thessaloniki, Thessaloniki 541 24, Greece*

HIGHLIGHTS

- Derivation and assessment of a multiphase DNS framework for Brownian motion.
- Langevin description of particle motion with mirroring immersed boundary method.
- Predictions of Brownian trajectories with ballistic-to-diffusive transition.
- Diffusivities agree with the Stokes-Cunningham-Einstein relation in unbounded flow.
- Applicable both to spherical particles and to combustion-generated aggregates.

ARTICLE INFO

ABSTRACT

In the mitigation of particulate matter (PM) using filters, the interplay between particle motion, geometry and flow conditions determines the overall performance. In such flows, molecular effects on the particle motion manifest as impeded momentum transfer and a meandering Brownian motion. Other particles and walls induce hydrodynamic interactions, which may further influence PM nucleation, growth and aggregation. Here, we formulate a multiphase direct numerical simulation framework to investigate these complex flows by including the molecular interactions in a consistent manner.

The basis for this framework is a coupling between the Langevin description of particle motion with a mirroring immersed boundary method. We show that the method is able to capture the diffusion dynamics of a Brownian particle, including its transition from a particle-inertia dominated, correlated ballistic regime to a non-correlated diffusive one, and that the method also can be used to reproduce the meandering motion of realistic soot particles.

1. Introduction

The diffusion of nanosized particles in a microchannel is of interest to both biological and physicochemical applications that deal with the transport of solid particles in a gas through porous media. A common gas-solid nanoscale system of high societal significance is the transport of combustion-generated particulate matter (PM) in exhaust gases from internal combustion engines, industrial energy converters, wood stoves and waste handling. The control of PM emissions is one of the most pressing sustain-

ability challenges of our time, owing to the global decline in urban air quality (Osseiran and Chriscaden, 2016) and due to the climate effects from accumulation of black carbon aerosols in the atmosphere (Bond et al., 2013). An efficient way to remove PM from a flowing gas is to pass it through a porous filter (Yang and Zelenyuk, 2009; Bensaid and Fino, 2010). The suspended nanoparticles would then deposit inside the narrow and tortuous pores, sticking to the walls due to the large surface forces involved, thereby cleaning the flow. The deposition efficiency within such filters reduces over time due to the dynamically changing pore geometry across sequential PM depositions. Thus these filters have to be regenerated (or cleansed) periodically so that they can be continually used.

---

* Corresponding author.
  E-mail addresses: ananda@chalmers.se (A.S. Kannan), henrik.strom@chalmers.se (H. Ström).

In many technical applications, this is achieved by the combustion of the deposited particles (Kostoglou and Konstandopoulos, 2003; Konstandopoulos and Papaioannou, 2008; Tripathi and Sadiki, 2018; Martirosyan and Luss, 2010; Sarli and Benedetto, 2015). This process leaves non-combustible ash residues at high temperatures that can further trigger chemical reactions between the ash, particles and the pore walls. Consequently, the combined effect of initial geometrical and flow properties, particle deposition pattern, particle clustering (aggregation), particle-particle and particle-wall interactions in the flow and spurious ash residue interactions will determine the efficiency and lifetime of a filter (i.e. whether the filter can eventually be emptied of the ash, or whether catastrophic pore clogging will render the filter unusable prematurely). Additionally, the inherent filter design has a significant influence on the overall pressure drop across the PM mitigation device, and this could amount to an extra penalty on the performance of the filter during the various stages of PM removal. Hence the design of effective mitigation technologies for PM emissions continues to remain an open-ended problem, and a deeper insight into the governing physics can aid in improving its understanding.

The inherent complexity in such systems is attributed to the hydrodynamic and molecular interactions that govern the deposition of PM. This is because both the hydraulic diameters of the pores in the filter, as well as the particle diameters, are comparable to the mean free path of the gas, λ. The flow may then be characterized by the Knudsen number ($Kn = \lambda/L$, where L is a characteristic length scale of the flow i.e. the duct or particle diameter or radius), which identifies the relative importance between molecular and hydrodynamic interactions. Systems that are strongly rarefied or at the 'limit of free molecular flow' are characterized by finite Knudsen numbers while the 'continuum flow limit' is characterized by $Kn \to 0$. In general, flows characterized by non-negligible particle Knudsen numbers are commonly known as kinetic or transition regime flows. Additionally, the Knudsen number can also aid in identifying the applicability of the continuum hypothesis to describe such systems. For Knudsen numbers below 0.015, the continuum hypothesis is assumed to hold. However, for finite Knudsen numbers, the hypothesis breaks down and continuum-based theories over-predict the interphase momentum exchange and do not predict the occurrence of Brownian motion. Hence any rigorous description of the underlying phenomena must simultaneously include both micro (molecular) and macro (hydrodynamic) scale interactions.

In general, combustion-generated PM are composed of fine primary particles that coagulate to form irregular fractal-clusters which have a broad size distribution (Köylü et al., 1995; Jiang et al., 2019). Considering PM from diesel fuel combustion as an example, where the mean free path due to high temperatures can be approximately 300 nm, the Knudsen number based on the filter channel diameter are initially of the order $0.01 - 0.02$ in the clean filter, whereas the particle Knudsen numbers are approximately in the range $0.5 - 10$ and the channels contain many particles at the same time. As particles accumulate in the filter by deposition, the pore-scale Knudsen numbers increase and the spatial distances between suspended particles and deposited particles become smaller. Under these conditions, the fractal-like PM aggregates can no longer be regarded as being in thermodynamic equilibrium with the fluid, and rarefaction effects are exhibited (Barber and Emerson, 2006; Kishore, 2016). This results in two primary phenomena; firstly the regular collisions act as a random driving force on the particle maintaining an incessant irregular motion and, secondly, they give rise to a frictional force (or drag) for a forced motion. The superposition of these two opposing effects gives rise to the meandering motion commonly referred to as Brownian motion. As a consequence, there is reduced momentum

transfer between the phases as well. Moreover, the coagulation induced due to this Brownian motion may be significant (Mountain et al., 1986; Sorensen et al., 1998; Sitarski and Seinfeld, 1977). This is further apparent as viscous resistance would inhibit coagulation, even in dilute systems, thereby reducing the coagulation rate (Matsuoka et al., 2012). Instead, fractal aggregates formed by diffusion-limited aggregation reach a critical size, and hence render inter-particle hydrodynamic interactions critical to the coagulation process. Hence, a simultaneous resolution of both molecular as well hydrodynamic interactions between the PM particles or bounding walls is desirable in such systems. Similar considerations are relevant also for gas-phase processes for nanoparticle synthesis (Kruis and Peled, 1998) (e.g. dry flame reactors (Stark and Pratsinis, 2002; Mueller and Pratsinis, 2003; Wegner and Pratsinis, 2003) as well as in aerosol generators and dispensers (Sjöblom et al., 2014; Park et al., 2018), where dense aerosol systems are often encountered.

Furthermore, there is also a motivation for evaluating this class of flows from a theoretical point of view, particularly due to the difficulty associated with exact analytical studies in the transition flow regime. Hydrodynamic interactions in this regime are complex already at lower Knudsen numbers, where deviations from the continuum hypothesis are small but finite (Cercignani, 2000). The earliest reported studies on these complex hydrodynamics in rarefied flows were performed by Epstein (1924), who used the kinetic theory to study a single sphere moving relative to a highly rarefied gas in the limit of small Mach numbers. This study was later extended by Cercignani and Pagani (1968) and Cercignani et al. (1968), who utilized a variational form of the linearized Bhatnager-Gross-Krook-Walender (BGKW) transport equations (Bhatnagar et al., 1954; Welander) to evaluate the flow of a rarefied gas past a sphere across a range of Knudsen numbers. The reported results were the earliest validation of the BGKW model for low speed flows, in acceptable agreement with Millikan's experimental data (Millikan, 1911). These studies were further extended to a flow past a cylinder by Yamamoto and Sera (1985), who obtained a solution to the linearized BGKW equations over two regions: the kinetic region adjacent to the cylinder and the near-continuum region outside it. Ying and Peters (1989) derived the resistance and mobility functions for the hydrodynamic interaction between two unequal sized spheres in the transition flow regime, by similarly obtaining the solution to the linearized BGKW equations in two regions (a Knudsen layer and a continuum region). These studies were extended towards translating interacting bodies at large particle Knudsen numbers and small Mach numbers by Gopinath and Koch (1999). The reported studies on hydrodynamics within rarefied flows were all based on analytical solutions to the linearized BGKW equations, which are non-trivial to use for realistic aerosol particles in complicated geometries with simultaneous Brownian motion. Consequently, there is a need for a method that can handle such practical weakly rarefied, hydrodynamically interacting gas-solid flows at reasonable computational loads.

For Brownian point particles in a liquid, the particle diffusion can be described with existing Lagrangian formulations that extended the fundamental theory of Einstein and Smoluchowski, i.e. the Langevin treatment (Langevin, 1908; Chandrasekhar, 1943). This treatment is based on a momentum equation for the particle with a random stochastic forcing for the non-equilibrium behaviour coupled with a friction force linear in instantaneous velocity (continuum-based hydrodynamic drag). This equation was further extended towards particulate aerosols by Ounis and Ahmadi (1990a), who additionally included the Cunningham correction (Cunningham, 1910) to the continuum steady drag used in the Langevin equation (Davies, 1945). This was done to account for the reduced momentum transfer between the PM and the rarefied gas. In this approach, hydrodynamic interactions are either

modelled or neglected and the particles are assumed to be point-particles. Consequently, these Lagrangian approaches inherently fail when the particles have a definite volume, such as the case during pore diffusion wherein the particles occupy a significant portion of the flow domain. Thus, the applicability of existing Lagrangian Langevin-based methods is limited to studying dispersion of dilute aerosols in channels where the particles are smaller than the characteristic channel dimension. Alternately, a different approach is represented by the Stokesian or Brownian Dynamics treatment, which was developed for describing particle-fluid suspensions (Ermak and McCammon, 1978; Brady and Bossis, 1988; Banchino and Brady, 2003). In these descriptions, the complete flow field around the particles is not resolved, meaning that these methods are not applicable to situations when the particle-particle and particle-wall interactions are significant yet not dominating. The hydrodynamic interaction terms in the transition flow regime could possibly be obtained from methods such as the one presented by Corson et al., who demonstrated that an extended Kirkwood-Riseman (EKR) theory (Corson et al., 2017) can be used to compute the translation, rotation, and coupling friction tensors along with the scalar rotational friction coefficient for hydrodynamically interacting aerosol fractal aggregates (Corson and Zachariah, 2018). However, given that the systems of interest here typically involve simultaneous heat and mass transfer with chemical reactions in the gas phase, as well as on and/or inside the particle, continuum-based descriptions are still expected to offer advantages over Stokesian Dynamics-based frameworks. The hydrodynamic interaction terms obtained with EKR-based methods may be used to correct also such continuum-based descriptions.

The most comprehensive resolution of the non-equilibrium dynamics in PM aerosols (including the resolved hydrodynamic and molecular interactions) can be achieved by directly solving the kinetic Boltzmann equation that governs such a system in its original form. This approach is however extremely time and memory consuming, since it requires a discretization of the kinetic equations in both physical and velocity spaces (Rovenskaya and Croce, 2016). Molecular event-driven methods such as the direct simulation Monte-Carlo method (DSMC) (Bird, 1994; Bird, 2013) and the slightly coarse-grained dissipative particle dynamics (Scanlon et al., 2010; Stefanov, 2011; Español and Warren, 1995; Groot and Warren, 1997) offer an attractive alternative to solve the kinetic Boltzmann equations, however these are also computationally expensive at the desired system scales and at the limit of weakly rarefied flow (i.e. at the relevant pore-scale Knudsen numbers). More recently, several research groups have used hybrid solvers that combine the aforementioned kinetic methods with a continuum fluid dynamics solver (Le Tallec and Mallinger, 1997; Roveda et al., 2000; Wijesinghe et al., 2004; Popov and Tcheremissine, 2005; Schwartzentruber and Boyd, 2006; La Torre et al., 2011; Rovenskaya and Croce, 2014; Rovenskaya and Croce, 2016) to study fluid rarefaction in micro-scale flows. These work on the condition that the rarefaction effect becomes relevant in a relatively small portion of the domain, which is generally not the case in PM applications.

Multiphase direct numerical simulation (DNS) methods available today are typically well equipped to handle complex geometries with many particles and simultaneous heat and trace species transport with chemical reactions. Such methods also intrinsically account for particle-particle and particle-wall interactions in the simulated system. However, these methods are based on continuum fluid dynamics and thus do not include any molecular effects. Thus, our aim with this paper is to present a novel multiphase DNS tool that can reasonably resolve both molecular and hydrodynamic effects within the transport of realistic combustion-generated nanoparticles in a computationally tractable manner. As Brownian fluctuations of the particle have been averaged out while deriving the continuum formulation, they are innately absent within any such DNS framework. Hence, we propose a novel method that extends the applicability of the Langevin method beyond the point-particle treatment. This is achieved by including the fully resolved flow around the particle within a governing Langevin equation that also includes the Cunningham correction for rarefaction. We formulate this novel method within a continuum based mirroring immersed boundary (IB) framework (Mark and van Wachem, 2008) that is coupled with a rigid body solver (Simo and Wong, 1991) that resolves the particle short-range dynamics including the stochastic forcing due to Brownian fluctuations. The combined method will be referred to as the IB-FSI framework throughout the paper (where FSI stands for fluid-structure interaction).

As a proof of concept for the proposed methodology, we evaluate the particle diffusion dynamics of a single spherical nanoparticle in a large (practically unbounded) domain. We analyse the consequences of resolving such ideal aerosols using the proposed framework and evaluate the diffusion dynamics (mean squared displacements, velocity auto-correlation functions and diffusion dynamics) of the transported particle. We further extend our assessments towards the transport of a realistic fractal aggregate and correspondingly assess similar particle dynamics. The results are also compared with a point-particle Lagrangian treatment to validate the performance of the method. Further, the method proposed here is independent of the multiphase DNS technique chosen, and the IB method has only been used as an example to demonstrate its feasibility.

This paper is organized as follows: in the succeeding section, we describe our numerical framework in detail, highlighting the modifications introduced to include both non-equilibrium rarefaction and Brownian behavior within the IB-FSI framework. In Section 3.1 we present a validation study undertaken to evaluate the accuracy of the framework. In Sections 3.2 and 3.3 we present results from our studies on the diffusion of nanoparticles of a fixed size in a large domain with ideal (spherical) and real (fractal) shapes. Finally, in Section 4 we summarize some of the major highlights from this work along with prospects for future research.

2. Numerical method

The current framework is built around extending a conventional continuum based multiphase DNS method to include non-equilibrium particle dynamics. Consequently, we describe this proposed framework in detail with particular emphasis on the conventional Langevin description of particle diffusion (Ounis and Ahmadi, 1990a,b), together with an account of the IB-FSI method, which includes our proposed extension to this conventional method. For the purpose of deriving and validating the proposed method, we only deal with nanoparticulate matter diffusion in the absence of nearby particles and walls.

2.1. Conventional Langevin description of particle diffusion

In order to be applicable to gas-solid aerosols, the original Langevin equation (Langevin, 1908) was extended by Ounis and Ahmadi (1990a,b) to include the empirical Cunningham correction C_c (Cunningham, 1910) which corrects the steady drag over the entire range of Knudsen numbers. For a particle with mass m_p and velocity u_p, this is given as:

$$m_p \frac{\mathrm{d}u_p}{\mathrm{d}t} = -\gamma_C u_p + F_{Brownian}, \qquad (1)$$

where γ_C is the Stokes friction factor (Eq. (2)) (Stokes, 1848) including the Cunningham correction (C_c). For practical applications

where solid nanoparticles are suspended in a rarefied gas, unsteady drag effects are known to be negligible (Maxey and Riley, 1983; Ounis and Ahmadi, 1990b). $F_{Brownian}$ represents the stochastic effects on particle motion experienced by a Brownian particle. Note that γ_C is defined for a fluid with dynamic viscosity μ_f as:

$$\gamma_C = \frac{3\pi\mu_f d_p}{C_c}, \tag{2}$$

and the particle time scale is given as:

$$\tau_p = \frac{m_p}{\gamma_C} \tag{3}$$

C_c is the empirical first-order slip velocity Cunningham correction factor (Cunningham, 1910) that is derived from hydrodynamic theory and is given as:

$$C_c(Kn) = 1 + AKn, \tag{4}$$

where A is further a function of Kn that is determined based on empirical data. Millikan (1911), and later Allen and Raabe (1985), confirmed experimentally that the drag reduction can be obtained using the Cunningham correction (C_c). In this work, we use the correlation proposed by Davies (1945):

$$C_c = 1 + Kn(1.257 + exp\{-1.1/Kn\}). \tag{5}$$

$F_{Brownian}$ is modelled as a Gaussian white noise process with spectral intensity S_{ij} given as:

$$S_{ij}^n = S_0 \delta_{ij}, \tag{6}$$

where

$$S_0 = \frac{216\mu_f k_B T}{\pi^2 d_p^5 \rho_p^2 C_c}. \tag{7}$$

Thus, $F_{Brownian}$ can be written as:

$$F_{Brownian} = m_p G \sqrt{\frac{\pi S_0}{\Delta t}}. \tag{8}$$

Here, G is a vector of normally distributed independent random numbers of zero mean and unit variance (Gaussian distribution), and Δt is the time step length during which the Brownian force is active (note that this is not necessarily the time step used in the integration of the particle equation of motion, as will be explained later). It should be noted that the white-noise assumption (in Eq. (8)) is satisfied when the particle density is sufficiently higher than the fluid density (Hinch, 1975).

The solution to Eq. (1) will reproduce the following analytical diffusive behaviour as postulated by Einstein (1905) i.e. for N particles diffusing over time, the root-mean-square displacement (MSD) in one dimension (MSD_x) is given as:

$$MSD_x = \left[\frac{1}{N}\sum_{n=1}^{N}(x(t+dt) - x(t))^2\right]^{\frac{1}{2}} = \sigma_{1D} \equiv \sqrt{2D\Delta t}, \tag{9}$$

where

$$D = \frac{k_B T}{\gamma_C} \tag{10}$$

is the Brownian diffusivity. This is extended to two and three dimensions, where the factor 2 on the right-hand side of Eq. (9) has to be replaced by 4 and 6, respectively (Bunde and Caro, 2018).

Eq. (1) is a stochastic differential equation (SDE), the integration of which is constrained by specific properties of the stochastic time integral as first defined by Itô (1973). The integration of Eq. (1) reproduces the variation in the root mean square displacement of a particle over sufficiently long times ($t >> \tau_p$), i.e. the analytical Stokes-Cunningham-Einstein diffusivity (Eq. (10)) is obtained. However, this result is entirely dependent on the condition that the total hydrodynamic force on the particle can be obtained from the steady drag. This is trivial to control in a Lagrangian simulation,

where the modeller explicitly chooses both formulations as a part of the modelling procedure. However, it becomes more sophisticated in a multiphase DNS framework, where the hydrodynamic coupling is resolved (by integrating the fluid stresses on the surface of the particle) and not modelled. In addition to unsteady effects, the full hydrodynamic coupling would also include effects from the presence of flow boundaries as well as proximity to other particles. Hence, as a proof of concept, in this paper we only address the Brownian diffusion of a single spherical nanoparticle at practically relevant particle-fluid density ratios in an unbounded domain.

2.2. Immersed boundary method coupled with Brownian dynamics: IB-FSI framework

The immersed boundary (IB) methods are a class of numerical techniques employed to obtain solutions to the Navier-Stokes (NS) equations of complex flow systems whilst facilitating its spatial discretization. This method, originally proposed by Peskin (1982), solves the governing equations in a non-body conforming Cartesian grid. In essence, an object, around which the flow is to be assessed, is immersed in a standard cartesian flow grid and its presence is accounted for by modifying the governing NS equations. It should be noted that a surface grid still has to be generated for the immersed body, however the volume grid on which the actual governing equations are solved for can be generated with no regard to this surface grid (Mittal and Iaccarino, 2005). Incorporating the presence of the IB in the NS equations is the primary challenge in setting up this framework. Usually, this modification takes the form of a source term (or forcing function) in the governing equations that reproduces the effect of the boundary. This is usually done in one of the following ways: (i) continuous forcing where the source term is introduced into the continuous NS equations (i.e. prior to the discretization), (ii) discrete forcing where in the source term is only introduced in the discretized NS equations around the vicinity of the IB (typically within the IB) and (iii) implicit forcing where a boundary condition is used (instead of a source term) within the discretized NS equations to constrain the velocity at the IB surface so that the correct behaviour is reproduced.

To deal with the sharply defined rigid bodies as in this paper, a discrete direct forcing approach that adds the necessary source terms to the discretized equations in the vicinity of the IB, could be employed. Such a method (developed by Uhlmann (2005) and later improved by Breugem (2012)) employs two grids: a fixed uniform Eulerian grid for the fluid phase and a uniform Lagrangian grid moving with the IB. A regularized delta function is used to communicate between the two grids (Breugem, 2012). Despite being second-order accurate, this approach is only explicitly formulated and can be unstable for unsteady flows. Alternately, an implicit forcing approach (as formulated by Mark and van Wachem (2008)) can also be used to treat such bodies. In this method, the velocity at the IB is constrained by an implicitly formulated immersed boundary condition (IBC) that is second-order accurate. This unique and stable treatment is central to the efficiency and accuracy of the multiphase DNS framework used in this paper.

2.2.1. Mirroring immersed boundary method

The governing equations for the flow around the immersed boundaries are given by the continuity and momentum equations for incompressible flows, i.e. the Navier-Stokes equations as:

$$\frac{\partial u_j}{\partial x_j} = 0,$$

$$\rho_f \frac{\partial u_i}{\partial t} + \rho_f u_j \frac{\partial u_i}{\partial x_j} = -\frac{\partial p}{\partial x_i} + \frac{\partial}{\partial x_j}\left(\mu_f \frac{\partial u_i}{\partial x_j}\right) + f_i, \tag{11}$$

where f_i represents any external source term. This set of equations is solved together with the implicit Dirichlet IB condition,

$$u_i = u_i^{ib}. \tag{12}$$

Note that, in this method, the coefficients obtained from the discretization of the Navier–Stokes equations are closed with a second-order accurate interpolation that arises from the IBC employed at the IB-fluid interface. The MIB method mirrors the velocity over the IB (the black cells in Fig. 1) to a velocity point in the flow domain. The velocity field at the interior nodes (u_{mi}) of the IB (i.e. the white cells in Fig. 1) is set so that a linear interpolation between that node and the velocity at the fictitious node (u_e) is exactly the implicit Dirichlet IB condition (Eq. (12)),

$$u_i^{ib} = \frac{u_{mi} + u_e}{2}. \tag{13}$$

Further, the IBC generates a fictitious reversed velocity field within the IB which is excluded when calculation fluid fluxes in the momentum equation and pressure equation source terms. The pressure is also not solved for cells inside the IB and pressure gradients are extrapolated over the IB interface. A more detailed description of the method is available at Mark et al., 2011; Mark and van Wachem, 2008.

The total force (acting on the IB) is given by the surface integral of the total fluid stress tensor consisting of pressure and viscous contributions over the IB, as follows:

$$\boldsymbol{F_{IB}} = \int_{IB} \left(-p\delta_{ij} + \tau_{ij} \right) n_j dS = \int_{IB} \left(-p\delta_{ij} + \mu \left(\frac{\partial u_i}{\partial x_j} + \frac{\partial u_j}{\partial x_i} \right) \right) n_j dS, \tag{14}$$

and the corresponding torque on the IB is estimated using –

$$T_{IB} = \int_{IB} \boldsymbol{r} \times \boldsymbol{\sigma} \cdot \boldsymbol{n} dS. \tag{15}$$

Here, $\boldsymbol{r}$ is the position vector of the IB and σ is the fluid stress tensor for a surface S with normal $\boldsymbol{n}$. In this paper, we use an in-house multiphase flow solver IPS IBOFlow, that utilizes the previously described mirroring immersed boundary method to handle the moving particles efficiently. In this solver, the continuity and momentum equations are discretized and solved on an adaptive Cartesian octree grid (Aftosmis, 1997), c.f. Fig. 1, which can be dynamically refined and coarsened. Fig. 1 illustrates this local refinement in the case of an immersed spherical particle along with the corresponding cell types. The pressure-velocity coupling
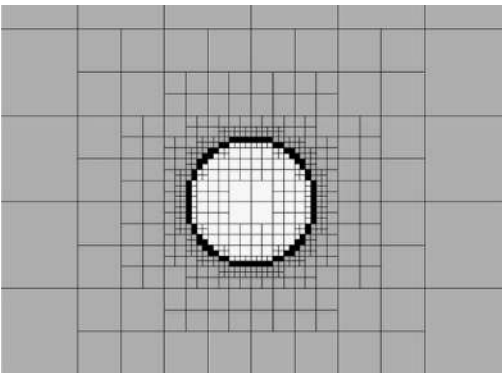

Fig. 1. 2D view of the adaptive dynamic grid refinement around an immersed spherical soot particle. Cell types shown are exterior (grey), interior (white) and mirror or IB cells (black).

in Eq. (11) is handled using the segregated SIMPLEC method (Doormaal and Raithby, 1984) which first approximates the momentum equation with an estimated pressure field, and then corrects the pressure by employing the continuity equation. All variables are stored in a co-located grid arrangement. The Rhie and Chow (1983) flux interpolation is used to suppress pressure oscillations. The IB method described above has been extensively validated and used for the DNS of complex multiphase flow phenomena (Mark et al., 2013).

Finally, it should be noted that the IB method determines the total hydrodynamic force $\boldsymbol{F_{IB}}$ as opposed to only the steady drag $-\gamma_C \boldsymbol{u_p}$. Deviations between these two force estimates will typically be small for solid nanoparticles in a gas, but may become significant for neutrally buoyant particles in a liquid.

2.2.2. Coupling the IB method with non-equilibrium particle dynamics

We can incorporate the relevant Brownian fluctuations by including a stochastic forcing term in our governing equations (either for the particle or fluid). The first possibility is to include the stochastic fluctuations only within the deterministic fluid description (by adding stochastic fluxes to the stress tensor) in order to reproduce the relevant non-equilibrium Brownian behaviour. This constitutes a group of methods referred to as the fluctuating hydrodynamic approach of Landau and Lifshitz (1987), which is derived using the fluctuating-dissipation theorem of statistical mechanics applicable at mesoscopic scales (Noetinger, 1990; Hauge, 1973). These methods have been used predominantly in liquid-solid systems (Groot and Warren, 1997; Español and Warren, 1995), wherein the breakdown of continuity occurs at considerably smaller length scales (Gad-El-Hak, 1329) (Kn is relatively smaller). Hence, no additional correction for the hindered momentum transfer due to rarefaction needs to be included even at nanoscales. However, such methods are not directly applicable to gas-solid rarefied flows, where there is also a pronounced decrease in the overall particle-fluid momentum exchange.

A stochastic forcing (in line with methods such as Brownian dynamics) appears more intuitive for gas-solid rarefied flows. We therefore extend the applicability of the Langevin approach by including the resolved hydrodynamics around the particle i.e. $\boldsymbol{F_{IB}}$ in Eq. (14). To our knowledge, this is the first continuum-based multiphase DNS method that can handle the dynamics of aerosol nanoparticles in a rarefied gas. It should be noted that this method is only valid as long as both the Cunningham correction and the Langevin equation have a sound basis (i.e. the particle-fluid density ratios should be sufficiently high). Thus, in our framework, the motion of a particle with mass m_p, translational velocity $\boldsymbol{u_p}$, angular velocity $\boldsymbol{\omega_p}$, moment of inertia $\boldsymbol{J}$ and including the stochastic forcing $\boldsymbol{F_{Brownian}}$ (c.f. Eq. (8)) is given as:

$$m_p \frac{d\boldsymbol{u_p}}{dt} = \frac{\boldsymbol{F_{IB}}}{C_c} + \boldsymbol{F_{Brownian}}, \tag{16}$$

$$\boldsymbol{J} \frac{d\boldsymbol{\omega_p}}{dt} = T_{IB} - \boldsymbol{\omega_p} \times \boldsymbol{J} \cdot \boldsymbol{\omega_p}. \tag{17}$$

The in-house IB flow solver (IPS IBOFlow) is coupled with an in-house finite-element (FEM) based rigid body solver (Simo and Wong, 1991) that can fully resolve the particle diffusion dynamics. The FEM solver computes the rigid body motion by solving the linear and angular momentum conservation equations (Eqs. (16) and (17)). The Newmark time scheme (Newmark, 1959) is used for the temporal integration of the stochastic differential equation (SDE). In this method, acceleration, velocity and displacement at time $t = t^{n+1}$ are obtained as a function of the values at $t = t^n$ by assuming a linear acceleration during that small time step. This one-step semi-implicit method can be represented by the following sets of equations:

$$\dot{u}_p^{n+1} = \dot{u}_p^n + \frac{\Delta t}{2}\left(\ddot{u}_p^n + \ddot{u}_p^{n+1}\right) \qquad (18)$$

$$u_p^{n+1} = u_p^n + \Delta t \dot{u}_p^n + \frac{1-2\beta}{2}\Delta t^2 \ddot{u}_p^n + \beta \Delta t^2 \ddot{u}_p^{n+1} \qquad (19)$$

This scheme is unconditionally stable with β a tuning parameter that has a default value of 0.25 (the constant average acceleration method) (Newmark, 1959). The scheme is also compliant with the Itô interpretation (Itô, 1973) of a stochastic integral.

A partitioned approach is employed to solve the coupled rigid body-IB problem. The grid and assembly are fully parallelized on the CPU, and the resulting large sparse-matrices are solved on the GPU with an Algebraic Multi-Grid (AMG) solver (Naumov et al., 2015). The use of such a coupled rigid body-IB solver would mean that we already have the infrastructure to account for particle-particle and particle-wall interactions as well. Additionally, as we use an IB method, we can easily add complex fractal-shaped aggregates within the framework. Moreover, this framework can also resolve particle deformation if needed (coupling between hydrodynamics and structural mechanics). However in this paper we limit ourselves to simulations of rigid PM aerosols.

2.3. Modelling fractal shaped soot particles

The proposed framework is also designed to handle complex fractal aggregates. Since we employ a rigid body solver, the dynamics of these complex fractal aggregates can inherently be handled, provided the physics of the system are consistently incorporated. In this sub-section we summarize the approach adopted to model such fractal shaped particles within the context of the IB-FSI framework.

2.3.1. Fractal aggregate generation

Real soot aggregates are formed from the growth of small primary particles into fractal aggregates (Kittelson, 1998). Such aggregates can thus be described as entities composed of a number of contacting or partially coalesced primary spheres, so that the radius of gyration (R_g) of the aggregate is defined as:

$$R_g = \frac{1}{H}\sum_{h=1}^{H} r_h^2, \qquad (20)$$

where H is the number of primary spheres in the entity and r is the distance between the center of mass of a primary sphere and the axis of rotation of the aggregate. For such an aggregate, the total number of primary spheres exhibits a power-law relationship with the radius of gyration (Rogak et al., 1993; Köylü et al., 1995) given as:

$$H = k_f \left(\frac{R_g}{a}\right)^{D_f}, \qquad (21)$$

where a, D_f, and k_f are the mean primary particle radius, fractal dimension (exponent) and fractal pre-factor, respectively. In order to accurately account for the diffusion dynamics of these fractal particles, we first generate them using standard particle–cluster (PC) aggregation algorithms (Skorupski et al., 2014). These algorithms attach one spherical sub-unit to the growing cluster at each step of the aggregation process in such a way that the scaling law (Eq. (21)) is fulfilled exactly at each step for prescribed values of the fractal dimension and pre-factor. The obtained fractal aggregates are then directly imported as a surface mesh to the IB-FSI framework (c.f. Fig. 2).

2.3.2. Characteristic dimensions of the fractal aggregate

The correlations for C_c (Eq. (4)) were derived based on regularly shaped spherical particles. Hence, in order to account for the drag reduction via C_c, a relevant equivalent characteristic dimension of
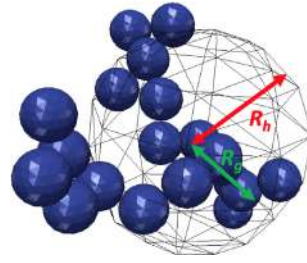

Fig. 2. A schematic representation of the hydrodynamic radius (R_h) in relation to a surface meshed fractal soot aggregate with pre-factor (k_f) 1.3 and dimension (D_f) 1.78.

the irregularly shaped fractal aggregate is needed. Recently, Zhang et al. (2012) showed that a correction analogous to the one used for spherical particles (as in Eq. (5)) can be obtained for an arbitrarily shaped aerosol particle across the entire Kn range, i.e. Eq. (5) may be used if the Kn of the fractal particle is defined in terms of the hydrodynamic radius of the non-spherical particle (R_h) (as originally defined by Hubbard and Douglas (1993)) and a projected area (A_p) as:

$$Kn = \frac{\lambda \pi R_h}{A_p}, \qquad (22)$$

This would mean that the aggregate Kn is a shape-independent relation that can be used to describe the low-Reynolds number, low-Mach number, orientationally averaged drag force on arbitrarily shaped particles (Zhang et al., 2012). We employ this idea to characterize the real fractal-shaped soot particles used in our IB-FSI framework as well. We use the algorithm described by Gopalakrishnan et al. (2011) for calculating an orientationally averaged R_h (c.f. Fig. 2). First passage time simulations (developed by Torquato and co-workers (Torquato and Avellaneda, 1991)) of inertialess Brownian walkers are used to estimate R_h based on Monte-Carlo collision events. These walkers are released from the surface of an imaginary sphere (one at a time) with radius $R_{outer} \gg R_g$ of the aggregate and thereafter moved by first passage time simulations. Finally, after n-steps, the Brownian walker either collides or escapes. The number of colliding and non-colliding walkers are then used to calculate R_h:

$$R_h = \frac{N_C R_{outer}}{N_C + N_{NC}} \qquad (23)$$

More details about this method are available in the supplementary material of the work by Gopalakrishnan et al. (2011).

The projected area (A_p), i.e. the maximum extent of the particle shape on an orthogonal projection plane, is calculated using a Monte-Carlo sampling technique. P uniformly distributed points are sampled from a rectangle (with area A) that encloses one specific orientation of the fractal aggregate completely. Each sampled point is checked to determine whether it is inside (N_{in}) the projection of the particle shape. The final A_p for this specific orientation is calculated as:

$$A_p = \frac{N_{in} A}{P} \qquad (24)$$

The calculation is repeated for 10^4 orientations, and the orientationally averaged projected area is taken as the arithmetic mean. An example of this Monte Carlo sampling method is shown for one particular aggregate orientation in Fig. 3. Based on these calculations, the simulated fractal aggregate is characterized by the dimensions listed in Table 1. The properties obtained are in good agreement with the open 20-particle aggregate investigated by Zhang et al. (2012).
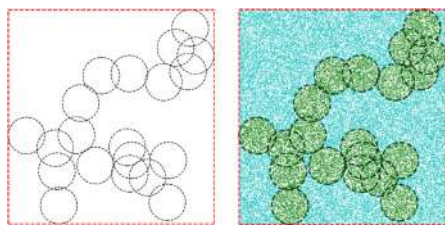
Fig. 3. Calculation of A_p using Monte Carlo sampling: The orthogonal projection of the aggregate (in the XY plane) is indicated by the black dashed circles (). P uniformly distributed points are sampled within a rectangle (box with red dashed lines) that encloses this specific orientation of the fractal aggregate. Each sampled point is checked to determine whether it is inside () or outside () the projection of the particle shape. (For interpretation of the references to colour in this figure legend, the reader is referred to the web version of this article.)

Table 1
Aggregate dimensions.

Fractal pre-factor (k_f)	1.3
Fractal dimension (D_f)	1.78
Hydrodynamic radius (R_h)	174.2 nm
Projected area (A_p)	6.42e−14 m^2

2.4. Simulation conditions

We now provide an overview of the numerical setup employed in the simulations. Note that these simulations employ the particle response time (τ_p) as a basis for determining the relevant temporal details. A spherical particle is initially placed at the center of our domain (which is symmetric on all sides) and is subjected to both the corrected hydrodynamic forces and the stochastic Brownian forcing. Further, the Brownian forcing is updated in intervals of $\tau_p/10$ to allow for an adequate resolution of the particle acceleration. A schematic of the domain is shown in Fig. 4. The simulation conditions are further listed in Table 2. The same domain dimensions are used for both the spherical (400 nm diameter) and the fractal aggregate (dimensions as in Table 1) simulations. The effect of particle-fluid density ratio on the diffusion dynamics is also analyzed for the spherical nanoparticles. The full list of cases that have been studied in this paper is shown in Table 3.

3. Results

Several numerical experiments have been carried out in the current IB-FSI framework. These experiments aim to demonstrate
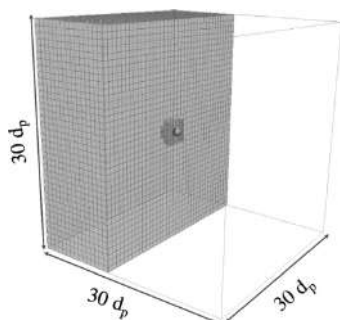

Fig. 4. Schematic of the simulation domain employed in the particle diffusion studies.

the feasibility of the proposed method to describe the dynamics of rarefied gas-solid PM aerosols. First, we present the framework validation studies using a standard Stokes settling case without Brownian motion. We next present our results from the diffusion of a 400 nm soot particle in an unbounded domain. The diffusion dynamics are quantified via the mean squared displacement (Eq. (9)). Further, they are non-dimensionalized by the square of a diffusional length scale ($MSD^* = MSD/D\tau_p$) to compensate for the density dependence of diffusivity. In this paper, we evaluate a single particle trajectory over very long periods of time, which represents multiple particle trajectories ensemble averaged over a much shorter duration (ergodicity hypothesis). Hence we include a brief account of a purely Lagrangian benchmark study (one-way coupled simulation) within this discussion to establish the minimum criteria to obtain reasonable statistics and further quantify the overall variability of the diffusion process studied. The obtained benchmarks are used to demonstrate the feasibility of the novel IB-FSI framework for the multiphase DNS of weakly rarefied aerosols. We then conclude with a discussion about the diffusion dynamics of fractal soot particle under similar conditions.

3.1. Validation of the IB-FSI framework

The IB-FSI framework used in this work is first validated using a standard non-Brownian Stokes settling case. A spherical aerosol particle accelerated by a constant force in the negative Z-direction is used for this test case. The particle has a diameter of 400 nm and a density of 1000 kg/m^3, which are relevant values for combustion-generated PM (Kittelson, 1998). The constant force was chosen so as to accelerate the particle to a terminal velocity proportional to the root mean square velocity ($V_{rms} = \sqrt{k_B T/m_p}$) of an equivalent Brownian motion. A detailed temporal and spatial (grid) convergence study was undertaken to show the sensitivity of this multiphase DNS method to the temporal and spatial discretization employed. The results from this assessment are shown in Fig. 5. Further, the relative error across the temporal and spatial resolutions in this study are summarized in the Table 4. This error between the simulations and the analytical results is calculated as:

$$Relative\ error = \frac{V_z^{analytic} - V_z^{simulation}}{V_z^{analytic}}. \tag{25}$$

A variety of grid resolutions were tested, at a fixed Courant number ($C = u\Delta t/\Delta x$) based on an initial temporal resolution of $\tau_p/200$ (i.e. the coarsest spatial resolution of 12 cells/diameter uses a temporal resolution (dt) of $\tau_p/200$). The successively finer spatial resolutions employ a correspondingly finer temporal resolution so as to maintain the same Courant number. A rule of thumb in such multiphase DNS simulations is to have at least 20 cells per particle diameter as the resolution, and this is realized in our assessments as well (c.f. Fig. 5a). The solution approaches grid independence if a minimum resolution of 24 cells/diameter is maintained. Moreover, although the reported relative error does decrease with a finer resolution, a larger mesh creates an increased computational overhead. Hence, in order to counter-balance computational demands and the expected accuracy, a grid resolution of 24 cells/diameter (with a relative error of $\approx 5\%$) will be used as the basis for all the studies presented henceforth.

In relation to the grid resolution employed, we stress that the purpose of the IB-FSI method is to obtain the total hydrodynamic force ($\boldsymbol{F_{IB}}$ in Eq. (14)) to be rescaled with the Cunningham correction. The resolution must therefore be sufficient to accurately describe the flow field around the particle, despite the fact that the Navier-Stokes equations are not intrinsically valid at these spatial scales (cf. Hocking, 1973; Sone, 1976; Beresnev et al., 1990 and the discussion in Bailey, 2004; Barber and Emerson, 2006). It is the

Table 2
Simulation settings and fluid properties.

Condition	Case: Grid convergence	Case: Time convergence	Case: Diffusion
System size (l × w × h), μm	10 × 10 × 10	10 × 10 × 10	10 × 10 × 10
Particulate phase: Spherical soot particle			
Diameter, nm	400	400	400
Density, kg/m³	1000	1000	2000, 1000, 500, 100
Particulate phase: Aggregate soot particle			
Diameter, nm	–	–	cf. Table 1
Density, kg/m³	–	–	1000
Fluid phase: Air			
Density, kg/m³	1	1	1
Dynamic viscosity, Pa s	1.8e−5	1.8e−5	1.8e−5
Simulation settings			
Spatial resolution, cells/diameter	12, 24, 48, 96	24	24
Temporal resolution or dt, s	$1/100\tau_p$, $1/200\tau_p$, $1/400\tau_p$, $1/800\tau_p$	$1/10$, $1/35$, $1/70$, $1/100$, $1/200\tau_p$	$1/200\tau_p$

Table 3
List of cases simulated using the IB-FSI framework.

Case	Particle/Fluid density ratio
Spherical particle of diameter 400 nm	
Case 1	2000
Case 2	1000
Case 3	500
Case 4	100
Aggregate of diameter 348 nm	
Case 5	1000

subsequent scaling with the Cunningham correction, implemented via the adjusted density method (Strom, 2011), that ensures that the hydrodynamic force experienced by the particle in the simulation leads to the correct dynamic behavior.

Next, the sensitivity of the IB-FSI framework to temporal discretization is shown in Fig. 5b. A temporal resolution of at least $\tau_p/70$ is needed to produce convergent solutions. Since the computational overhead from the time step demands are not as severe as those from the grid requirements, we select the temporal resolution of $\tau_p/200$ (with a relative error of $\approx 5\%$) to be used in all the simulations presented in this paper.

3.2. Diffusion of a 400 nm speherical soot particle in an unbounded domain

In order to demonstrate the feasibility of our method, we evaluate the diffusion of a single spherical soot nanoparticle (with a diameter of 400 nm) at practical particle-fluid density ratios in quiescent Stokes flow (as given in Table 3: cases 1–4) in an unbounded 3-dimensional domain (c.f. Fig. 4). We first establish the requirements on the statistical averaging to obtain meaningful results, using a purely point-particle based Langevin formulation. These simulations are performed across the chosen density ratios and would serve as the basis while describing the results obtained using our novel IB-FSI framework. This is followed by a detailed account of the diffusion dynamics assessed using our proposed framework.

3.2.1. Benchmark studies: Point-particle Langevin diffusion dynamics

The particle equation of motion is integrated using a forward Euler explicit time marching scheme (to solve the Langevin equation Eq. (1)) including the corrected Stokes drag (Eq. (2)) as the only hydrodynamic coupling between the particle and rarefied gas. In other words, this is a one-way coupled gas-solid system which is stochastically forced by the relevant model for Brownian
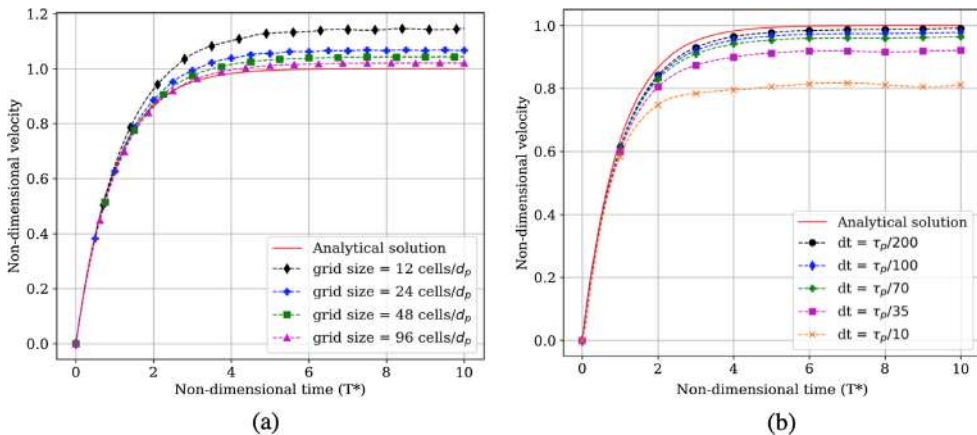
Fig. 5. Sensitivity assessments on the IB-FSI framework: (a) Grid and (b) temporal convergence based on time step dt after 10 response times. The solid red lines ( ) represent the analytical Stokes settling under a constant force in the negative Z-direction (solved by integrating the particle equation of motion using a forward Euler explicit solver). (For interpretation of the references to colour in this figure legend, the reader is referred to the web version of this article.)

Table 4
Spatial and temporal convergence for a spherical particle of density 1000 kg/m³ accelerated by a constant force in the negative Z-direction after 10 particle response times (τ_p). The values highlighted in **bold** are the chosen spatial and temporal resolutions for the DNS framework.

(a) Grid convergence	
Grid resolution	Error (%)
12 cells/dia	15.2%
24 cells/dia	**5.2%**
48 cells/dia	3.3%
96 cells/dia	2.1%
Temporal convergence	
Temporal resolution	Error (%)
$\tau_p/10$	17.8%
$\tau_p/35$	10.9%
$\tau_p/70$	7.5%
$\tau_p/100$	6.3%
$\mathbf{\tau_p/200}$	**5.2%**

motion (Eq. (8)), updated every $1/10^{th}$ particle response time τ_p and integrated (in time) using a temporal resolution of $\tau_p/200$. This assessment was done using a solver written in a Python environment. Note that the random seeds that have been used to initiate the stochastic process in these simulations are also used in the corresponding multiphase DNS treatments.

The one-way coupled simulations are used to determine the simulation duration and the lag time (averaging interval) required to get an adequate statistical description of the diffusion process. To avoid tail fluctuations, the lag time should not be too long. Additionally, the simulation duration should also be as long as possible. Our assessments showed that (across all the reported density ratios) the minimum criteria needed to obtain a reasonable statistical description of the diffusion process is a simulation duration of $150\tau_p$ and a lag time of $10\tau_p$. Further, the variation in the MSD^* across different particle trajectories (five different random seeds in the stochastic forcing) is also estimated (c.f. Fig. 6). Clearly, the choice of the random seed determines the final displacements of the particle. This variance is visualized in the inset of Fig. 6. This

estimate is used to determine the total variation (error bars) in the stochastic process while evaluating the results from the IB-FSI simulations.

3.2.2. General diffusion dynamics of a particle with density 1000 kg/m³

Some trends from the diffusion of a spherical soot particle with a density of 1000 kg/m³ are shown in Fig. 7. The left panel (i.e. Fig. 7a) depicts a typical Brownian trajectory while the right panel demonstrates the diffusion dynamics in terms of MSD^*. A very important property of Brownian diffusion, i.e. transition from a ballistic to a diffusive regime (Uhlenbeck and Ornstein, 1930), can clearly be seen in Fig. 7b. This noted transition between the regimes has also been observed experimentally (Huang et al., 2011) and can be attributed to the break down of the Stokes-Cunningham-Einstein description (Eq. (9)) at the shortest time-scales (Rahman, 1964). At these scales (referred to as the ballistic regime) the particle motion is highly correlated and therefore a definition of velocity is plausible (the root mean squared particle velocity V_{rms}). Further, as the results are averaged in 3D, these would approach the 1D Stokes-Cunningham-Einstein result. Correspondingly, the MSD approaches $(V_{rms}t)^2$ in the ballistic regime below τ_p, and reaches $2Dt$ (Stokes-Cunningham-Einstein result c. f. Eq. (9)) at larger times. Note also that the MSD^* predictions from the framework are in excellent agreement with the benchmark simulations and are further within the variability reported in the benchmark simulations (across different trajectories or 5 different random seeds). Additionally, particle positions and velocities also agree well between the benchmark and IB-FSI treatments (c.f. Fig. 8). In conclusion, this close correspondence can be considered as a qualitative validation of the performance of the framework.

3.2.3. Effect of density ratio on diffusion dynamics

The IB-FSI framework is used to evaluate whether the particle diffusion dynamics changes as a function of the particle-fluid density ratio, within a range of densities that might be relevant to actual applications (c.f. Table 3). The applicability of the proposed framework to handle a broad range of densities is shown in Fig. 9a, where the corresponding MSD^* values across realistic soot-particle densities compare very well with the benchmark results. The cho-
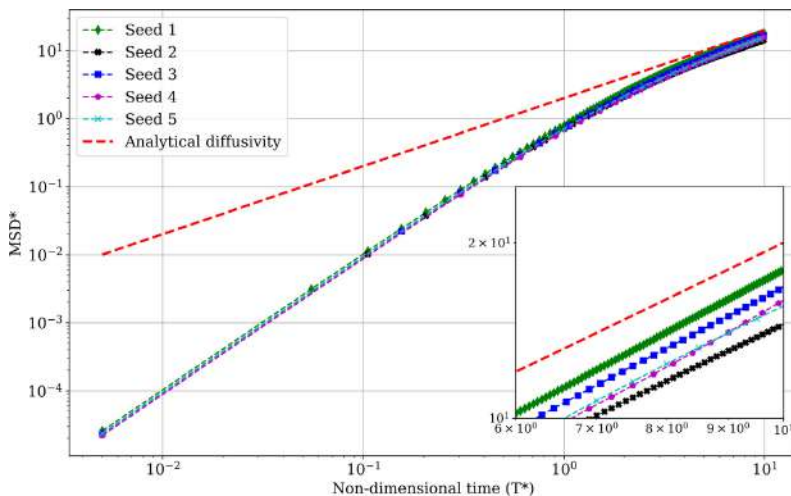
Fig. 6. Variation in particle diffusion dynamics across different random seeds: Averaged non-dimensional MSD across different particle trajectories (different seeds). The red dashed line ( ) represents the Stokes-Cunningham-Einstein analytical diffusivity (Eq. (9)). The inset emphasizes the variations across the seeds. (For interpretation of the references to colour in this figure legend, the reader is referred to the web version of this article.)
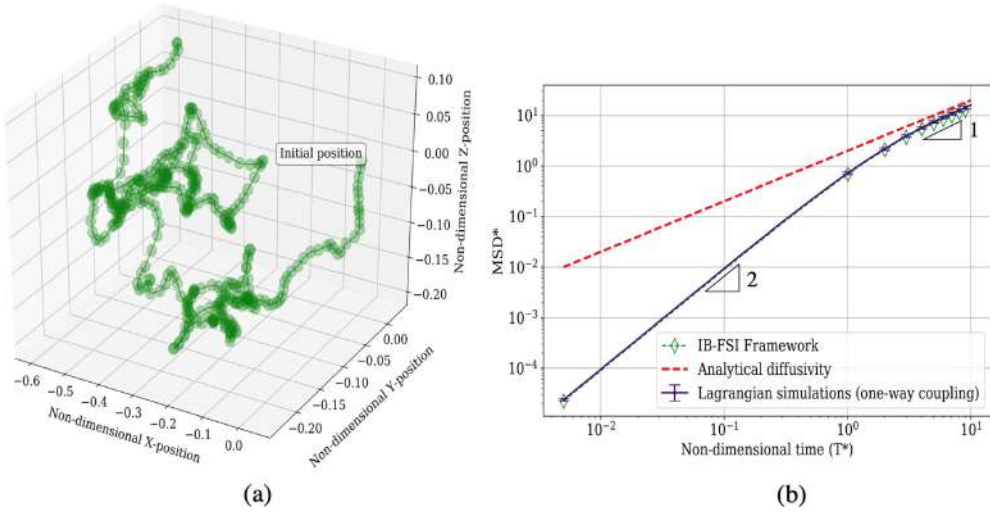
Fig. 7. Particle diffusion dynamics (IB-FSI simulations): (a) Trajectory of a 400 nm diameter particle (with density 1000 kg/m³) in non-dimensional units (scaled by particle diameter) and (b) averaged non-dimensional *MSD* after a lag time of 10 response times across different density ratios after 150 response times (the slopes indicate the ballistic and diffusive regimes). The red dashed line ( ) represents the Stokes-Cunningham-Einstein analytical diffusivity (Eq. (9)). (For interpretation of the references to colour in this figure legend, the reader is referred to the web version of this article.)
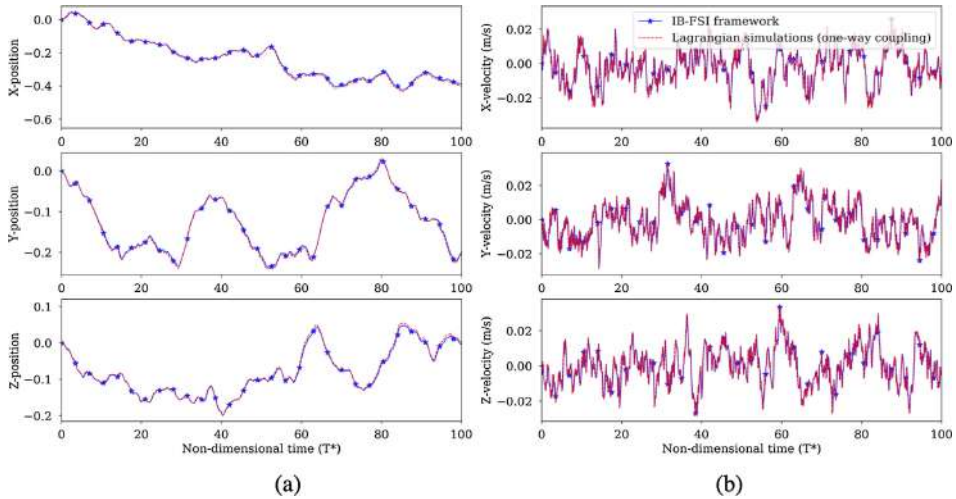

Fig. 8. Particle diffusion dynamics (IB-FSI simulations): (a) Position in non-dimensional units (scaled by particle diameter) and (b) velocity of a 400 nm diameter particle (with density 1000 kg/m³) after 100 response times.

sen non-dimensionalization of the results would compensate for the density dependence of diffusivity. This would mean that, if Stokes drag is the only hydrodynamic coupling between the phases, there should be no differences in the *MSD** across the simulations with different particle-fluid density ratios (as seen in Fig. 9a). This further confirms that at the chosen density ratios, the unsteady drag effects are negligible.

Additionally, the Gaussian nature of the stochastic forcing in Eq. (8) would mean that the consequent stochastic process is Markovian in nature. Hence, the auto-correlation function (v_{acf}) of the particle velocities v, given as:

$$v_{acf} = \langle \boldsymbol{v}(\boldsymbol{0}) \cdot \boldsymbol{v}(\boldsymbol{t}) \rangle = \frac{1}{N_t} \sum_{n=1}^{N_t} (\boldsymbol{v}(\boldsymbol{0}) \cdot \boldsymbol{v}(\boldsymbol{t})), \quad (26)$$

decays with an exponential tail, as shown in Fig. 9b. In this expression, N_t is the lag time interval (i.e. averaging using a lag of 1dt, 2dt... $N_t dt$). This classical result for Brownian particles with sufficiently high density ratios (von Smoluchowski, 1906; Chandrasekhar, 1943), is a further validation of the applicability of our framework towards such weakly rarefied gas-solid flows. Note that the analytical Stokes-Cunningham-Einstein exponential decay in Fig. 9b is slightly offset at the beginning (in the comparison with v_{acf} from both the IB-FSI and Lagrangian benchmark simula-
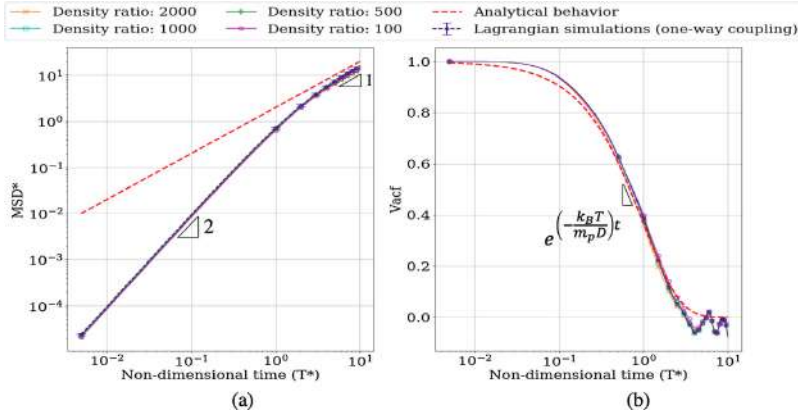
Fig. 9. Particle diffusion dynamics (IB-FSI simulations): (a) Averaged non-dimensional *MSD* variation and (b) averaged velocity auto-correlation function (v_{acf}) across different particle-fluid density ratios after 150 response times (all the Lagrangian benchmarks are represented by one curve). The red dashed lines () represent the Stokes-Cunningham-Einstein analytical behavior (Eq. (9)). (For interpretation of the references to colour in this figure legend, the reader is referred to the web version of this article.)
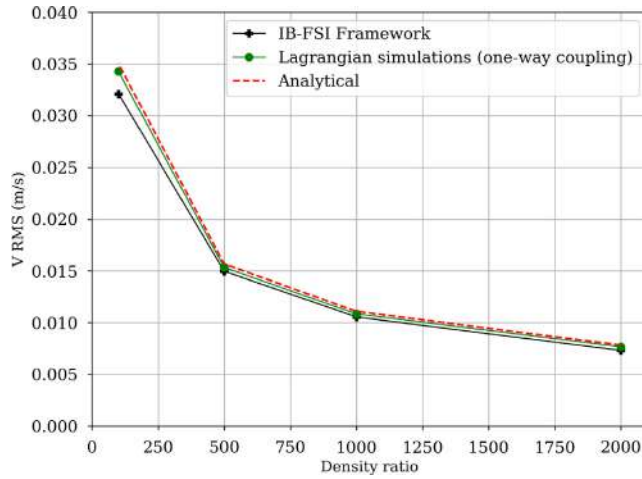

Fig. 10. Comparison of V_{rms} between the IB-FSI framework, Lagrangian benchmark and Analytical results across density ratios between 2000 and 100 kg/m3 after 150 response times. The red dashed line () represents the analytical values. (For interpretation of the references to colour in this figure legend, the reader is referred to the web version of this article.)

tions) due to the absence of a ballistic behaviour (which is accounted for in a Langevin treatment). This effect occurs because the analytical behaviour breaks down at the shortest time scales. Nevertheless, the two sets of curves do follow each other after this initial ballistic phase.

We further evaluate the accuracy of the current framework by comparing the root-mean squared velocities (V_{rms}) of the particle across the different particle-fluid density ratios. This is a good metric to judge if the stochastic behaviour is being correctly resolved. The analytical root mean square velocity is a function of the particle density (as a lighter particle is more easily accelerated by molecular collisions), and this trend is presented in Fig. 10. It can be seen that the IB-FSI framework closely follows the analytical trend. The relative difference between the V_{rms} values from the IB-FSI framework and the analytical values are used as a quantitative metric of accuracy. This relative error is given as:

$$Relative\ error = \frac{V_{rms}^{analytic} - V_{rms}^{simulation}}{V_{rms}^{analytic}} \qquad (27)$$

We report a maximal 5% error with our framework, synonymous with the error reported for our chosen spatial and temporal resolutions (as reported in the validation studies c.f. Fig. 5). This is considered acceptable, and further demonstrates the feasibility of this general method to study the dynamics of soot-like spherical particles in unbounded domains using continuum based multiphase DNS.

3.3. Diffusion of a fractal soot particle in an unbounded domain

The IB-FSI framework is extended to simulate the diffusion of a real soot aggregate (with the dimensions listed in Table 1) of density 1000 kg/m^3 in a large unbounded domain (c.f. Table 3). These results are compared with the Lagrangian simulations (or bench-

mark studies) of an ideal spherical particle with the same hydrodynamic radius ($r_H = A_p/\pi R_h$) and the same total mass as the aggregate. It is expected that, if the aggregate is characterized as reported in Table 1, the diffusion dynamics of a corresponding spherical particle is comparable with that of the aggregate with the same mass (Zhang et al., 2012). In these simulations, the effect of particle rotation have been approximated via the orientationally averaged hydrodynamic properties (i.e. only translation is explicitly calculated in the rigid body solver). This preliminary assessment is used to demonstrate that our framework has the built-in capability to handle real fractal shaped soot particles.

3.3.1. Diffusion of an aggregate with density 1000 kg/m³

The diffusion dynamics of a fractal aggregate is assessed over a duration of $150\tau_p$. An examination of the particle trajectories and the corresponding averaged MSD^* indicates that the IB-FSI framework is able to capture the relevant Brownian dynamics of an aggregate particle. This is particularly evident through the transition from the ballistic to a diffusive regime (see Fig. 11b), as shown earlier with a spherical particle. Further, a meandering Brownian trajectory of the aggregate is also identifiable (c.f. Fig. 11a). This qualitative validation further indicates that the utilized hydrodynamic properties of the aggregate can sufficiently describe the non-equilibrium particle dynamics in a rarefied gas.

A highlighting feature of this framework is that it can probe both particle-specific fields (such as position, velocity, displacements etc.) and fluid fields (such as species concentrations) around the particle. Such a detailed insight into these systems is seldom available, particularly at the desired system scales (such as the transport inside the pore of a porous material), yet constitutes a prerequisite for dealing with these flows, given the paramount importance of chemical reactions in PM transport problems. Fig. 12 shows the resolved flow field around the aggregate as an illustration of the level of detail available with the proposed tech-
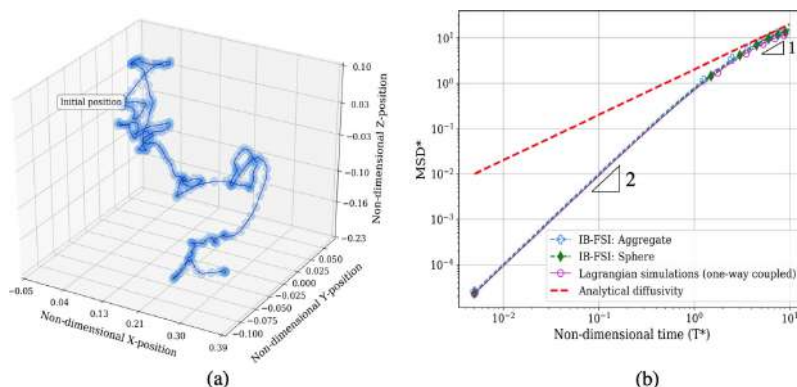
Fig. 11. Particle diffusion dynamics of a fractal aggregate (IB-FSI simulations): (a) Trajectory of a fractal aggregate of hydrodynamic diameter 348 nm with a density of 1000 kg/m³ and (b) averaged non-dimensional MSD after comparison between a sphere and an aggregate (with the same mass and hydrodynamic radius) in terms of the averaged non-dimensional MSD after a lag time of 10 response time units over a duration of 150 response times (the slopes indicate the ballistic and diffusive regimes). The red dashed line ( ) represents the Stokes-Cunningham-Einstein analytical diffusivity (Eq. (9)). (For interpretation of the references to colour in this figure legend, the reader is referred to the web version of this article.)
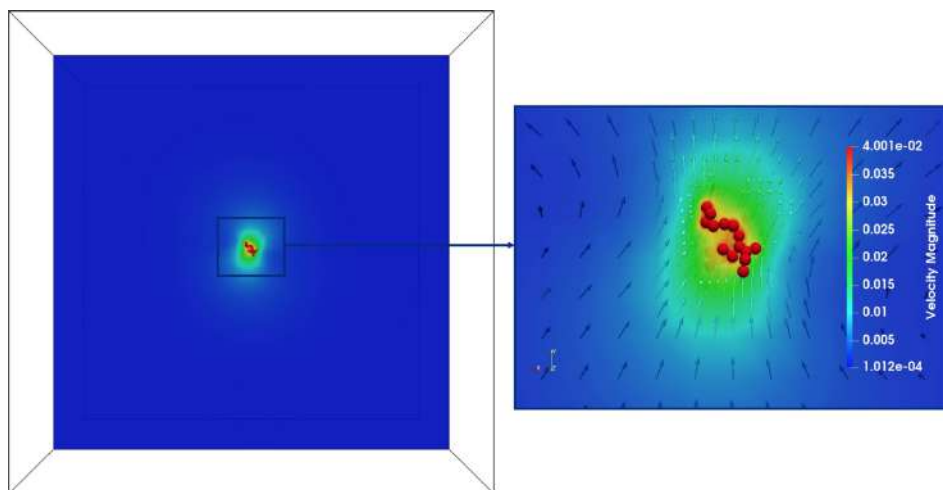
Fig. 12. Vectors of velocity magnitude (across a XY plane in the center of the simulation domain) for a fractal aggregate of hydrodynamic diameter 348 nm and with a density of 1000 kg/m³ after a duration of $150\tau_p$ at a timestep of $\tau_p/200$. Note that the contours are colored based on the velocity magnitude of the surrounding flow field. (For interpretation of the references to colour in this figure legend, the reader is referred to the web version of this article.)

Fig. 13. Comparison between an aggregate and a sphere with the same mass and hydrodynamic diameter of 348 nm: (a) Total hydrodynamic force (F_{IB}) on the particle and (b) Brownian forcing (F_{Br}) during a period of 20 response times.

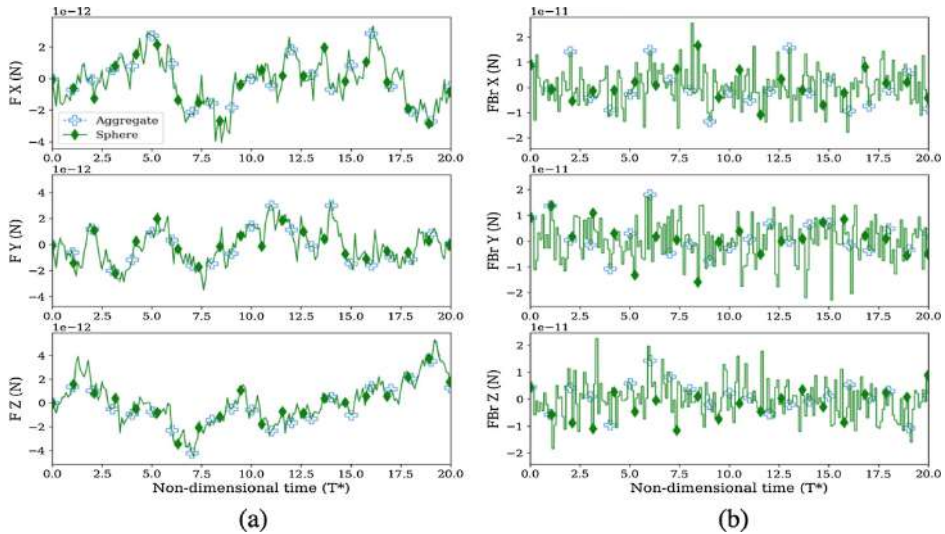nique. Consequently, the current framework provides a novel outlook into the governing phenomena at the pore scales, and can further be used to understand the complex transport of PM aerosols in weakly rarefied flows.

3.3.2. Comparison between a fractal aggregate and a spherical particle

The simulations with the aggregate were setup based on the assumption that the correlations for the empirical Cunningham correction could be extended to these complex shapes. This is plausible provided the Knudsen number (Kn) is calculated as shown in Eq. (22). Consequently, in order to indirectly validate this assumption, we compare the diffusion dynamics between a sphere and an aggregate with the same mass and hydrodynamic diameter. We first examine the net hydrodynamic force around the particle (F_{IB} in Eq. (14)) given the same stochastic forcing (F_{Br}). This comparison is depicted in Fig. 13. Clearly, both particles (i.e. the sphere and the aggregate) experience very similar hydrodynamic forces from the rarefied gas, meaning that the original assumption about the extension of the Cunningham correction is valid. Further, both particles also have a similar diffusive behaviour (transition from the ballistic to the diffusive regimes) and this closely matches the Lagrangian benchmark simulations of the spherical particle with the same hydrodynamic diameter and mass as the aggregate (c.f. Fig. 11b). We thus conclude that the methodology to handle realistic, non-spherical objects has been validated. We also stress that in a general situation with the presence of other particles and walls, the hydrodynamic interactions between objects of complex shapes will not be the same as that for spheres.

Thus, the framework presented here has an innate capability to account for the reduced momentum transfer on spherical as well as non-spherical nanoparticles, while also intrinsically accounting for hydrodynamic interactions of arbitrarily shaped objects via a complete resolution of the flow field.

4. Conclusions

In this paper, we present a novel continuum based multiphase DNS method to study the diffusion dynamics (Brownian transport) of combustion-generated nanoparticles. Modeling of such phenomena necessitates simultaneous descriptions of meandering Brownian trajectories, reduced momentum transfer between the gas and the solid, and hydrodynamic interactions with other particles and nearby walls. In this first step, we have chosen to focus on Brownian motion in very large (practically unbounded) domains. The original Langevin dynamics based method could reasonably account for both of these effects by including a Cunningham correction (for the drag reduction due to breakdown of continuity) and a stochastic point force (for the non-equilibrium Brownian fluctuations) within the particle equation of motion. However, as it is based on the point-particle assumption, this method will invariably fail when the particle has a definite volume. The failure is most linked to particle-particle and particle-wall interactions. Further, corrections to this model to include hydrodynamic interactions with particles of complex shapes are not trivial.

Future needs in computational optimization of PM mitigation devices call for a multiphase DNS treatment in which Brownian motion of non-spherical particles immersed in a weakly rarefied reactive gas can be handled. We address this need by proposing a novel method that utilizes a multiphase DNS framework to account for the particle-fluid coupling including the molecular interactions. This is achieved by modelling these non-equilibrium effects within the particle equation of motion, extending the conventional Langevin approach by incorporating the resolved hydrodynamics around the particle. Thus, we couple a mirroring immersed-boundary (MIB) method with a rigid body solver to compute the particle short range dynamics including the Brownian dynamics of the particle.

As a first step, we have demonstrated the capabilities of this novel technique to handle the diffusion of an ideal spherical soot particle in an unbounded domain. We were able to accurately capture the particle diffusion dynamics, including the transition from a ballistic regime to a diffusive regime, using the proposed framework. Further, the exponential decay of the velocity auto-correlation function was also noted in these simulations, confirming that the relevant non-equilibrium behaviour has been adequately represented in the governing equations of the dispersed particulate flow. We next extended this framework to evaluate the

diffusion dynamics of a realistic fractal particle. Such an extension was possible under the condition that the relevant hydrodynamic properties of the aggregate are calculated based on the methods described by Zhang et al. (2012). We were then able to demonstrate the capability of our framework to handle the Brownian dynamics of such a realistic fractal aggregate. The reported results were in good agreement with the traditional Langevin treatment of a spherical particle with the same mass and hydrodynamic properties as the aggregate.

It should be stressed that the proposed method is valid as long as the Langevin treatment and the Cunningham correction have a basis (i.e. high particle-fluid density ratios and unbounded flow domains). We note that, in typical applications of soot aerosols, the particle-fluid density ratios are sufficiently high to ensure the validity of the Langevin equation. Our future efforts will be directed towards analyzing the performance of the framework when wall effects and particle-particle interactions are also present. All the necessary infrastructure to account for these effects is already available in our framework. Furthermore, elaborate molecular methods such as discrete simulation Monte Carlo (DSMC) would provide a conclusive account of the relevant near-boundary behaviour (could be particle-particle or particle-wall), enabling the formulation of closures that can later be used in our framework to account for the correct physics. The inclusion of these two critical extensions to the framework will further enhance its applicability to real-world systems.

Declaration of Competing Interest

The authors declare that they have no known competing financial interests or personal relationships that could have appeared to influence the work reported in this paper.

Acknowledgements

References

Aftosmis, M.J., 1997. Lecture notes: Solution adaptive cartesian grid methods for aerodynamic flows with complex geometries.

Allen, M.D., Raabe, O.G., 1985. Slip correction measurements of spherical solid aerosol particles in an improved millikan apparatus. Aerosol Sci. Technol. 4 (3), 269–286. https://doi.org/10.1080/02786828508959055. issn: 0278-6826.

Bailey, C.L., Barber, R.W., Emerson, D.R., 2004, July. Is it safe to use Navier–Stokes for gas microflows. In: European Congress on Computational Methods in Applied Sciences and Engineering.

Banchino, A.J., Brady, J.F., 2003. Accelerated stokesian dynamics: Brownian motion. J. Chem. Phys. 118 (22), 10323–10332. https://doi.org/10.1063/1.1571819.

Barber, R.W., Emerson, D.R., 2006. Challenges in modeling gas-phase flow in microchannels: from slip to transition. Heat Transfer Eng. 27 (4), 3–12. https://doi.org/10.1080/01457630500522271. issn: 0145-7632.

Bensaid, S., Marchisio, D.L., Fino, D., 2010. Numerical simulation of soot filtration and combustion within diesel particulate filters. Chem. Eng. Sci. 65, 357–363. https://doi.org/10.1016/j.ces.2009.06.051.

Beresnev, S.A., Chernyak, V.G., Fomyagin, G.A., 1990. Motion of a spherical particle in a rarefied gas. Part 2. Drag and thermal polarization. J. Fluid Mech. 219, 405–421. https://doi.org/10.1017/S0022112090003007.

Bhatnagar, P.L., Gross, E.P., Krook, M., 1954. A model for collision processes in gases. i. Small amplitude processes in charged and neutral one-component systems. Phys. Rev. 94 (3), 511–525. https://doi.org/10.1103/PhysRev.94.511.

Bird, G.A., 1994. Molecular Gas Dynamics and Direct Simulation of Gas Flow. Oxford University Press, London.

Bird, G.A., 2013. The DSMC Method. CreateSpace Independent Publishing Platform. issn: 978-1492112907.

Bond, T.C., Doherty, S.J., Fahey, D.W., Forster, P.M., Berntsen, T., DeAngelo, B.J., Flanner, M.G., Ghan, S., et al., 2013. Bounding the role of black carbon in the climate system: a scientific assessment. J. Geophys. Res.: Atmospheres 118 (11), 5380–5552. https://doi.org/10.1002/jgrd.50171.

Brady, J.F., Bossis, G., 1988. Stokesian dynamics. Annu. Rev. Fluid Mech. 20 (1), 111–157. https://doi.org/10.1146/annurev.fl.20.010188.000551.

Breugem, W.-P., 2012. A second-order accurate immersed boundary method for fully resolved simulations of particle-laden flows. J. Comput. Phys. 231 (13), 4469–4498. https://doi.org/10.1016/j.jcp.2012.02.026. issn: 0021-9991.

Bunde, A., Caro, J., Kärger, J., Vogl, G., 2018. Diffusive Spreading in Nature, Technology and Society. Springer International Publishing AG, Cham, Switzerland, isbn: 978-3-319-67797-2. doi: 10.1007/978-3-319-67798-9.

Cercignani, C., 2000. Rarefied Gas Dynamics: From Basic Concepts to Actual Calculations. Cambridge University Press. issn: 9780521659925.

Cercignani, C., Pagani, C.D., Bassanini, P., 1968. Flow of a rarefied gas past an axisymmetric body. ii. Case of a sphere. Phys. Fluids 11 (7), 1399–1403. https://doi.org/10.1063/1.1692121.

Cercignani, C., Pagani, C.D., 1968. Flow of a rarefied gas past an axisymmetric body. i. General remarks. Phys. Fluids 11 (7), 1395–1399. https://doi.org/10.1063/1.1692120.

Chandrasekhar, S., 1943. Stochastic problems in physics and astronomy. Rev. Mod. Phys. 15 (1), 1–89. https://doi.org/10.1103/RevModPhys.15.1.

Corson, J., Mulholland, G.W., Zachariah, M.R., 2017. Friction factor for aerosol fractal aggregates over the entire knudsen range. Phys. Rev. E 95 (1), 013–103. https://doi.org/10.1103/PhysRevE.95.013103.

Corson, J., Mulholland, G.W., Zachariah, M.R., 2018. Hydrodynamic interactions between aerosol particles in the transition regime. J. Fluid Mech. 855, 535–553.

Cunningham, E., 1910. On, the velocity of steady fall of spherical particles through fluid medium. Proc. R. Soc. Lond. Ser. A 83 (563), 357–365.

Davies, C.N., 1945. Definitive equations for the fluid resistance of spheres. Proc. Phys. Soc. 57 (4), 259.

Doormaal, J.P.V., Raithby, G.D., 1984. Enhancements of the simple method for predicting incompressible fluid flows. Numer. Heat Transfer 7 (2), 147–163. https://doi.org/10.1080/01495728408961817.

Einstein, A., 1905. Über die von der molekularkinetischen theorie der wärme geforderte bewegung von in ruhenden flüssigkeiten suspendierten teilchen. Annalen der Physik 322 (8), 549–560. https://doi.org/10.1002/andp.19053220806.

Epstein, P.S., 1924. On the resistance experienced by spheres in their motion through gases. Phys. Rev. 23 (6), 710–733. https://doi.org/10.1103/PhysRev.23.710.

Ermak, D.L., McCammon, J.A., 1978. Brownian dynamics with hydrodynamic interactions. J. Chem. Phys. 69 (4), 1352–1360. https://doi.org/10.1063/1.436761. issn: 0021-9606.

Español, P., Warren, P., 1995. Statistical mechanics of dissipative particle dynamics. EPL (Europhysics Letters) 30 (4), 191. issn: 0295-5075.

Gad-El-Hak, M., 2006. Gas and liquid transport at the microscale. Heat Transfer Eng. 27 (4), 13–29. https://doi.org/10.1080/01457630500522305. issn: 0145-7632.

Gopalakrishnan, R., Thajudeen, T., Hogan, C.J., 2011. Collision limited reaction rates for arbitrarily shaped particles across the entire diffusive knudsen number range. J. Chem. Phys. 135 (5), 054–302. https://doi.org/10.1063/1.3617251.

Gopinath, A., Koch, D.L., 1999. Hydrodynamic interactions between two equal spheres in a highly rarefied gas. Phys. Fluids 11 (9), 2772–2787. https://doi.org/10.1063/1.870136.

Groot, R.D., Warren, P.B., 1997. Dissipative particle dynamics: Bridging the gap between atomistic and mesoscopic simulation. J. Chem. Phys. 107 (11), 4423–4435. https://doi.org/10.1063/1.474784. issn: 0021-9606.

Hauge, E.H., Martin-Löf, A., 1973. Fluctuating hydrodynamics and brownian motion. J. Stat. Phys. 7 (3), 259–281. https://doi.org/10.1007/BF01030307. issn: 1572-9613.

Hinch, E.J., 1975. Application of the langevin equation to fluid suspensions. J. Fluid Mech. 72 (3), 499–511. https://doi.org/10.1017/S0022112075003102.

Hocking, L., 1973. The effect of slip on the motion of a sphere close to a wall and of two adjacent spheres. J. Eng. Math. 7, 207–221.

Huang, K., Chavez, I., Taute, K.M., Lukić, B., Jeney, S., Raizen, M.G., Florin, E.-L., 2011. Direct observation of the full transition from ballistic to diffusive brownian motion in a liquid. Nat. Phys. 7, 576. https://doi.org/10.1038/nphys1953.

Hubbard, J.B., Douglas, J.F., 1993. Hydrodynamic friction of arbitrarily shaped brownian particles. Phys. Rev. E 47 (5), R2983–R2986. https://doi.org/10.1103/PhysRevE.47.R2983.

Itô, K., 1973. Stochastic integration. Academic Press, pp. 141–148. https://doi.org/10.1016/B978-0-12-702450-9.50020-8. issn: 978-0-12-702450-9.

Jiang, H., Li, T., Wang, Y., He, P., Wang, B., 2019. The evolution of soot morphology and nanostructure along axial direction in diesel spray jet flames. Combust. Flame 199, 204–212. https://doi.org/10.1016/j.combustflame.2018.10.030. issn: 0010-2180.

Kishore, N., Ramteke, R.R., 2016. Forced convective heat transfer from spheres to newtonian fluids in steady axisymmetric flow regime with velocity slip at fluid-solid interface. Int. J. Therm. Sci. 105, 206–217. https://doi.org/10.1016/j.ijthermalsci.2016.03.009.

Kittelson, D., 1998. Engines and nanoparticles: a review. J. Aerosol Sci. 29 (5–6), 575–588. https://doi.org/10.1016/S0021-8502(97)10037-4.

Konstandopoulos, A.G., Papaioannou, E., 2008. Update on the science and technology of diesel particulate filters. Kona Powder Part. J. 26, 36–65. https://doi.org/10.14356/kona.2008007.

Kostoglou, M., Housiada, P., Konstandopoulos, A.G., 2003. Multi-channel simulation of regeneration in honeycomb monolithic diesel particulate filters. Chem. Eng. Sci. 58, 3273–3283. https://doi.org/10.1016/S0009-2509(03)00178-7.

Köylü, Ü.Ö., Faeth, G.M., Farias, T.L., Carvalho, M.D.G., 1995. Fractal and projected structure properties of soot aggregates. Combust. Flame 100 (4), 621–633. https://doi.org/10.1016/0010-2180(94)00147-K. issn: 010-2180.

Kruis, F.E., Fissan, H., Peled, A., 1998. Synthesis of nanoparticles in the gas phase for electronic, optical and magnetic applications – a review. J. Aerosol Sci. 29, 511–535.

La Torre, F., Kenjereš, S., Moerel, J.L., Kleijn, C.R., 2011. Hybrid simulations of rarefied supersonic gas flows in micro-nozzles. Comput. Fluids 49 (1), 312–322. https://doi.org/10.1016/j.compfluid.2011.06.008. issn: 0045-7930.

Landau, L.D., Lifshitz, E.M., 1987. Chapter vi – Diffusion. In: Fluid Mechanics. second ed. Pergamon, pp. 227–237. https://doi.org/10.1016/B978-0-08-033933-7.50014-3. issn: 978-0-08-033933-7.

Langevin, P., 1908. Sur la théorie du mouvement brownien. C. R. Acad. Sci. (Paris) 146, 530–533. https://doi.org/10.1119/1.18725.

Le Tallec, P., Mallinger, F., 1997. Coupling boltzmann and navier–stokes equations by half fluxes. J. Comput. Phys. 136 (1), 51–67. https://doi.org/10.1006/jcph.1997.5729. issn: 0021-9991.

Mark, A., Rundqvist, R., Edelvik, F., 2011. Comparison between different immersed boundary conditions for simulation of complex fluid flows. Fluid Dyn. Mater. Process. 7, 241–258. https://doi.org/10.3970/fdmp.2011.007.241.

Mark, A., Svenning, E., Edelvik, F., 2013. An immersed boundary method for simulation of flow with heat transfer. Int. J. Heat Mass Transf. 56 (1), 424–435. https://doi.org/10.1016/j.ijheatmasstransfer.2012.09.010. issn: 0017-9310.

Mark, A., van Wachem, B.G.M., 2008. Derivation and validation of a novel implicit second-order accurate immersed boundary method. J. Comput. Phys. 227 (13), 6660–6680. https://doi.org/10.1016/j.jcp.2008.03.031. issn: 0021-9991.

Martirosyan, K.S., Chen, K., Luss, D., 2010. Behavior features of soot combustion in diesel particulate filter. Chem. Eng. Sci. 65, 42–46. https://doi.org/10.1016/j.ces.2009.01.058.

Matsuoka, Y., Fukasawa, T., Higashitani, K., Yamamoto, R., 2012. Effect of hydrodynamic interactions on rapid brownian coagulation of colloidal dispersions. Phys. Rev. E 86 (5), 051403. https://doi.org/10.1103/PhysRevE.86.051403.

Maxey, M.R., Riley, J.J., 1983. Equation of motion for a small rigid sphere in a nonuniform flow. Phys. Fluids 26 (4), 883–889. https://doi.org/10.1063/1.864230. issn: 0031-9171.

Millikan, R.A., 1911. The isolation of an ion, a precision measurement of its charge, and the correction of stokes's law. Phys. Rev. (Series I) 32 (4), 349–397. https://doi.org/10.1103/PhysRevSeriesI.32.349.

Mittal, R., Iaccarino, G., 2005. Immersed boundary methods. Annu. Rev. Fluid Mech. 37 (1), 239–261. https://doi.org/10.1146/annurev.fluid.37.061903.175743.

Mountain, R.D., Mulholland, G.W., Baum, H., 1986. Simulation of aerosol agglomeration in the free molecular and continuum flow regimes. J. Colloid Interface Sci. 114 (1), 67–81. https://doi.org/10.1016/0021-9797(86)90241-9. issn: 0021-9797.

Mueller, R., Mädler, L., Pratsinis, S.E., 2003. Nanoparticle synthesis at high production rates by flame spray pyrolysis. Chem. Eng. Sci. 58, 1969–1976.

Naumov, M., Arsaev, M., Castonguay, P., Cohen, J., Demouth, J., Eaton, J., Layton, S., Markovskiy, N., Reguly, I., Sakharnykh, N., Sellappan, V., Strzodka, R., 2015. Amgx: a library for gpu accelerated algebraic multigrid and preconditioned iterative methods. SIAM J. Sci. Comput. 37 (5), S602–S626. https://doi.org/10.1137/140980260.

Newmark, N.M., 1959. A method of computation for structural dynamics. J. Eng. Mech. Div. 85 (3), 67–94.

Noetinger, B., 1990. Fluctuating hydrodynamics and brownian motion. Phys. A: Stat. Mech. Appl. 163 (2), 545–558. https://doi.org/10.1016/0378-4371(90)90144-H. issn: 0378-4371.

Osseiran, N., Chriscaden, K., Press Release, 2016. [Online]. Available: <http://www.who.int/newsroom/detail/12-05-2016-air-pollution-levels-rising-in-many-of-the-world-s-poorestcities>.

Ounis, H., Ahmadi, G., 1990. Analysis of dispersion of small spherical particles in a random velocity field. J. Fluids Eng. 112 (1), 114–120. https://doi.org/10.1115/1.2909358. issn: 0098-2202.

Ounis, H., Ahmadi, G., 1990. A comparison of brownian and turbulent diffusion. Aerosol Sci. Technol. 13 (1), 47–53. https://doi.org/10.1080/02786829008959423. issn: 0278-6826.

Park, M., Joo, H.S., Lee, K., Jang, M., Kim, S.D., Kim, I., Borlaza, L.J.S., Lim, H., Shin, H., Chung, K.H., Choi, Y.H., 2018. Differential toxicities of fine particulate matters from various sources. Sci. Rep. 8, 1–11.

Peskin, C.S., 1982. The fluid dynamics of heart valves: experimental, theoretical, and computational methods. Annu. Rev. Fluid Mech. 14 (1), 235–259. https://doi.org/10.1146/annurev.fl.14.010182.001315.

Popov, S.P., Tcheremissine, F.G., 2005. A method of joint solution of the boltzmann and navier–stokes equations. AIP Conf. Proc. 762 (1), 82–87. https://doi.org/10.1063/1.1941518. issn: 0094-243X.

Rahman, A., 1964. Correlations in the motion of atoms in liquid argon. Phys. Rev. 136 (2A), A405–A411. https://doi.org/10.1103/PhysRev.136.A405.

Rhie, C.M., Chow, W.L., 1983. Numerical study of the turbulent flow past an airfoil with trailing edge separation. AIAA J. 21 (11), 1525–1532. https://doi.org/10.2514/3.8284.

Rogak, S.N., Flagan, R.C., Nguyen, H.V., 1993. The mobility and structure of aerosol agglomerates. Aerosol Sci. Technol. 18 (1), 25–47. https://doi.org/10.1080/02786829308959582.

Roveda, R., Goldstein, D.B., Varghese, P.L., 2000. Hybrid euler/direct simulation monte carlo calculation of unsteady slit flow. J. Spacecraft Rockets 37 (6), 753–760. https://doi.org/10.2514/2.3647. issn: 0022-4650.

Rovenskaya, O., Croce, G., 2014. Application a hybrid solver to gas flow through a slit at arbitrary pressure ratio. Vacuum 109, 266–274. https://doi.org/10.1016/j.vacuum.2014.04.018. issn: 0042-207X.

Rovenskaya, O.I., Croce, G., 2016. Numerical simulation of gas flow in rough microchannels: hybrid kinetic–continuum approach versus navier–stokes. Microfluidics Nanofluidics 20 (5), 81. https://doi.org/10.1007/s10404-016-1746-x. issn: 1613-4990.

Sarli, V.D., Benedetto, A.D., 2015. Modeling and simulation of soot combustion dynamics in a catalytic diesel particulate filter. Chem. Eng. Sci. 137, 69–78. https://doi.org/10.1016/j.ces.2015.06.011.

Scanlon, T.J., Roohi, E., White, C., Darbandi, M., Reese, J.M., 2010. An open source, parallel dsmc code for rarefied gas flows in arbitrary geometries. Comput. Fluids 39 (10), 2078–2089. https://doi.org/10.1016/j.compfluid.2010.07.014. issn: 0045-7930.

Schwartzentruber, T.E., Boyd, I.D., 2006. A hybrid particle-continuum method applied to shock waves. J. Comput. Phys. 215 (2), 402–416. https://doi.org/10.1016/j.jcp.2005.10.023. issn: 0021-9991.

Simo, J.C., Wong, K.K., 1991. Unconditionally stable algorithms for rigid body dynamics that exactly preserve energy and momentum. Int. J. Numer. Meth. Eng. 31 (1), 19–52. https://doi.org/10.1002/nme.1620310103.

Sitarski, M., Seinfeld, J.H., 1977. Brownian coagulation in the transition regime. J. Colloid Interface Sci. 61 (2), 261–271. https://doi.org/10.1016/0021-9797(77)90389-7. issn: 0021-9797.

Sjöblom, J., Ström, H., Kannan, A.S., Ojagh, H., 2014. Experimental validation of particulate matter (pm) capture in open substrates. Ind. Eng. Chem. Res. 53 (9), 3749–3752. https://doi.org/10.1021/ie404046y.

Skorupski, K., Mroczka, J., Wriedt, T., Riefler, N., 2014. A fast and accurate implementation of tunable algorithms used for generation of fractal-like aggregate models. Phys. A: Stat. Mech. Appl. 404, 106–117. issn: 0378-4371.

Sone, Y., Aoki, K., 1977. Forces on a spherical particle in a slightly rarefied gas. In: Rarefied gas dynamics; International Symposium, 10th, Aspen, Colo., July 18–23, 1976, Technical Papers. Part 1. (A77-36459 16-34) New York, American Institute of Aeronautics and Astronautics, Inc., pp. 417–433.

Sorensen, C.M., Hageman, W.B., Rush, T.J., Huang, H., Oh, C., 1998. Aerogelation in a flame soot aerosol. Phys. Rev. Lett. 80 (8), 1782–1785. https://doi.org/10.1103/PhysRevLett.80.1782.

Stark, W.J., Pratsinis, S.E., 2002. Aerosol flame reactors for manufacture of nanoparticles. Powder Technol. 126 (2), 103–108. https://doi.org/10.1016/S0032-5910(02)00077-3. issn: 0032-5910.

Stefanov, S., 2011. On dsmc calculations of rarefied gas flows with small number of particles in cells. SIAM J. Sci. Comput. 33 (2), 677–702. https://doi.org/10.1137/090751864. issn: 1064-8275.

Stokes, G.G., 1848. On the steady motion of incompressible fluids. Trans. Cambridge Philos. Soc. 7, 439.

Ström, H., Sasic, S., Andersson, B., 2011. A novel multiphase dns approach for handling solid particles in a rarefied gas. Int. J. Multiph. Flow 37, 906–918.

Torquato, S., Avellaneda, M., 1991. Diffusion and reaction in heterogeneous media: pore size distribution, relaxation times, and mean survival time, English (US). J. Chem. Phys. 95 (9), 6477–6489. issn: 0021-9606.

Tripathi, G., Dhar, A., Sadiki, A., 2018. Recent advancements in after-treatment technology for internal combustion engines — an overview. In: Advances in Internal Combustion Engine Research. Springer, pp. 159–179. https://doi.org/10.1007/978-981-10-7575-9_8.

Uhlenbeck, G.E., Ornstein, L.S., 1930. On the theory of the brownian motion. Phys. Rev. 36 (5), 823–841. https://doi.org/10.1103/PhysRev.36.823.

Uhlmann, M., 2005. An immersed boundary method with direct forcing for the simulation of particulate flows. J. Comput. Phys. 209 (2), 448–476. https://doi.org/10.1016/j.jcp.2005.03.017. issn: 0021-9991.

von Smoluchowski, M., 1906. Zur kinetischen theorie der brownschen molekularbewegung und der suspensionen. Annalen der Physik 326 (14), 756–780. https://doi.org/10.1002/andp.19063261405.28. issn: 0003-3804.

Wegner, K., Pratsinis, S., 2003. Scale-up of nanoparticle synthesis in diffusion flame reactors. Chem. Eng. Sci. 58, 4581–4589.

Welander, P. On the temperature jump in a rarefied gas. Arkiv Fysik.

Wijesinghe, H.S., Hornung, R.D., Garcia, A.L., Hadjiconstantinou, N.G., 2004. Three-dimensional hybrid continuum-atomistic simulations for multiscale hydrodynamics. J. Fluids Eng. 126 (5), 768–777. https://doi.org/10.1115/1.1792275. issn: 0098-2202.

Yamamoto, K., Sera, K., 1985. Flow of a rarefied gas past a circular cylinder. Phys. Fluids 28 (5), 1286–1293. https://doi.org/10.1063/1.865012.

Yang, J., Stewart, M., Maupin, G., Herling, D., Zelenyuk, A., 2009. Single wall diesel particulate filter (dpf) filtration efficiency studies using laboratory generated particles. Chem. Eng. Sci. 64, 1625–1634. https://doi.org/10.1016/j.ces.2008.12.011.

Ying, R., Peters, M.H., 1989. Hydrodynamic interaction of two unequal-sized spheres in a slightly rarefied gas: resistance and mobility functions. J. Fluid Mech. 207, 353–378. https://doi.org/10.1017/S0022112089002612.

Zhang, C., Thajudeen, T., Larriba, C., Schwartzentruber, T.E., Hogan Jr., C.J., 2012. Determination of the scalar friction factor for nonspherical particles and aggregates across the entire knudsen number range by direct simulation monte carlo (dsmc). Aerosol Sci. Technol. 46 (10), 1065–1078. https://doi.org/10.1080/02786826.2012.690543.

Paper B

Assessment of hindered diffusion in arbitrary geometries using a multiphase DNS framework

Assessment of hindered diffusion in arbitrary geometries using a multiphase DNS framework

Ananda Subramani Kannan [a],[*], Andreas Mark [b], Dario Maggiolo [a], Gaetano Sardina [a], Srdjan Sasic [a], Henrik Ström [a]
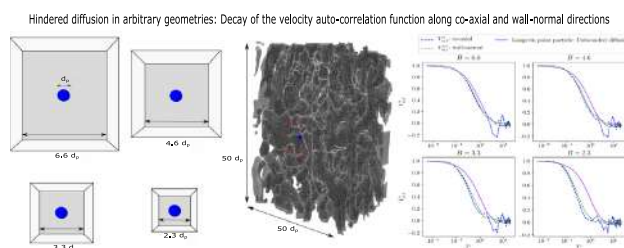
[a] *Department of Mechanics and Maritime Sciences, Division of Fluid Dynamics, Chalmers University of Technology, Göteborg 412 96, Sweden*
[b] *Fraunhofer-Chalmers Research Centre, Göteborg 412 88, Sweden*

HIGHLIGHTS

- A Langevin-multiphase DNS framework for assessing hindered diffusion.
- Basis is a two-way coupled continuum mechanics-discrete particle approach.
- Reduction in mobility estimated using instantaneous resolved particle hydrodynamics.
- Anisotropy in hydrodynamic resistances along co-axial direction of the channel.
- Particle mobility is heterogeneous and spatially dependant at sub-pore length scales.

GRAPHICAL ABSTRACT

Hindered diffusion in arbitrary geometries: Decay of the velocity auto-correlation function along co-axial and wall-normal directions

ABSTRACT

The hydrodynamics around a Brownian particle has a noticeable impact on its hindered diffusion in arbitrary geometries (such as channels/pores) due to reduced mobility close to walls. These effects are difficult to describe at sub-pore scales, wherein a complete analytical solution of the underlying hydrodynamics is challenging to obtain. Here, we propose a coupled Langevin-multiphase direct numerical simulation (DNS) framework, that fully resolves the hydrodynamics in such systems and consequently provides an on-the-fly capability to probe local instantaneous particle diffusivities.

We validate and establish the capabilities of this framework in square micro-channels (under varying degrees of hydrodynamic confinement) and in an arbitrary pore. Our results show that directional variations in mean-squared displacements, velocity auto-correlation functions and diffusivities of the Brownian particle, due to inherent asymmetries in the geometry are adequately captured. Further, a local anisotropy in the hydrodynamic resistances along the co-axial direction of the channel is also noted.

© 2020 Elsevier Ltd. All rights reserved.

1. Introduction

Hindered diffusion of Brownian particles within confined geometries, such as micro-channels or any other micro-porous materials, is of joint interest to several nano-engineering driven applications. A few typical examples include membrane transport of flexible macro-molecules (Davidson and Deen, 1988), entrapment of nano-sized particles (such as combustion generated debris) in filters used for the after-treatment of automotive exhausts (Kostoglou et al., 2003; Konstandopoulos and Papaioannou, 2008; Di Sarli and Di Benedetto, 2015), catalyst coating of the porous

---

* Corresponding author.
   E-mail address: ananda@chalmers.se (A.S. Kannan).

walls of such filters starting from colloidal suspension of nano-sized (catalyst) particles (Di Sarli et al., 2016), nanoelectrofuel consisting of a colloidal suspension of electro-active nanoparticles in redox flow batteries (Sokolov et al., 2016), nanofluids or engineered nanoparticle colloidal dispersions that are used as heat transfer fluids in micro-electronics (Sharaf et al., 2019), mixing and interface modulation in nanoparticle nucleation and growth processes (Zhang et al., 2018; Nashed et al., 2018; Strom et al., 2018), novel bio-engineering applications involving transport of magnetized nano-particles in lab-on-a-chip devices (Van Ommering et al., 2006; Derks et al., 2008; Van Ommering et al., 2009) and surface-based biosensors (Katelhon et al., 2016; Squires et al., 2008). In all these cases, nanoparticles have to diffuse in the vicinity of a wall, meaning that multiple effects (both molecular and hydrodynamic in nature) compete for dominance in governing the inherent transport. This type of micro-transport warrants some attention particularly as deeper insights into the inherent phenomena would aid in improving the performance of important existing and emerging technologies.

The dynamics of Brownian particles close to a wall are significantly affected by wall interactions. When a rigid particle approaches within a few radii from the wall, its mobility (i.e. ratio of the particle terminal velocity and hydrodynamic frictional force) is reduced owing to the additional drag of the displaced fluid on the wall (Lorentz, 1907; Pagac et al., 1996). This increase in drag is attributed to the alteration of the hydrodynamic interaction between the particle and the fluid generated by the boundaries. Independent measurements of the mobility and diffusion coefficient as well as theory have indicated that the latter are corrected by the same factor λ (Brenner, 1961; Frej and Prieve, 1993; Pagac et al., 1996), implying that these quantities are functions of the radial position of the Brownian particle in relation to the boundary walls. Direct measurements of such hindered Brownian motion were first reported by MacKay and Mason (1961) and further confirmed by Biondi and Quinn (1995) and Lobry and Ostrowsky (1996) using advanced particle tracking techniques. These studies noted that the particle motion becomes anisotropic due to the imbalance between the drag force parallel to the wall and that perpendicular to it, with the former typically lesser than the latter. More recent studies affirm these findings (Banerjee and Kihm, 2005; Bevan and Prieve, 2000; Gentile et al., 2015; Skaug et al., 2015; Choi et al., 1961; Mo et al., 2015; Sharma et al., 2010). Among these studies, Kihm and co-workers (Kihm et al., 2004) further validated that the reduction in mobility by the factor λ is well described by the analytical theories of Brenner (1961), Goldman et al. (1967). Additionally, Gentile et al. (2015) evaluated the spatial dependence of mobility in square micro-channels using confocal particle tracking to measure the local diffusion co-efficients. Most recently, Skaug et al. (2015) have reaffirmed the significant hydrodynamic damping of nanoparticle motion at sub-pore length scales, using single-particle tracking experiments that followed the pore-scale diffusion of individual nanoparticles, within a three-dimensional porous material of moderate porosity. Consequently, the mobility of the particle is heterogeneous and spatially dependent.

Experimental measurements in such highly confined Brownian systems are challenging due to the inherent difficulties with accurate measurements of local diffusion coefficients at these scales, as well as difficulties in ensuring proper access for the measurement techniques under such confinements. Thus, numerical modelling can offer a more tractable alternative for probing and understanding these complex systems. Historically, the problem of hindered diffusion has been approached from two opposing perspectives, i.e. building up from kinetic theory (in this case for pair-wise diffusion (Cukier et al., 1978; Cukier et al., 1981)) or projecting down from macroscopic hydrodynamics (Lorentz, 1907; Faxen, 1921;

Faxen, 1927; Brenner and Gaydos, 1977; Mavrovouniotis and Brenner, 1988; Felderhof, 2005; Mo et al., 2015; Michaelides, 2016), with varying degrees of success. The former has had limited success at high fluid packing densities, largely because of the complexity of molecular motions in dense fluids, while the latter overlooks details of the molecular nature of the surrounding fluid while predicting the diffusion behavior, as these are averaged out in the continuum description. Despite these shortcomings, the hydrodynamic approach has been the preferred choice when studying confinement effects on Brownian motion due to a relative ease in formulation.

The motion of a small sphere in a bounded viscous fluid is a well-studied problem. An overview of most analytical/theoretical developments including the relevant hydrodynamic expressions for the reduction in mobility (λ) can be found in the classical books of Happel and Brenner (1983) and Kim and Karrila (1991). The results from these analytical developments were extended to Brownian motion in a circular cylinder by Brenner and Gaydos (1977) and further towards cylindrical pores by Mavrovouniotis and Brenner (1988) and Nitsche and Balgi (1994, 1995). These authors proposed a general theory for calculating the hindered diffusion of Brownian particles within straight pores (of arbitrary cross section). A more detailed account of related hindered diffusion theories for Brownian motion are available in the reviews by Deen (1987), Burada et al. (2009), Radhakrishnan et al. (2019) and Mo and Raizen (2019). We have further listed some of the commonly used analytical expressions for λ in Table 1. It is evident from this table that expressions for the reduction in mobility (λ) are available only for simple systems, with well described solutions for the governing hydrodynamics. This is a consequence of the creeping flow assumption in these analytical descriptions, that linearizes the governing Navier–Stokes equations into the well described Stokes equations (Happel and Brenner, 1983; Kim and Karrila, 1991). Solutions to this equation system are further simplified under ideal conditions, such as for e.g. a spherical Brownian particle at the center-line of a cylindrical pore, due to symmetry considerations. This solution procedure gets progressively elaborate (in a mathematical sense) when describing asymmetrical particles (such as nanofibers, nanorods, nanosheets, nanowires or nanotubes (Zhang et al., 2018; Nashed et al., 2018)) and/or channels such as nanoparticle transport within an arbitrary pore. This is due to the direct dependence of the morphology (including shape, size and structure/composition.) of the particle on its corresponding hydrodynamic interaction (Kim and Karrila, 1991; Happel and Brenner, 1983). There is hence a perceived need for a tractable numerical method that can evaluate hindered diffusion of asymmetric mythologies in more arbitrary geometries.

Several recent studies have extended the conventional numerical modelling of hindered diffusion (Gentile et al., 2015; Goswami et al., 2020; Michaelides, 2017, 2019; Ramakrishnan et al., 2017; Sharaf et al., 2019; Simha et al., 2018; Uma et al., 2011; Andarwa et al., 2014; Felderhof, 2005; Imperio et al., 2011; Mo et al., 2015; Vitoshkin et al., 2016). These studies include computational methods that span many different scales, from rigorous direct simulations at a micro-scale, using multi-particle collision dynamics (MPCD) (Imperio et al., 2011), dissipative particle dynamics (DPD) (Español and Warren, 2017; Gubbiotti et al., 2019) and Monte-Carlo (Bird, 1994; Bird, 2013) methods (Berry and Chate, 2014; Michaelides, 2017; Goswami et al., 2020) coupled with a Langevin equation, to meso-scale simulations using the fluctuating lattice-Boltzmann equation (Ladd, 1994a; Ladd, 1994b; Mynam et al., 2011; Liu et al., 2019), and finally to more coarse-grained random-walk based approaches (Hlushkou et al., 2017; Katelhon et al., 2016; Sokolov et al., 2016; Eloul et al., 2015) and continuum based treatments such as fluctuating hydrodynamics (Uma et al., 2011; Vitoshkin et al., 2016; Ramakrishnan et al., 2017; Li et al.,

Table 1
Some reported correlations for the mobility correction factor λ for a spherical particle under creeping flow conditions.

Reference	Condition	Correlation for λ
Lorentz (1907)	Brownian sphere near a wall	$\begin{cases} \frac{1}{1-\frac{9r_p}{16h}} & \text{for } \parallel \text{ motion} \\ \frac{1}{1-\frac{9r_p}{8h}} & \text{for } \perp \text{ motion} \end{cases}$
Faxen (1927)	Motion of a sphere parallel to two plane walls	$\frac{1}{1-1.004(r_p/h)+0.418(r_p/h)^3+0.21(r_p/h)^4-0.169(r_p/h)^5}$
Wakiya (1953)	Motion of confined moving sphere in a circular pipe	$\frac{1}{\left(1-2.104\frac{r_p}{a}+2.09\frac{r_p^3}{a^3}-0.95\frac{r_p^5}{a^5}\right)}$
Haberman and Sayre (1958)	Axisymmetric flow past a confined sphere circular pipe	$\frac{\left(1-0.75857\frac{r_p^5}{r_p^5}\right)}{\left(1-2.1050\frac{a}{r_p}+2.0865\frac{a^3}{r_p^3}-1.7068\frac{a^5}{r_p^5}+0.72603\frac{a^6}{r_p^6}\right)}$.
Brenner (1961)	Sphere moving perpendicular to a plane wall	$\frac{4}{3}\sinh\alpha\sum_{n=1}^{\infty}\frac{n(n+1)}{(2n-1)(2n+3)}\left[\frac{2\sinh(2n+1)\alpha+(2n+1)\sinh 2\alpha}{4\sinh^2\left(n+\frac{1}{2}\right)\alpha-(2n+1)^2\sinh^2\alpha}-1\right]$ with $\alpha=\cosh^{-1}(h/r_p)$
Goldman et al. (1967)	Sphere moving perpendicular to a plane wall	$\begin{cases} \frac{6h^2+9r_ph+2r_p^2}{6h^2+2r_ph} & \text{for } h \geqslant 0 \\ 0 & \text{for } h < 0 \end{cases}$
Brenner and Gaydos (1977)	Brownian sphere diffusing within a long circular cylindrical pore	$(1-\frac{r_p}{a})^{-2}\left[1+(\frac{9}{8})(\frac{r_p}{a})\ln(\frac{r_p}{a})-1.539\frac{r_p}{a}\right]$
Mavrovouniotis and Brenner (1988)	Brownian sphere within circular cylindrical pore (including axial dispersion)	$(1-\frac{r_p}{a})^{-2}\left[1+(\frac{9}{8})(\frac{r_p}{a})\ln(\frac{r_p}{a})-1.539\frac{r_p}{a}\right]+$ $(1-\frac{r_p}{a})^{-6}(\frac{r_p}{a})^2\left[0.158\ln^2(\frac{r_p}{a})^{-1}-0.901\ln(\frac{r_p}{a})+1.385\right]$ for $(\frac{r_p}{a}) \ll 1$
Nitsche and Balgi (1994)	Brownian sphere within a circular cylindrical pore	$(1-\frac{r_p}{a})^{-2}\left[1+(\frac{9}{8})(\frac{r_p}{a})\ln(\frac{r_p}{a})-1.539\frac{r_p}{a}+1.2(\frac{r_p}{a})^2\right]$
Dechadilok and Deen (2006)	Brownian sphere within a circular cylindrical pore	$1+\frac{9}{8}\frac{r_p}{a}\ln\frac{r_p}{a}-1.56034\frac{r_p}{a}+0.528155(\frac{r_p}{a})^2+1.91521(\frac{r_p}{a})^3-2.81903(\frac{r_p}{a})^4$ $+0.270788(\frac{r_p}{a})^5+1.10115(\frac{r_p}{a})^6-0.435933(\frac{r_p}{a})^7$
Michaelides (2017)	Brownian sphere within a circular cylindrical pore	$\left\{1-2.3573(\frac{r_p}{a})^{0.603}\right\}\left[0.225\ln(\frac{r_p}{1nm})+0.217\right]$ for $5 < \frac{r_p}{a} < 140$ and $3\,nm < r_p < 100\,nm$

r_p is the radius of the particle.
h is the distance between the two plane walls.
a is the radius of the circular channel/pore.

2020). Some of these continuum treatments approximate analytical solutions to the governing Navier–Stokes equations using the point-particle approximation (Felderhof, 2005; Mo et al., 2015; Simha et al., 2018; Mo and Raizen, 2019), matched asymptotic expansions (O'Neill and Stewartson, 1967) or the method of reflections (Happel and Brenner, 1983), to name a few. Others, such as the fluctuating hydrodynamics approach, include stochastic components in the fluid stress tensor such that the fluctuation–dissipation theorem is satisfied (Hauge and Martin-Löf, 1973; Landau and Lifshitz, 1987; Noetinger, 1990; Espanol, 1998; Uma et al., 2011; Vitoshkin et al., 2016; Ramakrishnan et al., 2017; Li et al., 2020). An alternate continuum based approach was used by Gentile et al. (2015), wherein the resistance tensor of a spherical particle was determined a priori from the Stokes equations of the surrounding flow, and this tensor was used to evaluate the local diffusion tensor using the Stokes–Einstein relation. The rigorous microscale studies are limited by the simplicity and physical scale of the assessment i.e. only simplified geometries at scales relative to the mean free path of the surrounding fluid can be assessed, while the more coarse-grained and continuum based approaches are restricted by the availability of valid expressions for the hydrodynamic mobility in more arbitrary geometries. Moreover, they are computationally expensive as well.

Thus, among these reported frameworks, DPD coupled with a Langevin equation, meso-scale and continuum-based multiphase direct numerical simulations (or DNS) including fluctuating hydrodynamics, that can simultaneously account for both the particle dynamics via a solution to the equation of particle transport and the fluid hydrodynamics via a solution to governing fluid equations along with the accompanying interactions, have the potential to model confinement effects in arbitrary geometries. Amongst these, the fluctuating hydrodynamics approach is extensively involved and challenging to implement (Bell et al., 2007). The continuum-based approaches, which do not employ the fluctuating Navier–Stokes equation, incorporate molecular effects on the particle

dynamics as a stochastic noise in the particle equation of motion, as shown by Ahmadi and co-workers (Ounis and Ahmadi, 1990a; Ounis and Ahmadi, 1990b; Li and Ahmadi, 1992). A similar approach is also followed in the meso-scale treatments where a fluctuating Boltzmann equation is solved in conjunction with the Langevin equation (Ladd, 1994a; Ladd, 1994a). These meso- and continuum-based DNS approaches can be designed to be two-way coupled where the particle effects on the fluid are inherently incorporated. However, the point-particle assumption (that the particles are assumed to have negligible volume but finite mass), which is central to these numerical treatments, limits their application to systems where the fluid hydrodynamics around the particle need not be fully resolved but can instead be modelled.

From this overview it is evident that both numerical and experimental studies that extend beyond simple confining geometries are scarce. Exact solutions are available for only the simplest of systems (see Table 1). Rigorous descriptions of these systems require both a resolution of the near and far-field hydrodynamic interactions and the accompanying Brownian motion, necessitating elaborate mathematical treatments. In addition, the inherent pore-scale heterogeneity of many natural and synthetic porous materials increases the difficulty in modeling sub-porous Brownian diffusion particularly as the underlying microscopic processes are often poorly understood. Some of these difficulties were overcome by Michaelides (2017), Michaelides (2019) by coupling a Lagrangian description of the Brownian motion with a microscale resolution of the fluid (using Monte Carlo methods). However, this framework cannot account for the presence of other particles in the computational domain, meaning that it is applicable to dilute particle–fluid systems (Michaelides, 2017). More recently, Gubbioti and co-workers used DPD to account for a spatially dependent mobility field determined a priori. This field was solved in conjunction with a rigid body Langevin equation (Gubbioti et al., 2019; Lau et al., 2007) to assess hindered diffusion. This method is perfectly suited for studying pore scale diffusion in sym-

metric pores, however the a priori determination of the mobility field gets progressively harder in heterogeneous pores, limiting its applicability. Thus, multiphase DNS methods have the potential to handle such heterogeneous systems as they can inherently resolve particle short-range and long-range dynamics in any arbitrary geometry. Such an approach is also favorable since it is simpler to formulate and easier to implement (Michaelides, 2016). However, available methods need to be extended to also handle systems where the Brownian particle does not have negligible volume, such as a single Brownian particle in a narrow pore. Hence, an improved multiphase DNS framework that can simultaneously handle particle–fluid and fluid-particle coupling, as well as the accompanying Brownian dispersion of the particle at high solid volume fractions, would be ideally suited to describe hindered diffusion dynamics in pores.

In a previous work (Kannan et al., 2019), we have developed and validated such a DNS framework for unbounded Brownian diffusion. This was achieved by coupling a continuum-based mirroring immersed-boundary (IB) framework (Mark and van Wachem, 2008) with the Langevin description for the particle motion. We have established that continuum-based multiphase DNS frameworks can be utilized to evaluate Brownian phenomena. The aim with this paper is to extend this framework to study hindered diffusion of Brownian particles in micro-channels. The resolved hydrodynamics around the Brownian particle are used to estimate the reduction in mobility (λ), which is further used in describing the Brownian behavior of the particle through the Stokes–Einstein relation, obviating the reliance on analytical solutions for the flow. As a proof of concept, we evaluate the hindered diffusion of a single spherical Brownian nanoparticle in a square channel across different confinements. We analyse the consequences of resolving such ideal colloidal suspensions using the proposed framework and evaluate the inherent diffusion dynamics. Since in our framework a solution for the hydrodynamic mobility is intrinsically available at all regions in the domain, we further evaluate the variation in the estimated reduction in mobility λ due to the instantaneous changes in the displacement of the particle (i.e movement away from the channel center-line of symmetry). This capability to estimate λ on-the-fly is a unique feature of this framework that makes it well suited to study such localized pore diffusion behavior. The obtained results are compared with conventional hindered diffusion theories (Haberman and Sayre, 1958; Brenner and Gaydos, 1977) in order to establish their accuracy. To further demonstrate the novel capabilities of this framework, the localized diffusion of a spherical Brownian nanoparticle in an arbitrary pore is also investigated. It should be noted that the general method outlined in this work is independent of the multiphase DNS technique chosen, and the IB framework has been used as an example to demonstrate its feasibility.

This paper is organized as follows: in the succeeding section we describe our numerical framework. In Section 3 we present our results starting with a validation study of a settling sphere in a cylindrical channel (synonymous with the study undertaken by Haberman and Sayre (1958)) to evaluate the accuracy of the framework. This is followed by results of the hindered diffusion of a spherical Brownian nanoparticle under different confinements along with an account of pore-scale diffusion in an arbitrary non-uniform pore. Finally, in Section 4 we summarize some of the major highlights from this work along with prospects for further development.

2. Numerical framework

The proposed framework extends the applicability of existing multiphase DNS methods (such as the IB framework) to study

the hindered diffusion of Brownian particles. In this section, we describe this in brief within the context of coupling an existing IB framework to the conventional Langevin description of particle diffusion (Ounis and Ahmadi, 1990a; Ounis and Ahmadi, 1990b; Li and Ahmadi, 1992) including confinement/wall effects. We further include a description of the numerical setup used in this paper. For a more comprehensive review and description of this framework (including a thorough validation for unbounded Brownian diffusion), the reader is directed to our previous work (Kannan et al., 2019). It should be noted that, for the purpose of deriving and validating this method and without any loss of generality regarding the hydrodynamic interactions, we only deal with the hindered diffusion of spherical nanoparticles with high particle-to-fluid density ratios in confinement. This choice is made since we employ the standard form of the Langevin equation (Langevin, 1908; Li and Ahmadi, 1992) which is valid only under conditions of negligible fluid inertia (Hindi, 1975). We emphasize that this framework can similarly be used with the fractional form of the Langevin equation (Kubo, 1966; Mainardi et al., 2009).

2.1. Multiphase DNS framework for hindered diffusion dynamics: Langevin-Immersed Boundary method (LaIBM)

The multiphase DNS framework proposed in this paper (*LaIBM*) couples a continuum description of the surrounding fluid with a Lagrangian Langevin description of the Brownian particle. The continuum description is resolved using the immersed boundary method (IBM), which is a class of multiphase DNS techniques, that solves the governing transport equations in a non-body conforming Cartesian grid through a finite-volume discretization (Peskin, 1982; Mittal and Iaccarino, 2005). In essence, an object, around which the flow is to be studied, is immersed in a standard Cartesian flow grid and its presence is accounted for by modifying the governing Navier–Stokes equations through a boundary condition or a source term. There are several ways of accomplishing this (Mittal and Iaccarino, 2005), and in this paper we utilize the implicit forcing method, where a boundary condition is used (instead of a source term) within the discretized equations, to constrain the velocity at the IB surface so that the correct behaviour is reproduced (Mark et al., 2011; Mark and van Wachem, 2008; Kannan et al., 2019). This unique and stable second-order accurate implicitly formulated immersed-boundary condition (IBC) is central to the efficiency and accuracy of the multiphase DNS framework used in this paper. In the subsequent sections, we briefly discuss this continuum IB treatment followed by the conventional Langevin description of hindered diffusion. We then present the coupling between these two descriptions, which is the essence of *LaIBM*.

2.1.1. Continuum description of the fluid

The governing equations for the flow around the immersed boundaries are given by the following continuity and momentum equations for incompressible flows (i.e. the Navier–Stokes equations):

$$\frac{\partial u_i}{\partial x_j} = 0,$$

$$\rho_f \frac{\partial u_i}{\partial t} + \rho_f u_j \frac{\partial u_i}{\partial x_j} = -\frac{\partial p}{\partial x_i} + \frac{\partial}{\partial x_j}\left(\mu_f \frac{\partial u_i}{\partial x_j}\right) + f_i, \quad (1)$$

where f_i represents any external source term. This set of equations is solved together with the implicit Dirichlet IB condition,

$$u_i = u_i^{ib}. \quad (2)$$

Note that in this method, the coefficients obtained from the discretization of the Navier–Stokes equations are closed with a second-order accurate interpolation that arises from the IBC employed at the IB-fluid interface. A more detailed description of

the method is available in Mark et al. (2011), Mark and van Wachem (2008), Kannan et al. (2019).

The total force (acting on the IB) is given by the surface integral of the total fluid stress tensor consisting of the pressure and viscous contributions over the IB, as follows:

$$\mathbf{F_{IB}} = \int_{IB} \left(-p\delta_{ij} + \tau_{ij}\right) n_j dS = \int_{IB} \left(-p\delta_{ij} + \mu\left(\frac{\partial u_i}{\partial x_j} + \frac{\partial u_j}{\partial x_i}\right)\right) n_j dS, \quad (3)$$

and the corresponding torque on the IB is estimated using:

$$T_{IB} = \int_{IB} \mathbf{r} \times \boldsymbol{\sigma} \cdot \mathbf{n} dS. \quad (4)$$

Here, $\mathbf{r}$ is the position vector of the IB and σ is the fluid stress tensor for a surface S with normal n. In this paper, we use an in-house multiphase flow solver IPS IBOFlow (Centre, 2015), that utilizes the previously described mirroring immersed-boundary method to handle the moving particles efficiently. This solver is described in detail in our previous work (Kannan et al., 2019).

2.1.2. Langevin description of hindered diffusion

The Langevin equation (Langevin, 1908; Chandrasekhar, 1943) models particle motion as a balance between the hydrodynamic drag (included via the steady Stokes drag (Stokes, 1848)) experienced by the nanoparticle and the molecular-scale Brownian fluctuations (usually modelled as a Gaussian white noise). Unsteady effects, such as Basset history and added mass forces (Maxey and Riley, 1983), can also be included within a fractional form of the Langevin equation (Kubo, 1966; Mainardi et al., 2009) enabling its use in modeling a wider range of realistic applications. For the hindered diffusion of a particle with mass m_p and velocity $\mathbf{u_p}$ that is studied in this paper, this Langevin equation is expressed as:

$$m_p \frac{d\mathbf{u_p}}{dt} = -\gamma \mathbf{u_p}\lambda + \mathbf{F_{Brownian}}, \quad (5)$$

where γ is the Stokes friction factor (Eq. (6)) or the inverse of the mobility of the particle. In order to account for the additional hydrodynamic confinement effects (due to the presence of walls and/or other particles), this mobility is adjusted using a correction factor λ which is a function of the longitudinal distance from the bounding plane(s). The hindered diffusion theories of Brenner (1961), Brenner and Gaydos (1977), Goldman et al. (1967), Brenner (1982) can be used to provide an estimate for λ for geometrically well-defined systems (see Table 1). In this paper, we propose an on-the-fly estimation of λ, denoted henceforth as λ_{IB}, which reflects the instantaneous hydrodynamics around the particle, as will be explained in the subsequent section. The Stokes friction factor γ is defined for a fluid with the dynamic viscosity μ_f as:

$$\gamma = 3\pi\mu_f d_p, \quad (6)$$

with the relevant particle time scale given as:

$$\tau_p = \frac{m_p}{\gamma \lambda_{IB}} \quad (7)$$

The force $\mathbf{F_{Brownian}}$, which represents the Brownian fluctuations in the particle motion, is modelled as a Gaussian white noise process with the vector of spectral intensity $\mathbf{S_{ij}^n}$ given as:

$$\mathbf{S_{ij}^n} = \mathbf{S_0}\delta_{ij}, \quad (8)$$

where the vector $\mathbf{S_0}$ is a function of the directional Brownian diffusivity D_i (where i can be x, y or z) that reflects the presence of walls and/or other particles (note that the diffusion is asymmetric):

$$S_{0_i} = \frac{2\gamma^2 \lambda_{IB}^2}{\pi} D_i. \quad (9)$$

This corrected directional diffusivity (D_i) can be calculated from the balance of the thermal kinetic motion with the viscous drag force, i.e. D_∞ (or bulk diffusivity) as given by the Stokes–Einstein equation with a further reduction by λ_{IB} (in accordance with (Brenner, 1982; Pagac et al., 1996; Bevan and Prieve, 2000; MacKay and Mason, 1961; Biondi and Quinn, 1995)) to account for the confinement effects. Hence, D_i is related to the diffusivity for a freely diffusing Brownian particle as:

$$D_i = \frac{D_\infty}{\lambda_{IB}}, \quad (10)$$

leading to the general form (from (Einstein, 1905)):

$$D_i = \frac{k_B T}{\gamma \lambda_{IB}}, \quad (11)$$

where k_B and T are the Boltzmann constant and absolute temperature respectively. This Eq. (11) shows the inverse dependence of the particle diffusivity on the particle diameter. Further in Eq. (11) the directional details are confounded within λ. Thus, $\mathbf{F_{Brownian}}$ can be written as:

$$\mathbf{F_{Brownian}}(t) = m_p \mathbf{G} \sqrt{\frac{\pi \mathbf{S_0}}{\Delta t}}. \quad (12)$$

Here, $\mathbf{G}$ is a vector of normally distributed independent random numbers of zero mean and unit variance (Gaussian distribution), and Δt is the time step length during which the Brownian force is active (note that this is not necessarily the time step used in the integration of the particle equation of motion, as will be explained later).

The solution to Eq. (5), which is a stochastic differential equation (SDE), would reproduce the analytical diffusive behaviour for confined Brownian motion, such that for N particles diffusing over time, the root-mean-square displacement (MSD) in one dimension (MSD_x) is given as:

$$MSD_x = \left[\frac{1}{N}\sum_{n=1}^{N}(x(t+dt) - x(t))^2\right]^{\frac{1}{2}} = \sigma_{1D} \equiv 2D\Delta t. \quad (13)$$

However, the integration of Eq. (5) is constrained by specific properties of the stochastic time integral as first defined by Ito (1973). If solved correctly, the variation in the root mean squared displacement of the particle over sufficiently long times ($t \gg \tau_p$) should reproduce the analytical Stokes–Einstein diffusivity (Eq. (11)). However, this result is entirely dependent on the condition that the total hydrodynamic force on the particle can be obtained from the steady drag and that the hydrodynamic interactions can be obtained from a standardized correlation for λ (see Table 1). In the framework proposed here, we instead obtain the total hydrodynamic force on the particle, including the hydrodynamic interaction effects, by directly integrating the fluid stresses on the surface of the particle. The coupling needed between the continuum and Langevin descriptions is further explained below.

2.1.3. Coupling the continuum and Langevin descriptions

The coupling between the continuum-resolved description of the surrounding liquid and the Lagrangian Langevin basis of the Brownian particle forms the crux of the numerical method presented in this paper. This coupling is achieved using the reduction in mobility λ (see Eq. (5)). In our framework, the resolved hydrodynamics around the particle can be directly accounted within λ_{IB} by normalizing the magnitude of the hydrodynamic force on the confined Brownian particle ($\mathbf{F_{IB}}$) with the magnitude of the Stokes drag on the same particle when diffusing in an unbounded domain. This is given as:

$$\lambda_{IB} = \frac{\|\mathbf{F_{IB}}\|}{\gamma \|\mathbf{u_p}\|}. \tag{14}$$

The Eq. (14) indicates that the particle's parallel and perpendicular motion with respect to the wall are clumped into a single λ_{IB} valid along the current direction of motion of the particle. This approach is motivated as follows. In stationary low Reynolds number flows in confined geometries, the correction to the mobility of a particle (λ) becomes a vector, with one element per coordinate direction. A theoretical requirement for that description to be valid is that the hydrodynamic force on the particle is a linear function of the relative velocity between the particle and the surrounding fluid. Due to this linearity, the particle's parallel and perpendicular motion with respect to the wall can be decomposed and handled separately. However in the case of Brownian motion, particles continuously accelerate and decelerate leading to instantaneous changes in their direction of motion, meaning unsteady hydrodynamic effects cannot in general be disregarded. For instance, the added mass effects from the relative acceleration of the particle and the fluid contribute unsteady effects that are not linear in relative velocity (Mo et al., 2015; Mo and Raizen, 2019). This presents us with two opportunities for the development of the current framework: either we maintain the complexity of a heterogeneous mobility matrix where unsteady effects are lumped into the form of a steady drag, or we use the ineluctable lumping of unsteady and steady effects as a motivation to simplify the mobility matrix to a scalar where directional information is also lumped. In this work, we have chosen the latter approach, to enable a comprehensive assessment of the overall methodology at a moderate level of abstraction and computational cost. There is nothing in the basic layout of the method as described here that precludes a later redevelopment along the lines of the former approach instead.

Thus, the estimated λ_{IB} is directly used instead of the analytically derived λ within the Langevin description (see Eq. (5)) to account for the hydrodynamic mobility ($\gamma \lambda_{IB}$) and the stochastic forcing (i.e. $\mathbf{F_{Brownian}}$ which correspondingly includes the corrected diffusivity D, see Eqs. (12) and (11)). In our framework, the motion of a particle with mass m_p, translational velocity $\mathbf{u_p}$, angular velocity $\boldsymbol{\omega_p}$, moment of inertia J with the inclusion of stochastic forcing $\mathbf{F_{Brownian}}$ (see Eq. (12)) is thus described as:

$$m_p \frac{d\mathbf{u_p}}{dt} = \mathbf{F_{IB}} + \mathbf{F_{Brownian}}, \tag{15}$$

$$\mathbf{J} \frac{d\boldsymbol{\omega_p}}{dt} = T_{IB} - \boldsymbol{\omega_p} \times \mathbf{J} \cdot \boldsymbol{\omega_p}. \tag{16}$$

These linear and angular momentum conservation equations (Eqs. (15) (16)) are integrated using the Newmark time-marching scheme (Newmark, 1959). In this method, the acceleration, velocity and displacement at time $t = t^{n+1}$ are obtained as functions of the values at $t = t^n$ by assuming a linear acceleration during that small

time step. This one-step semi-implicit method can be represented by the following set of equations:

$$\dot{u}_p^{n+1} = \dot{u}_p^n + \frac{\Delta t}{2} (\ddot{u}_p^n + \ddot{u}_p^{n+1}) \tag{17}$$

$$u_p^{n+1} = u_p^n + \Delta t \dot{u}_p^n + \frac{1-2\kappa}{2} \Delta t^2 \ddot{u}_p^n + \kappa \Delta t^2 \ddot{u}_p^{n+1} \tag{18}$$

The scheme is unconditionally stable with κ as a tuning parameter that has a default value of 0.25 (the constant average acceleration method) (Newmark, 1959). Note that this scheme is also compliant with the Itô interpretation (Ito, 1973) of a stochastic integral. A partitioned approach is employed to solve the coupled Langevin-IB problem. The grid and assembly are fully parallelized on the CPU, and the resulting large sparse-matrices are solved on the GPU with an Algebraic Multi-Grid (AMG) solver (Naumov et al., 2015). The use of an IB method enables the straightforward incorporation of complex fractal-shaped particles and complex pore structures within the framework. However in this paper we limit ourselves to simulations of spherical Brownian nanoparticles in simple and complex geometries. The ability of this framework to handle complex aggregates is already validated in our previous work (Kannan et al., 2019).

2.2. Simulation conditions

The numerical experiments carried out using *LaIBM* are based on a particle–fluid colloidal system given by the conditions specified in Table 2. Note that these simulations are carried out at a low particle Reynolds number ($Re_p = d_p V_{rms}^\infty \rho_p / \mu_f = 3 \cdot 10^{-3}$, where the root mean square velocity $V_{rms}^\infty = \sqrt{k_B T/m_p} = 1 \cdot 10^{-4}$ m/s is for an equivalent unbounded Brownian motion of a 400 nm particle) and at a particle–fluid density ratio of 1000. These choices are made so as to maintain the validity of the Langevin Eq. (5) (unsteady effects such as history and added mass forces are negligible). All simulations presented use the particle response time (τ_p see Eq. (7)) and particle diameter (d_p) as a basis for determining the relevant temporal and spatial details, respectively. The chosen simulation setups along with the axis of orientation (x is the co-axial direction while y and z are the wall-normal directions) are shown in Fig. 1. Correspondingly, a validation study in a cylindrical channel (see Fig. 1a), a hindered diffusion study in a square channel (see Fig. 1 and a hindered diffusion study in an arbitrary pore (see Fig. 1c) are carried out using a single spherical Brownian nanoparticle with a diameter of 400 nm. The corresponding domains described in Fig. 1 represent the different numerical environments that have been simulated using the proposed framework. The cylindrical channels have solely been used for the purpose of validation (since the corresponding analytical expressions (Haberman and Sayre, 1958) were derived for this setup), while the square channels are used for simulating the hindered diffusion under different hydro-

Table 2
Simulation conditions for the different cases.

Case	Validation: Grid convergence	Validation: Time convergence	Hindered diffusion
Domain shape			
	Cylindrical pore	Cylindrical pore	Square micro-channel and arbitrary pore*
Domain height+			
in d_p	6.6, 4.6, 3.3 and 2.3	6.6, 4.6, 3.3 and 2.3	6.6, 4.6, 3.3 and 2.3
Simulation details			
Spatial resolution (in $cells/d_p$)	24, 48 and 96	96	96
Temporal resolution dt (in τ_p)	1/200	1/50, 1/100 and 1/200	1/200
Total duration T (in τ_p)	100	100	100

l = w = h = 10 and a total duration T (in τ_p) as 10.
+ Length of the domain is 20 d_p in the co-axial direction.
* Simulations in the arbitrary pore have the same physical and simulation conditions, except a domain size (in d_p) given by –.
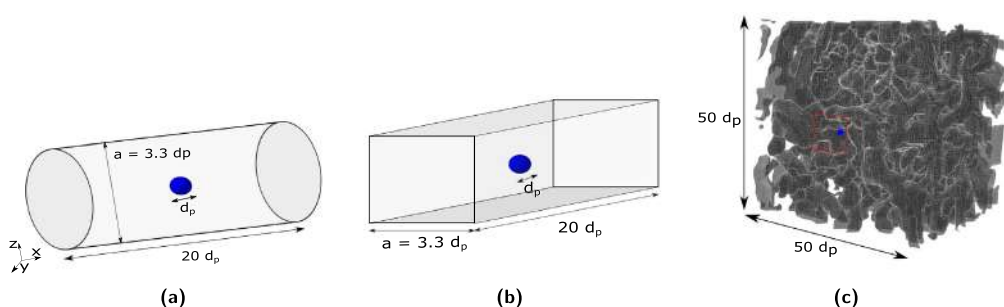
Fig. 1. Schematic of the simulation domain: (a) cylindrical channel with blockage ratio (B) 3.3 used in the validation studies, (b) straight square micro-channel with blockage ratio (B) 3.3 and (c) arbitrary pore used in the hindered diffusion studies. The dimensions are in terms of the particle diameter (d_p). Note that for the cylindrical and square micro-channels, x is the co-axial direction (of the pore) while y and z are the wall-normal directions.

dynamic confinements. The arbitrary pore represents a 'real-world' scenario, and hindered diffusion simulations in this geometry showcase the advanced capabilities of the presented numerical method. Note that, the validation studies represents a 400 nm particle settling under a fictitious force along the axis of a channel for a sufficiently long time (until terminal velocity is reached) to extract the relevant λ_{IB}. The constant force was chosen so as to accelerate the particle to a terminal velocity proportional to the root mean square velocity (V_{rms}^{∞}) of an equivalent unbounded Brownian motion for the 400 nm particle. This choice is made so as to have similar hydrodynamic scales of motion in both the validation and hindered diffusion cases in order to employ the same temporal and spatial resolutions across these cases. A cylindrical channel is chosen in order to reproduce the Haberman and Sayre (1958) study, while a square micro-channel is chosen from the application perspective (as this is more common in lab-on-a-chip applications due to constraints in manufacturing) and further represents a somewhat more complex geometry than cylindrical channels. The arbitrary pore simulations, on the other hand, demonstrate the capability of our framework in assessing the diffusive behavior of the same Brownian particle in an arbitrary asymmetric domain, for which *a priori* estimates of λ are unavailable. This arbitrary pore domain is generated using a tomography image of a widely available porous material. The respective surfaces of this porous media are extracted using an iso-surface mesh, which is then directly read into *LaIBM*.

In this paper the degree of hydrodynamic confinement is represented in terms of a blockage ratio B given as a/r_p. Correspondingly, the validation and the square channel simulations are carried out at four selected blockage ratios (B) which represent conditions that vary from weak to strong confinement, while the arbitrary pore simulations have spatially varying confinements as dictated by the geometry. The longitudinal extent of the domain is 20 d_p for the validation and square channel cases, with periodic conditions imposed along this direction. This length is chosen so as to minimize any inlet/outlet effects due to the applied boundary conditions on the particle motion. The pore simulations are carried out using a cubical domain with sides of 10 d_p, representing the region around the particle in the pore where the local diffusion is to be studied. These pore simulations are carried out at 5 randomly chosen locations in the pore network.

These validation cases are used as the basis to determine the minimum spatial and temporal resolutions needed for accurately estimating λ_{IB}. The hindered diffusion simulations (both in the square channel and in the arbitrary pore) are carried out at these determined resolutions. Further, since we deal with nanoparticle motion in all of these simulations, gravitational acceleration is deemed negligible. The Brownian forcing is updated in intervals

of $\tau_p/10$ to allow for an adequate resolution of the particle acceleration (Kannan et al., 2019). We also compare these *LaIBM* simulations (in the square channel) with a pure Langevin treatment of the same problem, where the Brownian particle is treated as a point-particle occupying negligible volume and diffusing only along the center-line of the domain. This is achieved by integrating the Langevin Eq. (5) using a forward Euler explicit time marching scheme along with an *a priori* estimated λ_{IB} extracted from the corresponding *LaIBM* simulation of the Brownian particle settling along the axis of an equivalent square micro-channel (similar to the validation cases). Note that this treatment represents a one-way coupled fluid–solid system with the Stokes drag (Eq. (6)) as the only hydrodynamic coupling between the two phases. The pure Langevin treatment thus represents a significant simplification, which is only possible due to the simplistic geometry and the limiting assumption that the particle stays along the center-line of the channel at all times (which is not strictly true for a Brownian particle), meaning a single constant value of λ_{IB} can be used for each pure Langevin simulation case respectively. Nevertheless, the Langevin treatment is used to establish the minimum criteria (in terms of duration and time averaging interval), including the variability of the stochastic process across several random seeds. The derivation of these criteria using a pure Langevin treatment have been extensively discussed in our previous work (Kannan et al., 2019) and a similar approach is adopted for describing the results presented in this paper as well (note that we use the same random number sequence as used in (Kannan et al., 2019)). For brevity, we directly report the final criteria chosen, namely a duration (T) of 100 τ_p and an averaging interval of 5 τ_p in the *MSD* calculations (see Eq. (13)), meaning the diffusivities that have been reported in this paper are calculated after a 5 τ_p period (i.e. by fitting the linear relation Eq. (13) to the *MSD* data over this period). The pore diffusion cases are carried out over a duration of 10 τ_p with an averaging interval of 2 τ_p for the *MSD* calculations, each to demonstrate a proof-of-concept that *LaIBM* can capture the spatially varying λ_{IB} in an arbitrary pore.

These simulations are run on a standard desktop (8 cores @ 3.4 GhZ and with 4 memory channels) equipped with an NVIDIA GeForce GTX 1070 graphic card. *LaIBM* scales linearly with the number of cores, with the grid and assembly fully parallelized on the CPU. The resulting large sparse-matrices are solved on the GPU with an Algebraic Multi–Grid solver (AmgX) (Naumov et al., 2015) at a processing efficiency of 200 GFLOPS (Giga Floating Point Operations Per Second) in double precision, while distributed over 1920 CUDA cores. A typical hindered diffusion simulation (of duration 100 τ_p and with 20000 time steps) needs a total simulation time of around two weeks.

3. Results and discussion

In this section, we present our results from the *LaIBM* framework. First, we present the results from the validation study which was designed to reproduce the Haberman and Sayre (1958) assessment. The spatial and temporal resolutions needed for the hindered diffusion studies are chosen based on these validation cases. We next present our hindered diffusion results. The diffusion dynamics are quantified via the directional mean squared displacement (MSD_i^* in Eq. (13)) and velocity auto-correlation functions (V_{acf}^i). In this paper, we choose to obtain the statistical description of particle motion by evaluating a single particle trajectory over long periods of time, which consequently represents multiple particle trajectories ensemble averaged over a much shorter duration (ergodicity hypothesis). Further, the mean-squared displacements are non-dimensionalized by the diffusional length scale for unbounded diffusion i.e. $MSD_i^* = MSD_i/D_\infty \tau_p^\infty$, where i is the direction of motion (x, y or z) and τ_p^∞ is the response time of an unbounded Brownian particle (obtained by setting $\lambda = 1$ in Eq. (7)), for ease of interpretation. These directional MSD_i^* are calculated for a 5 τ_p period of motion, while the V_{acf}^i are estimated over a 20 τ_p period. These periods are chosen for a reasonable representation of the underlying statistics for the total simulated duration of 100 τ_p. Note that the presented results are also compared with the pure Langevin treatment to qualitatively demonstrate the feasibility of this framework.

3.1. Validation studies: non-Brownian sphere moving along the axis of an infinitely long circular cylinder

In the validation study, a particle is accelerated with a constant force along the co-axial direction (or *x-axis*) of a cylindrical pore that contains a viscous liquid under creeping flow conditions (see Fig. 1a). The constant force is chosen so as to accelerate the particle to a terminal velocity proportional to the root mean square velocity ($V_{rms}^\infty = \sqrt{k_B T/m_p}$) of an equivalent unbounded Brownian motion of a 400 nm particle. Here, a root mean square velocity of $1 \cdot 10^{-4}$ m/s, corresponding to a particle Reynolds number of $3 \cdot 10^{-3}$, is used. At terminal velocity, the drag on the particle is counter-balanced by this constant force (in the absence of gravitational effects). This simple setup is used to determine the reduction in mobility (λ_{IB}) for the various confinements chosen. The λ_{IB} is estimated using Eq. (14) and is compared with the corresponding analytical expression for λ given as:

$$\lambda = \frac{\left(1 - 0.75857 B^{-5}\right)}{\left(1 - 2.1050 B^{-1} + 2.0865 B^{-3} - 1.7068 B^{-5} + 0.72603 B^{-6}\right)}. \tag{19}$$

Note that this expression is the equivalent form of the Haberman and Sayre correlation (see Table 1), represented in terms of a blockage ratio B given as a/r_p, where a is the pore size and r_p is the particle radius. This comparison is used as a basis for a detailed temporal and spatial (grid) convergence study. This is required since *LaIBM* is sensitive to both the temporal and spatial discretizations of the governing equations (Eqs. 1, 15 and 16). The results from this assessment are shown in Fig. 2. This figure directly compares the estimated values of λ_{IB} from our framework across various temporal and spatial resolutions with the analytical values.

The minimum spatial resolution needed was determined at a fixed temporal resolution of $\tau_p/200$. This temporal condition satisfied the Courant number ($C = u\Delta t/\Delta x$) requirement of the DNS framework. A rule of thumb in such multiphase DNS simulations

is to have at least 20 cells/d_p as the resolution, and this is realized in our assessments as well (see Fig. 2a). Consequently, the estimated values of λ_{IB} agree well with the analytical values at a grid resolution of 96 cells/d_p. In a similar way, the minimum temporal resolution required was established at a fixed grid resolution of 96 cells/d_p and determined to be $\tau_p/200$. Note that this conceptual validation study has been carried out at the same spatial and temporal scales as that of the hindered diffusion simulations. Hence, the determined minimum temporal and spatial resolutions are applicable for the diffusion cases as well. A similar simulation was run in the square micro-channels (at the finalized spatial and temporal resolutions) in order to estimate the λ_{IB} that are used in the pure Langevin hindered diffusion treatment. The estimated λ_{IB} for the cylindrical and square micro-channels along with the corresponding λ estimated using Eq. (19) are listed in Table 3.

3.2. Hindered diffusion of a spherical Brownian particle in a square channel

The diffusion of a Brownian particle under varying degrees of hydrodynamic confinement has been studied. These diffusion dynamics are evaluated in terms of the non-dimensional and directional particle MSD_i^* and are compared with both bounded and unbounded point-particle Langevin diffusion. Note that, we represent the respective directional non-dimensional MSD_{i*} along co-axial (x) and wall-normal (obtained by averaging along y and z) directions, due to y-z symmetry. We re-iterate that in the pure Langevin treatment for hindered diffusion, we are limited to assuming that the reduction in mobility λ is a constant for each chosen blockage ratio as given by Eq. (19). Hence, to probe the actual diffusion behavior in the *LaIBM* framework, we further evaluate λ_{IB} that is perceived by the particle and study its distribution. In this way, we can establish the local variations in λ_{IB} due to the instantaneous changes in the position and direction of motion of the Brownian nanoparticle in the channel. These studies demonstrate the efficacy and further validate the performance of the proposed framework in studying instantaneous pore diffusion phenomena.

3.2.1. General diffusion dynamics at blockage ratio 3.3

The general Brownian behavior of the spherical nanoparticle is discussed in terms of a square channel with $B = 3.3$. In conjunction with this discussion, a non-dimensional position vector P^* (i.e. P/d_p) is shown in Fig. 3a. The pure Langevin unbounded diffusion ($\lambda = 1$) is also shown in this figure. There is a marked difference between these two Brownian trajectories, calculated using the same sequence for the random vector $\mathbf{G}$, with a noticeable confinement effect visible. A direct comparison between the mean drift, estimated as the displacement from the origin: $\mathbf{P}^*(\mathbf{x},\mathbf{y},\mathbf{z}) - \mathbf{P}_{\text{origin}}^*$, between a freely diffusing and a confined Brownian particle over a 100 τ_p period clearly elucidates these differences. The freely diffusing Brownian nanoparticle (Fig. 3b) is displaced almost evenly in all the directions when compared with hindered diffusion, which seems to have a restricted displacement along all the directions (from the same initial position). The differences in $\mathbf{P}_{\mathbf{x}}^*$, which is along the co-axial direction of motion, are more pronounced than the corresponding y and z non-dimensional position vectors, indicative of a directional bias (anisotropic behavior) in the hydrodynamic resistance on the particle. This will be revisited in detail in the subsequent sections. Thus the relevant diffusion dynamics (due to the increased hydrodynamic resistance on the particle) are qualitatively captured by the *LaIBM* simulations. Note that in Fig. 3b and subsequent figures, the time axis is represented in terms of a non-dimensional T^* given as t/τ_p.

A qualitative evaluation of the performance of the framework is established by assessing the directional MSD_{i*} over 5 τ_p and veloc-
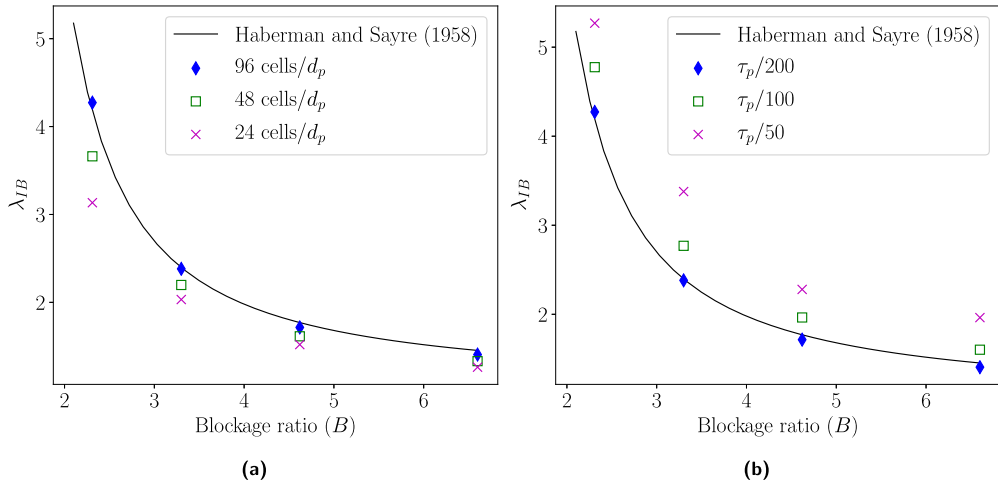
Fig. 2. Sensitivity of the λ_{IB} estimated from the LaIBM framework to (a) spatial and (b) temporal discretization. The black lines (——) represent the analytical estimate (see Eq. (19)) for λ.

Table 3
Reduction in mobility (λ) for the cylindrical and square micro-channels compared with the analytically estimated value by Haberman and Sayre (1958): motion along the longitudinal (co-axial) axis of the pore.

Blockage ratio	Haberman and Sayre (1958): Cylindrical pore	LaIBM: Cylindrical pore	LaIBM: Square micro-channel
6.6	1.453	1.406	1.513
4.6	1.770	1.715	1.798
3.3	2.397	2.381	2.374
2.3	4.173	4.272	4.133

ity auto-correlation functions (V_{acf}^i) over 20 τ_p. Fig. 4a illustrates the general hindered diffusion dynamics along the co-axial direction in a channel with $B = 3.3$. These results are further compared with the corresponding unbounded Langevin diffusion calculation.

Both these results demonstrate the transition from a ballistic to a diffusive regime (Uhlenbeck and Ornstein, 1930) due to the breakdown of the Stokes–Einstein description (Eq. (13)) at the shortest timescales (Rahman, 1964; Li et al., 2010; Huang et al., 2011; Kheifets et al., 2014). At these scales, the particle motion is highly correlated and therefore a definition of velocity is plausible i.e. the root mean squared particle velocity V_{rms}. Correspondingly, the MSD_x approaches $(V_{rms}t)^2$ in the ballistic regime below τ_p, and reaches the Stokes–Einstein result $2D_x t$ (see Eq. (13)) at larger times. Note that the bounded diffusion cases approach a lower diffusivity, i.e. the MSD_x approaches $2D_x t$ rather than $2D_\infty t$, due to the resistance to particle movement from hydrodynamic confinement effects in the channel (see inset of Fig. 4a). Note that a similar qualitative behavior was observed along the x and y directions and for the other blockage ratios as well (see Fig. 5).
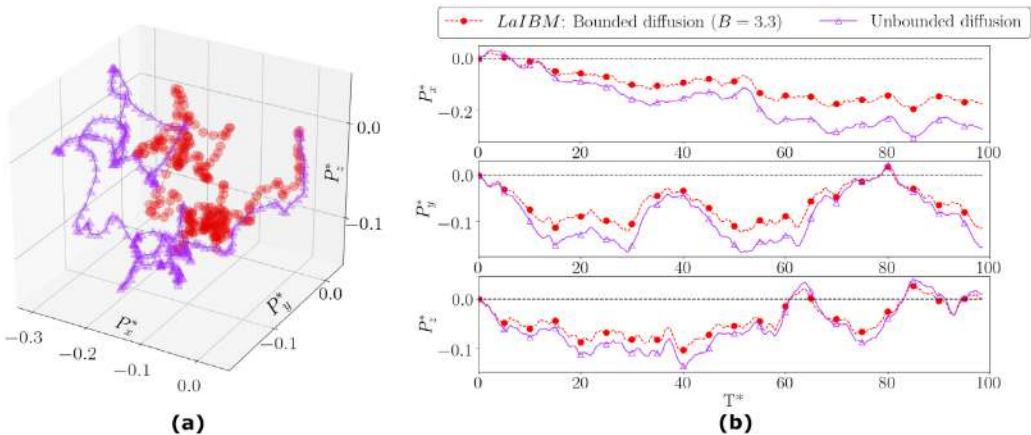

Fig. 3. Snapshot of the trajectory of a spherical 400 nm Brownian particle (in non-dimensional units i.e. $\mathbf{P}^*(\mathbf{x}, \mathbf{y}, \mathbf{z})$): (a) the red line indicates hindered diffusion in a square channel with $B = 3.3$ while the purple one indicates unbounded diffusion (point-particle case) and (b) the mean non-dimensional drift/displacement of the particle from the origin (estimated as $\mathbf{P}^*(\mathbf{x}, \mathbf{y}, \mathbf{z}) - \mathbf{P}_{origin}$) over a 100 τ_p period. Both trajectories are calculated using the same random number sequence ($\mathbf{G}$). (For interpretation of the references to colour in this figure legend, the reader is referred to the web version of this article.)
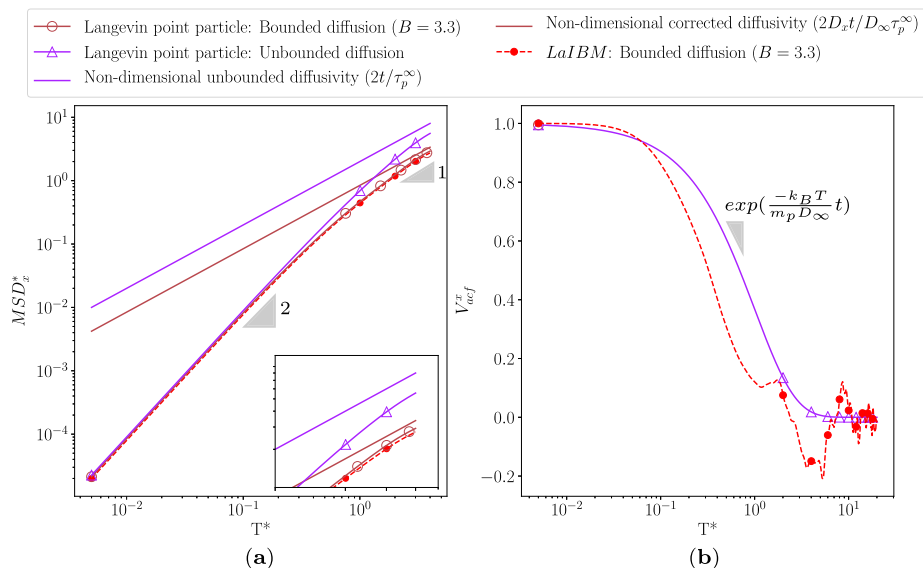
Fig. 4. Hindered diffusion dynamics of a 400 nm Brownian particle along the co-axial direction of a square micro-channel with $B = 3.3$: (a) non-dimensional MSD_x compared with an unbounded Langevin point-particle diffusion simulation over 5 τ_p and b) decay of the velocity auto-correlation function (V_{acf}^x) over 20 τ_p. The solid purple lines (⸺) represent the unbounded Langevin point-particle diffusion simulations. The slopes indicate the ballistic and diffusive regimes and the exponential decay of the V_{acf}^x. Inset: tail behavior of MSD_{x*} showing that the bounded diffusion cases approach a lower diffusivity. (For interpretation of the references to colour in this figure legend, the reader is referred to the web version of this article.)

Further, the MSD_{x*} trends are qualitatively similar for both the *LaIBM* framework and pure Langevin treatments at $B = 3.3$, albeit with a slight difference at the tail due to the different λ estimates used in solving for the Brownian trajectories (see Eq. (5)). The pure

Langevin treatment assumes that the particle is not displaced from the center-line of the channel, which is an unphysical restriction for a real Brownian particle. This leads to an under-prediction of the hydrodynamic resistance, as the particle is always assumed
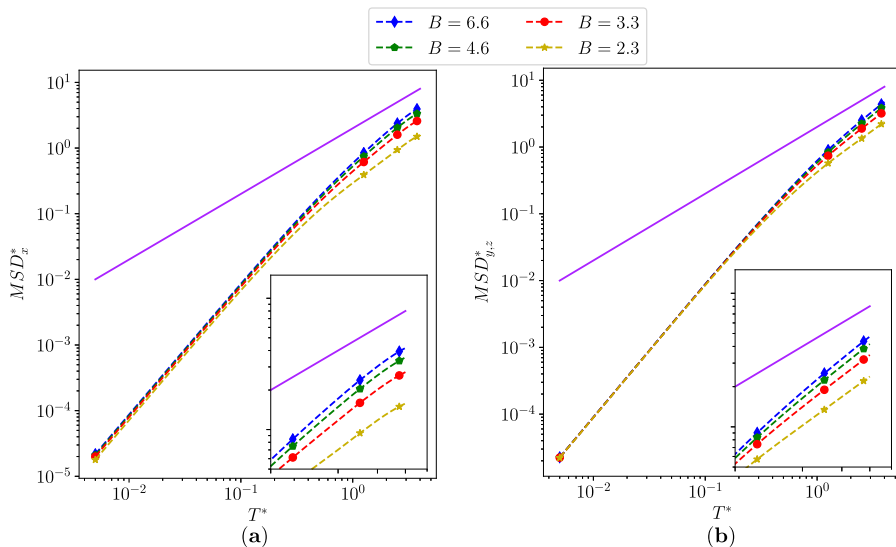
Fig. 5. Hindered diffusion dynamics of a 400 nm Brownian particle under varying degrees of confinement (represented as the blockage ratios (*B*) 6.6, 4.6, 3.3 and 2.3 respectively): (a) the non-dimensional MSD_{x*} along the co-axial and (b) $MSD_{y,z*}$ along the wall-normal directions evaluated over 5 τ_p. The solid lines (⸺) represents the analytical non-dimensionalized Stokes–Einstein behavior for unbounded Brownian motion (Eq. (10)). The insets show that the linear diffusive regimes attained individually along each of these directions have decreasing diffusivities with increasing confinement (or decreasing blockage ratio). These differences are further elaborated in Table 4, where it can be seen that the diffusivities vary by a factor of 2.6 in panel (a) and a factor of 2.0 in panel (b) from .$B = 2.3$ to 6.6.

to be in the center of the channel, leading to an over-prediction of the diffusivity (as seen in the inset of Fig. 4a). Moreover, in a square micro-channel the diffusivity is direction dependent, as the hydrodynamic resistances on the particle are asymmetric (as can be inferred from the trajectories in Fig. 3b), meaning the diffusive behavior varies across the three principal directions of motion (x, y and z). Nevertheless, these comparative studies can be used to qualitatively validate the relevant hindered diffusion behavior (in terms of the transition from ballistic to diffusive regimes). We emphasize that our *LaIBM* framework provides a dynamic description for such systems which is well beyond the scope of the pure Langevin approach.

The velocity auto-correlation function of the Langevin processes studied in this paper should rapidly decay to zero due to the Gaussian nature of the stochastic forcing in Eq. (12), making the stochastic process Markovian in nature. Hence, the V_{acf}^i, given as the equilibrium ensemble average of the particle velocities v_i along the ith direction:

$$V_{acf}^i = \langle \mathbf{v_i}(\mathbf{0}) \cdot \mathbf{v_i}(\mathbf{t}) \rangle = \frac{1}{N_t} \sum_{n=1}^{N_t} (\mathbf{v_i}(\mathbf{0}) \cdot \mathbf{v_i}(\mathbf{t})), \tag{20}$$

decays with an exponential tail, as shown in Fig. 4b. In this expression, N_t is the lag time interval (i.e. averaging using a lag of $1dt$, $2dt$ ... $N_t dt$). This classical result for Brownian nanoparticles with sufficiently high density ratios (von Smoluchowski, 1906; Chandrasekhar, 1943), is a further validation of the applicability of our framework for studying such ideal colloids. Note however that the V_{acf}^z of the Brownian nanoparticle under hydrodynamic confinement decays quicker than the unbounded Langevin point-particle diffusion calculations. This type of behavior has been previously reported by Felderhof (2006), Jeney and co-workers (Jeney et al., 2008; Franosch and Jeney, 2009) and more recently by Mo and co-workers (Mo et al., 2015; Simha et al., 2018; Mo and Raizen, 2019). These authors noted confinement effects in both the long term diffusive regime, as well as the short timescale ballistic regime. This leads to a faster decay of the velocity autocorrelation function for the confined Brownian particle when compared with an unbounded particle. The rapidly decaying behavior is attributed to the reflected flow from the wall, which cancels the tail of the velocity auto-correlation function. Thus, the reported velocity auto-correlation function trends serve as an additional qualitative validation of the *LaIBM* framework. Note that the studies of Felderhof (2006) and Mo and co-workers (Mo et al., 2015; Simha et al., 2018; Mo and Raizen, 2019) report a long-tail decay of the velocity auto-correlation function, while we report an exponential decay. This is because in our proof-of-concept studies the inertial effects of the fluid have been neglected. Similar decays are noted along the wall-normal directions as well (see Fig. 7).

3.2.2. Effect of blockage ratio on particle directional diffusivity D_i

The degree of hydrodynamic resistance (represented by the blockage ratio) on the particle has a direct impact on its hindered diffusion behavior. This effect is noticeable in Fig. 5 which shows the corresponding results from *LaIBM*. The relevant diffusive regimes attained have decreasing diffusivities with increasing degrees of confinement (or decreasing blockage ratio), which is expected due to increasing hydrodynamic resistance at tighter confinements. This would mean that at $B = 2.3$, the corresponding directional particle diffusivities are the lowest, as the estimated λ_{IB} in general are higher (see Table 4). Note that, we list the respective directional diffusivities (in the non-dimensional form D_i/D_∞), along the corresponding co-axial and wall-normal directions after a 5 τ_p period, in Table 4. The results listed in this table are of the same order of magnitude as that of Gentile et al. (2015), who per-

formed similar assessments (both numerical and experimental) in square-channels. Additionally, these results correspond with analogous studies in circular channels by Gubbiotti et al. (2019), Uma et al. (2011) and Dechadilok and Deen (2006) as well. These qualitative comparisons further confirm that the relevant particle diffusion dynamics are adequately captured. We re-emphasize that the qualitative trends in the MSD_{i*} are correspondingly similar (as described earlier) across all the blockage ratios. The reduction in diffusivity with decreasing blockage ratios is directly related to the estimated reduction in mobility λ_{IB}. These confinement effects are also noticeable in the decay of the velocity auto-correlation function (along the co-axial direction) over a 20 τ_p period as shown in Fig. 6. Note that the V_{acf}^x of the Brownian nanoparticle under the highest hydrodynamic confinement (i.e. $B = 2.3$) decays the quickest, with increasing time of decay as the degree of confinement decreases. Similar decays are noted along the wall-normal directions as well (see Fig. 7).

3.2.3. Anisotropy in the hydrodynamic resistances

Figs. 3b, 5 and Table 4 further indicate a directional bias (anisotropic behavior) in the reduction in non-dimensional diffusivity D_i/D_∞. In general, it is seen that the reduction in diffusivity is more pronounced along the co-axial direction (x) when compared to the wall-normal (y and z) directions. The same trend is observed across all the blockage ratios. These trends have also been reported by Gentile et al. (2015) in similar experimental studies in square micro-channels and Uma et al. (2011) in numerical studies in cylindrical channels. This bias is attributed to the higher hydrodynamic resistance along the co-axial direction of motion when compared with the corresponding wall-normal direction. This can be explained by the distribution of the fluid volume around the particle in the square-micro channel. A relatively smaller volume of fluid is squeezed between the particle and the bounding walls. Thus a smaller fraction of the total fluid opposes the wall-normal motion when compared with co-axial movement, leading to less pronounced hydrodynamic resistances. This behavior is directly reflected in the diffusivities reported in Table 4, with lower co-axial values when compared with the corresponding wall-normal values. Additionally, the relative difference between the diffusivities along these two principal directions increases with decreasing blockage ratio (or increasing confinement). This is due to the increasing asymmetry in the fluid distribution around the Brownian particle as the channel gets narrower (where a progressively lesser volume of fluid is squeezed between the particle and walls). This bias in the directional diffusivities (D_i/D_∞) are also reflected in the corresponding V_{acf}^i along the co-axial (V_{acf}^x) and wall-normal (obtained by averaging V_{acf}^y and V_{acf}^z) directions of motion. The Fig. 7 shows the differences between the decay of the V_{acf}^i along these two principle directions over 20 τ_p. In general, the V_{acf}^x decays faster than $V_{acf}^{y,z}$ indicating a higher dampening (due to hydrodynamic resistance) along the co-axial direction. Further, this difference between the decays is more noticeable at the lowest blockage

Table 4
Effect of the blockage ratios on the non-dimensional directional diffusivities of a 400 nm Brownian particle in the co-axial (D_x/D_∞) and wall-normal ($D_{y,z}/D_\infty$) directions after 5 τ_p.

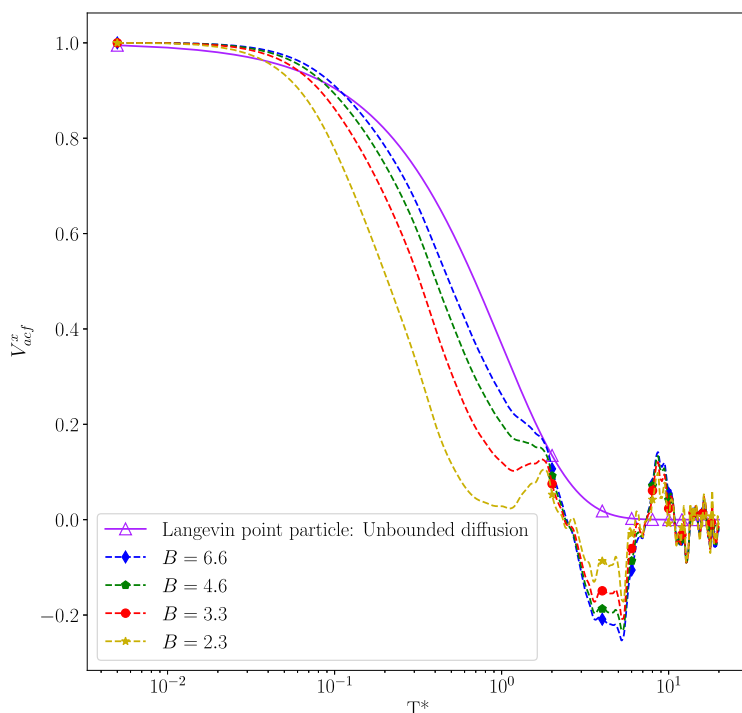| Blockage ratio	$D_{co-axial}/D_\infty$	$D_{wall-normal}/D_\infty$
6.6	0.523	0.592
4.6	0.443	0.521
3.3	0.342	0.432
2.3	0.198	0.298

$D_\infty = 6.3 \cdot 10^{-11}$ m^2/s.

Fig. 6. Decay of the velocity auto-correlation function for a 400 nm Brownian particle along the co-axial direction (V_{acf}^{x}) across different blockage ratios (B: 6.6, 4.6, 3.3 and 2.3 respectively) over 20 τ_{p}. The solid line (——) represents the exponential decay for an unbounded Langevin point-particle over the same period.

ratios indicative of the increased geometrical asymmetries around the particle.

This bias is further confirmed by individually examining the analytical behavior reported (for non-Brownian systems) by Chang and Keh (2006) for wall normal motion and that of Haberman and Sayre (1958) for longitudinal or co-axial motion. Note that due to the lack of constitutive analytical correlations for wall-normal motion of a particle in a cylindrical/square micro-channel, the Chang and Keh study (Chang and Keh, 2006), which is applicable for particle motion between two parallel walls (under creeping flow conditions), is used as a general baseline for approximating the behavior of such systems. From this study, we relate the ratio a/b (where $b = h$ is the distance between the two parallel plates and a is the particle diameter) to the inverse of the blockage ratio B. This comparison is shown in Fig. 8. It is evident that for any given blockage ratio, the resistance along the axial direction of motion is more pronounced than the corresponding resistance in the wall-normal direction. Further, this effect is also confirmed using simulations (similar to those described in the validation studies) setup in *LaIBM*. A spherical non-Brownian particle is accelerated to a terminal velocity proportional to the root mean square velocity (V_{rms}^{∞}) with a constant force along a representative wall-normal direction (*y-direction*). The corresponding λ_{IB} is extracted from the simulations across the chosen blockage ratios and these are compared with those shown in Fig. 2 and Table 3 (for co-axial motion). This comparison is also shown in Fig. 8, with the estimated λ_{IB} supporting our analytical basis for the bias of the hydrodynamic resistances. Note that the correspondence with the Chang and Keh study is poor as the corresponding *LaIBM* simulations represent a micro-channel and not flow between two parallel plates. Hence, the hydrodynamic resistance

to wall-normal motion is more pronounced in the *LaIBM* simulations. These results show that *LaIBM* is able to capture the directional variation in hindered diffusion behavior with the lumped λ_{IB} procedure adopted in the current work.

3.2.4. Estimation of the lumped reduction in mobility: λ_{IB}

The highlighting feature of *LaIBM* is its ability to estimate the reduction in mobility (λ_{IB}) on-the-fly based on a fully resolved fluid flow field. Hence, instantaneous as well as local particle diffusivities can be evaluated and their evolution over time can easily be studied. In this framework, λ_{IB} is computed using Eq. (14). Fig. 9 compares values seen by the particle in the simulations for the various confinements. These are obtained by smoothing the raw data using a moving average filter over a time-averaging window of 100 dt or 0.5 τ_{p}. The chosen window reasonably represents the white-noise signal from *LaIBM*. λ_{IB} increases with decreasing blockage ratios (or increasing confinement), leading to higher hydrodynamic resistance and correspondingly lesser mean displacement from the initial position at lower values of blockage ratios (see Fig. 10). Moreover, the estimated values of λ_{IB} vary at every time-instant. Such a variation is an indication of two simultaneous phenomena: the probing of a lumped λ_{IB} by *LaIBM* along the direction of motion of the particle, and the off-center-line displacement of the Brownian particle. The first phenomenon relates to the fact that Eq. (14) always estimates the reduction of mobility in the current direction of motion of the particle, so that the frequent changes to this direction due to the Brownian motion show up as variations in λ_{IB} at a similar frequency. The latter phenomenon is discussed as follows.

Most analytical theories assume that the nanoparticles which are released in the center of the channel do not drift away from this initial position. This is definitely true (on average) over longer peri-
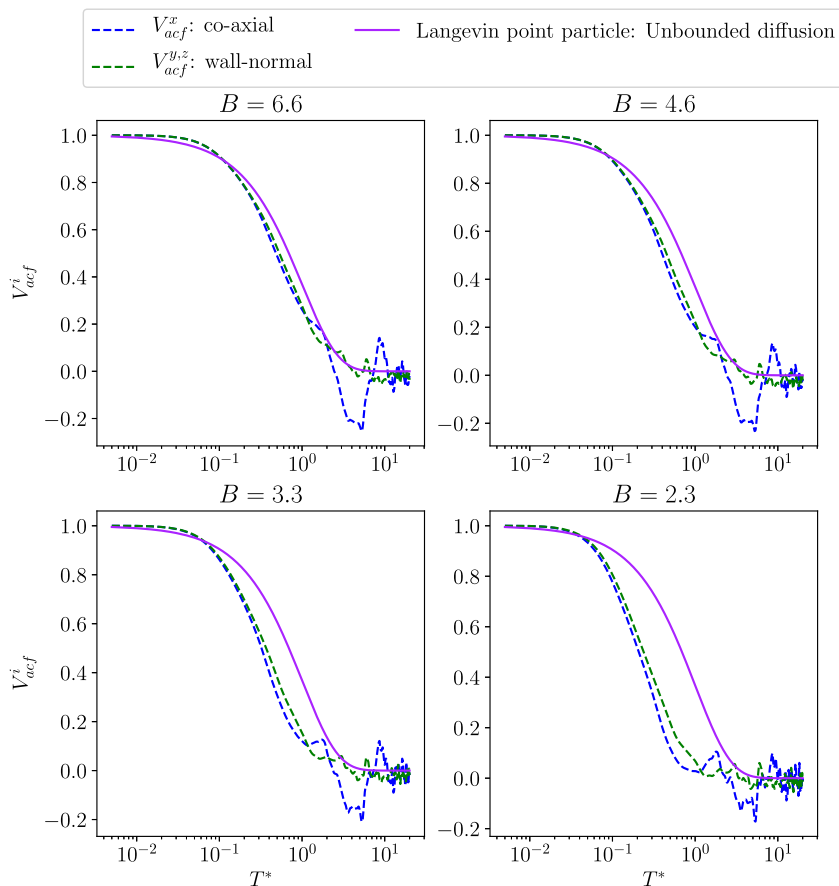
Fig. 7. Anisotropy in the hydrodynamic resistances across different blockage ratios (B: 6.6, 4.6, 3.3 and 2.3 respectively): Decay of the velocity auto-correlation function (V_{acf}^{i}) along the co-axial (x) and wall-normal directions (y, z) over 20 τ_p . The solid line (——) represents the exponential decay for an unbounded Langevin point-particle over the same period. In general, the co-axial (V_{acf}^{x}) decay is faster than the wall-normal ($V_{acf}^{y,z}$) one due to a dominant hydrodynamic resistance along. that direction.

ods of Brownian diffusion, when the mean displacement around the origin (or the initial position) is zero. However, the displacement from the initial position during shorter diffusion periods is not negligible, as individual particles do tend to drift away from this origin, as seen in Fig. 10. This hypothesis was first explored by Brenner and Gaydos (1977) and later by Mavrovouniotis and Brenner (1988) using an axial Taylor dispersivity of the hindered axial molecular diffusion coefficient for Brownian spheres in cylindrical channels. Since these authors relied on an analytical representation for the governing flow field, they estimated this dispersivity using the method of matched asymptotic expansions to piece together a composite solution for the required hydrodynamic resistance coefficients or mobility γ (see Eq. (6)). This was needed due to the absence of uniformly valid expressions for the required hydrodynamic resistances over the complete span of the channel. In our *LaIBM* framework, the complete flow field around the Brownian particle is resolved, meaning we can estimate the reduction in mobility at any given distance from the confining walls, without the reliance on such an analytical basis. Hence, this framework is more naturally suited to evaluate local and instantaneous diffusion phenomena, wherein the off-center-axis drift could significantly affect the mobility of the Brownian particle.

3.2.5. Distribution of λ_{IB}

The time-varying estimate of λ_{IB} is further analyzed in order to ascribe a general behavior to it. The objective with this is to provide a function for the spatial and temporal variation of λ_{IB}, which best represents our data. The variation of the estimated λ_{IB} is already shown in Fig. 9, wherein the raw data has been smoothed using a moving average filter over a time-averaging window of 100 dt or 0.5 τ_p. The data collected here is valid for Brownian motion in square micro-channels, but the approach presented is generally applicable to arbitrary geometries.

Based on a χ^2 goodness-of-fit test on the smoothed λ_{IB}, we further confirm that the β-distribution can be best used to describe our data. The probability density function of this distribution is given as:

$$f_X(\lambda_{\dagger}^{*}) = \frac{\Gamma(\alpha+\beta)}{\Gamma(\alpha)\Gamma(\beta)} \lambda_{\dagger}^{*\,\alpha-1}(1-\lambda_{\dagger}^{*})^{\beta-1}, \quad 0 \leqslant \lambda_{\dagger}^{*} \leqslant 1, \tag{21}$$

where $\lambda_{\dagger}^{*}$ is defined in the interval *[0, 1]* (see Supplementary Material for more details) and parametrized by two positive shape parameters denoted by α, β respectively, and a Γ function. λ_{IB} is hence scaled and shifted into the interval *[0, 1]* in order to fit a sin-
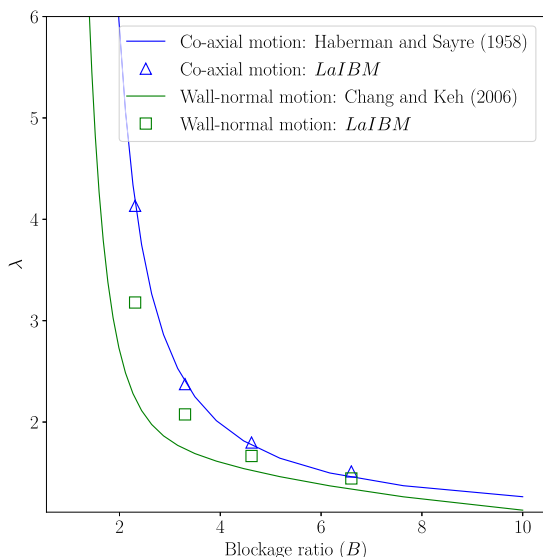
Fig. 8. Anisotropy in the hydrodynamic resistances (analytical basis): co-axial vs. wall-normal movement of the particle. The co-axial hydrodynamic resistances are more pronounced than the corresponding wall-normal resistances for motion in a micro-channel. The open symbols represent the corresponding *LaIBM* simulations.

gle distribution to all the reported cases. We shall henceforth refer to this scaled variable as $\lambda_\dagger^*$. Fig. 11 shows $\lambda_\dagger^*$ for the chosen blockage ratios (B) fitted to a standard β-distribution. In addition, the figure also includes an averaged distribution function, which is obtained

by averaging the coefficients of the respective fitted β-distributions across the chosen blockage ratios (B). This averaged function (with $\alpha = 1.4856$ and $\beta = 2.5368$) can be used to describe the general distribution of $\lambda_\dagger^*$ across any of the chosen confinements. Thus, the statistical behavior observed in our data, for the spatially varying λ_{IB}, can be directly reproduced by sampling from the β-distribution given by the Eq. (21). A more detailed account on the scaling adopted to obtain $\lambda_\dagger^*$ along with the goodness of fit tests and the procedures for sampling are provided in the Supplementary Material.

We stress that the characteristics of the distributions for $\lambda_\dagger^*$ obtained in Fig. 11 show that the instantaneous hydrodynamics around the Brownian particle need to be accounted for while evaluating hindered diffusion in narrow arbitrary geometries. Assuming that the particle remains in a purely co-axial motion along the center-line of the channel, in order to use the correlations listed in Table 1, has adverse consequences while extracting fundamental properties from such a system. For example, if the particle is assumed to remain in co-axial motion along the center-line, the heat and mass transfer to the particle would always be erroneous as the underlying hydrodynamic interaction with the channel is incorrect. This is because, by constraining the Brownian particle to the center-line, the fluctuations in the relative velocities between the particle and fluid will not accurately reflect the influence of off-centerline and wall-normal motion. Another example would be when a direct observation of Brownian motion is used to infer the size of a suspended macromolecule. In this case, neglecting the spatial variation of the hydrodynamic interactions would imply that the size would be erroneous as an inaccurate effective λ is used in Eq. (11). The approach outlined in this paper enables the derivation of distributions for λ as seen by a diffusing particle in an arbitrary geometry, which ensures that the underlying hydrodynamic interaction with the channel is accurately represented in the hindered diffusion dynamics.
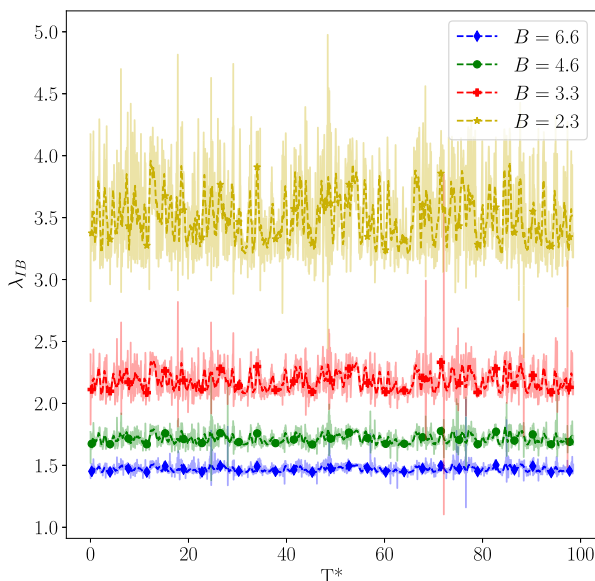

Fig. 9. Variation of the estimated reduction in mobility (λ_{IB}) for the different degrees of confinement represented as the blockage ratios (B): 6.6, 4.6, 3.3 and 2.3 respectively, over 100 τ_p. The raw data (represented by the solid lines) is smoothed using a moving average filter over a time-averaging window of 100 dt or 0.5 τ_p.
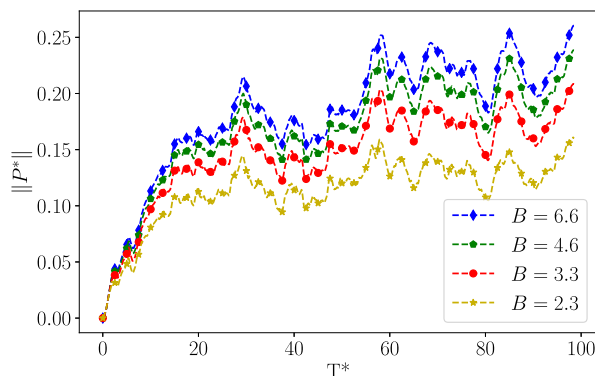
Fig. 10. Magnitude of non-dimensional drift/displacement of the particle from the origin (estimated as $\|\mathbf{P}^*(\mathbf{x}, \mathbf{y}, \mathbf{z}) - \mathbf{P}^*_{\text{origin}}(\mathbf{x}, \mathbf{y}, \mathbf{z})\|$) over a duration of 100 τ_p. The drift reduces with increasing confinement (or decreasing blockage ratio B). All trajectories are calculated using the same sequence for the random number **G**.
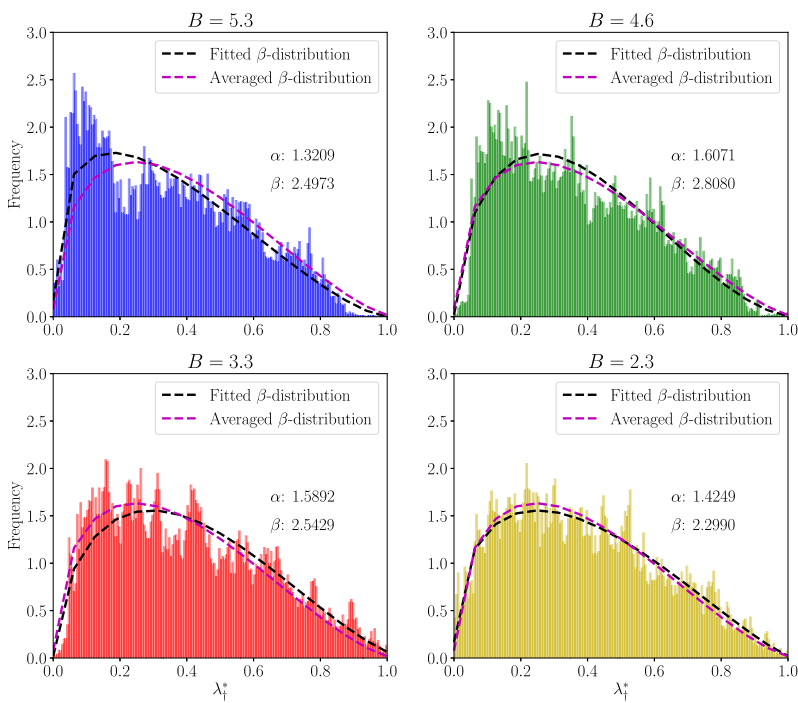

Fig. 11. β-distribution fitted to $\lambda_\uparrow^*$ across the blockage ratios (B): 6.6, 4.6, 3.3 and 2.3 respectively, evaluated over a duration of 100 τ_p. The corresponding shape parameters of the fitted β-distribution (α and β) are listed in each panel. The averaged β-distribution (obtained by averaging the coefficients of the respective individual β-distributions), with $\alpha = 1.4856$ and $\beta = 2.5368$ can be used to describe the general distribution of $\lambda_\uparrow^*$ across all the chosen confinements.

3.3. Hindered diffusion in a pore

The hindered diffusion of the spherical Brownian particle is assessed at five random positions (as shown in Fig. 12) chosen in an arbitrary pore. The objective with this assessment is to demonstrate the capability of *LaIBM* to estimate the local mobility ($1/\gamma\lambda_{IB}$) and the corresponding diffusivity for a Brownian particle on-the-fly and in any arbitrary geometry. The particle diffusion is assessed over a 2 τ_p period (for a total simulation duration of 10 τ_p). Since

the flow field around the particle is fully resolved (meaning the hydrodynamic resistances are available for the entire porous domain under consideration), these types of simulations can be used to study localized pore-diffusion phenomena in greater detail.

Fig. 13 showcases the qualitative capabilities of the *LaIBM* framework in resolving the hydrodynamics around a Brownian particle diffusing in an arbitrary pore. As an example, we show the contours of velocity magnitude in a $y - z$ plane passing through the center of the particle which is diffusing around *position 2* (see
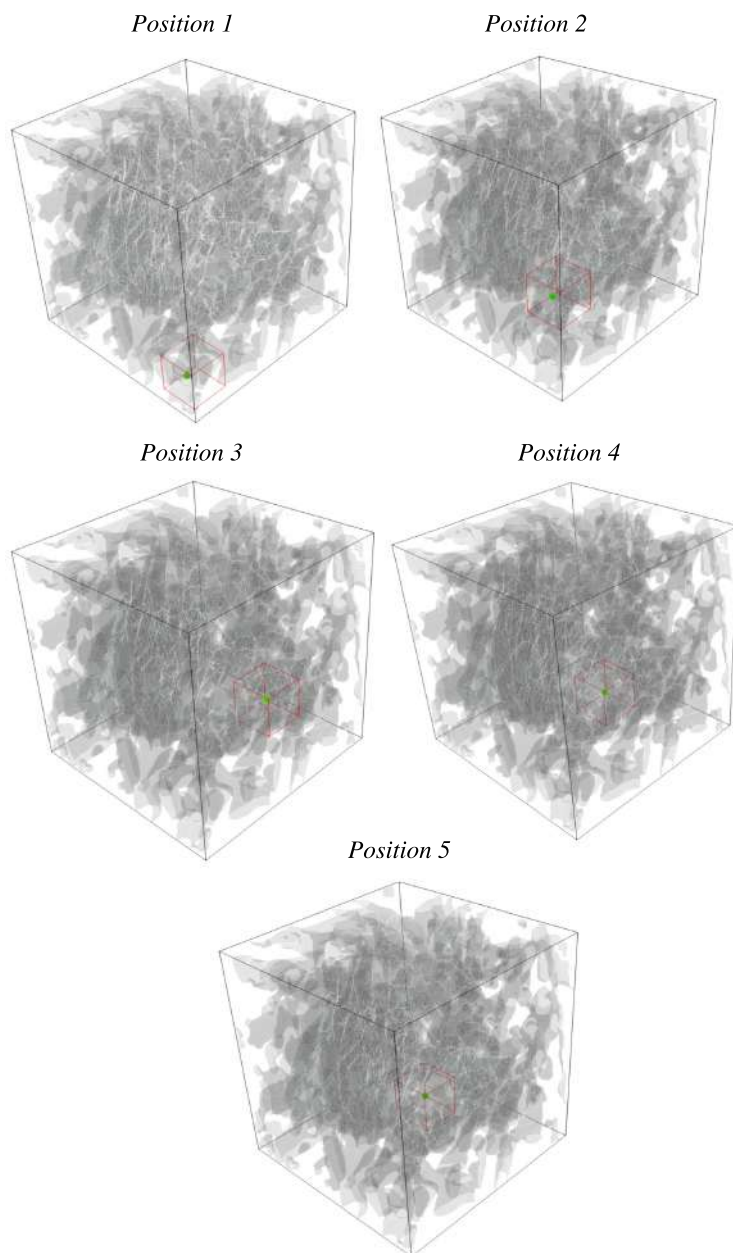
Fig. 12. Locations in the chosen porous matrix at which hindered diffusion is assessed. The red box represents the local simulation domain. (For interpretation of the references to colour in this figure legend, the reader is referred to the web version of this article.)

Fig. 12). The availability of the resolved hydrodynamics around the particle enables the estimation of the reduction in mobility (λ_{IB}) at each location. The corresponding variation of λ_{IB} over the simulation duration and across the different locations is shown in Fig. 14a. Further, the estimated averaged non-dimensional diffusivities (D/D_{∞}) are listed in Table 5. These diffusivities are obtained

from the averaged $MSD_{avg}*$ (which is nothing but $MSD_{i}*$ averaged over x, y and z directions) shown in Fig. 14b after a 2 τ_p period. Note that directionally-averaged values are used since they reasonably represent the overall local diffusive behavior of the Brownian particle in the pore. The Fig. 14b shows the variation in the non-dimensional mean-squared behavior across the random locations
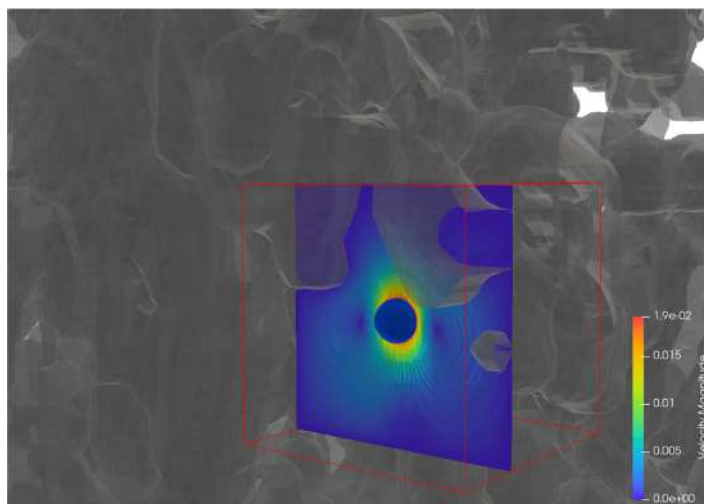
Fig. 13. Localized simulation domain at *position 2* in the porous matrix (instantaneous snapshot at 10 τ_p): contours of velocity magnitude on a *yz*-plane passing through the center of the Brownian particle.

in the pore over a 2 τ_p period. These can be used in tandem with λ_{IB} to determine the nature of the local environment in which the particle is diffusing.

The averaged non-dimensional diffusivities (listed in Table 5) indicate that the diffusivity of the Brownian particle is directly affected by its location in the pore. Based on the reported data, we can say that *position 3* consists of a relatively dense region of

porous networks since it has a comparatively lower non-dimensional diffusivity, indicative of increased hydrodynamic resistances (higher λ_{IB}, see Fig. 14a). *Position 4*, on the other hand, has a comparatively less denser pore network among the chosen locations due to a relatively higher non-dimensional diffusivity. These results further concur with the experimental observations by Skaug and co-workers, who reported a heterogeneous and spa-
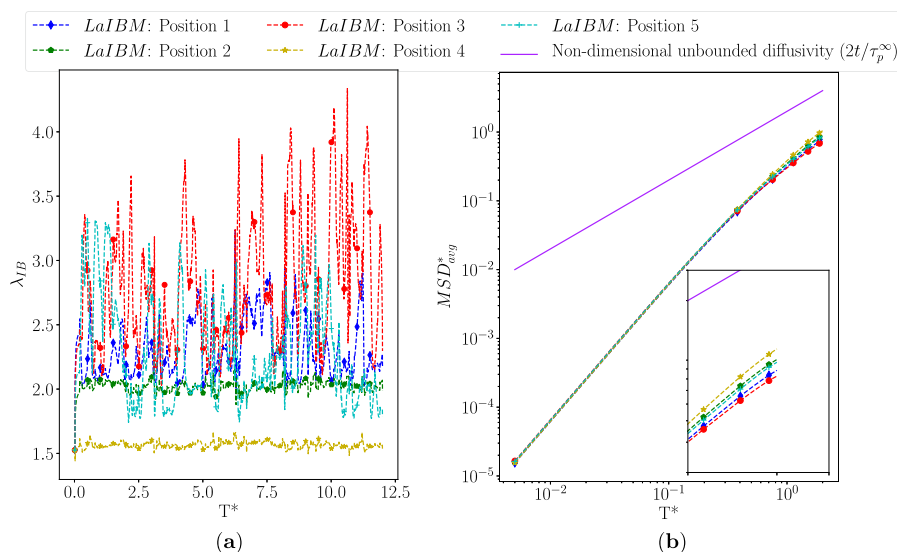
Fig. 14. Effect of position in the pore on hindered diffusion: (a) variation of the estimated reduction in mobility (λ_{IB}) and (b) the non-dimensional $MSD_{avg}*$ (averaged over *x, y and z* directions) evaluated over 2 τ_p. The solid line (——) represents the analytical non-dimensionalized Stokes–Einstein behavior for unbounded Brownian motion (Eq. (10)). The inset shows the variations in the linear (diffusive) regimes attained by the spherical Brownian particle at the various randomly chosen locations in the pore.

Table 5
Non-dimensional diffusivity D/D_∞ (estimated from the MSD_{i^*} averaged over x, y and z directions) for a 400 nm Brownian particle diffusing at five random locations in an arbitrary pore after a duration of 2 τ_p.

Location in the pore	D/D_∞
Position 1	0.349
Position 2	0.403
Position 3	0.323
Position 4	0.465
Position 5	0.389

$D_\infty = 2.8 \cdot 10^{-12}$ m^2/s.

tially dependant mobility at sub-pore length scales in an arbitrary pore (Skaug et al., 2015). The presented results are of the same order of magnitude as reported by these experimental studies.

4. Conclusions

In this paper, we present and discuss a novel continuum-based multiphase DNS framework, *LaIBM*, to study hindered diffusion of Brownian nanoparticles in arbitrary geometries. This framework leverages a resolved solution of the hydrodynamics around the Brownian particle to estimate the relevant reduction in mobility. The proposed method is not limited by the availability of uniform solutions to the hydrodynamic resistances nor symmetry considerations, such as other methods reported in literature (Brenner and Gaydos, 1977; Brenner, 1982; Felderhof, 2005; Mo et al., 2015), making it suitable for studying both simplified systems such as a square micro-channel and complex pore diffusion phenomena. To our best knowledge, this is the first continuum-based framework that directly includes the resolved instantaneous hydrodynamics around the Brownian particle (*without the need for an a priori determination of the relevant mobility tensors) into the particle Langevin equation of motion.* Consequently, we show that the hindered diffusion behavior for any relevant system can be assessed using a two-way coupled continuum mechanics-discrete particle approach. As a proof-of-concept, we assess the Brownian diffusion of a spherical nanoparticle under creeping flow conditions and correspondingly employ the fundamental form of the Langevin equation with an additional correction factor λ to correct for the increased hydrodynamic wall resistances. We lump steady and unsteady effects along with directional details into λ, thereby simplifying it into a scalar.

We demonstrate the capabilities of this numerical technique in handling the hindered diffusion of an ideal spherical Brownian nanoparticle in a simple square micro-channel as well as a complex pore. The relevant hindered diffusion phenomena are studied in a square channel at varying degree of confinement. Brownian diffusion dynamics, including the transition from a ballistic to a diffusive regime and exponential decay of the velocity autocorrelation function (due to creeping flow conditions in the test cases), are adequately captured across all investigated degrees of confinement. Further, we show that the velocity auto-correlation function decays more rapidly for a bounded Brownian sphere when compared with an unbounded one, in accordance with earlier studies (Felderhof, 2006; Jeney et al., 2008; Franosch and Jeney, 2009; Mo et al., 2015; Mo and Raizen, 2019). We also establish the directional variation of the hindered diffusion phenomena due to the perceived asymmetries in the flow geometry. The non-dimensional directional diffusivity estimates obtained reasonably match similar studies reported in literature (Gentile et al., 2015; Gubbiotti et al., 2019; Dechadilok and Deen, 2006). Moreover, these calculations also reveal an inherent anisotropy of the hydrodynamic resistances on the Brownian particle, an observation that

is also corroborated with relevant analytical (Haberman and Sayre, 1958; Chang and Keh, 2006) and experimental (Gentile et al., 2015) studies from literature. These results show that *LaIBM* manages to preserve the relevant bias in the hydrodynamic resistances. Thus, *LaIBM* can thus be used as a tool to study such fundamental hydrodynamic behavior of colloidal Brownian nanoparticles. This unique ability to incorporate such instantaneous hydrodynamics into a Langevin description of the Brownian particle on-the-fly makes *LaIBM* ideally suited to study hindered diffusion in arbitrary geometries. Note that for hindered diffusion in square micro-channels, the estimated λ_{IB} is found to fit reasonably well with a β-distribution. Thus, the relevant hydrodynamic resistances, for the chosen blockage ratios, can be directly obtained from the reported data. We further demonstrate the capabilities of our framework in dealing with more realistic pore diffusion cases using an arbitrary pore. The local (and averaged) instantaneous diffusivity of the particle is directly estimated using our framework, making it an ideal candidate to replace complex pore diffusion experiments, which already have inherent measurement difficulties. Hence, a more *in silico* driven assessment of complex pore diffusion phenomena is made possible. Such an effort would reduce both the time and costs incurred during prototyping. Moreover, detailed evaluation of transport-dependent pore accessibility of the void space in the porous material could also be feasible with our framework. These type of detailed in silico assessments would open-up challenging research frontiers at the micro/pore scales.

Our future efforts will be directed towards analyzing these complex colloidal pore-scale phenomena and further improving the performance of this framework by assessing the effects of particle–particle interactions on hindered diffusion phenomena. *LaIBM* already has the necessary capabilities to account for particle–particle interactions, including collisions. These effects can be included by including the relevant reduction in mobility due to the presence of surrounding particles, which is estimated from the forces acting on the respective particle, in the corresponding Langevin description of the particle. Moreover, as we use an IB method, we can easily include complex fractal-shaped particles as well as any other form of particle including (but not limited to) nanofibers, nanoparticles, nanorods, nanosheet, nanowires, nanotubes, or droplets (Zhang et al., 2012; Kannan et al., 2019). By including these additional capabilities, our framework can be used to simultaneously study the hindered diffusion behavior of several particles in micro-channels and arbitrary pores. Since the framework relies on a continuum-based solution to the surrounding flow field, additional transport of temperature and/or species can be directly incorporated by solving the relevant transport equations. Hence, our framework has the inherent capability to provide a detailed insight into reactive pore-scale phenomena as well.

This framework can also resolve particle deformation if needed (coupling between hydrodynamics and structural mechanics). Moreover, it can also be extended towards rarefied aerosol systems, provided the reduced momentum transfer between the gas and the solid is accounted for in a reasonable manner (for instance as shown in our previous work (Kannan et al., 2019)). Thus, a lot of the future capabilities are already inherently built-into the framework. In its current form, this framework can be directly applied to evaluate the behaviour of a single inert nanoparticle in a micro-channel/pore, aiding in probing the complex hydrodynamic interactions between the particle and its surrounding environment, which are often challenging to obtain using experimental techniques. Detailed insight into such pore-scale diffusive phenomena can aid in improving the understanding of several localized phenomena including deposition of nanoparticles and attachment of macromolecules. Since this framework is highly adaptable, it has a potential relevance in several applications including (but not lim-

ited to) studying *in silico* drug delivery, particulate emission dispersion and mitigation, nanofluids and short-time-scale Brownian motion, which further opens new avenues into the experimental study of statistical mechanics (Mo et al., 2015; Mo and Raizen, 2019).

CRediT authorship contribution statement

Ananda Subramani Kannan: Conceptualization, Methodology, Software, Validation, Formal analysis, Validation, Data curation, Writing - original draft. **Andreas Mark:** Methodology, Software, Validation, Validation, Resources, Data curation, Writing - review & editing. **Dario Maggiolo:** Conceptualization, Methodology, Writing - review & editing. **Gaetano Sardina:** Conceptualization, Methodology, Writing - review & editing. **Srdjan Sasic:** Conceptualization, Methodology, Writing - review & editing, Supervision. **Henrik Ström:** Conceptualization, Methodology, Writing - review & editing, Funding acquisition, Supervision, Supervision, Writing - review & editing.

Declaration of Competing Interest

None.

Appendix A. Supplementary material

Supplementary data associated with this article can be found, in the online version, at https://doi.org/10.1016/j.ces.2020.116074.

References

Andarwa, S., Basirat Tabrizi, H., Ahmadi, G., 2014. Effect of correcting near-wall forces on nanoparticle transport in a microchannel. Particuology, vol. 16, pp. 84–90, 2014. DOI: 10.1016/j.partic.2013.11.007, ISSN: 16742001.

Banerjee, A., Kihm, K.D., 2005. Experimental verification of near-wall hindered diffusion for the Brownian motion of nanoparticles using evanescent wave microscopy. Phys. Rev. E - Stat., Nonlinear, Soft Matter Phys. 72 (4), 1–4. https://doi.org/10.1103/PhysRevE.72.042101. ISSN: 15393755.

Bell, J.B., Garcia, A.L., Williams, S.A., 2007. Numerical methods for the stochastic landau-lifshitz navier-stokes equations. Phys. Rev. E, vol. 76, p. 016 708, 1 2007. DOI: 10.1103/PhysRevE. 76.016708.

Berry, H., Chate, H., 2014. Anomalous diffusion due to hindering by mobile obstacles undergoing Brownian motion or Orstein-Ulhenbeck processes. Phys. Rev. E - Stat., Nonlinear, Soft Matter Phys. 89 (2), 1–9. https://doi.org/10.1103/PhysRevE.89.022708. eprint: 1103.2206, ISSN: 15502376.

Bevan, M.A., Prieve, D.C., 2000. Hindered diffusion of colloidal particles very near to a wall: revisited. J. Chem. Phys. 113 (3), 1228–1236. https://doi.org/10.1063/1.481900. ISSN: 00219606.

Biondi, S.A., Quinn, J.A., 1995. Direct observation of hindered brownian motion. AIChE J. 41 (5), 1324–1328. https://doi.org/10.1002/aic.690410528. ISSN: 15475905.

Bird, G.A., 1994. Molecular Gas Dynamics and Direct Simulation of Gas Flow. Oxford University Press, London.

Bird, G.A, 2013. The DSMC method. CreateSpace Independent Publishing Platform, 2013, ISBN: 978-1492112907.

Brenner, H., 1961. The slow motion of a sphere through a viscous fluid towards a plane surface. Chem. Eng. Sci. 16 (3–4), 242–251. https://doi.org/10.1016/0009-2509(61)80035-3. ISSN: 00092509.

Brenner, H., 1982. A general theory of taylor dispersion phenomena iv. direct coupling effects. Chem. Eng. Commun. 18 (5–6), 355–379. https://doi.org/10.1080/00986448208939976.

Brenner, H., Gaydos, L.J., 1977. The constrained brownian movement of spherical particles in cylindrical pores of comparable radius. Models of the diffusive and convective transport of solute molecules in membranes and porous media. J. Colloid Interface Sci. 58 (2), 312–356. https://doi.org/10.1016/0021-9797(77)90147-3. ISSN: 00219797.

Burada, P.S., Hanggi, P., Marchesoni, F., Schmid, G., Talkner, P., 2009. Diffusion in confined geometries. ChemPhysChem 10 (1), 45–54. https://doi.org/10.1002/cphc.200800526. eprint:0808.2345, ISSN: 14397641.

F.C. Centre, Ips iboflow. [Online]. Available: http://www.fcc.chalmers.se/software/ips/ iboflow/.

Chandrasekhar, S., 1943. Stochastic problems in physics and astronomy. Rev. Mod. Phys. 15 (1), 1–89. https://doi.org/10.1103/RevModPhys. 15.1.

Chang, Y., Keh, H., 2006. Slow motion of a slip spherical particle perpendicular to two plane walls. J. Fluids Struct. 22 (5), 647–661. https://doi.org/10.1016/j.jfluidstructs.2006.02.006. ISSN: 0889-9746.

Choi, C.K., Margraves, C.H., Kihm, K.D., 1961. Examination of near-wall hindered Brownian diffusion of nanoparticles: Experimental comparison to theories by Brenner (1961) and Goldman et al. (1967), Physics of Fluids, vol. 19, no. 10, 2007. DOI: 10.1063/1.2798811, ISSN: 10706631.

Cukier, R.I., Mehaffey, J.R., Kapral, R., 1978. Kinetic theory derivation of a pair configuration space diffusion equation. J. Chem. Phys. 69 (11), 4962–4975. https://doi.org/10.1063/1.436485. ISSN: 00219606.

Cukier, R.I., Kapral, R., Mehaffey, J.R., 1981. Kinetic theory of the hydrodynamic interaction between two particles. J. Chem. Phys. 74 (4), 2494–2504. https://doi.org/10.1063/1.441318. ISSN: 00219606.

Davidson, M.G., Deen, W.M., 1988. Hydrodynamic theory for the hindered transport of flexible macromolecules in porous membranes. J. Membr. Sci. 35 (2), 167–192. https://doi.org/10.1016/S0376-7388(00)82442-4. ISSN: 03767388.

Dechadilok, P., Deen, W.M., 2006. Hindrance factors for diffusion and convection in pores. Industr. Eng. Chem. Res. 45 (21), 6953–6959. https://doi.org/10.1021/ie051387n.

Deen, W.M., 1987. Hindered transport of large molecules in liquid-filled pores. AIChE J. 33 (9), 1409–1425. https://doi.org/10.1002/aic.690330902. ISSN: 15475905.

Derks, R.J., Frijns, A.J., Prins, M.W., Dietzel, A.H., 2008. Self-organized twinning of actuated particles for microfiuidic pumping. Appl. Phys. Lett., vol. 92, no. 2, 2008. DOI: 10.1063/1.2834851, ISSN: 00036951.

Di Sarli, V., Di Benedetto, A., 2015. Modeling and simulation of soot combustion dynamics in a catalytic diesel particulate filter. Chem. Eng. Sci. 137, 69–78. https://doi.org/10.1016/j.ces.2015.06.011. ISSN: 00092509.

Di Sarli, V., Landi, G., Lisi, L., Saliva, A., Di Benedetto, A., 2016. Catalytic diesel particulate filters with highly dispersed ceria: Effect of the soot-catalyst contact on the regeneration performance. Appl. Catal. B: Environ., vol. 197, pp. 116–124, Forty years of catalysis by ceria: a success story. doi: 10.1016/j.apcatb.2016.01.073, ISSN: 0926-3373.

Einstein, A., 1905. ber die von der molekularkinetischen theorie der warme erforderte bewegung von in ruhenden fliissigkeiten suspendierten teilchen. Ann. Phys. 322 (8), 549–560. https://doi.org/10.1002/andp.19053220806.

Eloul, S., Katelhon, E., Batchelor-Mcauley, C., Tschulik, K., Compton, R.G., 2015. Diffusional nanoim-pacts: The stochastic limit. J. Phys. Chem. C, vol. 119, no. 25, pp. 14 400–14 410, 2015. DOI: 10.1021/acs.jpcc.5b03210, ISSN: 19327455.

Espafiol, P., Warren, P.B., 2017. Perspective: Dissipative particle dynamics. J. Chem. Phys. 146 (15), 150 901. https://doi.org/10.1063/1.4979514.

Espanol, P., 1998. Stochastic differential equations for non-linear hydrodynamics. Phys. A 248 (1), 77–96. https://doi.org/10.1016/S0378-4371(97)00461-5. ISSN: 0378-4371.

Faxen, H., 1921. Einwirkung der gefasswande auf den widerstand gegen die bewegung einer kleinen kugel in einer zahen fliissigkeit (PhD thesis), Ph.D. dissertation. Uppsala University.

Faxen, H., 1927. Die bewegung einer starren kugel langs der achse eines mit zaher flfisigkeit fefiillten rohres. Arkiv for Matematik Astronomi och Fysik 17 (27), 1–28.

Felderhof, B.U., 2005. Effect of the wall on the velocity autocorrelation function and long-time tail of Brownian motion. J. Phys. Chem. B, vol. 109, no. 45, pp. 21 406–21 412, 2005. DOI: 10.1021/jp051335b, ISSN: 15206106.

Felderhof, B.U., 2006. Diffusion and velocity relaxation of a brownian particle immersed in a viscous compressible fluid confined between two parallel plane walls. J. Chem. Phys. 124 (5), 054111. https://doi.org/10.1063/1.2165199.

Franosch, T., Jeney, S., 2009. Persistent correlation of constrained colloidal motion. Phys. Rev. E, vol. 79, p. 031402, 3 2009. DOI: 10.1103/PhysRevE. 79.031402.

Frej, N.A., Prieve, D.C., 1993. Hindered diffusion of a single sphere very near a wall in a nonuniform force field. J. Chem. Phys. 98 (9), 7552–7564. https://doi.org/10.1063/1.464695.

Gentile, F.S., Santo, I.D., D'Avino, G., Rossi, L., Romeo, G., Greco, F., Netti, P.A., Maffettone, P.L., 2015. Hindered Brownian diffusion in a square-shaped geometry. J. Colloid Interface Sci. 447, 25–32. https://doi.org/10.1016/j.jcis.2015.01.055. ISSN: 10957103.

Goldman, A.J., Cox, R.G., Brenner, H., 1967. Slow viscous motion of a sphere parallel to a plane wall-I Motion through a quiescent fluid. Chem. Eng. Sci., vol. 22, no. 4, pp. 637–651, 1967, ISSN:00092509. DOI: 10.1016/0009-2509(67)80047-2.

Goswami, P., Baier, T., Tiwari, S., Lv, C., Hardt, S., Klar, A., 2020. Drag force on spherical particle moving near a plane wall in highly rarefied gas. J. Fluid Mech. 883, A47. https://doi.org/10.1017/jfm.2019.921.

Gubbiotti, A., Chinappi, M., Casciola, C.M., 2019. Confinement effects on the dynamics of a rigid particle in a nanochannel. Phys. Rev. E, vol. 100, p. 053 307, 5 2019. DOI: 10.1103/PhysRevE. 100.053307.

Haberman, W.L., Sayre, R.M., 1958. Motion of rigid and fluid spheres in stationary and moving liquids inside cylindrical tubes, Department of the navy - David Taylor model basin, Tech. Rep., 1958. [Online]. Available: http://hdl.handle.net/1721.3/48988.

Happel, J., Brenner, H., 1983. Low Reynolds number hydrodynamics. Martinus Nijhoff publishers, 1983, ISBN: 13: 978-90-247-2877-0. DOI: 10.1007/978-94-009-8352-6.

Hauge, E.H., Martin-Löf, A., 1973. Fluctuating hydrodynamics and brownian motion. J. Stat. Phys. 7 (3), 259–281. https://doi.org/10.1007/BF01030307. ISSN: 1572-9613.

Hindi, E.J., 1975. Application of the langevin equation to fluid suspensions. J. Fluid Mech. 72 (3), 499–511. https://doi.org/10.1017/S0022112075003102.

Hlushkou, D., Svidrytski, A., Tallarek, U., 2017. Tracer-Size-Dependent Pore Space Accessibility and Long-Time Diffusion Coefficient in Amorphous, Mesoporous Silica. J. Phys. Chem. C 121 (15), 8416–8426. https://doi.org/10.1021/acs.jpcc.7b00264. ISSN: 19327455.

Huang, R., Chavez, I., Taute, K.M., Lukic, B., Jeney, S., Raizen, M.G., Florin, E.-L., 2011. Direct observation of the full transition from ballistic to diffusive brownian motion in a liquid. Nat. Phys. 7, 576. https://doi.org/10.1038/nphys953.

Imperio, A., Padding, J.T., Briels, W.J., 2011. Diffusion of spherical particles in microcavities. J. Chem. Phys., vol. 134, no. 15, 2011. DOI: 10.1063/1.3578186, ISSN: 00219606.

Ito, K., 1973. Stochastic integration. In: Tucker, D.H., Maynard, H.B. (Eds.), Vector and Operator Valued Measures and Applications. Academic Press, pp. 141–148. https://doi.org/10.1016/B978-0-12-702450-9.50020-8.

Jeney, S., familyi=c, given=Branimir, giveni=B., Kraus, J.A., Franosch, T., Forro, L., 2008. Anisotropic memory effects in confined colloidal diffusion. Phys. Rev. Lett., vol. 100, p. 240 604, 24 2008. DOI: 10.1103/PhysRevLett.100.240604.

Kannan, A.S., Naserentin, V., Mark, A., Maggiolo, D., Sardina, G., Sasic, S., Strom, H., 2019. A continuum-based multiphase DNS method for studying the Brownian dynamics of soot particles in a rarefied gas. Chem. Eng. Sci., vol. 210, p. 115 229, 2019. DOI: 10.1016/j.ces.2019.115229, ISSN: 0009-2509.

Katelhon, E., Sokolov, S.V., Compton, R.G., 2016. Near-wall hindered diffusion: Implications for surface-based sensors. Sens. Actuat., B: Chem. 234, 420–425. https://doi.org/10.1016/j.snb.2016.05.016. ISSN: 09254005.

Kheifets, S., Simha, A., Melin, K., Li, T., Raizen, M.G., 2014. Observation of brownian motion in liquids at short times: Instantaneous velocity and memory loss. Science 343 (6178), 1493–1496. https://doi.org/10.1126/science.1248091. ISSN: 0036-8075.

Kihm, K.D., Banerjee, A., Choi, C.K., Takagi, T., 2004. Near-wall hindered Brownian diffusion of nanoparticles examined by three-dimensional ratiometric total internal reflection fluorescence microscopy (3-D R-TIRFM). Exp. Fluids 37 (6), 811–824. https://doi.org/10.1007/s00348-004-0865-4. ISSN: 07234864.

Kim, S., Karrila, S.J., 1991. Microhydrodynamics: principles and selected applications. Butterworth-Heinemann. ISBN: 9781483161242.

Konstandopoulos, A.G., Papaioannou, E., 2008. Update on the science and technology of diesel particulate filters. KONA Powder Part. J. 26 (March), 36–65. https://doi.org/10.14356/kona.2008007. ISSN: 21875537.

Kostoglou, M., Housiada, P., Konstandopoulos, A.G., 2003. Multi-channel simulation of regeneration in honeycomb monolithic diesel particulate filters. Chem. Eng. Sci. 58 (14), 3273–3283. https://doi.org/10.1016/S0009-2509(03)00178-7. ISSN: 00092509.

Kubo, R., 1966. The fluctuation-dissipation theorem. Rep. Prog. Phys. 29 (1), 255–284. https://doi.org/10.1088/0034-4885/29/1/306. ISSN: 00344885.

Ladd, A.J.C., 1994a. Numerical simulations of particulate suspensions via a discretized boltzmann equation, part 1. theoretical foundation. J. Fluid Mech. 271, 285–309. https://doi.org/10.1017/S0022112094001771.

Ladd, A.J.C., 1994b. Numerical simulations of particulate suspensions via a discretized boltzmann equation, part 2. numerical results. J. Fluid Mech. 271, 311–339. https://doi.org/10.1017/S0022112094001783.

Landau, L.D., Lifshitz, E.M., 1987. Chapter vi - diffusion, in Fluid Mechanics (Second Edition). Pergamon, 227–237, ISBN: 978-0-08-033933-7. doi: 10.1016/B978-0-08-033933-7.50014-3.

Langevin, P., 1908. Sur la theorie du mouvement brownien. C.R. Acad. Sci. (Paris) 146, 530–533. https://doi.org/10.1119/1.18725.

Lau, A.W.C., Lubensky, T.C., 2007. State-dependent diffusion: Thermodynamic consistency and its path integral formulation. Phys. Rev. E, vol. 76, p. 011123, 1 2007. DOI: 10.1103/PhysRevE.76.011123.

Li, A., Ahmadi, G., 1992. Dispersion and deposition of spherical particles from point sources in a turbulent channel flow. Aerosol Sci. Technol. 16 (4), 209–226. https://doi.org/10.1080/02786829208959550.

Li, T., Kheifets, S., Medellin, D., Raizen, M.G., 2010. Measurement of the instantaneous velocity of a brownian particle. Science 328 (5986), 1673–1675. https://doi.org/10.1126/science.1189403. ISSN: 0036-8075.

Li, J., Jiang, X., Singh, A., Heinonen, O.G., Hernandez-Ortiz, J.P., de Pablo, J.J., 2020. Structure and dynamics of hydrodynamically interacting finite-size brownian particles in a spherical cavity: Spheres and cylinders. J. Chem. Phys. 152 (20), 204 109. https://doi.org/10.1063/1.5139431.

Liu, Z., Zhu, Y., Clausen, J.R., Lechman, J.B., Rao, R.R., Aidun, C.K., 2019. Multiscale method based on coupled lattice-boltzmann and langevin-dynamics for direct simulation of nanoscale particle/polymer suspensions in complex flows. Int. J. Numer. Meth. Fluids 91 (5), 228–246. https://doi.org/10.1002/fld.4752.

Lobry, L., Ostrowsky, N., 1996. Diffusion of Brownian particles trapped between two walls: Theory and dynamic-light-scattering measurements. Phys. Rev. B - Condensed Matter Mater. Phys. 53 (18), 12050–12056. https://doi.org/10.1103/PhysRevB.53.12050. ISSN: 1550235X.

Lorentz, H.A., 1907. Abhandlungen u'ber theoretische Physik. B.G. Teubner, 23–42.

MacKay, G.D.M., Mason, S.G., 1961. Approach of a solid sphere to a rigid plane interface. J. Colloid Sci. 16 (6), 632–635. https://doi.org/10.1016/0095-8522(61)90049-6. ISSN: 0095-8522.

Mainardi, F., Mura, A., Tampieri, F., 2009. Brownian motion and anomalous diffusion revisited via a fractional Langevin equation. Modern Probl. Stat. Phys., vol. 8, pp. 3–23, 2009. [Online]. Available: http://arxiv. org/abs/1004.3505.

Mark, A., van Wachem, B.G.M., 2008. Derivation and validation of a novel implicit second-order accurate immersed boundary method. J. Comput. Phys. 227 (13), 6660–6680. https://doi.org/10.1016/j.jcp.2008.03.031. ISSN: 0021-9991.

Mark, A., Rundqvist, R., Edelvik, F., 2011. Comparison between different immersed boundary conditions for simulation of complex fluid flows. Fluid Dynam. Mater. Process. 7, 241–258. https://doi.org/10.3970/fdmp.2011.007.241.

Mavrovouniotis, G.M., Brenner, H., 1988. Hindered sedimentation, diffusion, and dispersion coefficients for brownian spheres in circular cylindrical pores. J. Colloid Interface Sci. 124 (1), 269–283. https://doi.org/10.1016/0021-9797(88)90348-7. ISSN: 00219797.

Maxey, M.R., Riley, J., 1983. Equation of motion for a small rigid sphere in a nonuniform flow. Phys. Fluids 26 (4), 883–889. https://doi.org/10.1063/1.864230. ISSN: 0031-9171.

Michaelides, E.E., 2016. Wall Effects on the Brownian Movement, Thermophoresis, and Deposition of Nanoparticles in Liquids. J. Fluids Eng., vol. 138, no. 5, Jan. 2016. DOI: 10.1115/1.4032030, ISSN: 0098-2202.

Michaelides, E.E., 2017. Nanoparticle diffusivity in narrow cylindrical pores. Int. J. Heat Mass Transf. 114, 607–612. https://doi.org/10.1016/j.ijheatmasstransfer.2017.06.098. ISSN: 0017-9310.

Michaelides, E., 2019. Hindered electrophoresis of nanoparticles in narrow pores. J. Therm. Anal. Calonm. 135 (2), 1363–1371. https://doi.org/10.1007/sl0973-018-7462-x.

Mittal, R., Iaccarino, G., 2005. Immersed boundary methods. Annu. Rev. Fluid Mech. 37 (1), 239–261. https://doi.org/10.1146/annurev.fluid.37.061903.175743.

Mo, J., Raizen, M.G., 2019. Highly resolved brownian motion in space and in time. Annu. Rev. Fluid Mech. 51 (1), 403–428. https://doi.org/10.1146/annurev-fluid-010518-040527.

Mo, J., Simha, A., Raizen, M.G., 2015. Broadband boundary effects on brownian motion, Phys. Rev. E, vol. 92, p. 062106, 6 2015. DOI: 10.1103/PhysRevE.92.062106.

Mynam, M., Sunthar, P., Ansumali, S., 2011. Efficient lattice boltzmann algorithm for brownian suspensions. Philos. Trans. Roy. Soc. A: Math., Phys. Eng. Sci. 369 (1944), 2237–2245. https://doi.org/10.1098/rsta.2011.0047.

Nashed, O., Partoon, B., Lai, B., Sabil, K.M., Shariff, A.M., 2018. Review the impact of nanoparticles on the thermodynamics and kinetics of gas hydrate formation. J. Nat. Gas Sci. Eng. 55, 452–465. https://doi.org/10.1016/j.jngse. 2018.05.022. ISSN: 1875-5100.

Naumov, M., Arsaev, M., Castonguay, P., Cohen, J., Demouth, J., Eaton, J., Layton, S., Markovskiy, N., Reguly, I., Sakharnykh, N., Sellappan, V., Strzodka, R., 2015. Amgx: A library for gpu accelerated algebraic multigrid and preconditioned iterative methods. SIAM J. Scient. Comput. 37 (5), S602–S626. https://doi.org/10.1137/140980260.

Newmark, N.M., 1959. A method of computation for structural dynamics. J. Eng. Mech. Divis., vol. 85, pp. 67–94, 3 1959

Nitsche, J.M., 1995. Pore Diffusion of Nonspherical Brownian Particles. Ind. Eng. Chem. Res. 34 (10), 3606–3620. https://doi.org/10.1021/ie00037a050. ISSN: 15205045.

Nitsche, J.M., Balgi, G., 1994. Hindered Brownian Diffusion of Spherical Solutes within Circular Cylindrical Pores. Ind. Eng. Chem. Res. 33 (9), 2242–2247. https://doi.org/10.1021/ie00033a030. ISSN: 15205045.

Noetinger, B., 1990. Fluctuating hydrodynamics and brownian motion. Phys. A 163 (2), 545–558. https://doi.org/10.1016/0378-4371(90)90144-H. ISSN: 0378-4371.

O'Neill, M.E., Stewartson, K., 1967. On the slow motion of a sphere parallel to a nearby plane wall. J. Fluid Mech. 27 (4), 705–724. https://doi.org/10.1017/S0022112067002551.

Ounis, H., Ahmadi, G., 1990a. Analysis of dispersion of small spherical particles in a random velocity field. J. Fluids Eng. 112 (1), 114–120. https://doi.org/10.1115/1.2909358. ISSN: 0098-2202.

Ounis, H., Ahmadi, G., 1990b. A comparison of brownian and turbulent diffusion. Aerosol Sci. Technol. 13 (1), 47–53. https://doi.org/10.1080/02786829008959423. ISSN: 0278-6826.

Pagac, E.S., Tilton, R.D., Prieve, D.C., 1996. Hindered mobility of a rigid sphere near a wall. Chem. Eng. Commun. 148–50 (May), 105–122. https://doi.org/10.1080/00986449608936511. ISSN: 00986445.

Peskin, C.S., 1982. The fluid dynamics of heart valves: Experimental, theoretical, and computational methods. Annu. Rev. Fluid Mech. 14 (1), 235–259. https://doi.org/10.1146/annurev.fl.14.010182.001315.

Radhakrishnan, R., Farokhirad, S., Eckmann, D.M., Ayyaswamy, P.S., 2019. Chapter two - nanoparticle transport phenomena in confined flows. In: Sparrow, E.M., Abraham, J.P., Gorman, J.M., Minkowycz, W. (Eds.), Advances in Heat Transfer, ser. Advances in Heat Transfer, vol. 51. Elsevier, pp. 55–129. https://doi.org/10.1016/bs.aiht.2019.08.002.

Rahman, A., 1964. Correlations in the motion of atoms in liquid argon. Phys. Rev. 136 (2A), A405–A411. https://doi.org/10.1103/PhysRev.136.A405.

Ramakrishnan, N., Wang, Y., Eckmann, D.M., Ayyaswamy, P.S., Radhakrishnan, R., 2017. Motion of a nano-spheroid in a cylindrical vessel flow: Brownian and hydrodynamic interactions. J. Fluid Mech. 821, 117–152. https://doi.org/10.1017/jfm.2017.182.

Sharaf, O.Z., Al-Khateeb, A.N., Kyritsis, D.C., Abu-Nada, E., 2019. Numerical investigation of nanofluid particle migration and convective heat transfer in microchannels using an eulerian-lagrangian approach. J. Fluid Mech. 878, 62–97. https://doi.org/10.1017/jfm.2019.606.

A high-precision study of hindered diffusion near a wall. Appl. Phys. Lett., vol. 97, no. 10, pp. 1–4, 2010. DOI: 10.1063/1.3486123, ISSN: 00036951.

Simha, A., Mo, J., Morrison, P.J., 2018. Unsteady stokes flow near boundaries: The point-particle approximation and the method of reflections. J. Fluid Mech. 841, 883–924. https://doi.org/10.1017/jfm.2018.87.

Skaug, M.J., Wang, L., Ding, Y., Schwartz, D.K., 2015. Hindered nanoparticle diffusion and void accessibility in a three-dimensional porous medium. ACS Nano 9 (2), 2148–2156. https://doi.org/10.1021/acsnano.5b00019.

Sokolov, S.V., Katelhon, E., Compton, R.G., 2016. Near-wall hindered diffusion in convective systems: Transport limitations in colloidal and nanoparticulate systems. J. Phys. Chem. C, vol. 120, no. 19, pp. 10 629–10 640, 2016. DOI: 10.1021/acs. jpcc.6b01640, ISSN: 19327455.

Squires, T.M., Messinger, R.J., Manalis, S.R., 2008. Making it stick: Convection, reaction and diffusion in surface-based biosensors. Nat. Biotechnol. 26 (4), 417–426. https://doi.org/10.1038/nbtl388. ISSN: 10870156.

Stokes, G.G., 1848. On the Steady Motion of Incompressible Fluids. Trans. Cambridge Philos. Soc. 7, 439.

Strom, L., Strom, H., Carlsson, P.-A., Skoglundh, M., Harelind, H., 2018. Catalytically active pdag alloy nanoparticles synthesized in microemulsion template. Langmuir 34, 9754–9761. https://doi.org/10.1021/acs.langmuir.8bO1838.

Uhlenbeck, G.E., Ornstein, L.S., 1930. On the theory of the brownian motion. Phys. Rev. 36 (5), 823–841. https://doi.org/10.1103/PhysRev.36.823.

Uma, B., Swaminathan, T.N., Radhakrishnan, R., Eckmann, D.M., Ayyaswamy, P.S., 2011. Nanoparticle brownian motion and hydrodynamic interactions in the presence of flow fields. Phys. Fluids 23 (7), 073 602. https://doi.org/10.1063/1.3611026.

Van Ommering, K., Nieuwenhuis, J.H., Van Ijzendoorn, L.J., Koopmans, B., Prins, M. W., 2006. Confined Brownian motion of individual magnetic nanoparticles on a chip: Characterization of magnetic susceptibility. Appl. Phys. Lett., vol. 89, no. 14, 2006. DOI: 10.1063/1.2360246, ISSN: 00036951.

Van Ommering, K., Lamers, C.C., Nieuwenhuis, J.H., Van Ijzendoorn, L.J., Prins, M.W., 2009. Analysis of individual magnetic particle motion near a chip surface. J. Appl. Phys., vol. 105, no. 10, 2009. DOI: 10.1063/1.3118500, ISSN: 00218979.

Vitoshkin, H.,Yu, H.-Y., Eckmann, D.M., Ayyaswamy, P.S., Radhakrishnan, R., 2016. Nanoparticle stochastic motion in the inertial regime and hydrodynamic interactions close to a cylindrical wall. Phys. Rev. Fluids, vol. 1, p. 054104, 5 2016. DOI: 10.1103/PhysRevFluids. 1.054104.

von Smoluchowski, M., 1906. Zur kinetischen theorie der brownschen molekularbewegung und der suspen-sionen. Ann. Phys. 326 (14), 756–780. https://doi.org/10.1002/andp.19063261405. ISSN: 0003-3804.

Wakiya, S., 1953. A spherical obstacle in the flow of a viscous fluid through a tube. J. Phys. Soc. Jpn. 8 (2), 254–256. https://doi.org/10.1143/JPSJ.8.254.

Zhang, C., Thajudeen, T., Larriba, C., Schwartzentruber, T.E., Jr, C.J.H., 2012. Determination of the scalar friction factor for nonspherical particles and aggregates across the entire knudsen number inertial range by direct simulation monte carlo (dsmc). Aerosol Sci. Technol. 46 (10), 1065–1078. https://doi.org/10.1080/02786826.2012.690543.

Zhang, Z., Cai, J., Chen, F., Li, H., Zhang, W., Qi, W., 2018. Progress in enhancement of co2 absorption by nanofluids: A mini review of mechanisms and current status. Renew. Energy 118, 527–535. https://doi.org/10.1016/j.renene.2017.11.031. ISSN: 0960-1481.

Paper C

A hydrodynamic basis for off-axis Brownian diffusion under intermediate confinements in micro-channels

A hydrodynamic basis for off-axis Brownian diffusion under intermediate confinements in micro-channels

Ananda Subramani Kannan[a],[*], Andreas Mark[b], Dario Maggiolo[a], Gaetano Sardina[a], Srdjan Sasic[a], Henrik Ström[a]

[a]*Department of Mechanics and Maritime Sciences, Division of Fluid Dynamics, Chalmers University of Technology, Göteborg, 412 96, Sweden.*

[b]*Fraunhofer-Chalmers Research Centre, Göteborg, 412 88, Sweden.*

Abstract

The mobility of a Brownian particle diffusing in a micro-channel is heterogeneous and spatially dependent on the surrounding hydrodynamic resistance fields. The positional asymmetry of such a diffusing particle further leads to anisotropies in the observed diffusive behavior. In this paper, we probe such directionally varying diffusive behavior of a spherical nanoparticle diffusing at a location off-set from the centerline of a square micro-channel in a quiescent fluid. This investigation is carried out over varying degrees of intermediate hydrodynamic confinements. A coupled Langevin-immersed boundary method is used for these assessments. We observe that the co-axial diffusivity is enhanced during off-axis hindered diffusion when compared with a corresponding centerline diffusive behavior. We attribute this increased particle diffusivity to a reduced co-axial fluid resistance through a hydrodynamic basis derived using steady-state CFD simulations. For co-axial motion, the particle creates a recirculating flow pattern around itself when moving along the centerline, whereas it drags along the fluid in between itself and the wall when in close proximity to the latter. These contrasting flow behaviors are responsible for the unexpected enhancement of the co-axial diffusivity for off-axis hindered diffusion under intermediate hydrodynamic confinements.

Keywords: Brownian diffusion; CFD; Hindered diffusion; Hydrodynamic resistance; Immersed boundary method; Micro-channel and Mobility

1. Introduction

The diffusion of Brownian particles in confined environments is a well-explored problem [1]. An in-depth understanding of the hindered transport of such nanoparticles can aid in developing novel nanoengineering-based concepts for a wide range of applications. Some typical

[*]Corresponding author: ananda@chalmers.se

examples include designing filters for the entrapment of particulate matter [2], evaluating the performance of nano-electrofuels in redox flow batteries [3], bio-engineering applications involving transport of magnetized nano-particles in lab-on-a-chip devices [4], surface-based biosensors [5] and targeted drug delivery using functionalized nanocarriers [6]. In optimizing these applications, the ability to predict the behavior of individual nanoparticles in confined environments is of utmost importance. Such predictions are challenging as the non-equilibrium thermal fluctuations in the system render the relationship between the characteristics of the particle (and its surrounding environment) and its observable behavior a stochastic event. These challenges are further aggravated by the fact that under tight confinements, the hydrodynamic effect on the particle from the surrounding fluid changes nature – it is no longer a monotonous function of the particle-wall distance as the balance between parallel and normal hydrodynamic resistances is shifted [7].

It is well established that the mobility (defined as the ratio of the particle terminal velocity to the hydrodynamic frictional force) of a Brownian particle in a confined system is reduced in relation to the free (or unbounded) diffusion case [8–13]. This effect is due to the increased drag from the alteration of the hydrodynamic interaction between the particle and the fluid due to external boundaries [14]. Correspondingly, the mobility and (consequently) diffusivity of the particle are functions of the position of the Brownian particle in relation to the boundary walls, implying that the mobility is heterogeneous and spatially dependent [15]. It follows that these quantities can be corrected by a factor λ (also termed as the reduction in mobility), which represents the extent of the deviation from the analytical unbounded behavior [1, 9–11, 14, 16], in order to accurately represent hindered diffusion. For a more detailed account of related hindered diffusion theories, the reader is referred to the reviews by Deen [17], Burada et al. [18], Radhakrishnan et al. [19], Mo and Raizen [13] and to the classical books by Happel and Brenner [1] and Kim and Karilla [20].

Correspondingly, for a particle that is small in relation to the bounding geometry, well-established rules of thumb indicate that the hydrodynamic resistance to motion increases as the particle is positioned closer to the wall and that this effect is larger for wall-normal motion than for parallel motion. However, Gubbiotti et al. [21] found that as the confinement increases, the hydrodynamic effect for parallel motion will eventually surpass wall-normal motion in the central region of a small duct, as the minimum in the hydrodynamic influence on the wall-parallel particle motion shifts from the centerline to an off-axis position. In a recent paper [7], we identified a similar bias in the hydrodynamic resistances along the co-axial and wall normal directions on a Brownian particle diffusing in a square micro-channel. We noted that the former was greater than the latter for a particle diffusing co-axially along the centerline of the micro-channel. Such effects have not yet been fully understood or characterized previously. Consequently, in this work, we analyze the impact of such tight confinements on the Brownian motion of a spherical particle by further extending the range of confinements and by focusing on the pure hydrodynamic effect of confinement (without the action of any external field). Fully understanding this hydrodynamic bias is relevant when assessing Brownian transport in micro-channels with nanoparticles that are not negligible in size when compared with the channel width.

2

The existing body of work in this field mainly extends the hydrodynamic theories of Brenner and others [1, 14, 22, 23] for a spherical Brownian particle moving co-axially in a cylindrical channel towards off-axis diffusion. Mavrovouniotis and Brenner [24] achieved this by including an extra dispersion contribution (due to the positional asymmetry) in addition to the direct hindered-diffusion effect of the tube walls upon the mean co-axial diffusivity. Further, Dechadilok and Deen [25] presented an improved correlation based on the off-axis hydrodynamic results of Higdon and Muldowney [26] and Mavrovouniotis and Brenner [24]. A hydrodynamic basis cannot be derived from the expressions presented in that work [25] since all directional information is contained within a single scalar expression for λ, whereas λ is a function of both the position and direction of motion of the particle. More recently, Uma et al. [27] used an iterative fluctuating hydrodynamics (FH) approach to estimate the dependence of the co-axial and wall-normal estimates of λ as a function of the distance from the walls of a circular vessel in a quiescent medium. Gubbiotti et al. [21] used the dissipative particle dynamics (DPD) framework (a kinetic-theory-based approach) to construct a spatial mobility field for a Brownian particle diffusing in a cylindrical channel.

While these recent efforts have in principle probed the anisotropy in the hydrodynamic resistances, similar studies on hindered diffusion in arbitrary geometries and under asymmetric conditions are scarce. Moreover, the origin of the anisotropy in the hydrodynamic resistances felt by a Brownian particle under confinement has not been adequately probed. Thus, with this paper we aim at providing fresh insights into such systems. We present the relevant hydrodynamic basis for Stokesian off-axis hindered diffusion in a square micro-channel under intermediate confinement (i.e. the particle size is non-negligible in relation to the channel size while still smaller than the hydraulic diameter). We use a previously developed and validated multiphase direct numerical simulation (DNS) technique, a Langevin-immersed Boundary method or *LaIBM* [2, 7], to probe the relevant hydrodynamic fields around the Brownian particle. We evaluate the hindered diffusion initiated along the centerline (co-axial) of the channel as well as at a location that is off-set from this centerline (midway between the center and walls), under different confinements or blockage ratios (B given as a/d_p, where a is the side of the square duct and d_p the diameter of the spherical particle). The obtained results are compared with continuum-resolved (steady state) simulations for the single particle hydrodynamics using a settling particle in a channel. This is done in order to establish the necessary hydrodynamic basis for the observed hindered diffusion phenomena at high resolutions.

2. Methodology

We combine two separate computational frameworks for the current analysis: *LaIBM* (for the hindered Brownian diffusion simulations) and steady-state *CFD* simulations (for in-depth analysis of the hydrodynamic fields). This is done in order to establish the relevant hydrodynamic basis for hindered diffusion. These are both introduced in the following.

2.1. Langevin-Immersed Boundary method (*LaIBM*)

The *LaIBM* framework handles the particle in the Lagrangian frame of reference and the fluid in the Eulerian one, respectively. The immersed boundary method (IBM) [28, 29] is used to couple these descriptions. In this method, the Navier-Stokes equations are discretized on a Cartesian grid and the presence of the particle is modeled using boundary conditions or source terms. Furthermore, *LaIBM* utilizes a dynamic octree grid for the necessary refinements (around the IB) and a second-order accurate mirroring immersed boundary method [2, 7, 30, 31] to implicitly impose the necessary no-slip boundary condition at the IB surface. This unique and stable second-order accurate implicitly formulated immersed-boundary condition (IBC) is central to the efficiency and accuracy of this framework.

The Eulerian (or continuum) description of the fluid around the immersed particle is given by the Navier-Stokes equations:

$$\rho_f \left(\frac{\partial}{\partial t} \boldsymbol{v} + \boldsymbol{v} \cdot \boldsymbol{\nabla} \boldsymbol{v} \right) = * \boldsymbol{\nabla} P + \mu_f \boldsymbol{\nabla}^2 \boldsymbol{v} + f_i,$$
$$\boldsymbol{\nabla} \cdot \boldsymbol{v} = 0, \tag{1}$$

where, ρ_f, μ_f, v and P represent the fluid density, dynamic viscosity, velocity and pressure, respectively. The term f_i represents any external source term. This set of equations is solved together with an implicit Dirichlet IB condition. A more detailed description of the method is available in [30, 31]. The fluid force acting on the IB is calculated by integrating the fluid stresses over the surface of the IB as:

$$\mathbf{F_{IB}} = \int_{IB} \boldsymbol{\sigma} \cdot \mathbf{n} dS = \int_{IB} \left(* P\delta_{ij} + \tau \right) \cdot \mathbf{n} dS = \int_{IB} \left(* P\delta_{ij} + \mu_f \boldsymbol{\nabla}^2 \boldsymbol{v} \right) \cdot \mathbf{n} dS, \tag{2}$$

where, δ_{ij} is the Kronecker delta and σ is the total fluid stress tensor with $P\delta_{ij}$ and τ as the pressure and viscous contributions (from the fluid) for a surface S with normal $\boldsymbol{n}$, respectively. The corresponding torque on the IB with a position vector $\mathbf{r}$ is calculated using:

$$\mathbf{T_{IB}} = \int_{IB} \mathbf{r} \times \boldsymbol{\sigma} \cdot \mathbf{n} dS. \tag{3}$$

The particulate phase in the *LaIBM* framework is governed by the Lagrangian Langevin equation of motion [32–36]. This equation balances the macro-scale hydrodynamic drag on the particle with the molecular-scale Brownian fluctuations. For the hindered diffusion of a particle with mass m_p, translational velocity $\mathbf{u_p^i}$, angular velocity $\boldsymbol{\omega_p^i}$ and moment of inertia $\boldsymbol{J}$ (where the index i represents the degrees of freedom for the particle in a Cartesian basis),

the corresponding Langevin equation along the ith direction is described as:

$$m_p \frac{\mathrm{d}\mathbf{u_p^i}}{\mathrm{d}t} = \mathbf{F_{IB}^i} + \mathbf{F_{Brownian}^i}, \tag{4}$$

$$\mathbf{J} \frac{\mathrm{d}\omega_\mathbf{p}^\mathbf{i}}{\mathrm{d}t} = \mathbf{T_{IB}^i} * \boldsymbol{\omega}_p^i \times \mathbf{J} \cdot \boldsymbol{\omega}_p^i. \tag{5}$$

In Eqs. (4) and (5), note that the continuum resolved translational ($\mathbf{F_{IB}^i}$) and rotational ($\mathbf{T_{IB}^i}$) hydrodynamic fields are directly used in the Langevin equation, thus enforcing a direct coupling of the Eulerian solution with the corresponding Langevin equation of motion. Consequently, the directional reduction in mobility λ^i, which is directly required in the stochastic forcing term used in $\mathbf{F_{Brownian}^i}$, is estimated on-the-fly by normalizing the magnitude of the hydrodynamic force on the confined Brownian particle ($\mathbf{F_{IB}^i}$) with the corresponding Stokes drag (along the ith direction) on the same particle when diffusing in an unbounded domain. This is given as:

$$\lambda^i = \frac{\mathbf{F_{IB}^i}}{\gamma \mathbf{u_p^i}}. \tag{6}$$

Here, the Stokes friction factor γ is defined for a fluid with the dynamic viscosity μ_f as $\gamma = 3\pi \mu_f d_p$, and the relevant particle time scale (τ_p) is given as:

$$\tau_p = \frac{m_p}{\gamma \|\lambda^i\|} \tag{7}$$

The force $\mathbf{F_{Brownian}^i}$, which represents the Brownian fluctuations in the particle motion, is modeled as a linear time-invariant system represented as a Gaussian white noise process as given by [33, 35–37]:

$$\mathbf{F_{Brownian}^i}(\mathbf{t}) = m_p \mathbf{G} \sqrt{\frac{\pi \mathbf{S_0^i}}{\Delta t}}. \tag{8}$$

Here, $\mathbf{G}$ is a vector of normally distributed independent random numbers of zero mean and unit variance (Gaussian distribution), and Δt is the time step length during which the Brownian force is active. The vector of spectral intensity $\mathbf{S_0^i}$, is a function of the directional Brownian diffusivity D^i given as:

$$D^i = \frac{D^\infty}{\lambda^i} = \frac{k_B T}{\gamma \lambda^i}, \tag{9}$$

where, D^∞ (or bulk diffusivity) is given by the Stokes-Einstein equation with a further reduction by λ^i (in accordance with [24, 25, 38]) to account for confinement effects. The linear and angular momentum conservation equations (Eqs. (4) and (5)) are integrated using the Newmark time-marching scheme [39]. Note that this scheme is also compliant with the Itô interpretation [40] of a stochastic integral. Thus, the variation in the root-mean-squared displacement of the particle over sufficiently long times ($t >> \tau_p$) should reproduce the analytical Stokes-Einstein diffusivity, given as:

$$MSD^i = [\frac{1}{N} \sum_{n=1}^{N} (i(t+dt) * i(t))^2]^{\frac{1}{2}} = \sigma_{1D} \equiv 2D^i t, \tag{10}$$

along the ith direction. This result is dependent on the condition that the total hydrodynamic force on the particle can be obtained from the resolved force $\mathbf{F_{IB}^i}$ with the current hydrodynamic interaction effect obtained from Eq. (6) [7]. We use an in-house multiphase flow solver `IPS IBOFlow`, that utilizes the mirroring immersed-boundary method to handle the moving particles efficiently [41–48]. An overview of the $LaIBM$ framework is shown in Fig. 1. For more details on the framework, including the exact formulation of the spectral intensities $\mathbf{S_0^i}$, as well as a thorough validation of the $LaIBM$ framework, the reader is referred to our previous works [2, 7].
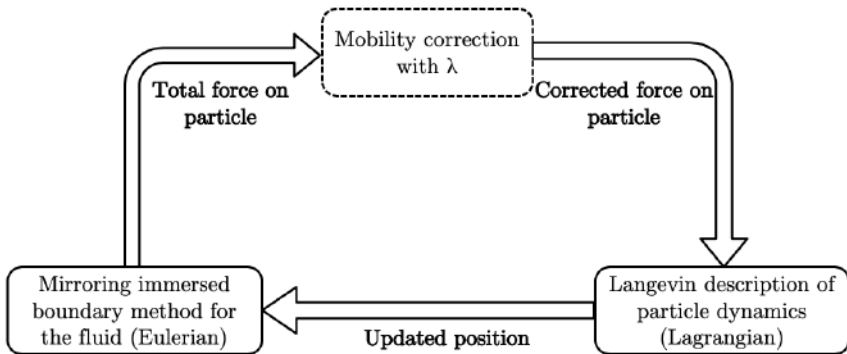
Figure 1: Overview of the $LaIBM$ framework: the particle dynamics are handled on a Lagrangian basis while the surrounding fluid is resolved in an Eulerian framework. Note that the Lagrangian basis utilizes the resolved fluid stresses on the particle (from the Eulerian solution) to compute/correct the particle mobility. This framework is 2-way coupled.

2.2. Steady-state computational fluid dynamics *(CFD)*

In addition to the continuum-based multiphase DNS framework $LaIBM$, we also use a conventional steady-state computational fluid dynamics *(CFD)* framework to establish a hydrodynamic basis for the results presented in this paper. This framework is chosen so as to off-set

the computational requirements of the proposed DNS method, thereby permitting a wider configuration space. Consequently, the steady-state Navier-Stokes equations are discretized within a finite volume framework [49] and solved using the pseudo-transient pressure-based solver available in `ANSYS Fluent 2019 R3`, with second-order accurate spatial discretization schemes used for all involved terms.

$$\rho_f \left(\boldsymbol{v} \cdot \boldsymbol{\nabla v} \right) = * \, \boldsymbol{\nabla} P + \mu_f \boldsymbol{\nabla}^2 \boldsymbol{v},$$
$$\boldsymbol{\nabla} \cdot \boldsymbol{v} = 0, \tag{11}$$

The particulate phase is defined as a fixed volume wherein the desired velocity is prescribed. The resulting hydrodynamic fields around this boundary region are utilized to extract the necessary hydrodynamic bases.
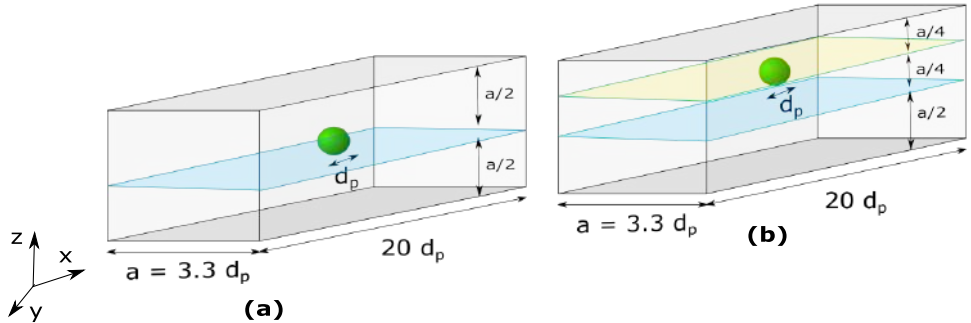
3. Numerical setup

Figure 2: Examples of the simulation domain: a) diffusion in the vicinity of the centerline (at $a/2$) inside a straight square micro-channel and b) diffusion originating from an off-axis position (at $a/4$) inside a straight square micro-channel. The dimensions are in terms of the particle diameter (d_p). Note that x is the co-axial direction, while z is the wall-normal direction under study here. The corresponding x-y planes at different z positions are depicted in the square micro-channel schematics.

The particle-fluid system studied in this paper is specified in Table 1. The hydrodynamic confinements are represented in terms of a blockage ratio, B, given as a/d_p (where a and d_p are the channel width and particle diameter, respectively). The assessments are carried out using a single spherical Brownian nanoparticle with a diameter of 400 nm. Further, the longitudinal extent of all the domains used in the diffusion simulations of this study is $20d_p$, with periodic conditions imposed along this direction. This length is chosen to minimize any inlet/outlet effects due to the applied boundary conditions on the particle motion. The

corresponding domain, along with the axis of orientation (x is the co-axial direction while y and z are the wall-normal directions), is shown in Fig. 2. The radial locations of the particle in the micro-channel are also indicated in this figure with the off-axis diffusion carried out at a location midway between the centerline and the wall. These simulations are done at a low particle Reynolds number ($Re_p = d_p V_{rms}^\infty \rho_p / \mu_f = 3 \cdot 10^{-3}$, where the root mean square velocity $V_{rms}^\infty = \sqrt{k_B T / m_p} = 1 \cdot 10^{-4}$ m/s is for an equivalent unbounded Brownian motion of a 400 nm particle) and at a particle-fluid density ratio of 1000, with k_B and T the Boltzmann constant and temperature of the fluid, respectively. These choices are made to maintain the validity of the current form of the Langevin equation (i.e. in Eq. (4) – unsteady effects such as history and added mass forces are negligible). In the simulation setup presented (in Table 1) we use the particle response time τ_p (see Eq. (7)) and the particle diameter d_p for non-dimensionalizing the temporal and spatial details, respectively. Further, since we deal with nanoparticle motion, gravitational acceleration is deemed negligible. These simulations are carried out under varying degrees of hydrodynamic confinement, to gauge the impact of particle blockage in the channel.

Domain details[+]	Square micro-channel
size (in d_p)	$a, h = 4.6$, $l = 20$ $a, h = 3.3$, $l = 20$ $a, h = 2.3$, $l = 20$
Simulation details	
Spatial resolution, in $cells/d_p$	96
Temporal resolution dt, in τ_p	1/200
Total duration T, in $\tau_p{}^*$	100

[+]l is the length, a is the width and h is the height

Table 1: Simulation details for the hindered diffusion cases (both centerline and off-axis)

We use steady-state continuum computational fluid dynamics simulations of a constant-velocity spherical particle in a square micro-channel to establish a hydrodynamic basis for the hindered diffusion studies. In these studies, we investigate several different locations radially in the channel for the spherical particle, from the centerline to a z-location close to the wall. Furthermore, we run simulations at blockage ratios (B) 4.6, 3.3 and 2.3, in order to span the requisite degree of intermediate confinements needed to establish a relevant hydrodynamic basis. To ensure Stokes flow, the Reynolds number (based on the hydrodynamic radius of the duct) is maintained at $1 \cdot 10^{-3}$. Mesh convergence is obtained by successively refining a base mesh in regions of large gradients of velocity and pressure, until the total force on the spherical particle does not change more than a factor 10^{-3} with further refinements. The base mesh uses a resolution of $1/10^{th}$ of the particle radius in the region occupied by the particle and $1/20^{th}$ of the duct radius in the far-field, which yields approximately 650,000 cells. The total number of cells after refinement varied with the geometrical configuration, but was within the range 1.5 - 5 million. The length of the cylindrical duct is 20 times its hydrodynamic radius, with the particle positioned in the middle along this co-axial coordinate direction.

8

No-slip boundary conditions are enforced along the duct walls and free-slip conditions at the far-field ends.

4. Validation of the numerical methods

The performance of the $LaIBM$ framework has been thoroughly validated in our earlier work [2, 7]. Correspondingly, the simulations are carried out at these predetermined spatial and temporal resolutions. Further, the Brownian forcing (see Eq. (8)) is updated in intervals of $\tau_p/10$ to allow for an adequate resolution of the particle acceleration. We have used a pure one-way coupled Langevin point-particle unbounded diffusion case to establish the minimum criteria in terms of simulation duration and time-averaging interval. Other details on the statistical variability in the modeled stochastic process are available in our previous work [2, 7]. The final criteria chosen (based on this prior work) are a total simulation duration (T) of $100\tau_p$ and an interval of $5\tau_p$ for the MSD calculations. These simulation settings are further listed in Table 1.

The steady state CFD framework is validated by comparing its performance to the analytical results of Haberman and Sayre [50] for cylindrical ducts. This analytical result is given (in terms of B) as:

$$\lambda_{HS1958} = \frac{(1 * 0.75857B^{-5})}{(1 * 2.1050B^{-1} + 2.0865B^{-3} * 1.7068B^{-5} + 0.72603B^{-6})}.$$ (12)

The reduction in particle mobility due to hydrodynamic confinement is deduced from the CFD results as:

$$\lambda_{CFD}^{i} = \frac{F^{i}}{F_{Stokes}^{i}},$$ (13)

where F^{i} and F_{Stokes}^{i} are the total drag forces on the particle along the ith direction under confinement and when unbounded, respectively. We have confirmed that we are able to reproduce the analytical results of Haberman and Sayre [50] (Eq. (12)) within $\pm 1\%$ in a cylindrical duct with this approach for B ranging from 20 to 2. These results are presented in Table 2. Furthermore, the DPD results of Gubbiotti et al. [21] are also listed in this table to demonstrate the accuracy attained in the steady-state CFD framework.

5. Results and discussion

In this paper we assess the off-axis hindered diffusion behavior of a spherical nanoparticle diffusing under intermediate confinements in a square micro-channel. These assessments are

Table 2: Validation of the steady-state CFD methodology against the analytical solution of Haberman and Sayre [50], λ_{HS1958}, for co-axial motion of a particle along the centerline of a cylindrical duct. Also listed are comparisons with the DPD results of Gubbiotti et al. [21], λ_{G2019}.

Blockage ratio	λ_{HS1958}	λ_{CFD}	λ_{G2019}
20.00	1.12	1.12	
4.87	1.71	1.70	1.63
4.00	1.98	1.96	
2.87	2.87	2.86	2.68
2.00	5.87	5.84	

undertaken to characterize and probe the relevant hydrodynamic behavior of such Brownian particles. Furthermore, a hydrodynamic basis is derived using steady-state CFD simulations in order to support the observed trends. These results are elaborated in the following.

5.1. Off-axis hindered diffusion under intermediate confinements

The diffusion of a Brownian particle at a location off-set from the centerline of a square micro-channel is assessed under the conditions specified in Table 1. These assessments are carried out at a non-dimensional radial location given as:

$$X^* = \frac{2p^z * a}{a * d_p},$$
(14)

where, p^z is the radial location (along the wall-normal z-direction) of the particle between the center of the channel and the walls (i.e. at $X^* = 0$ the particle is located on the centerline, while at $X^* = 1$ the particle touches the wall). Note that the non-dimensional radial locations listed in Table 3 correspond with the initial off-axis position midway between the centerline and the wall as shown in Fig. 2b.

Table 3: Non-dimensional radial location X^*, which corresponds to the off-axis position $a/4$ in Fig. 2b, at which the $LaIBM$ assessments are carried out (for each chosen blockage ratio).

Blockage ratio	X^*
4.60	0.638
3.30	0.717
2.30	0.882

Fig. 3 summarizes the off-axis hindered diffusion assessments done, showing both the particle drift/displacements (in the top panel) and the resulting directional mean-squared-displacements (MSD^i) that are calculated using Eq. (10) (bottom panel). We represent the drift of the particle in terms of a non-dimensional displacement (along the ith direction from the particle origin) as:

$$P^{i*} = p^{i*} * p^{i*}_{origin},$$ (15)

where, p^{i*} is the non-dimensional particle location given as $p^{i*} = p^i/d_p$. The mean-squared displacements are non-dimensionalized by the diffusional length scale for unbounded diffusion as:

$$MSD^{i*} = \frac{MSD^i}{D^\infty \tau_p^\infty},$$ (16)

where, τ_p^∞ is the response time of an unbounded Brownian particle. Note that the wall-normal motion is represented by the z-coordinate as the particle is off-set along this direction (y-symmetric).

Under these intermediate confinements, there is a noticeable difference in the mean drift of the Brownian particle across different blockage ratios as well as for the centerline and off-axis positions. The displacement of a freely diffusing Brownian particle ($\lambda = 1$) is also shown in Fig. 3 to appreciate the overall effect from the confinement. It is evident that the Brownian particle under confinement is displaced lesser than a corresponding unbounded particle. This is expected since the confinement increases the hydrodynamic resistance on the Brownian particle leading to its net lower drift (owing to the enhanced particle drag). There is, however, an interesting trend noticeable when comparing diffusion along the centerline with the corresponding off-axis cases listed in Table 3 (at $a/4$), under such intermediate confinements. In the co-axial direction, we can notice that a Brownian particle diffusing in the off-axis region is displaced more than the corresponding centerline case. Along the wall-normal direction, however, the opposite trend is observed with the Brownian particle in the off-axis cases being displaced significantly lesser than their corresponding centerline counterparts. These trends are also reflected in the reported MSD^{i*}.

We further summarize these anisotropic trends in terms of the respective directional diffusivities in the non-dimensional form D^i/D^∞ in Table 4. The particle diffusivity is estimated after the linear Stokes-Einstein regime is attained in the directional mean-squared-displacements (MSD^i). All D^i/D^∞ values decrease with blockage B (i.e. going downwards along the columns of Table 4), whereas the corresponding difference between the centerline and the off-axis positions at the same B is characterized by an increase in co-axial motion but a decrease in wall-normal motion (looking sideways along the rows of Table 4). This enhancement along
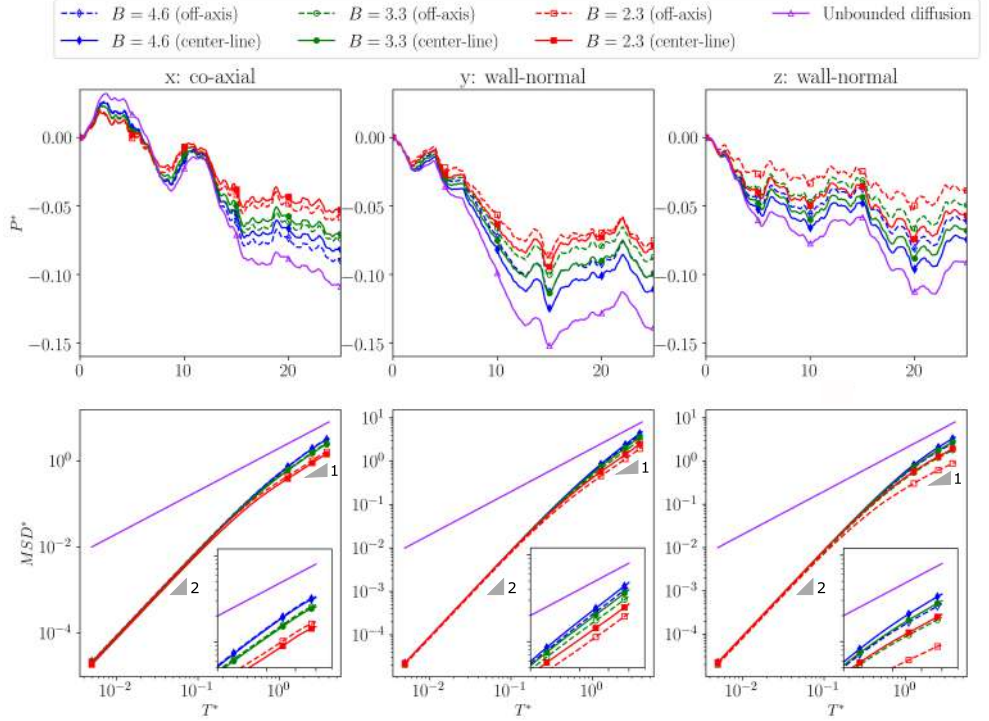
11

Figure 3: Comparison of the centerline and off-axis hindered diffusion for a 400 nm Brownian particle under varying degrees of confinement (represented as the blockage ratios (B) 4.6, 3.3 and 2.3, respectively) along the co-axial (x) and wall-normal (z) directions. **Top panel**: the mean non-dimensional drift/displacement of the particle from the origin (estimated as $P^{i*} = p^{i*} * p^{i*}_{origin}$) over a 25 τ_p period. **Bottom panel**: the non-dimensional directional MSD^{i*} evaluated over $5\tau_p$ for a $100\tau_p$ period of motion. The purple solid lines (——) represent the analytical non-dimensionalized Stokes-Einstein behavior for unbounded Brownian motion (Eq. (9)). The insets show the linear diffusive regimes attained individually along each of these directions. Note the transition from a ballistic *(slope = 2)* to a linear diffusive regime. All reported drifts are calculated using the same random number sequence (**G**).

the co-axial direction is also listed in Table 4. The hydrodynamic basis for this observed counter-intuitive trend is explained in terms of particle mobility enhancement below using the steady-state CFD framework.

Table 4: Anisotropy in the non-dimensional directional diffusivities of a 400 nm Brownian particle in the x (co-axial) and z (wall-normal) directions after $5\tau_p$. Predictions of D^i/D_∞ from *LaIBM* are compared with $1/\lambda^i_{CFD}$, which is the mobility reduction deduced from steady-state CFD simulations (non-Brownian). Notice the enhanced diffusivity (due to lower mobility reduction) along the co-axial direction for the off-axis cases (at $a/4$) in both scenarios. The results listed in this table are of the same order of magnitude as those of [12, 21, 27], that performed similar assessments.

	Centerline				Off-axis				% enhancement	
Blockage ratio	x_{LaIBM}	x_{CFD}	z_{LaIBM}	z_{CFD}	x_{LaIBM}	x_{CFD}	z_{LaIBM}	z_{CFD}	x_{LaIBM}	x_{CFD}
4.6	0.638	0.605	0.690	0.653	0.655	0.609	0.522	0.518	2.66%	0.72%
3.3	0.496	0.467	0.576	0.528	0.513	0.478	0.359	0.355	1.95%	2.34%
2.3	0.304	0.293	0.399	0.365	0.324	0.298	0.172	0.122	6.17%	1.76%

D_∞ is estimated from the corresponding unbounded Brownian diffusion simulations ($\lambda = 1$).

5.2. Mobility enhancement in the co-axial direction

The noted anisotropy in the diffusive behavior is explained using the the directional reduction in mobility, λ^i, of a non-Brownian spherical particle moving under similar conditions (a quiescent fluid). The reduction is deduced from the steady-state CFD simulations using Eq. (13). Owing to the theoretical relationship between D^i and λ^i (as shown in Eq. (9)), the expected effect on the diffusivity (in the diffusion simulations) of the Brownian particle can be directly estimated as:

$$\frac{D^i}{D^\infty} = \frac{1}{\lambda^i_{CFD}}. \tag{17}$$

Note that Eq. (17) is used to estimate the mobility reduction listed in Table 4. We emphasize that the CFD results are valid at the off-axis location $a/4$ exactly, while the *LaIBM* results represent an averaged behavior in the vicinity of this location due to the continuous motion of the particle. To provide a broader illustration of these enhancement effects from the CFD simulations, we also list the maximum enhancement found and the corresponding location of these maxima (in terms of X^*) in Table 5. In general, it is clear that a relatively minor displacement towards the centerline from the off-axis location (at $a/4$) results in a noticeable increase in the enhancement of the co-axial diffusivity, which may at least partly explain why the *LaIBM* results (which depict a Brownian particle under continuous motion) are higher than the corresponding CFD results (which depict a non-Brownian particle) for two out of three blockage ratios in Table 4. We furthermore stress that Table 5 does not necessarily reflect the global maxima, but only the maximum enhancement found in the locations probed in the CFD simulations.

Table 5: Maximum % enhancements and their corresponding positions along the co-axial direction when moving from a position on the centerline to an off-center position as obtained from the steady-state CFD analyses.

Blockage ratio	% enhancement	X^*_{max}
4.60	1.38%	0.436
3.30	2.52%	0.428
2.87	2.92%	0.423
2.30	5.19%	0.823

Overall we find that, as B decreases (i.e. the degree of confinement increases), the corresponding λ^i along the co-axial direction reduces to a distinct minimum value as the particle is shifted off-axis, before increasing again. This trend in λ^i is plotted in Fig. 4. We also note that the existence of a minimum is in agreement with the data presented by Gubbiotti et al. [21] (see Table 5 and the inset in Fig. 4). The noted enhancement along the co-axial direction is small enough to possibly be due to numerical uncertainties, however there could also be a hydrodynamic basis for the observed behavior. A strong argument for the latter hypothesis is that this effect is present in both our *LaIBM* and steady-state CFD results for the square duct, as well as in the DPD results of Gubbiotti et al. [21] and our steady-state CFD results for a cylindrical duct – i.e. that the effect has been observed in three independent frameworks and in two different geometries. Moreover, as this phenomenon is absent in the limits of $B \to \infty$ (point particle) and $B \to 0$ (particle touching the walls), it is also clear that it can only exist in some range of intermediate values of B, thus making it more difficult to observe by chance. Furthermore, since a Brownian particle does not remain at an exact location as in the steady state (non-Brownian) simulations, slight differences in the particle mobility are expected. Despite these differences, the underlying hydrodynamic basis is still reflected in a continuum multiphase DNS approach (such as the *LaIBM*) as the hydrodynamic fields around the particle are resolved to a reasonable degree of accuracy. Correspondingly, the mean λ^i, extracted from the particle mean-squared behavior as the inverse of the values listed in Table 4, is plotted in Fig. 4 as well (with an error bar indicating the span of X^* visited by the particle). This comparison further confirms that the obtained particle mobilities are in agreement with the established hydrodynamic bases (under the period of observation). Furthermore, the steady-state CFD results are more closer to the analytical solution of Haberman and Sayre [50] than the DPD results of Gubbiotti et al. [21] (as shown in Table 2), since the latter considers the effect of slip walls. This leads to lower predictions of λ as opposed to the no-slip walls considered by Haberman and Sayre [50] and our CFD setup. Despite these differences, the appearance of the minima in both sets of results, increases the plausibility of the described hydrodynamic basis.

5.3. A hydrodynamic basis for the anisotropy

In the limit of high values of B (not shown in this paper), the particle is small in relation to the duct and interacts with the walls only in its closest proximity. It is in this situation that
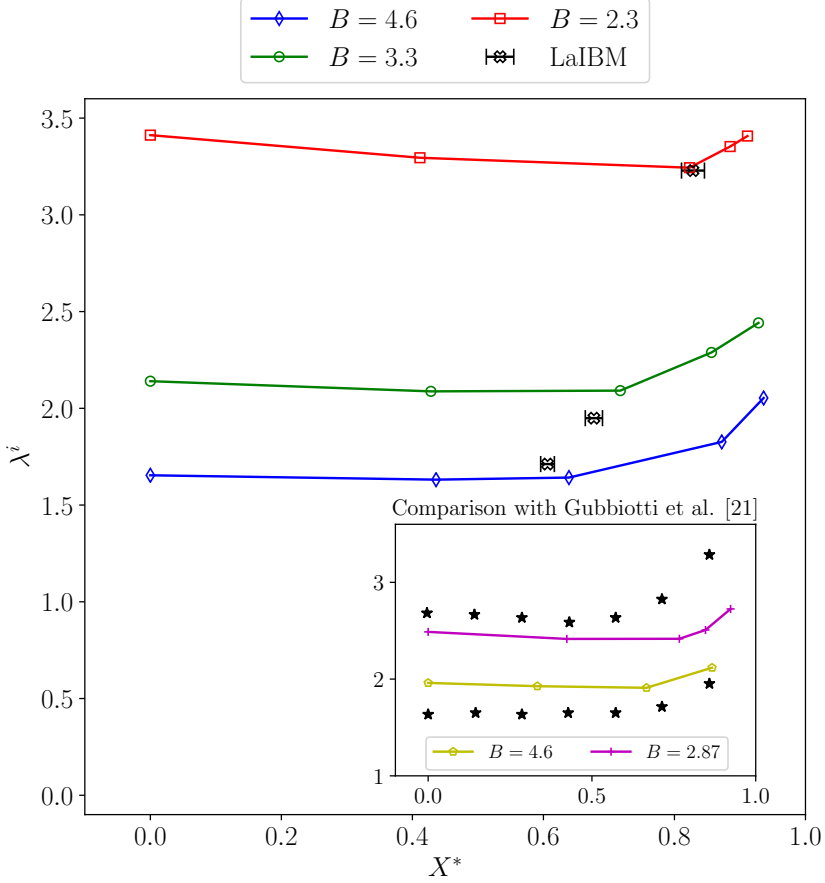
Figure 4: Directional reduction in mobility, λ^i, along the co-axial direction at the blockage ratios (B) 4.6, 3.3 and 2.3, respectively, for the CFD simulations in a square micro-channel. Here, X^* is the non-dimensional radial location of the particle between the center of the channel and the walls. The inset shows the comparison between the DPD data of Gubbiotti et al. [21] and our steady state CFD results in a cylindrical channel. Also plotted are the the mean λ^i, extracted from the particle mean-squared behavior in the $LaIBM$ framework with an error bar indicating the span of X^* visited by the particle in the simulation. Note the distinct minimum in λ^i as the particle is shifted off-axis.

λ^i is a monotonous function of the particle-wall distance, with the wall-normal interactions dominant over corresponding co-axial ones (as shown by Brenner [14]). However, as the confinement becomes more pronounced, the walls around the entire duct perimeter start to influence the flow field around the particle, implying that friction along all wall-bounded sides contribute to the overall λ^i. More specifically, the co-axial motion of the particle necessitates that the fluid in its path is displaced in a recirculating motion where it fills the region between the particle and the confining walls due to continuity (see Fig. 5). These flows are symmetric on the centerline and asymmetric for off-axis positions.
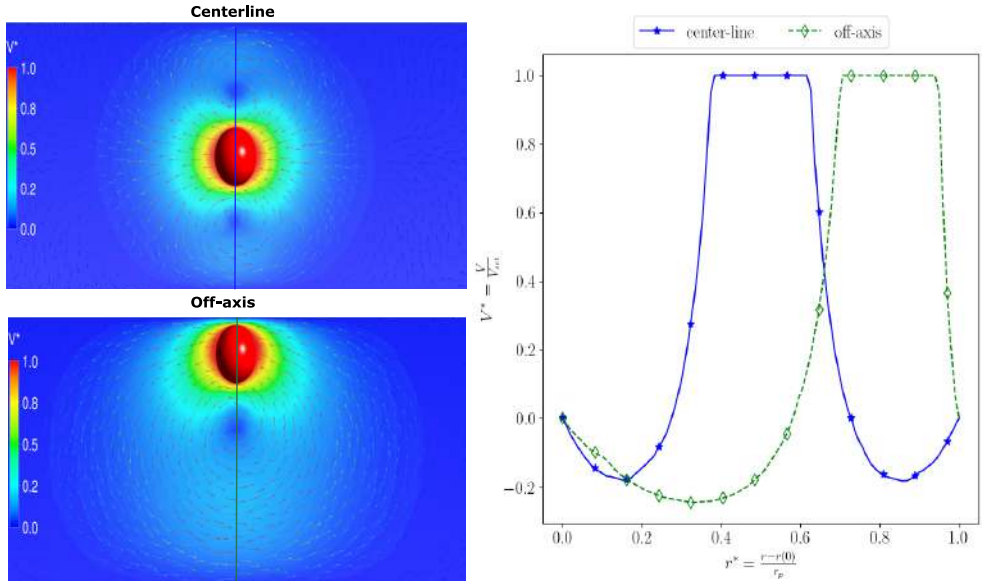

Figure 5: **Left panel:** Re-circulation zones around a particle located at centerline and off-center positions. Contours of normalized co-axial fluid velocity ($V^* = \frac{V}{V_p}$) overlaid with flow vectors along the same direction (from the steady-state CFD simulations) in an x-z plane at $6.5d_p < x < 13.5d_p$ (i.e. a 6 d_p co-axial span around the particle), $y = w/2$ and $0 < z < a$. This normalization is done for a simplified visualization of the hydrodynamic zones. **Right panel**: V^* over a line passing through the center of the particle (i.e. $x = l/2$, $y = w/2$ and $0 < z < a$) plotted as a function of the non-dimensional distance $r^* = \frac{r-r(0)}{r_p}$ ($r^* = 0$ and $r^* = 1$ represent the location of the walls along the z-direction) at $B = 4.6$. Note the lack of a flow reversal in the region between the particle and the wall in the off-axis configuration.

The cross-sectional area available for the displaced fluid to pass the particle is independent of the particle radial position, but the resistance to this flow varies with the geometrical configuration. As the particle comes in close proximity to the wall, there is no longer room for a re-circulation pattern to develop in the narrow slit between the particle and the wall. The flow field asymmetry is therefore significantly enhanced as the flow reversal between the particle and the wall dies out and the sphere, instead, drags along the fluid in this

16

narrow region. This lack of flow-reversal in between the particle and the wall is evident in the right panel of Fig. 5, which shows the normalized co-axial fluid velocity over a line passing a through the center of the particle across a centerline and off-axis motion at $B = 4.6$. Moving the particle off the centerline towards a wall increases the effective hydraulic diameter of the cross-section available for the flow without affecting the total flow rate, thus contributing to a lowering of the overall resistance. At the same time, the velocity gradient at the particle surface in the region between the particle and the wall goes to infinity as the particle-wall distance reduces, eventually causing a steep increase in the hydrodynamic resistance associated with the co-axial motion at small particle-wall separations. However, before that, the change of direction in the fluid motion within the narrow slit between the particle and the wall gives rise to the noticed minimum in λ^i.

Further, as B decreases, the particle fills up a larger portion of the channel cross-section and thus creates a relatively larger fluid displacement as it moves, leading to an increase in the overall hydrodynamic resistance. An increase in the effective hydraulic diameter, as obtained by moving the particle away from the centerline, therefore becomes more influential on the resistance, while at the same time shifting the location of minimal co-axial resistance further towards the wall as B decreases (see Fig. 4). The wall-normal motion, on the other hand, does not exhibit such a fundamental change of regimes, as the fluid in the region between the particle and the wall always has to be squeezed out irrespective of the wall-particle distance. Thus, these trends in the hydrodynamic resistances are responsible for the unexpected increase in co-axial diffusivity noted in the off-axis hindered diffusion of the Brownian particle.

5.4. Implications for simulations of Brownian motion at intermediate confinements

The existence of an enhancement effect on the Brownian motion (of a spherical particle in a micro-channel) at intermediate confinements has several important implications for simulations of such phenomena at varying levels of abstraction. For example, the application of wall corrections to the hydrodynamics in non-interface resolving methods must be done with great care, as these are generally derived in the $B \to \infty$ limit where enhancement effects are not present. It is also still an open question as to how this enhancement effect may change due to the presence of other Brownian particles or in a pressure-driven flow through the channel (with inertial effects from the fluid). Further, one must expect that the delicate balance between hydrodynamic effects, thermal fluctuations and additional external fields not accounted for here (e.g. van der Waals-interactions or electrostatic double-layer interactions) can be very sensitive to the exact geometrical configuration in the near-wall region of narrow channels, indicating that failure to correctly account for the true hydrodynamic environment around the Brownian particle will lead to erroneous predictions of the extent of particle-wall interaction. Such facets are very relevant in several reactive or biological systems. In conclusion, these facts point to the importance of probing Brownian motion at intermediate confinements with a numerical simulation model that can leverage the local hydrodynamic environment on-the-fly to dictate the ensuing diffusion.

6. Conclusions

In this paper, we evaluate the off-axis diffusion of a spherical Brownian particle in a square micro-channel, under intermediate hydrodynamic confinements (i.e. the particle size is non-negligible in relation to the channel size while still not touching the walls). We show that, under these conditions, the co-axial diffusivity of a particle diffusing off-axis may be enhanced when compared with a corresponding centerline diffusion. This effect is augmented as the particle confinement increases. We attribute this increased particle diffusivity to a reduced co-axial fluid resistance when the particle is displaced off-center, through a hydrodynamic basis derived using steady-state CFD simulations of a spherical particle moving in a channel. More specifically, the direction of fluid motion in the narrow region between the particle and the wall changes with the particle-wall distance at low blockages B (where $B = a/d_p$, a is the side of the duct and d_p is the particle diameter), creating a position of minimum hydrodynamic resistance for co-axial motion at an off-axis location (which in turn is a function of B). Such a minimum was noted in both our coupled continuum mechanics-Langevin multiphase DNS ($LaIBM$) and steady-state CFD results, as well as in the results reported in literature (the dissipative particle dynamics (DPD) results of Gubbiotti et al. [21]). Thus, the noted enhancement along the co-axial direction for off-axis hindered diffusion – although small enough to blend-in with numerical uncertainties at a coarser resolution – does seem to have a firm hydrodynamic basis. Consequently, we demonstrate how the $LaIBM$ framework, which incorporates the instantaneous hydrodynamics into the Langevin equation of motion, can be used to probe such anisotropies in hindered diffusion phenomena. These inferences open up new avenues for advanced functional material design, where the complex influence of nano-structured system boundaries on the Brownian behavior of nanoparticles can be probed and optimized *in silico*. A large number of applications in rapidly emerging nano-engineering fields would significantly benefit from such capabilities.

Acknowledgments

References

[1] J. Happel, H. Brenner, Low Reynolds number hydrodynamics, Martinus Nijhoff publishers, 1983. `doi:10.1007/978-94-009-8352-6`.

[2] A. S. Kannan, V. Naserentin, A. Mark, D. Maggiolo, G. Sardina, S. Sasic, H. Ström, A continuum-based multiphase DNS method for studying the Brownian dynamics of soot particles in a rarefied gas, Chemical Engineering Science 210 (2019) 115229. `doi:10.1016/j.ces.2019.115229`.

[3] S. V. Sokolov, E. Kätelhön, R. G. Compton, Near-wall hindered diffusion in convective systems: Transport limitations in colloidal and nanoparticulate systems, Journal of Physical Chemistry C 120 (19) (2016) 10629–10640. `doi:10.1021/acs.jpcc.6b01640`.

[4] R. J. Derks, A. J. Frijns, M. W. Prins, A. H. Dietzel, Self-organized twinning of actuated particles for microfluidic pumping, Applied Physics Letters 92 (2) (2008). `doi:10.1063/1.2834851`.

[5] T. M. Squires, R. J. Messinger, S. R. Manalis, Making it stick: Convection, reaction and diffusion in surface-based biosensors, Nature Biotechnology 26 (4) (2008) 417–426. `doi:10.1038/nbt1388`.

[6] P. S. Ayyaswamy, V. Muzykantov, D. M. Eckmann, R. Radhakrishnan, Nanocarrier Hydrodynamics and Binding in Targeted Drug Delivery: Challenges in Numerical Modeling and Experimental Validation, Journal of Nanotechnology in Engineering and Medicine 4 (1) (07 2013). `doi:10.1115/1.4024004`.

[7] A. S. Kannan, A. Mark, D. Maggiolo, G. Sardina, S. Sasic, H. Ström, Assessment of hindered diffusion in arbitrary geometries using a multiphase dns framework, Chemical Engineering Science 230 (2021) 116074. `doi:10.1016/j.ces.2020.116074`.

[8] G. D. M. MacKay, S. G. Mason, Approach of a solid sphere to a rigid plane interface, Journal of Colloid Science 16 (6) (1961) 632–635. `doi:https://doi.org/10.1016/0095-8522(61)90049-6`.

[9] M. A. Bevan, D. C. Prieve, Hindered diffusion of colloidal particles very near to a wall: revisited, Journal of Chemical Physics 113 (3) (2000) 1228–1236. `doi:10.1063/1.481900`.

[10] E. R. Dufresne, T. M. Squires, M. P. Brenner, D. G. Grier, Hydrodynamic coupling of two brownian spheres to a planar surface, Physical Review Letters 85 (15) (2000) 3317–3320. `doi:10.1103/PhysRevLett.85.3317`.

[11] C. K. Choi, C. H. Margraves, K. D. Kihm, Examination of near-wall hindered Brownian diffusion of nanoparticles: Experimental comparison to theories by Brenner (1961) and Goldman et al. (1967), Physics of Fluids 19 (10) (2007). `doi:10.1063/1.2798811`.

[12] F. S. Gentile, I. D. Santo, G. D'Avino, L. Rossi, G. Romeo, F. Greco, P. A. Netti, P. L. Maffettone, Hindered Brownian diffusion in a square-shaped geometry, Journal of Colloid and Interface Science 447 (2015) 25–32. `doi:10.1016/j.jcis.2015.01.055`.

[13] J. Mo, M. G. Raizen, Highly resolved brownian motion in space and in time, Annual Review of Fluid Mechanics 51 (1) (2019) 403–428. `doi:10.1146/annurev-fluid-010518-040527`.

[14] H. Brenner, The slow motion of a sphere through a viscous fluid towards a plane surface, Chemical Engineering Science 16 (3-4) (1961) 242–251. `doi:10.1016/0009-2509(61)80035-3`.

[15] M. J. Skaug, L. Wang, Y. Ding, D. K. Schwartz, Hindered nanoparticle diffusion and void accessibility in a three-dimensional porous medium, ACS Nano 9 (2) (2015) 2148–2156. `doi:10.1021/acsnano.5b00019`.

[16] K. D. Kihm, A. Banerjee, C. K. Choi, T. Takagi, Near-wall hindered Brownian diffusion of nanoparticles examined by three-dimensional ratiometric total internal reflection fluorescence microscopy (3-D R-TIRFM), Experiments in Fluids 37 (6) (2004) 811–824. `doi:10.1007/s00348-004-0865-4`.

[17] W. M. Deen, Hindered transport of large molecules in liquid-filled pores, AIChE Journal 33 (9) (1987) 1409–1425. `doi:10.1002/aic.690330902`.

[18] P. S. Burada, P. Hänggi, F. Marchesoni, G. Schmid, P. Talkner, Diffusion in confined geometries, ChemPhysChem 10 (1) (2009) 45–54. `arXiv:0808.2345, doi:10.1002/cphc.200800526`.

[19] R. Radhakrishnan, S. Farokhirad, D. M. Eckmann, P. S. Ayyaswamy, Chapter two - nanoparticle transport phenomena in confined flows, in: E. M. Sparrow, J. P. Abraham, J. M. Gorman, W. Minkowycz (Eds.), Advances in Heat Transfer, Vol. 51 of Advances in Heat Transfer, Elsevier, 2019, pp. 55 – 129. `doi:https://doi.org/10.1016/bs.aiht.2019.08.002`.

[20] S. Kim, S. J. Karrila, Microhydrodynamics: principles and selected applications, Butterworth-Heinemann, 1991.

[21] A. Gubbiotti, M. Chinappi, C. M. Casciola, Confinement effects on the dynamics of a rigid particle in a nanochannel, Phys. Rev. E 100 (2019) 053307. `doi:10.1103/PhysRevE.100.053307`.

[22] B. U. Felderhof, Effect of the wall on the velocity autocorrelation function and long-time tail of Brownian motion, Journal of Physical Chemistry B 109 (45) (2005) 21406–21412. `doi:10.1021/jp051335b`.

[23] E. E. Michaelides, Wall Effects on the Brownian Movement, Thermophoresis, and Deposition of Nanoparticles in Liquids, Journal of Fluids Engineering 138 (5) (01 2016). `doi:10.1115/1.4032030`.

[24] G. M. Mavrovouniotis, H. Brenner, Hindered sedimentation, diffusion, and dispersion coefficients for brownian spheres in circular cylindrical pores, Journal of Colloid And Interface Science 124 (1) (1988) 269–283. `doi:10.1016/0021-9797(88)90348-7`.

[25] P. Dechadilok, W. M. Deen, Hindrance factors for diffusion and convection in pores, Industrial & Engineering Chemistry Research 45 (21) (2006) 6953–6959. `doi:10.1021/ie051387n`.

[26] J. J. L. Higdon, G. P. Muldowney, Resistance functions for spherical particles, droplets and bubbles in cylindrical tubes, Journal of Fluid Mechanics 298 (1995) 193–210. `doi:10.1017/S0022112095003272`.

[27] B. Uma, T. N. Swaminathan, R. Radhakrishnan, D. M. Eckmann, P. S. Ayyaswamy, Nanoparticle brownian motion and hydrodynamic interactions in the presence of flow fields, Physics of Fluids 23 (7) (2011) 073602. `doi:10.1063/1.3611026`.

[28] C. S. Peskin, The fluid dynamics of heart valves: Experimental, theoretical, and computational methods, Annual Review of Fluid Mechanics 14 (1) (1982) 235–259. `doi:10.1146/annurev.fl.14.010182.001315`.

[29] R. Mittal, G. Iaccarino, Immersed boundary methods, Annual Review of Fluid Mechanics 37 (1) (2005) 239–261. `doi:10.1146/annurev.fluid.37.061903.175743`.

[30] A. Mark, B. G. M. van Wachem, Derivation and validation of a novel implicit second-order accurate immersed boundary method, Journal of Computational Physics 227 (13) (2008) 6660–6680. `doi:https://doi.org/10.1016/j.jcp.2008.03.031`.

[31] A. Mark, R. Rundqvist, F. Edelvik, Comparison between different immersed boundary conditions for simulation of complex fluid flows, Fluid Dynamics and Materials Processing 7 (2011) 241–258. `doi:10.3970/fdmp.2011.007.241`.

[32] P. Langevin, Sur la théorie du mouvement brownien, C. R. Acad. Sci. (Paris) 146 (1908) 530–533. `doi:https://doi.org/10.1119/1.18725`.

[33] G. E. Uhlenbeck, L. S. Ornstein, On the theory of the brownian motion, Physical Review 36 (5) (1930) 823–841. `doi:10.1103/PhysRev.36.823`.

[34] S. Chandrasekhar, Stochastic problems in physics and astronomy, Reviews of Modern Physics 15 (1) (1943) 1–89. `doi:10.1103/RevModPhys.15.1`.

[35] H. Ounis, G. Ahmadi, A comparison of brownian and turbulent diffusion, Aerosol Science and Technology 13 (1) (1990) 47–53. `doi:10.1080/02786829008959423`.

[36] A. Li, G. Ahmadi, Dispersion and deposition of spherical particles from point sources in a turbulent channel flow, Aerosol Science and Technology 16 (4) (1992) 209–226. `doi:10.1080/02786829208959550`.

[37] H. Ounis, G. Ahmadi, Analysis of dispersion of small spherical particles in a random velocity field, Journal of Fluids Engineering 112 (1) (1990) 114–120. `doi:10.1115/1.2909358`.

[38] H. Brenner, A general theory of taylor dispersion phenomena iv. direct coupling effects, Chemical Engineering Communications 18 (5-6) (1982) 355–379. `doi:10.1080/00986448208939976`.

[39] N. M. Newmark, A method of computation for structural dynamics, Journal of the Engineering Mechanics Division 85 (1959) 67–94.

[40] K. Itô, Stochastic integration, Academic Press, 1973, pp. 141–148. `doi:https://doi.org/10.1016/B978-0-12-702450-9.50020-8`.

[41] R. Rundqvist, A. Mark, B. Andersson, A. Ålund, F. Edelvik, S. Tafuri, J. S. Carlson, Simulation of spray painting in automotive industry, in: G. Kreiss, P. Lötstedt, A. Målqvist, M. Neytcheva (Eds.), Numerical Mathematics and Advanced Applications 2009, Springer Berlin Heidelberg, Berlin, Heidelberg, 2010, pp. 771–779. `doi: 10.1007/978-3-642-11795-4_83`.

[42] J. Göhl, A. Mark, S. Sasic, F. Edelvik, An immersed boundary based dynamic contact angle framework for handling complex surfaces of mixed wettabilities, International Journal of Multiphase Flow (2018). `doi:10.1016/j.ijmultiphaseflow.2018.08.001`.

[43] J. Göhl, K. Markstedt, A. Mark, K. Håkansson, P. Gatenholm, F. Edelvik, Simulations of 3d bioprinting: predicting bioprintability of nanofibrillar inks, Biofabrication 10 (3) (2018) 034105.
URL `http://stacks.iop.org/1758-5090/10/i=3/a=034105`

[44] A. Mark, E. Svenning, F. Edelvik, An immersed boundary method for simulation of flow with heat transfer, International Journal of Heat and Mass Transfer 56 (1) (2013) 424 – 435. `doi:10.1016/j.ijheatmasstransfer.2012.09.010`.

[45] T. Johnson, S. Jakobsson, B. Wettervik, B. Andersson, A. Mark, F. Edelvik, A finite volume method for electrostatic three species negative corona discharge simulations with application to externally charged powder bells, Journal of Electrostatics 74 (2015) 27 – 36. `doi:10.1016/j.elstat.2014.12.009`.

[46] B. Wettervik, T. Johnson, S. Jakobsson, A. Mark, F. Edelvik, A domain decomposition method for three species modeling of multi-electrode negative corona discharge – with applications to electrostatic precipitators, Journal of Electrostatics 77 (2015) 139 – 146.
`doi:https://doi.org/10.1016/j.elstat.2015.08.004`.
URL `http://www.sciencedirect.com/science/article/pii/S0304388615300346`

[47] S. Ingelsten, A. Mark, F. Edelvik, A lagrangian-eulerian framework for simulation of transient viscoelastic fluid flow, Journal of Non-Newtonian Fluid Mechanics 266 (2019) 20 – 32. `doi:10.1016/j.jnnfm.2019.02.005`.

[48] S. Ingelsten, A. Mark, K. Jareteg, R. Kádár, F. Edelvik, Computationally efficient viscoelastic flow simulation using a lagrangian-eulerian method and gpu-acceleration, Journal of Non-Newtonian Fluid Mechanics 279 (2020) 104264. `doi:10.1016/j.jnnfm.2020.104264`.

[49] H. K. Versteeg, W. Malalasekera, An introduction to computational fluid dynamics - the finite volume method., Addison-Wesley-Longman, 1995.

[50] W. L. Haberman, R. M. Sayre, Motion of rigid and fluid spheres in stationary and moving liquids inside cylindrical tubes, Tech. rep., Department of the navy - David Taylor model basin (1958).
URL `http://hdl.handle.net/1721.3/48988`

Paper D

Hindered diffusion of nanoparticles in a liquid re-visited with a continuum based direct numerical simulation framework

A. S. Kannan, A. Mark, D. Maggiolo, G. Sardina, S. Sasic, and H. Ström. Hindered diffusion of nanoparticles in a liquid re-visited with a continuum based direct numerical simulation framework. *To be submitted to a journal* (2021)

Hindered diffusion of nanoparticles in a liquid re-visited with a continuum based direct numerical simulation framework

Ananda Subramani Kannan[a,*], Andreas Mark[b], Dario Maggiolo[a], Gaetano Sardina[a], Srdjan Sasic[a], Henrik Ström[a]

[a]*Department of Mechanics and Maritime Sciences, Division of Fluid Dynamics, Chalmers University of Technology, Göteborg, 412 96, Sweden.*

[b]*Fraunhofer-Chalmers Research Centre, Göteborg, 412 88, Sweden.*

Abstract

In this paper we revisit the hindered diffusion problem in a liquid, wherein hydrodynamic interactions mediated by the fluid (such as particle-particle or particle-wall effects) influence the governing particle dynamics, using a continuum based direct numerical simulation (DNS) technique. We show that the expected hindered diffusion behavior near a no-slip boundary is captured using both the directional mean squared displacement and velocity auto-correlation functions, correspondingly reflecting the increased hydrodynamic resistance. We further extend this discussion towards diffusion near a soft-boundary (formed at the interface of two liquids) by integrating the dynamics of the evolving interface with the motion of the nearby Brownian particle, through a volume of fluid (VOF) coupling. We show that the particle mobility is enhanced near such a soft-boundary due to significant reduction in the hydrodynamic resistances that result from the lowered fluid shear near this interface. Finally, we also assess the pairwise diffusion of Brownian particles using this framework. As expected, the inter-particle interactions mediated by the fluid leads to a correlated motion between the pair of particles as a result of being accelerated by each other's wakes. Thus, the developed numerical method can be used to complement existing experimental techniques for assessing the dynamics of such interacting Brownian nanoparticles.

Keywords: Brownian particle; Hindered diffusion; Hydrodynamic interaction; DNS; Mobility; Nanoparticles; Soft-boundaries and VOF.

---

*Corresponding author: ananda@chalmers.se

Manuscript to be submitted to a journal

1. Introduction

In this paper we revisit the hindered diffusion problem in a liquid, i.e the diffusion of a Brownian nanoparticle near a boundary (could be a wall, an interface or another particle) using a continuum based simulation technique. The primary motivation with this endeavor is to address some of the shortcomings of the existing alternate approaches and further improve upon them as hindered diffusion plays a crucial role in several relevant physical and physico-chemical problems. Some common examples include, membrane transport of flexible macro-molecules [1], entrapment of nano-sized particles (such as combustion generated debris) in filters used for the aftertreatment of automotive exhausts [2–4], micro-manipulation of colloidal particles using solvent-mediated long-range interactions [5], bio-engineering applications involving transport of magnetized nano-particles in lab-on-a-chip devices [6, 7], nanocarrier mediated drug delivery [8], micro-swimmers [9] and surface-based biosensors [10, 11]. More recently, the space-time correlation of the Brownian motion of dilute tracer particles in a medium has been used to probe its rheological properties (including its wettability [12]), an approach referred to as microrheology [13, 14]. In all these cases, nanoparticles have to diffuse in the vicinity of a wall, meaning that multiple effects (both molecular and hydrodynamic in nature) compete for dominance in governing the inherent transport. Furthermore, the presence of a boundary alters the underlying hydrodynamic field around the Brownian particles, ultimately affecting their diffusive behavior as reflected by their altered mobility (or ratio of the particle terminal velocity and the viscous frictional force). Correspondingly, a comprehensive insight into the complex interplay between the micro- and macro scale phenomena at these scales is crucial to improving our understanding of the underlying transport phenomena in these systems. Moreover, as the aforementioned systems involve very fine particles, experimentally forecasting the hydrodynamics is challenging due to the simultaneous prevalence of disparate length and time scales. This necessitates the parallel development of numerical approaches that complement existing experimental techniques.

The Brownian motion of a small particle in an unbounded viscous fluid is a classical problem that has been extensively studied and reviewed, some selected works include [15–25]. These studies have contributed to developing the existing theories for hindered diffusion as shown by [13, 26–29], to name a few. Physically, most of the reported studies assume that the momentum of a Brownian particle relaxes to an equilibrium through its interaction with the immediately surrounding fluid, i.e. the system is strongly overdamped by the viscous friction forces. This limit in a liquid, where the Brownian particle interacts through continuum-level forces, permits a macro-scale abstraction of molecular level phenomena. Several numerical methods take the computational advantages at this level of abstraction, such as the popular particle-based Brownian dynamics (BD) [30] and Stokesian dynamics (SD) [31] approaches. Despite being able to include particle-particle, particle-boundary, thermal fluctuations, and long-range many-body hydrodynamic interactions (mediated by the fluid), the applicability of these methods is limited. This is because the included thermal fluctuations and hydrodynamic interactions are modeled and not resolved. Nevertheless, these are still more computationally tractable at larger length and time scales than the rigorous kinetic theory based micro- and meso-scale methods such as molecular dynamics (MD) [32], direct simulation Monte-Carlo (DSMC) [33], fluctuating lattice Boltzmann method (LBM) [34, 35], dissipative particle

dynamics (DPD) [36–38] and multi-particle collision dynamics, to name a few. This is due – in part – to the reason that only the time-dependent behavior and evolution of a molecular system is evaluated with these approaches. Correspondingly, a continuum based approach is the preferred choice in this paper.

These continuum approaches are a coarse-grained abstraction of the micro- and meso-scale descriptions that permits the governing equation system to be simplified into non-linear partial differential equations (PDEs), i.e. the Navier-Stokes equations [39–41]. These equations can be solved using advanced iterative techniques such as computational fluid dynamics (CFD). Alternately, these can be linearized by neglecting fluid inertia (creeping flow), leading to an equation system (the Stokes equations) that can be determined by semi-analytical solutions. The latter are predominantly used in BD [30] and SD [31] where Brownian particles interact through continuum-level forces, while the former are used in direct numerical simulations (DNS) [4, 42–44], wherein the hydrodynamic field around the Brownian particle is discretized and solved on a computational grid. Since the non-linear PDEs are solved directly (either analytically or using CFD), these continuum-based approaches resolve the hydrodynamic fields. However, the relevant molecular details in the Brownian description are absent as they have been averaged out while deriving such a description. Thus, the primary challenge in these numerical approaches is to consistently account for the thermal fluctuations. Langevin [16] and later others [17, 18, 30, 31, 45] showed that these fluctuations can be incorporated as a stochastic forcing with specific properties dictated by the fluctuation-dissipation theorem of statistical mechanics. Consequently, in a continuum description of Brownian phenomena the thermal fluctuations can either be included in the particle equation of motion (as shown by Langevin [16]) or in the fluid equations (the fluctuating hydrodynamics (FH) approach of Landau and Lifshitz [46]).

The analytical descriptions, such as the method of reflections, pioneered by Smoluchowski [47] and extensively used by several others including Brenner [26] and Felderhof [27, 48, 49], to name a few, as well as the particle-based simulation methods such as BD and SD include the stochastic forcing on the particle. Both these approaches utilize a simplification of the governing continuum equations to model the hydrodynamic forces on the particle. BD and SD neglect unsteady particle inertia, while some of the analytical methods, such as those by Felderhof [27, 48, 49], Ardekani and Rangel [50] and Simha et al. [51] (to name a few) account for these. Nevertheless, these approaches may not be analytically tractable in a closed-form without an approximation (despite the linearity) particularly in situations with reduced symmetry. Moreover, the solution procedure gets progressively elaborate (in a mathematical sense) when describing asymmetrical systems (such as a fractal aggregate or diffusion in an arbitrary pore), thus, limiting their applicability to simplified symmetric particle-fluid systems. Consequently, due to these limitations, the iterative solution technique (for the governing Navier-Stokes equation) through direct numerical simulations (DNS) has gained in popularity. Note that within the context of this paper, DNS (also to referred to as multiphase DNS) refers to a numerical framework where the fluid equations are solved coupled with the equation of motion of the particles.

In this multiphase DNS method, the two phases are represented as an Eulerian-Lagrangian

combination, with the particle represented in the Lagrangian basis. The thermal fluctuations can be added directly on either the particle or on the fluid. The latter approach, which consists of the FH based methods, have recently been explored using a finite volume CFD framework by Sharma and Patankar [52, 53] and others [8, 43, 54, 55]. Further, a stochastic immersed boundary method (which is an alternate iterative approach to solving the Navier-Stokes equations) proposed by Atzberger et al. [42, 56–58] also uses the same basis. Despite being a popular DNS implementation, the main difficulty associated with these FH based methods is in devising a discretization scheme for the stochastic differential equation. This is primarily due to the correlation between the form of the required fluctuation-dissipation relations and the choice of discretization scheme [59]. An additional difficulty is that such finite-volume discretizations naturally impose a grid-scale regularization (smoothing) of the stochastic forcing. Moreover, the non-linear LLNS equations are ill-behaved stochastic partial differential equations that are challenging to integrate [60]. This is because the stability properties of the available numerical schemes for the nonlinear Landau and Lifshitz Navier-Stokes equation system are not well understood and the whole notion of stability is different from those in regular deterministic schemes [61].

Thus, in this paper an alternate DNS approach is put-forth, where the particle motion is modeled using a stochastic differential equation (in the spirit of the Langevin description adopted in BD and SD) and leaving the fluid equations unaltered. In this way, some of the shortcomings of the FH based methods are overcome (by discretizing the traditional Navier-Stokes equations), however, with the inclusion of an additional complexity of generating the necessary stochastic forcing term (which is in-turn dependent on the hydrodynamic resistance tensor). Previously [4, 44], we have shown using a Langevin immersed boundary method ($LaIBM$) that the original Langevin formulation [16] for the particle can be used in conjunction with an immersed boundary based (finite volume) solution of the hydrodynamic fields around it, provided the particle inertia is negligible. Consequently, we extend this idea towards describing the interaction of a Brownian particle with a no-slip wall, a soft boundary or another Brownian particle (pairwise interaction) under creeping flow conditions. We analyze the consequences of resolving such ideal colloidal suspensions using the proposed framework and evaluate the inherent diffusion dynamics.

This paper is organized as follows: in the subsequent section, we introduce the hindered diffusion problem and establish a hydrodynamic context for the same. In Section 3, we provide an overview of the Langevin immersed boundary method followed by a brief account of the numerical setup and validation in Sections 4 and 5, respectively. Next, in Section 6 we elaborate on the results from the hindered diffusion studies in an ideal colloid. Finally in Section 7, we summarize the major conclusions from this work along with prospects for further development.

2. The hindered diffusion problem

Hindered diffusion can be broadly defined as the diffusion of a Brownian particle in an environment where other interactions mediated by the fluid (see Fig. 1), such as particle-

particle (p-p) or particle-wall (p-boundary) effects, assume a governing role in dictating the dynamics of the system (i.e. the free diffusion of a Brownian particle is 'hindered' by additional hydrodynamic effects mediated by the fluid). The particle dynamics is well represented by its mobility, as shown in [62–65]. Correspondingly, it is well known that this mobility is altered by the additional hydrodynamic resistances in the system. The presence of a no-slip surface such as a wall or another particle increases the hydrodynamic resistance on the particle, thereby reducing its mobility. These effects of the altered hydrodynamic fields on the particle can be accounted as a deviation (by a factor λ) from the ideal unbounded Stokes behavior, as shown by [26, 28, 63–73]. Thus, anomalous (or hindered) diffusion of Brownian particles can be evaluated using the representative particle mobility, which in-turn is a function of the position of the particle in relation to the confining boundaries and the inter-particle separation distance (in the case of n-particle Brownian diffusion). An overview of most analytical/theoretical developments including the relevant hydrodynamic expressions for the reduction in mobility (λ) in the vicinity of boundaries (no-slip and free-slip) can be found in the classical books of Happel and Brenner [62] and Kim and Karilla [74], while those governing n-particle Brownian motion are reported in [48, 68, 75–81]. Some of these theoretical developments which are relevant within the context of this paper are elaborated in this section.
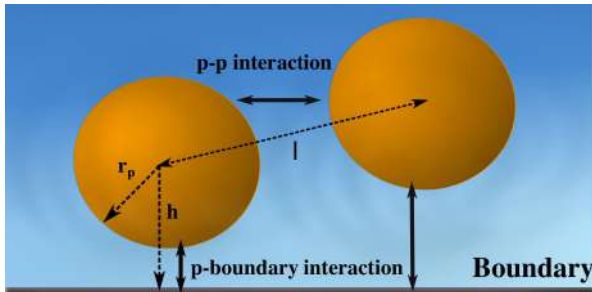

Figure 1: Hindered diffusion due to p-p and p-boundary interaction in a liquid. The pair of Brownian particles are spherical with a radius r_p, separated by a p-p distance l and a p-boundary distance h.

The hindered diffusion of a Brownian particle (at a macro-scale abstraction), with mass m_p and velocity $\mathbf{u_p}$ under creeping flow conditions is given by the Langevin equation [26, 28, 63, 64, 68]:

$$m_p \frac{\mathrm{d}\mathbf{u_p}}{\mathrm{d}t} = * \, \gamma \mathbf{u_p} \lambda + \mathbf{F_{Brownian}}, \tag{1}$$

where, γ is the Stokes friction factor or the inverse of particle mobility, which is defined for a fluid with dynamic viscosity μ_f as: $\gamma = 3\pi\mu_f d_p$. In order to account for the additional hydrodynamic effects (due to the presence of a boundary and/or other particles), the mobility (or $1/\gamma$) is adjusted using the correction factor λ which is in-turn a function of the distance(s)

from the bounding plane(s)/particles. The force $\mathbf{F_{Brownian}}$ represents the Brownian fluctuations in the particle motion when modeled as a Gaussian white noise process. Thus, the Langevin Eq. (1) clearly shows that the Brownian particle relaxes to equilibrium through hydrodynamic interactions with the fluid. Correspondingly, the hindered diffusion dynamics of Brownian particles near a boundary (such as a no-slip or free-slip wall) is usually discussed in terms of its hydrodynamic mobility along two principal directions relative to the boundary yielding a co-axial (or parallel) and wall-normal (or perpendicular) mobilities, respectively. Moreover, the boundary condition that is imposed at the wall also influences this mobility. Consequently, the behavior of the particle depends on the degree of slippage, with no-slip and free-slip representing the limiting cases.
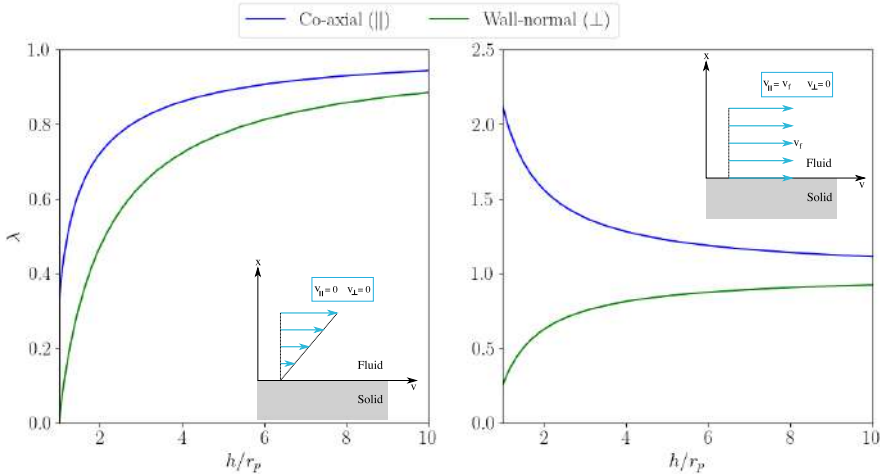

Figure 2: Particle mobility near a boundary along co-axial ($\parallel$) and wall-normal ($\perp$) directions: variation of λ as a function of non-dimensional distance (h/r_p) from a no-slip wall (left panel) and a free-slip wall (right panel), respectively. The insets represent the corresponding boundary conditions (v_f is the fluid velocity in the co-axial direction). Note that these curves are plotted using Eqs. (2), (3), (4) and (5).

The hydrodynamic effect of a no-slip boundary can be understood by examining the corresponding analytical expressions derived by Faxén [82, 83] and Brenner [84] for the mobility reductions along the co-axial and wall-normal directions, respectively. Faxén's result is given as:

$$\lambda_{\parallel} = \frac{1}{1 * \frac{9}{16}\left(\frac{r_p}{h}\right) + \frac{1}{8}\left(\frac{r_p}{h}\right)^3 * \frac{45}{256}\left(\frac{r_p}{h}\right)^4 * \frac{1}{16}\left(\frac{r_p}{h}\right)^5}, \tag{2}$$

while an approximation of Brenner's [84] result is given as [25]:

$$\lambda_\perp = \frac{6 * 3(\frac{r_p}{h}) * (\frac{r_p}{h})^2}{6 * 10(\frac{r_p}{h}) + 4(\frac{r_p}{h})^2} \tag{3}$$

where, h is the distance from the center of the sphere to the plane-wall surface and r_p is the particle radius. In this case, a no-slip wall is an idealization adopted while solving fluid flow problems, which is defined by a boundary condition where the normal and tangential components of the fluid velocity (v) is set to zero. Correspondingly, the variation of mobility correction λ as a function of non-dimensional distance (h/r_p) from such a boundary is shown in Fig. 2a. It is evident that the wall-normal motion is impeded more strongly than the co-axial one. This is expected since, during wall-normal motion, the fluid between the particle and the wall needs to be squeezed out leading to an increased resistance. Moreover, as the particle moves away from the no-slip wall, both the co-axial and wall-normal mobilities tend to Stokes free mobility (i.e. $1/\gamma$), as the influence of the wall is diminished (meaning free diffusion is eventually attained). For particles confined by such no-slip walls, the strength of the hydrodynamic interactions decay as $1/h^2$ [78, 85]. It follows that, for this analysis to be valid, the particle must be small in relation to any bounding geometry (else the wall effects will never completely vanish), which is not the case in most applications of interest discussed in Section 1. This is further described in our earlier work on Brownian transport in micro-channels under intermediate confinements [44, 86].
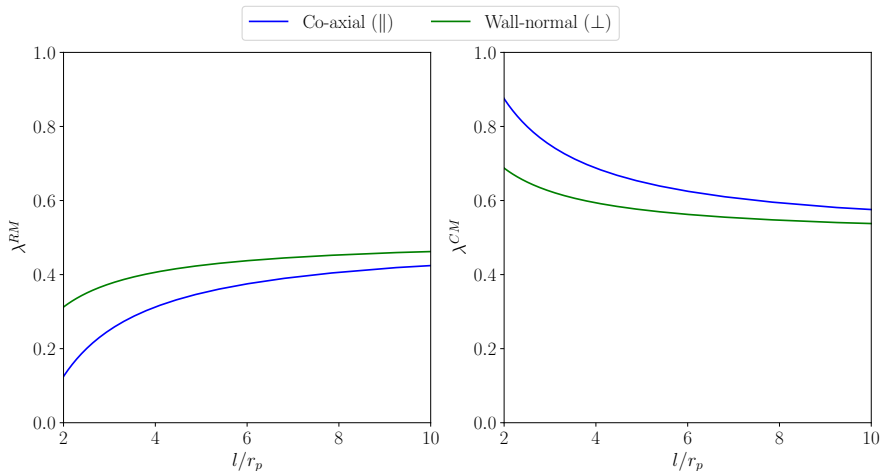

Figure 3: Pairwise particle mobility: variation of λ as a function of dimensionless center-to-center separation (l/r_p), along co-axial and wall-normal [29] directions. Note that, mobilities are decomposed along the direction of relative motion of the two sphere's with respect to each other (left panel) and along the direction of common motion of the two sphere's center of mass (right panel). These curves are plotted using Eqs. (6), (7), (8) and (9).

A slip-wall is defined by a boundary condition where the normal component of the fluid velocity is set to zero, but the tangential component is permissible. The simplest and most natural violation of the no-slip condition would involve a surface slip velocity that varies in proportion to the local shear rate, thus introducing a finite slip length b. The first order expressions for the alteration in mobility along the co-axial and wall-normal directions for large slip lengths (i.e. $b \gg h$) were derived by Lauga and Squires [29] as:

$$\lambda_\parallel \approx \frac{1}{1 + \frac{3}{8} \left(\frac{r_p}{h} \right) \left(1 + \frac{5h}{b} \ln \frac{h}{b} \right)}, \tag{4}$$

$$\lambda_\perp \approx \frac{1}{1 * \frac{3}{4} \left(\frac{r_p}{h} \right) \left(1 + \frac{h}{4b} \right)}. \tag{5}$$

When $b \to \infty$, we recover Brenner's original result [84] for a free-slip wall. Higher order terms in r_p/h and h/b are excluded in Eqs. (4) and (5), meaning, these expressions are first-order accurate. These equations can be used to establish a simple hydrodynamic basis for hindered diffusion near a slip wall. Correspondingly, the variation of λ as a function of non-dimensional distance (h/r_p) from a free-slip wall is shown in Fig. 2b. It is evident that the mobility near a free-slip wall is reduced to a lesser degree, when compared with the corresponding no-slip case. This is due to the significant drag reduction achieved due to zero wall shear (infinite slip), consequently leading to an enhanced mobility. Further, it is noticed that the mobility along the co-axial direction is enhanced, while the wall-normal mobility is reduced. This enhancement arises because the particle must displace less fluid in the tangential direction to a free-slip wall. Moreover, as the particle moves away from the free-slip wall, both the co-axial and wall-normal mobilities tend to Stokes free mobility, just as in the no-slip case.

Similarly, a Brownian particle diffusing in the vicinity of a neighboring one would perceive the presence of the latter, through the developed hydrodynamic fields mediated by the fluid. Correspondingly, the relevant hydrodynamic basis can be understood from Batchelor's studies on a pair of spherical particles [68], which extended the original results by Stimson and Jeffery [87]. He showed that the sphere's motion can be decomposed into two parts: the relative motion of the two spheres with respect to each other and the common motion of the two spheres' center of mass. Each of these two motions are in turn described by a pair of mobilities, yielding the following four mobility coefficients:

$$\lambda_\parallel^{RM} = \frac{2}{\left[1 * \frac{3}{2\eta} + \frac{1}{\eta^3} * \frac{15}{4\eta^4} + O\left(\eta^{-6} \right) \right]}, \tag{6}$$

$$\lambda_\perp^{RM} = \frac{2}{\left[1 * \frac{3}{4\eta} * \frac{1}{2\eta^3} + O\left(\eta^{-6} \right) \right]}, \tag{7}$$

$$\lambda_{\parallel}^{CM} = \frac{2}{\left[1 + \frac{3}{2\eta} * \frac{1}{\eta^3} * \frac{15}{4\eta^4} + O\left(\eta^{-6}\right)\right]}, \qquad (8)$$

$$\lambda_{\perp}^{CM} = \frac{2}{\left[1 + \frac{3}{4\eta} + \frac{1}{2\eta^3} + O\left(\eta^{-6}\right)\right]}, \qquad (9)$$

where, η is the dimensionless center-to-center separation given by l/r_p and the superscripts, RM and CM, represent motion decomposed along the center-to-center axis (relative motion, RM) and common motion (CM) axis of the center of mass (of the particle system), respectively. These expressions are only valid when the two spheres have the same radius, no external torques are applied and the pair are free to rotate in response to each other's flow field. The lowest order terms in these equations sufficiently describe the mobilities when the spheres are separated by more than a few radii [25, 88]. Fig. 3 shows the variation of λ as decomposed along the relative motion and common motion components, respectively. It is observed that the relative diffusivities (shown in the left panel) are suppressed while the common center of mass diffusivities (right panel) are enhanced. This suppression of the relative diffusivities is caused by the resistance of the fluid between the spheres to being sheared or squeezed out of the gap. Conversely, the diffusion of the center of mass is enhanced by the fluid entrained by one sphere, which is pulling along the other. These relative effects diminish as the center-to-center distance increases.

Thus, these hydrodynamic effects from the fluid on the particle will be reflected in its diffusive behavior and consequently the primary objective of this paper is to show that a continuum-based multiphase DNS method (*LaIBM*), which can innately handle polydisperse particles of complex shapes in arbitrary geometries (as shown in our previous works [4, 44]), can reproduce the aforementioned hydrodynamic observations from classical hindered diffusion theory. This DNS method is further discussed below.

3. Langevin-Immersed Boundary method (*LaIBM*)

The *LaIBM* framework represents a multiphase DNS method that handles the particle in a Lagrangian basis and the fluid in an Eulerian one. The continuum Eulerian description is resolved using an immersed boundary method (IBM) [89, 90], which is a CFD-based finite-volume approach for solving the governing fluid equations. In the IBM, the object around which the flow is to be studied is immersed in a Cartesian flow grid and its presence is accounted for by modifying the governing Navier-Stokes equations through boundary conditions or source terms. In *LaIBM*, we utilize a dynamic octree grid to spatially discretize the fluid volume around the object and a second-order accurate mirroring immersed boundary method to constrain the velocity at the IB surface. This is done so that the correct conditions are satisfied at the boundaries [4, 44, 86, 91].

The Eulerian description of the fluid around the immersed particle is given by the following continuity and momentum equations for incompressible flows (i.e. the Navier-Stokes equations):

$$\rho_f \left(\frac{\partial}{\partial t} \boldsymbol{v} + \boldsymbol{v} \cdot \boldsymbol{\nabla} \boldsymbol{v} \right) = * \boldsymbol{\nabla} P + \mu_f \boldsymbol{\nabla}^2 \boldsymbol{v} + f_i,$$
$$\boldsymbol{\nabla} \cdot \boldsymbol{v} = 0, \tag{10}$$

where, f_i represents any external source term. This set of equations is solved together with an implicit Dirichlet IB condition as detailed in [91, 92]. The total force (acting on the IB) is calculated by integrating the fluid stresses over the surface of the IB:

$$\mathbf{F_{IB}} = \int_{IB} \boldsymbol{\sigma} \cdot \mathbf{n} dS = \int_{IB} \left(* P\delta_{ij} + \tau \right) \cdot \mathbf{n} dS = \int_{IB} \left(* P\delta_{ij} + \mu_f \boldsymbol{\nabla}^2 \boldsymbol{v} \right) \cdot \mathbf{n} dS, \tag{11}$$

where, δ_{ij} is the Kronecker delta and σ is the total fluid stress tensor with $P\delta_{ij}$ and τ as the pressure and viscous contributions (from the fluid) for a surface S with normal $\boldsymbol{n}$, respectively. The corresponding torque on the IB is calculated using:

$$\mathbf{T_{IB}} = \int_{IB} \mathbf{r} \times \boldsymbol{\sigma} \cdot \mathbf{n} dS. \tag{12}$$

Here, $\mathbf{r}$ is the position vector of the IB and σ is the fluid stress tensor for a surface S with normal $\boldsymbol{n}$.

Furthermore, the volume of fluid method (VOF) [93, 94] is used to track the interface between two immiscible fluids. This is especially needed when studying the hindered diffusion of a particle near a soft boundary (such as a liquid-liquid or gas-liquid interface). Soft boundaries may exhibit slip, and may also deform due to the motion in either phase. The VOF method accounts for the volume fractions, α, of each phase, so that the density and viscosity in the Cartesian grid can be estimated as:

$$\rho_f = \alpha \rho_{k1} + (1 * \alpha) \rho_{k2},$$
$$\mu_f = \alpha \mu_{k1} + (1 * \alpha) \mu_{k2}, \tag{13}$$

where, the subscripts $k1$ and $k2$ represent the corresponding fluid phase. Consequently, the distribution of the fluid volume fraction is solved using a transport equation for the volume fraction field as:

$$\frac{\partial \alpha}{\partial t} + \nabla \cdot (\alpha \boldsymbol{v}) = 0. \tag{14}$$

The particulate phase in the *LaIBM* framework is governed by the Lagrangian Langevin equation of motion [16]. This equation balances the macro-scale hydrodynamic drag on the particle with the molecular-scale Brownian fluctuations. Such a balance satisfies the requirement that the Brownian particles interact through continuum-level forces (which is a crucial assumption in the proposed method). Thus, for the hindered diffusion of a particle with mass m_p, a translational velocity $\mathbf{u_p^i}$, an angular velocity $\boldsymbol{\omega}_p^i$ and moment of inertia $\boldsymbol{J}$ (where the index i represents the degrees of freedom for the particle in a Cartesian basis), the corresponding Langevin Eq. (1) is re-written as:

$$m_p \frac{\mathrm{d}\mathbf{u_p^i}}{\mathrm{d}t} = \mathbf{F_{IB}^i} + \mathbf{F_{Brownian}^i}, \tag{15}$$

$$\mathbf{J}\frac{\mathrm{d}\boldsymbol{\omega}_\mathbf{p}^\mathbf{i}}{\mathrm{d}t} = \mathbf{T_{IB}^i} * \boldsymbol{\omega}_p^i \times \mathbf{J} \cdot \boldsymbol{\omega}_p^i. \tag{16}$$

In Eqs. (15) and (16), note that the continuum resolved translational ($\mathbf{F_{IB}^i}$) and rotational ($\mathbf{T_{IB}^i}$) hydrodynamic fields are included within the Langevin description, thus enforcing a direct coupling of the Eulerian solution with the corresponding Lagrangian Langevin equation of motion. Further, since we deal with the motion of very small particles, gravitational acceleration is deemed negligible. Consequently, the directional alteration in mobility λ^i, which is required in the stochastic forcing term used in $\mathbf{F_{Brownian}^i}$, is estimated by normalizing the magnitude of the hydrodynamic force on the hindered Brownian particle ($\mathbf{F_{IB}^i}$) with the corresponding Stokes drag (along the ith direction) on the same particle when diffusing in an unbounded fluid. This is given as:

$$\lambda^i = \frac{\mathbf{F_{IB}^i}}{\gamma \mathbf{u_p^i}}. \tag{17}$$

The relevant particle time scale (τ_p) is given as:

$$\tau_p = \frac{m_p}{\gamma \|\lambda^i\|}. \tag{18}$$

The force $\mathbf{F_{Brownian}^i}$, which represents the Brownian fluctuations in the particle motion, is modeled as a Gaussian white-noise process with the vector of spectral intensity $\mathbf{S_{IJn}^i}$ given as [18, 45, 95]:

$$\mathbf{S_{IJn}^i} = \mathbf{S_0^i}\delta_{IJ}, \tag{19}$$

where the vector $\mathbf{S_0^i}$ is a function of the directional Brownian diffusivity D^i that reflects the

presence of walls and/or other particles (note that the diffusion is asymmetric):

$$S_0^i = \frac{2\gamma^2 {\lambda_{IB}^i}^2}{\pi} D^i. \tag{20}$$

This corrected directional diffusivity (D^i) can be calculated from the bulk diffusivity (D^∞) using a balance between the thermal kinetic motion and the hydrodynamic (viscous) drag force, as given by the Stokes-Einstein equation with a further correction by λ_{IB}^i (in accordance with [26, 28, 64, 67]). This correction accounts for the hindered effects (such as a confining boundary or a neighboring particle or both). Hence, D^i is related to the diffusivity of a freely diffusing Brownian particle as:

$$D^i = \frac{D^\infty}{\lambda_{IB}^i}, \tag{21}$$

leading to the general form (using the Stokes-Einstein equation [15]):

$$D^i = \frac{k_B T}{\gamma \lambda_{IB}^i}, \tag{22}$$

where k_B and T are the Boltzmann constant and absolute temperature, respectively. Thus, $\mathbf{F_{Brownian}^i}$ can be written as [45, 95]:

$$\mathbf{F_{Brownian}^i}(\mathbf{t}) = m_p \mathbf{G} \sqrt{\frac{\pi \mathbf{S_0^i}}{\Delta t}}. \tag{23}$$

Here, $\mathbf{G}$ is a vector of normally distributed independent random numbers of zero mean and unit variance (Gaussian distribution) and Δt is the time step length during which the Brownian force is active.

The solution to Eq. (15), which is a stochastic differential equation (SDE), would reproduce the analytical diffusive behavior for confined Brownian motion. Correspondingly, for N particles diffusing over time, the root-mean-square displacement (MSD) in one dimension (MSD^i) is given as:

$$MSD^i = [\frac{1}{N} \sum_{n=1}^{N} \big(i(t+dt) * i(t)\big)^2]^{\frac{1}{2}} = \sigma_{1D} \equiv 2D\Delta t. \tag{24}$$

The linear and angular momentum conservation equations (Eqs. (15) and (16)) are integrated using the Newmark time-marching scheme [96]. In this method, the acceleration, velocity and displacement at time $t = t^{n+1}$ are obtained as functions of the values at $t = t^n$ by assuming

a linear acceleration during that small time step. This one-step semi-implicit method can be represented by the following set of equations:

$$\dot{u_p}^{n+1} = \dot{u_p}^n + \frac{\Delta t}{2}\left(\ddot{u_p}^n + \ddot{u_p}^{n+1}\right) \tag{25}$$

$$u_p^{n+1} = u_p^n + \Delta t\dot{u_p}^n + \frac{1 * 2\kappa}{2}\Delta t^2\ddot{u_p}^n + \kappa\Delta t^2\ddot{u_p}^{n+1} \tag{26}$$

The scheme is unconditionally stable with κ as a tuning parameter that has a default value of 0.25 (the constant average acceleration method) [96]. Note that this scheme is also compliant with the Itô interpretation [97] of a stochastic integral. Thus, if solved correctly, the variation in the root-mean-squared displacement of the particle over sufficiently long times ($t >> \tau_p$) should reproduce the analytical Stokes-Einstein diffusivity (Eq. (22)). This result is entirely dependent on the condition that the total hydrodynamic force on the particle can be obtained from the steady drag and that the hydrodynamic interactions can be obtained from Eq. (17).

We use an in-house finite-volume-based incompressible multiphase flow solver `IPS IBOFlow` [98], that utilizes the previously described mirroring immersed-boundary method to handle the moving particles efficiently. Further, when the VOF coupling is activated (i.e. for the cases of Brownian diffusion near a soft boundary), the corresponding transport equation for the volume fraction field (Eq. 14) is discretized using the compressive interface capturing scheme for arbitrary meshes (CICSAM) [99]. A partitioned approach is employed to solve the resulting coupled Langevin-IB problem. The grid and assembly are fully parallelized on the CPU and the resulting large sparse-matrices are solved on the GPU with an Algebraic Multi-Grid (AMG) solver [100]. The use of an IB method enables the straightforward incorporation of complex fractal-shaped particles and complex pore structures within the framework. Further, the ability of this framework to handle complex aggregates as well as hindered diffusion under varying degrees of confinement is already described in our previous work [4, 44, 86].

4. Numerical setup

The hindered diffusion problem investigated is specified by the conditions in Table 1. These simulations are carried out at a low particle Reynolds number ($Re_p = d_p V_{rms}^\infty \rho_p/\mu_f = 3 \cdot 10^{-3}$, where the root mean square velocity $V_{rms}^\infty = \sqrt{k_B T/m_p} = 1 \cdot 10^{-4} \ m/s$ is for an equivalent unbounded Brownian motion of a 400 nm particle) and at a particle-fluid density ratio of 1000. These choices are made so as to maintain the validity of the steady state Langevin Eq. (15) (unsteady effects such as history and added mass forces are negligible). All simulations presented use the particle response time (τ_p, see Eq. (18)) and particle diameter (d_p) as a basis for determining the relevant temporal and spatial details, respectively.

Further, the longitudinal extent of all the domains in this study (the x-direction) is $10d_p$, with symmetric conditions imposed along this direction (no flow or scalar flux across the

boundary, i.e. zero-shear slip walls). This length is chosen so as to enable the representation of Brownian particle interaction with different types of boundaries under confined conditions, as would be the case in the relevant applications (e.g., flow in porous media or micro/nano-channel flow), while minimizing the influence of the applied far-field boundary conditions on the particle motion. With this setup, the wall-normal interactions will resemble those in semi-infinite systems reasonably well, whereas the parallel interactions will be significantly higher, in line with what would be expected in for example a cavity within a natural porous medium.

All simulations are carried out at predetermined spatial and temporal resolutions obtained from the validation studies presented in the subsequent sections. Further, the Brownian forcing (see Eq. (23)) is updated in intervals of $\tau_p/10$ to allow for an adequate resolution of the particle acceleration [4, 44]. We use a pure one-way coupled Langevin (point-particle) unbounded diffusion case to establish the minimum criteria (in terms of duration and time averaging interval), including the variability of the stochastic process across several random seeds, for the statistical analysis reported in this paper (cf. [4, 44]). The final criteria chosen are a total simulation duration (T) of $100\tau_p$ and an averaging interval of $5\tau_p$ in the *MSD* calculations.

Table 1: Simulation conditions for the hindered diffusion cases

Case	No-slip wall	Soft boundary	Pairwise diffusion
Particle diameter (in nm)	400	400	400
Domain size (in d_p)$^+$	h, w = 3.3, l = 10	h = 6.6, w = 3.3, l = 10	h, w = 3.3, l = 10
Simulation details			
Spatial resolution, in $cells/d_p$	96	96	96
Temporal resolution dt, in τ_p	1/200	1/200	1/200
Total duration T, in τ_p	100	100	100

$^+$l, w and h are respectively aligned along the x, y and z co-ordinate axes.

Correspondingly, the respective cases (as listed in Table 1) are set-up and simulated. The hindered diffusion near a no-slip boundary is studied using a single spherical particle which is initially located at a distance $1d_p$ away from the wall (i.e. $h = d_p$). This simulation is carried out in a domain which has symmetric boundary conditions imposed at all faces, except at the bottom, which is defined as a no-slip wall. The hindered diffusion near a soft boundary is set-up in a domain with two immiscible fluids (as shown in Fig. 4). The spherical Brownian particle diffuses in the *Fluid 1* with the properties specified by the dimensionless numbers stated earlier. This *Fluid 1* co-exists with another immiscible *Fluid 2*, such that each fluid occupies half of the total volume of the domain. *Fluid 2* has the same density as *Fluid 1*. However, its viscosity is 100 times lower. Such a fluid combination is chosen for the present investigation to avoid large density ratios that may be particularly challenging to deal in the VOF method (errors are manifested by spurious velocities at the interface that can lead to numerical instabilities) [101, 102]. Moreover, since we are in the creeping flow regime, any inertial contributions from the fluids are anyway negligible. The Brownian particle diffuses at an initial location $1d_p$ away from the interface (soft-boundary) between the fluids. In this simulation, the VOF coupling is additionally activated in the solver to adequately resolve the

dynamics of the evolving interface topology, which may be influenced by the motion of the nearby Brownian particle. Further, all the faces in this domain are symmetric boundaries. The pairwise simulations are carried out with two identical Brownian particles *P1* and *P2* (as specified in Table 1) in a domain which has symmetric boundary conditions at all faces and with the initial inter-particle separation, l, as $2d_p$. We emphasize that in all the simulations presented in this paper, the confinement effects due to the symmetric boundaries (from the shorter vertical span of the domain) are equally consistent. Thus, the resulting hindered diffusion dynamics can be correspondingly compared across these individual cases to establish the relevant hydrodynamic bases.
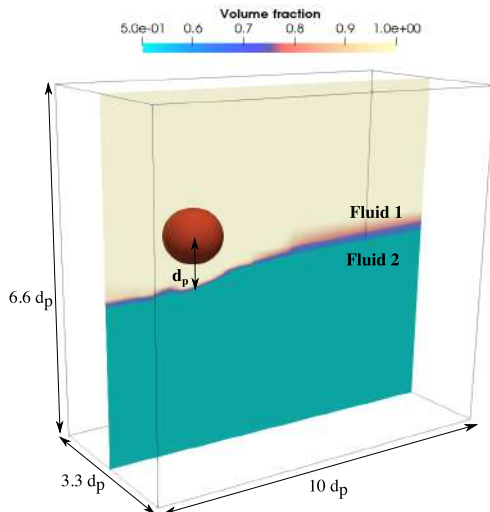

Figure 4: Snapshot from the hindered diffusion simulation near a soft-boundary that indicates the two immiscible liquids: *Fluid 1* and *Fluid 2*. The volume fraction across a plane in the x-z direction depicts the location of the interface in relation to the particle.

5. Validation of the framework

The capabilities of the *LaIBM* framework in resolving the hydrodynamic fields resulting from the diffusion of a single particle has been thoroughly validated in our earlier work [4, 44]. Correspondingly in this paper, we present only the validation for the hydrodynamic treatment of a pair of particles. This is accomplished by validating the framework with the experimental results of Adamczyk et al. [103]. These experiments estimate the correction factor λ (along the direction of motion) as a function of the dimensionless center-to-center separation (l/r_p) for the slow motion of a solid sphere towards another identical stationary one under a constant force (gravity in this case) in a quiescent fluid. These experimental results further confirm the hydrodynamic bases in the analytical developments of Stimson and Jeffery [87], Batchelor [88] and Brenner [67].
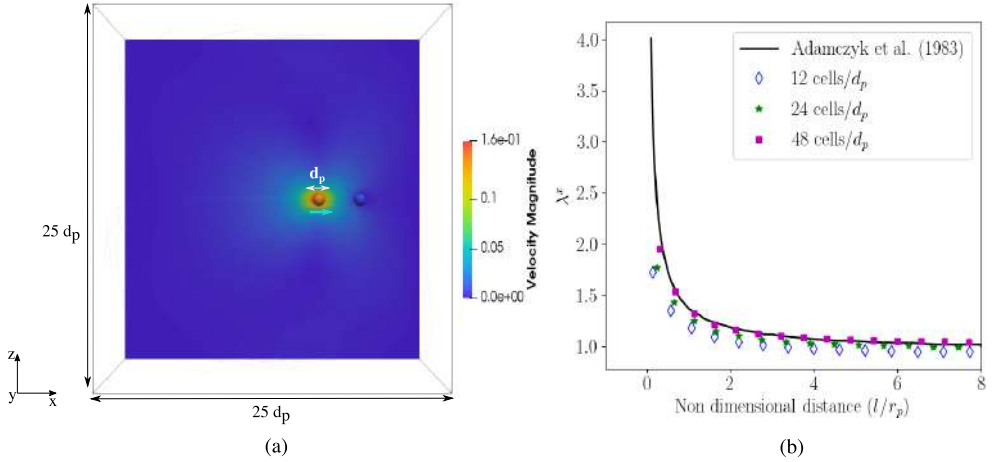
15

Figure 5: Slow motion of a solid sphere in a quiescent fluid towards an identical stationary one under a constant force: a) - Contours of velocity magnitude in a x-z plane (at y = 12.5 d_p) overlayed with flow-streamlines (after a duration of 50 τ_p) indicating the extent of the computational domain and b) - grid convergence of the estimated λ^x from   at a constant temporal resolution of $\tau_p/200$. The blue arrow indicates the direction of motion. The solid line (—) represents the experimental results from Adamczyk et al. [103].

This experimental study is recreated in $LaIBM$ using the spherical particle described in Table 1 within a cuboidal domain with side 25 d_p (as shown in Fig. 5a). The stationary particle is initially located 20 d_p away from the moving one. The latter is accelerated with a constant force along the x-direction in a viscous liquid (under creeping flow conditions) towards the former. This constant force and fluid properties are chosen so as to accelerate the particle to a terminal velocity proportional to V_{rms}^∞, leading to the Re_p defined in Section 4. Note that this terminal velocity is set as the initial condition for particle motion such that the drag on the particle is counter-balanced by the constant force (in the absence of gravitational effects). Further, all the boundaries in this domain are modeled as a symmetry-plane except for the boundaries along the flow (x) direction which are a traditional inlet-outlet pair. These constraints are imposed to minimize boundary effects on the immediate hydrodynamic fields around the pair of particles (as maintained in the experiments). This setup is used to determine the reduction in mobility (λ^x as computed using Eq. (17)), along the direction of motion of the particle, as a function of the dimensionless center-to-center separation distance (l/r_p).

Such a study is needed since $LaIBM$ is sensitive to both the temporal and spatial discretizations of the governing equations (Eqs. (10), (15) and (16)). The temporal discretization determined in our previous studies [4, 44] are applicable here as well since the particle dynamics is being resolved at similar time-scales. Consequently, the minimum spatial resolution needed is determined at this minimum (required) temporal resolution of $\tau_p/200$. Furthermore, this temporal condition satisfied the Courant number ($C = u\Delta t/\Delta x$) requirement of

16

the DNS framework. A rule of thumb in such multiphase DNS simulations is to have at least 20 cells/d_p as a minimum resolution and this is realized in our assessments as well (cf. Fig 5b). Consequently, the estimated values of λ^x agree well with the experimental values already at a grid resolution of 48 cells/d_p ($\approx 2\%$ error). Thus, in keeping with the discretization limits established in our previous work, we retain the spatial and temporal discretizations as 96 cells/d_p and $\tau_p/200$, respectively. Note that this conceptual validation study has been carried out at the same spatial and temporal scales as that of the hindered diffusion simulations. Thus, the determined minimum temporal and spatial resolutions are applicable in these cases as well.

6. Results

In this paper, we quantify the diffusion dynamics via the directional mean squared displacement (MSD_i^* in Eq. (24)) and velocity auto-correlation functions (V_{acf}^i). This is given as the equilibrium ensemble average of the particle velocities v_i along the ith direction:

$$V_{acf}^i = \langle \mathbf{v_i(0)} \cdot \mathbf{v_i(t)} \rangle = \frac{1}{N_t} \sum_{n=1}^{N_t} \left(\mathbf{v_i(0)} \cdot \mathbf{v_i(t)} \right). \qquad (27)$$

We choose to obtain the statistical description of particle motion by evaluating a single particle trajectory over long periods of time, which consequently represents multiple particle trajectories ensemble averaged over a much shorter duration (due to the ergodicity hypothesis). Further, the mean-squared displacements are non-dimensionalized by the length scale for unbounded diffusion, such that $MSD^{i*} = MSD^i/D^\infty \tau_p^\infty$, where i is the direction of motion (x, y or z) and τ_p^∞ is the response time of an unbounded Brownian particle (obtained by setting $\lambda = 1$ in Eq. (18)), for ease of interpretation. These directional MSD^{i*} are calculated for a $5\tau_p$ period of motion, while the V_{acf}^i are estimated over a $20\tau_p$ period. These periods are chosen for a reasonable representation of the underlying statistics within the total simulated duration of $100\tau_p$. Note that the presented results are also compared with an analytical basis for free diffusion which is obtained by integrating the Langevin Eq. (1) using an explicit forward Euler time marching scheme.

6.1. Hindered diffusion near a boundary

The classical problem of hindered diffusion near a boundary is revisited with the *LaIBM* technique. The behavior of a single spherical nanoparticle is evaluated in the vicinity of a wall (at a distance $1d_p$ away from it). The diffusion dynamics of the particle, as represented by the MSD^{i*} and the V_{acf}^i, is shown in Fig. 6 with the top panel depicting the former while the bottom panel depicting the latter. The MSD^{i*} captures the transition from a ballistic (due to the breakdown of the Stokes-Einstein description at the shortest timescales [23, 24, 104, 105]) to a linear diffusive regime [18]. Furthermore, it is evident that the particle
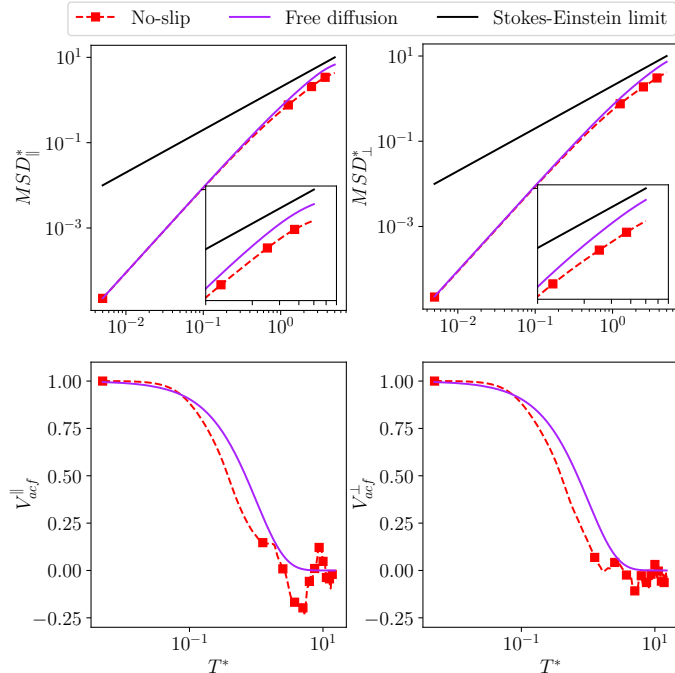
Figure 6: Hindered diffusion near a no-slip boundary: **Top panel** - the non-dimensional MSD^{i*} evaluated over 5 τ_p, along the co-axial ($\parallel$) and wall normal ($\perp$) directions. The solid lines (—) represents the analytical non-dimensionalized Stokes-Einstein behavior for free diffusion (Eq. (21)). The insets show the linear diffusive regimes attained individually along each of these directions (top panel). **Bottom panel** - decay of the directional velocity auto-correlation function (V_{acf}^i) over 20 τ_p period. The solid line (—) represents the exponential decay for free diffusion over the same period.

diffusing close to the no-slip boundary is resisted more in comparison with a freely diffusing particle. Consequently, the hindered diffusion cases approach a lower diffusivity, i.e. the MSD^{i*} approaches $2D^i t$ rather than $2D^\infty t$, due to the resistance to particle movement from the no-slip wall and other confining boundaries (including the zero-shear walls). This extra hindrance to the diffusive behavior is also visible when assessing the corresponding V_{acf}^i. Along all the directions, the hindered diffusion cases decay faster than the corresponding free diffusion ones due to the reflected flow from the wall, which cancels the tail of the auto-correlation function [51, 106–110]. The hydrodynamic theories for diffusion near a no-slip wall, discussed in Section 2, support these observed results as well with the wall normal mobility hindered more than the corresponding co-axial mobility (along the x-direction, see Table 2). Note that the wall-normal motion is represented by the z-coordinate as the particle is off-set along this direction (y-symmetric).
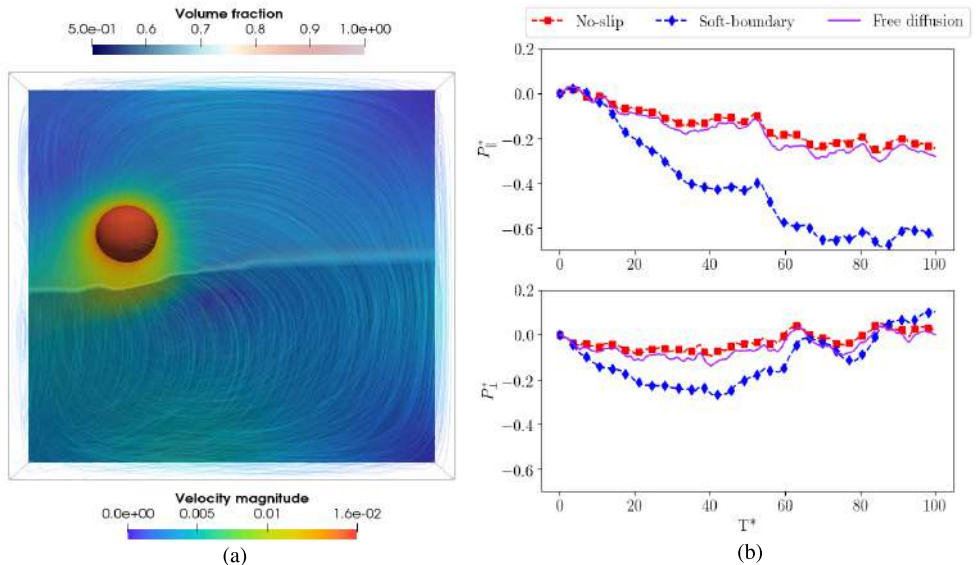
Figure 7: Hindered diffusion near a soft-boundary: a) contours of velocity magnitude along an x-z plane with the flow streamlines around the Brownian particle (the volume fraction contour is overlaid in this visualization to indicate the location of the interface between the two liquids) and b) the mean non-dimensional drift/displacement along the co-axial ($\parallel$) and wall normal ($\perp$) directions of the particle from the origin (estimated as $\mathbf{P}^*(\mathbf{x}, \mathbf{y}, \mathbf{z}) * \mathbf{P}^*_{\mathbf{initial}}(\mathbf{x}, \mathbf{y}, \mathbf{z})$) over a 100 τ_p period (all trajectories are calculated using the same random number sequence $\mathbf{G}$).

Furthermore, we use the $LaIBM$ framework to also assess the diffusion of a spherical Brownian particle near a soft boundary formed at the interface of two liquids (with a viscosity ratio of 100), as shown in Fig. 4. Such a case is not easily described using the analytical methods discussed in Section 1, since both the liquids on either side of the soft-boundary are impacted by the presence of the diffusing particle. Consequently, derivation of an analytical basis that spans across the liquids is not straightforward, thereby necessitating the use of advanced multiphase DNS techniques that can solve the coupled equation system for all three phases that co-exist in such a system. $LaIBM$ is inherently capable of solving the diffusion dynamics in such a complex system due to its in-built capability to resolve the interface between the two miscible liquids using a VOF method and further accurately predicting the developing hydrodynamic fields around the Brownian particle. A snapshot of this ability is shown in Fig. 7a wherein the resolved hydrodynamic field around the particle (spanning both the liquids) is visualized as contours of velocity magnitude along an x-z plane. The volume fraction field is overlaid on this contour to indicate the location of the interface between the liquids. It can be observed in the figure that the flow streamlines around the particle extend across both the liquids and are reflected at the boundary faces (due to the symmetry conditions imposed here).

To further evaluate the hindered diffusion behavior, the mean non-dimensional drift/displacement of the particle from its initial position (estimated as $\mathbf{P}^*(\mathbf{x}, \mathbf{y}, \mathbf{z}) * \mathbf{P}^*_{\mathbf{initial}}(\mathbf{x}, \mathbf{y}, \mathbf{z})$, where $P^*(x, y, z) = P(x, y, z)/d_p$) is calculated over the entire 100 τ_p simulation period. This is shown in Fig. 7b along with the corresponding drifts for the no-slip and free diffusion cases. Note that the diffusion near a no-slip and soft-boundary can be compared as the initial particle (i.e the diffusion starts a location which is $1d_p$ away from the boundary) and simulation configurations are identical in both cases. Correspondingly, it is noticeable that the particle diffusing near the soft-boundary is displaced the most (along all the directions), followed by the freely diffusing and the particle near a no-slip wall. Further, these differences among the displacements (across the different cases) is most pronounced along the co-axial (x) direction when compared with the wall normal (z) direction (due to the higher wall resistance in latter as explained earlier). This observed behavior is in accordance with the hydrodynamic theories discussed in Section 2. Note that the computational domain in the no-slip case is smaller as the boundary is already defined at the initial location of the fluid-fluid interface.

The soft-boundary represents a type of slip-wall, with a boundary condition permitting both normal and tangential components of the fluid velocity at the interface. Thus both co-axial and wall-normal mobilities are enhanced when compared with a corresponding no-slip wall. This is due to the significant drag reduction achieved (in this case) because of lowered fluid shear (along these directions) near the interface. Consequently, the effective viscosity (due to the joint effect of both liquids) felt by the particle is reduced. In essence, we can consider the particle to be diffusing in a fluid which has a net lower viscosity (than the original fluid it was diffusing in), leading to an increased mobility. This could be the probable cause for the pronounced mobility near a soft-boundary when compared with the corresponding free and no-slip diffusion cases. The additional enhancement of particle mobility along the co-axial direction manifests as less fluid is displaced in this direction. The enhancement along the wall-normal direction is possible due to the ability of the particle to modulate the interface topology. These mobility enhancements are summarized as directional diffusivities in the non-dimensional form D^i/D^∞ in Table 2.

Table 2: Enhancement in the non-dimensional directional diffusivities of a 400 nm Brownian particle diffusing near a soft-boundary along the co-axial (D^x/D^∞) and wall-normal (D^z/D^∞) directions after $5\tau_p$.

Case	$\frac{D^x}{D^\infty}$	$\frac{D^z}{D^\infty}$
No-slip	0.630	0.554
Soft boundary	1.804	1.982

D_∞ is estimated from the unbounded Brownian diffusion simulations.

6.2. Pairwise diffusion

The pairwise diffusion of two identical Brownian particles ($P1$ and $P2$) which are $2d_p$ apart (center-to-center distance) is also re-visited using the $LaIBM$ framework. In order to ap-
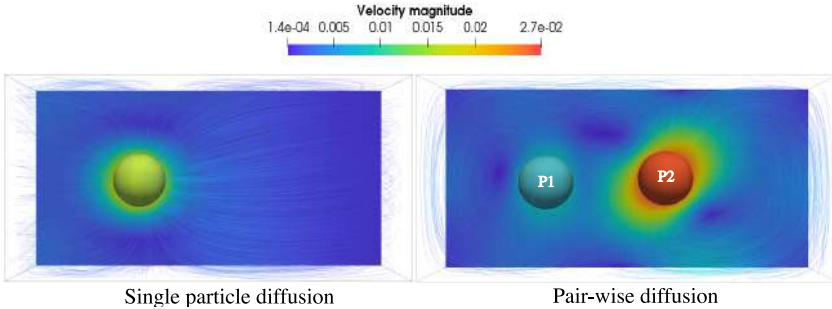
Figure 8: Comparison between single and pairwise diffusion (in a domain with symmetric boundaries): contours of velocity magnitude overlayed with flow streamlines around the particle after a duration of 10 τ_p.

preciate the inter-particle hydrodynamic effect, the diffusion behavior of the pair of particles is compared with the corresponding diffusion of a single particle in the same domain. Note that the particle *P1* in this pair is simulated with same random number sequence ($\mathbf{G}$) as that of the single particle diffusion case, while *P2* is simulated with an alternate random sequence. Fig. 8 compares hydrodynamic fields resulting from single and pairwise diffusion in the same domain. It is noticeable that the flow streamlines and the contours of velocity magnitude are markedly altered in the presence of the second particle, thereby impacting the diffusive behavior. Further, it is evident that the dual-particle system is at a lower velocity when compared to the single particle diffusion, indicative of an altered hydrodynamic behavior in the former. This impact of the hydrodynamic field of *P2* on the diffusion of *P1* is further exemplified by comparing the maximum span (absolute values are taken) of the mean non-dimensional drift (P_i^*), as listed in Table 3. It is evident that *P1* drifts more along the co-axial direction of motion, when compared to the corresponding maximum displacement for the single particle diffusion case (a 14% increase is noted). This further confirms that *P2* alternately drags *P1* along and pushes *P1* away (in the co-axial direction), leading to a correlated diffusive behavior for the pair of particles. Furthermore, the net resistance on the particle-*P1* in the pairwise diffusion case is higher than the corresponding single particle diffusion case (a 12% increase in λ is noted). This is demonstrated by comparing the time-averaged hydrodynamic resistance on the particles (represented as the correction to Stokes mobility, λ) across both cases, as listed in Table 4.

Table 3: Maximum span of the non-dimensional displacement (P_i^*) along the co-axial and wall normal directions after 50 tau_p.

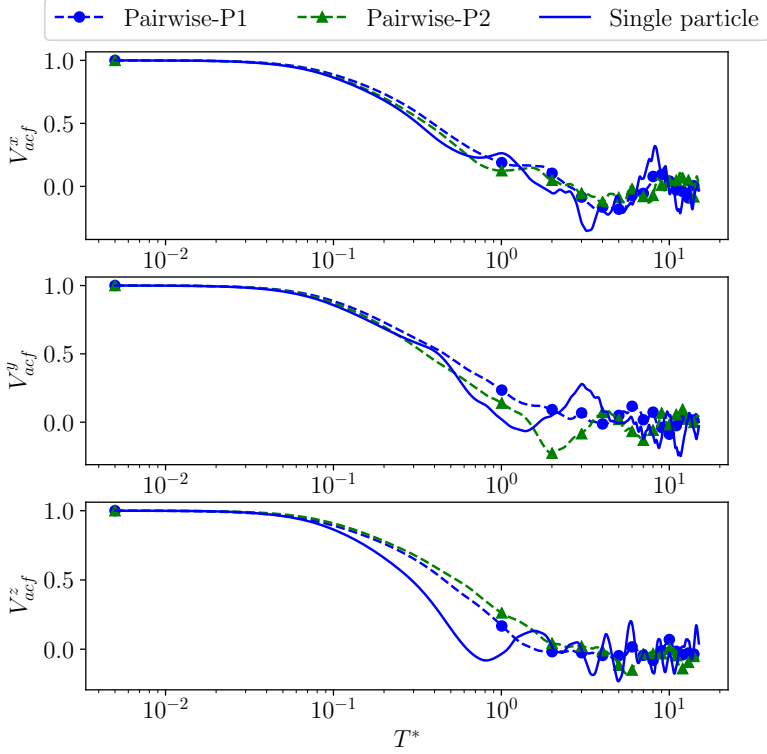| Case	Co-axial (x)	Wall-normal (z)
Single particle	0.072	0.0515
Pairwise-*P1*	0.082	0.051

Figure 9: Comparison between single and pairwise diffusion (in a domain with symmetric boundaries): decay of the directional velocity auto-correlation function (V_{acf}^i) over a 20 τ_p period. The trajectories of the single and particle-*P1* are calculated using the same random number sequence **G**, while particle-*P2* is simulated with an alternate sequence.

The correlated hydrodynamic behavior is also identifiable when comparing the decay of the auto-correlation (V_{acf}^i) for particle velocities across the single and pairwise diffusion cases as well (see Fig. 9). The V_{acf}^i for the single particle diffusion case decays earlier along all the directions of motion due to the effect of the boundaries, while in the pairwise *P1* case the decay (under the same boundary effects) is delayed indicating that *P1* travels in the wake of *P2*. Thus, it is shown that the *LaIBM* framework is able to account for the two simultaneous fundamental effects on a diffusing pair of particles (as identified in the hydrodynamic bases of Batchelor [68]), which are the increased overall hydrodynamic resistances and the correlated motion of the pair, respectively. Note that these effects inherently include the accompanying p-p interaction mediated by the fluid.

Table 4: Time averaged net hydrodynamic resistance on the particles (represented as the correction to Stokes mobility i.e. λ) along the co-axial and wall normal directions after 20 τ_p.

Case	Co-axial (x)	Wall-normal (z)
Single particle	1.944	1.797
Pairwise-*P1*	2.174	2.042

7. Conclusions

In this paper, we revisit some classical results from hindered diffusion theory with a continuum-based multiphase DNS framework, $LaIBM$, which has previously been shown to handle hindered diffusion in arbitrary geometries (such as micro-channels and pores) [44, 86]. This framework leverages a resolved solution of the hydrodynamics around the Brownian particle to estimate its mobility, thereby making it perfectly suited to describe the complex diffusive behavior of Brownian particles. This is of particular importance in the classical studies reported in literature (for e.g. [26, 68]), where other interactions (mediated by the fluid) such as particle-particle (p-p) or particle-wall (p-boundary) effects assume a governing role. To our best knowledge, this is the first continuum-based framework that simultaneously solves for Brownian dynamics with the inclusion of an evolving interface (for the diffusion near a soft-boundary) through a VOF coupling. The incorporation of the resolved hydrodynamics around a diffusing particle (in its transport equation) obviates the need to resort to assumptions about the interface topology or an *a-priori* determination of hydrodynamic mobility tensors, as required by the conventional analytical treatments [26, 49, 51] and classical particle-based simulation techniques such as SD and BD.

Consequently, we show that the hindered diffusion behavior can be assessed using a two-way coupled continuum mechanics-discrete particle approach. The expected effects of a no-slip wall on the diffusion of a spherical Brownian particle is illustrated using the directional mean squared displacement (MSD_i^*) and velocity auto-correlation functions (V_{acf}^i). The former captured the standard diffusion dynamics of the particle including the transition from a ballistic to a linear regime, while the latter showed an expected exponential decay (due to creeping flow conditions in the system). Further, both the MSD_i^* and V_{acf}^i also reflect the increased hydrodynamic resistance in the diffusion near a no-slip boundary, thereby confirming the reduced particle mobility. Next, the hindered diffusion behavior near a soft boundary (formed at the interface of two liquids with a viscosity ratio of 100) is also investigated using the $LaIBM$ framework. This case represents a more complex three-phase problem (i.e. *Fluid 1*, *Fluid 2* and the solid nanoparticle), which is beyond the scope of analytical and commonly used particle-based simulation methods like BD and SD. The $LaIBM$ framework is extended to these complex problems via a seamless integration between the dynamics of the evolving interface and the motion of the nearby Brownian particle through a *VOF-LaIBM* coupling. Consequently, we show that the particle mobility is enhanced near a soft-boundary due to a significant reduction in the hydrodynamic resistances that results from the lowered fluid shear

near such an interface. Finally, we also assess the pairwise diffusion of Brownian particles (*P1-P2*) in a symmetric domain (no flow or scalar flux across the boundary i.e. zero-shear slip walls). As expected, the p-p interactions mediated by the fluid lead to a correlated motion between the pair of particles as a result of being accelerated by each other's wakes. Thus, a particle *P1* in the pair when compared with an identical particle diffusing alone in the same domain (i.e. the two particles are forced using the same random number sequence **G**), exhibits a different mobility along the co-axial direction as it is influenced by the nearby motion of *P2* (along this direction).

Hence, we have shown that the $LaIBM$ framework can be used to handle a variety of challenging theoretical cases. This further opens up new avenues to assess the hindered diffusion problem of Brownian particles. In its current form, the applicability of our framework is constrained by the Langevin basis used (i.e. creeping flow conditions must prevail). Nevertheless, it can be extended to study problems beyond the reach of existing methods, such as the diffusion of a particle in an inertial fluid (where memory effects are included) or in a non-Newtonian fluid (the IB method has been demonstrated to handle such fluids in [111, 112]), by including the appropriate Langevin basis. Moreover, as we use an IB method, we can also include complex (such as nanorods, nanowires etc.) and fractal-shaped particles [4]. Further, since the framework relies on a continuum-based solution to the surrounding flow field, additional transport of temperature and/or species can be directly incorporated by solving the relevant transport equations. Hence, this framework also has the inherent capability to provide a detailed insight into reactive Brownian phenomena. In conclusion, this framework is highly adaptable and has the inherent capability in evaluating hindered diffusion phenomena over a wide range of applications including (but not limited to) evaluating nano-carrier mediated drug delivery and particulate emission dispersion and mitigation.

Acknowledgments

References

[1] M. G. Davidson, W. M. Deen, Hydrodynamic theory for the hindered transport of flexible macromolecules in porous membranes, Journal of Membrane Science 35 (2) (1988) 167–192. `doi:10.1016/S0376-7388(00)82442-4`.

[2] M. Kostoglou, P. Housiada, A. G. Konstandopoulos, Multi-channel simulation of regeneration in honeycomb monolithic diesel particulate filters, Chemical Engineering Science 58 (14) (2003) 3273–3283. `doi:10.1016/S0009-2509(03)00178-7`.

[3] A. G. Konstandopoulos, E. Papaioannou, Update on the science and technology of diesel particulate filters, KONA Powder and Particle Journal 26 (March) (2008) 36–65. `doi:10.14356/kona.2008007`.

[4] A. S. Kannan, V. Naserentin, A. Mark, D. Maggiolo, G. Sardina, S. Sasic, H. Ström, A continuum-based multiphase DNS method for studying the Brownian dynamics of soot particles in a rarefied gas, Chemical Engineering Science 210 (2019) 115229. `doi: 10.1016/j.ces.2019.115229`.

[5] F. Martínez-Pedrero, P. Tierno, Advances in colloidal manipulation and transport via hydrodynamic interactions, Journal of Colloid and Interface Science 519 (2018) 296 – 311. `doi:https://doi.org/10.1016/j.jcis.2018.02.062`.

[6] K. Van Ommering, J. H. Nieuwenhuis, L. J. Van Ijzendoorn, B. Koopmans, M. W. Prins, Confined Brownian motion of individual magnetic nanoparticles on a chip: Characterization of magnetic susceptibility, Applied Physics Letters 89 (14) (2006). `doi:10.1063/1.2360246`.

[7] K. Van Ommering, C. C. Lamers, J. H. Nieuwenhuis, L. J. Van Ijzendoorn, M. W. Prins, Analysis of individual magnetic particle motion near a chip surface, Journal of Applied Physics 105 (10) (2009). `doi:10.1063/1.3118500`.

[8] R. Radhakrishnan, B. Uma, J. Liu, P. Ayyaswamy, D. Eckmann, Temporal multiscale approach for nanocarrier motion with simultaneous adhesion and hydrodynamic interactions in targeted drug delivery, Journal of Computational Physics 244 (2013) 252 – 263, multi-scale Modeling and Simulation of Biological Systems. `doi: 10.1016/j.jcp.2012.10.026`.

[9] E. Lauga, T. R. Powers, The hydrodynamics of swimming microorganisms, Reports on Progress in Physics 72 (9) (2009) 096601. `doi:10.1088/0034-4885/72/9/096601`.

[10] E. Kätelhön, S. V. Sokolov, R. G. Compton, Near-wall hindered diffusion: Implications for surface-based sensors, Sensors and Actuators B: Chemical 234 (2016) 420 – 425. `doi:https://doi.org/10.1016/j.snb.2016.05.016`.

[11] T. M. Squires, R. J. Messinger, S. R. Manalis, Making it stick: Convection, reaction and diffusion in surface-based biosensors, Nature Biotechnology 26 (4) (2008) 417–426. `doi:10.1038/nbt1388`.

[12] J. Mo, A. Simha, M. G. Raizen, Brownian motion as a new probe of wettability, The Journal of Chemical Physics 146 (13) (2017) 134707. `doi:10.1063/1.4979177`.

[13] J. C. Crocker, M. T. Valentine, E. R. Weeks, T. Gisler, P. D. Kaplan, A. G. Yodh, D. A. Weitz, Two-point microrheology of inhomogeneous soft materials, Phys. Rev. Lett. 85 (2000) 888–891. `doi:10.1103/PhysRevLett.85.888`.

[14] R. N. Zia, Active and passive microrheology: Theory and simulation, Annual Review of Fluid Mechanics 50 (1) (2018) 371–405. `doi:10.1146/annurev-fluid-122316-044514`.

[15] A. Einstein, Über die von der molekularkinetischen theorie der wärme geforderte bewegung von in ruhenden flüssigkeiten suspendierten teilchen, Annalen der Physik 322 (8) (1905) 549–560. `doi:10.1002/andp.19053220806`.

[16] P. Langevin, Sur la théorie du mouvement brownien, C. R. Acad. Sci. (Paris) 146 (1908) 530–533. `doi:https://doi.org/10.1119/1.18725`.

[17] M. Smoluchowski, On the mutual action of spheres which move in a viscous liquid, Bull. Int. Acad. Polonaise Sci. Lett. 1A (757) (1911) 28.

[18] G. E. Uhlenbeck, L. S. Ornstein, On the theory of the brownian motion, Physical Review 36 (5) (1930) 823–841. `doi:10.1103/PhysRev.36.823`.

[19] S. Chandrasekhar, Stochastic problems in physics and astronomy, Reviews of Modern Physics 15 (1) (1943) 1–89. `doi:10.1103/RevModPhys.15.1`.

[20] R. Zwanzig, M. Bixon, Hydrodynamic theory of the velocity correlation function, Phys. Rev. A 2 (1970) 2005–2012. `doi:10.1103/PhysRevA.2.2005`.

[21] E. J. Hinch, Application of the langevin equation to fluid suspensions, Journal of Fluid Mechanics 72 (3) (1975) 499–511. `doi:10.1017/S0022112075003102`.

[22] F. Mainardi, A. Mura, F. Tampieri, Brownian motion and anomalous diffusion revisited via a fractional Langevin equation, Modern Problems of Statistical Physics 8 (2009) 3–23.
URL `http://arxiv.org/abs/1004.3505`

[23] R. Huang, I. Chavez, K. M. Taute, B. Lukić, S. Jeney, M. G. Raizen, E.-L. Florin, Direct observation of the full transition from ballistic to diffusive brownian motion in a liquid, Nature Physics 7 (2011) 576. `doi:10.1038/nphys1953`.

[24] S. Kheifets, A. Simha, K. Melin, T. Li, M. G. Raizen, Observation of brownian motion in liquids at short times: Instantaneous velocity and memory loss, Science 343 (6178) (2014) 1493–1496. `doi:10.1126/science.1248091`.

[25] X. Bian, C. Kim, G. E. Karniadakis, 111 years of Brownian motion, Soft Matter 12 (30) (2016) 6331–6346. `doi:10.1039/c6sm01153e`.

[26] G. M. Mavrovouniotis, H. Brenner, Hindered sedimentation, diffusion, and dispersion coefficients for brownian spheres in circular cylindrical pores, Journal of Colloid And Interface Science 124 (1) (1988) 269–283. `doi:10.1016/0021-9797(88)90348-7`.

[27] B. Felderhof, Hydrodynamic interaction between two spheres, Physica A: Statistical Mechanics and its Applications 89 (2) (1977) 373 – 384. `doi:https://doi.org/10.1016/0378-4371(77)90111-X`.

[28] P. Dechadilok, W. M. Deen, Hindrance factors for diffusion and convection in pores, Industrial & Engineering Chemistry Research 45 (21) (2006) 6953–6959. `doi:10.1021/ie051387n`.

[29] E. Lauga, T. M. Squires, Brownian motion near a partial-slip boundary: A local probe of the no-slip condition, Physics of Fluids 17 (10) (2005) 103102. `doi:10.1063/1.2083748`.

[30] D. L. Ermak, J. A. McCammon, Brownian dynamics with hydrodynamic interactions, The Journal of Chemical Physics 69 (4) (1978) 1352–1360. `doi:10.1063/1.436761`. URL `https://doi.org/10.1063/1.436761`

[31] J. F. Brady, G. Bossis, Stokesian dynamics, Annual Review of Fluid Mechanics 20 (1) (1988) 111–157. `doi:10.1146/annurev.fl.20.010188.000551`.

[32] B. J. Alder, T. E. Wainwright, Studies in molecular dynamics. i. general method, The Journal of Chemical Physics 31 (2) (1959) 459–466. `doi:10.1063/1.1730376`.

[33] G. A. Bird, Monte carlo simulation of gas flows, Annual Review of Fluid Mechanics 10 (1) (1978) 11–31. `doi:10.1146/annurev.fl.10.010178.000303`.

[34] P. Ahlrichs, B. Dünweg, Lattice-boltzmann simulation of polymer-solvent systems, International Journal of Modern Physics C 09 (08) (1998) 1429–1438. `doi:10.1142/S0129183198001291`.

[35] M. Mynam, P. Sunthar, S. Ansumali, Efficient lattice boltzmann algorithm for brownian suspensions, Philosophical Transactions of the Royal Society A: Mathematical, Physical and Engineering Sciences 369 (1944) (2011) 2237–2245. `doi:10.1098/rsta.2011.0047`.

[36] X. Bian, S. Litvinov, R. Qian, M. Ellero, N. A. Adams, Multiscale modeling of particle in suspension with smoothed dissipative particle dynamics, Physics of Fluids 24 (1) (2012) 012002. `doi:10.1063/1.3676244`.

[37] P. Español, P. B. Warren, Perspective: Dissipative particle dynamics, The Journal of Chemical Physics 146 (15) (2017) 150901. `doi:10.1063/1.4979514`.

[38] A. Gubbiotti, M. Chinappi, C. M. Casciola, Confinement effects on the dynamics of a rigid particle in a nanochannel, Phys. Rev. E 100 (2019) 053307. `doi:10.1103/PhysRevE.100.053307`.

[39] G. Stokes, On the theories of internal friction of fluids in motion and of the equilibrium and motion of elastic solids, Trans. Camb. Phil. Soc. 8 (1845) 24–40.

[40] G. G. Stokes, On the Steady Motion of Incompressible Fluids, Transactions of the Cambridge Philosophical Society 7 (1848) 439.

[41] O. Darrigol, Between hydrodynamics and elasticity theory: The first five births of the navier-stokes equation, Archive for History of Exact Sciences 56 (2) (2002) 95–150. `doi:10.2307/41134138`.

[42] P. J. Atzberger, P. R. Kramer, C. S. Peskin, A stochastic immersed boundary method for fluid-structure dynamics at microscopic length scales, Journal of Computational Physics 224 (2) (2007) 1255 – 1292. `doi:10.1016/j.jcp.2006.11.015`.

[43] B. Uma, T. N. Swaminathan, R. Radhakrishnan, D. M. Eckmann, P. S. Ayyaswamy, Nanoparticle brownian motion and hydrodynamic interactions in the presence of flow fields, Physics of Fluids 23 (7) (2011) 073602. `doi:10.1063/1.3611026`.

[44] A. S. Kannan, A. Mark, D. Maggiolo, G. Sardina, S. Sasic, H. Ström, Assessment of hindered diffusion in arbitrary geometries using a multiphase dns framework, Chemical Engineering Science (in press) (2020).

[45] H. Ounis, G. Ahmadi, Analysis of dispersion of small spherical particles in a random velocity field, Journal of Fluids Engineering 112 (1) (1990) 114–120. `doi:10.1115/1.2909358`.

[46] L. D. Landau, E. M. Lifshitz, CHAPTER VI - Diffusion, Pergamon, 1987, pp. 227–237. `doi:10.1016/B978-0-08-033933-7.50014-3`.

[47] M. von Smoluchowski, Zur kinetischen theorie der brownschen molekularbewegung und der suspensionen, Annalen der Physik 326 (14) (1906) 756–780. `doi:10.1002/andp.19063261405`.

[48] B. U. Felderhof, Diffusion of interacting brownian particles 11 (5) (1978) 929–937. `doi:10.1088/0305-4470/11/5/022`.

[49] B. U. Felderhof, Effect of the wall on the velocity autocorrelation function and long-time tail of brownian motion, The Journal of Physical Chemistry B 109 (45) (2005) 21406–21412. `doi:10.1021/jp051335b`.

[50] A. M. Ardekani, R. H. Rangel, Unsteady motion of two solid spheres in stokes flow, Physics of Fluids 18 (10) (2006) 103306. `doi:10.1063/1.2363351`.

[51] A. Simha, J. Mo, P. J. Morrison, Unsteady stokes flow near boundaries: the point-particle approximation and the method of reflections, Journal of Fluid Mechanics 841 (2018) 883–924. `doi:10.1017/jfm.2018.87`.

[52] N. Sharma, N. A. Patankar, Direct numerical simulation of the brownian motion of particles by using fluctuating hydrodynamic equations, Journal of Computational Physics 201 (2) (2004) 466 – 486. `doi:10.1016/j.jcp.2004.06.002`.

[53] B. E. Griffith, N. A. Patankar, Immersed methods for fluid–structure interaction, Annual Review of Fluid Mechanics 52 (1) (2020) 421–448. `doi:10.1146/annurev-fluid-010719-060228`.

[54] A. Donev, A. Nonaka, Y. Sun, G. Fai, Thomas, A. L. Garcia, J. B. Bell, Low mach number fluctuating hydrodynamics of diffusively mixing fluids, Communications in Applied Mathematics and Computational Science 9 (1) (2014) 47–105. `doi:10.2140/camcos.2014.9.47`.

[55] N. Ramakrishnan, Y. Wang, D. M. Eckmann, P. S. Ayyaswamy, R. Radhakrishnan, Motion of a nano-spheroid in a cylindrical vessel flow: Brownian and hydrodynamic interactions, Journal of Fluid Mechanics 821 (2017) 117–152. `doi:10.1017/jfm.2017.182`.

[56] P. R. Kramer, C. S. Peskin, P. J. Atzberger, On the foundations of the stochastic immersed boundary method, Computer Methods in Applied Mechanics and Engineering 197 (25) (2008) 2232 – 2249, immersed Boundary Method and Its Extensions. `doi:10.1016/j.cma.2007.11.010`.

[57] Inertial coupling method for particles in an incompressible fluctuating fluid, Computer Methods in Applied Mechanics and Engineering 269 (2014) 139 – 172. `doi:10.1016/j.cma.2013.10.029`.

[58] Y. Wang, H. Lei, P. J. Atzberger, Fluctuating hydrodynamic methods for fluid-structure interactions in confined channel geometries, Applied Mathematics and Mechanics 39 (1) (2018) 125–152. `doi:10.1007/s10483-018-2253-8`.

[59] G. De Fabritiis, M. Serrano, R. Delgado-Buscalioni, P. V. Coveney, Fluctuating hydrodynamic modeling of fluids at the nanoscale, Physical Review E 75 (2) (2007) 026307. `doi:10.1103/PhysRevE.75.026307`.

[60] J. Vom Scheidt, Kloeden, p. e.; platen, e., numerical solution of stochastic differential equations. berlin etc., springer-verlag 1992. xxxvi, 632 pp., 85 figs., dm 118,oo. isbn 3-540-54062-8 (applications of mathematics 23), ZAMM - Journal of Applied Mathematics and Mechanics / Zeitschrift für Angewandte Mathematik und Mechanik 74 (8) (1994) 332–332. `doi:10.1002/zamm.19940740806`.

[61] A. Donev, A. Nonaka, A. K. Bhattacharjee, A. L. Garcia, J. B. Bell, Low mach number fluctuating hydrodynamics of multispecies liquid mixtures, Physics of Fluids 27 (3) (2015) 037103. `doi:10.1063/1.4913571`.

[62] J. Happel, H. Brenner, Low Reynolds number hydrodynamics, Martinus Nijhoff publishers, 1983. `doi:10.1007/978-94-009-8352-6`.

[63] E. S. Pagac, R. D. Tilton, D. C. Prieve, Hindered mobility of a rigid sphere near a wall, Chemical Engineering Communications 148-50 (May) (1996) 105–122. `doi:10.1080/00986449608936511`.

[64] M. A. Bevan, D. C. Prieve, Hindered diffusion of colloidal particles very near to a wall: revisited, Journal of Chemical Physics 113 (3) (2000) 1228–1236. `doi:10.1063/1.481900`.

[65] K. D. Kihm, A. Banerjee, C. K. Choi, T. Takagi, Near-wall hindered Brownian diffusion of nanoparticles examined by three-dimensional ratiometric total internal reflection fluorescence microscopy (3-D R-TIRFM), Experiments in Fluids 37 (6) (2004) 811–824. `doi:10.1007/s00348-004-0865-4`.

[66] H. A. Lorentz, Abhandlungen über theoretische Physik, B.G. Teubner, 1907.

[67] H. Brenner, A general theory of taylor dispersion phenomena iv. direct coupling effects, Chemical Engineering Communications 18 (5-6) (1982) 355–379. `doi:10.1080/00986448208939976`.

[68] G. K. Batchelor, Brownian diffusion of particles with hydrodynamic interaction, Journal of Fluid Mechanics 74 (1) (1976) 1–29. `doi:10.1017/S0022112076001663`.

[69] N. A. Frej, D. C. Prieve, Hindered diffusion of a single sphere very near a wall in a nonuniform force field, The Journal of Chemical Physics 98 (9) (1993) 7552–7564. `doi:10.1063/1.464695`.

[70] P. Huang, K. S. Breuer, Direct measurement of anisotropic near-wall hindered diffusion using total internal reflection velocimetry, Physical Review E - Statistical, Nonlinear, and Soft Matter Physics 76 (4) (2007) 1–4. `doi:10.1103/PhysRevE.76.046307`.

[71] J. Mo, A. Simha, M. G. Raizen, Broadband boundary effects on brownian motion, Phys. Rev. E 92 (2015) 062106. `doi:10.1103/PhysRevE.92.062106`.

[72] E. E. Michaelides, Wall Effects on the Brownian Movement, Thermophoresis, and Deposition of Nanoparticles in Liquids, Journal of Fluids Engineering 138 (5) (01 2016). `doi:10.1115/1.4032030`.

[73] E. E. Michaelides, Nanoparticle diffusivity in narrow cylindrical pores, International Journal of Heat and Mass Transfer 114 (2017) 607 – 612. `doi:https://doi.org/10.1016/j.ijheatmasstransfer.2017.06.098`.

[74] S. Kim, S. J. Karrila, Microhydrodynamics: principles and selected applications, Butterworth-Heinemann, 1991.

[75] W. Hess, R. Klein, Generalized hydrodynamics of systems of brownian particles, Advances in Physics 32 (2) (1983) 173–283. `doi:10.1080/00018738300101551`.

[76] R. I. Cukier, Diffusion of interacting brownian particles in a fluid with fixed macroparticles, The Journal of Chemical Physics 79 (8) (1983) 3911–3920. `doi:10.1063/1.446259`.

[77] L. Bocquet, J.-P. Hansen, J. Piasecki, Friction tensor for a pair of brownian particles: Spurious finite-size effects and molecular dynamics estimates, Journal of Statistical Physics 89 (1) (1997) 321–346. `doi:10.1007/BF02770768`.

[78] E. R. Dufresne, T. M. Squires, M. P. Brenner, D. G. Grier, Hydrodynamic coupling of two brownian spheres to a planar surface, Phys. Rev. Lett. 85 (2000) 3317–3320. `doi:10.1103/PhysRevLett.85.3317`.

[79] J. C. Crocker, Measurement of the hydrodynamic corrections to the brownian motion of two colloidal spheres, The Journal of Chemical Physics 106 (7) (1997) 2837–2840. `doi:10.1063/1.473381`.

[80] S. Savel'ev, F. Marchesoni, A. Taloni, F. Nori, Diffusion of interacting brownian particles: Jamming and anomalous diffusion, Phys. Rev. E 74 (2006) 021119. `doi:10.1103/PhysRevE.74.021119`.

[81] K. Misiunas, S. Pagliara, E. Lauga, J. R. Lister, U. F. Keyser, Nondecaying hydrodynamic interactions along narrow channels, Phys. Rev. Lett. 115 (2015) 038301. `doi:10.1103/PhysRevLett.115.038301`.

[82] H. Faxén, Einwirkung der gefässwände auf den widerstand gegen die bewegung einer kleinen kugel in einer zähen flüssigkeit (PhD thesis), Ph.D. thesis, Uppsala University (1921).

[83] H. Faxén, Die bewegung einer starren kugel langs der achse eines mit zaher flfisigkeit fefiillten rohres, Arkiv för Matematik Astronomi och Fysik 17 (27) (1927) 1–28.

[84] H. Brenner, The slow motion of a sphere through a viscous fluid towards a plane surface, Chemical Engineering Science 16 (3-4) (1961) 242–251. `doi:10.1016/0009-2509(61)80035-3`.

[85] P. P. Lele, J. W. Swan, J. F. Brady, N. J. Wagner, E. M. Furst, Colloidal diffusion and hydrodynamic screening near boundaries, Soft Matter 7 (2011) 6844–6852. `doi:10.1039/C0SM01466D`.

[86] A. S. Kannan, A. Mark, D. Maggiolo, G. Sardina, S. Sasic, H. Ström, A hydrodynamic basis for off-axis brownian diffusion under intermediate confinements in micro-channels, International Journal of Multiphase Flow (2020) (submitted).

[87] M. Stimson, G. B. Jeffery, L. N. G. Filon, The motion of two spheres in a viscous fluid, Proceedings of the Royal Society of London. Series A, Containing Papers of a Mathematical and Physical Character 111 (757) (1926) 110–116. `doi:10.1098/rspa.1926.0053`.

[88] G. K. Batchelor, Transport properties of two-phase materials with random structure, Annual Review of Fluid Mechanics 6 (1) (1974) 227–255. `doi:10.1146/annurev.fl.06.010174.001303`.

[89] C. S. Peskin, The fluid dynamics of heart valves: Experimental, theoretical, and computational methods, Annual Review of Fluid Mechanics 14 (1) (1982) 235–259. `doi:10.1146/annurev.fl.14.010182.001315`.

[90] R. Mittal, G. Iaccarino, Immersed boundary methods, Annual Review of Fluid Mechanics 37 (1) (2005) 239–261. `doi:10.1146/annurev.fluid.37.061903.175743`.

[91] A. Mark, B. G. M. van Wachem, Derivation and validation of a novel implicit second-order accurate immersed boundary method, Journal of Computational Physics 227 (13) (2008) 6660–6680. `doi:10.1016/j.jcp.2008.03.031`.

[92] A. Mark, E. Svenning, F. Edelvik, An immersed boundary method for simulation of flow with heat transfer, International Journal of Heat and Mass Transfer 56 (1) (2013) 424 – 435. `doi:10.1016/j.ijheatmasstransfer.2012.09.010`.

[93] C. Hirt, B. Nichols, Volume of fluid (vof) method for the dynamics of free boundaries, Journal of Computational Physics 39 (1) (1981) 201 – 225. `doi:10.1016/0021-9991(81)90145-5`.

[94] R. Scardovelli, S. Zaleski, Direct numerical simulation of free-surface and interfacial flow, Annual Review of Fluid Mechanics 31 (1) (1999) 567–603. `doi:10.1146/annurev.fluid.31.1.567`.

[95] H. Ounis, G. Ahmadi, A comparison of brownian and turbulent diffusion, Aerosol Science and Technology 13 (1) (1990) 47–53. `doi:10.1080/02786829008959423`.

[96] N. M. Newmark, A method of computation for structural dynamics, Journal of the Engineering Mechanics Division 85 (1959) 67–94.

[97] K. Itô, Stochastic integration, Academic Press, 1973, pp. 141–148. `doi:10.1016/B978-0-12-702450-9.50020-8`.

[98] F. C. Centre, Ips iboflow.
URL `http://www.fcc.chalmers.se/software/ips/iboflow/`

[99] O. Ubbink, R. Issa, A method for capturing sharp fluid interfaces on arbitrary meshes, Journal of Computational Physics 153 (1) (1999) 26 – 50. `doi:10.1006/jcph.1999.6276`.

[100] M. Naumov, M. Arsaev, P. Castonguay, J. Cohen, J. Demouth, J. Eaton, S. Layton, N. Markovskiy, I. Reguly, N. Sakharnykh, V. Sellappan, R. Strzodka, Amgx: A library for gpu accelerated algebraic multigrid and preconditioned iterative methods, SIAM Journal on Scientific Computing 37 (5) (2015) S602–S626. `doi:10.1137/140980260`.

[101] H. Ding, P. D. Spelt, C. Shu, Diffuse interface model for incompressible two-phase flows with large density ratios, Journal of Computational Physics 226 (2) (2007) 2078 – 2095. `doi:10.1016/j.jcp.2007.06.028`.

[102] M. Raessi, H. Pitsch, Consistent mass and momentum transport for simulating incompressible interfacial flows with large density ratios using the level set method, Computers Fluids 63 (2012) 70 – 81. `doi:10.1016/j.compfluid.2012.04.002`.

[103] Z. Adamczyk, M. Adamczyk, T. van de Ven, Resistance coefficient of a solid sphere approaching plane and curved boundaries, Journal of Colloid and Interface Science 96 (1) (1983) 204 – 213. `doi:10.1016/0021-9797(83)90022-X`.

[104] A. Rahman, Correlations in the motion of atoms in liquid argon, Phys. Rev. 136 (1964) A405–A411. `doi:10.1103/PhysRev.136.A405`.

[105] T. Li, S. Kheifets, D. Medellin, M. G. Raizen, Measurement of the instantaneous velocity of a brownian particle, Science 328 (5986) (2010) 1673–1675. `doi:10.1126/science.1189403`.

[106] B. U. Felderhof, Diffusion and velocity relaxation of a brownian particle immersed in a viscous compressible fluid confined between two parallel plane walls, The Journal of Chemical Physics 124 (5) (2006) 054111. `doi:10.1063/1.2165199`.

[107] S. Jeney, B. Lukić, J. A. Kraus, T. Franosch, L. Forró, Anisotropic memory effects in confined colloidal diffusion, Phys. Rev. Lett. 100 (2008) 240604. `doi:10.1103/PhysRevLett.100.240604`.

[108] T. Franosch, S. Jeney, Persistent correlation of constrained colloidal motion, Phys. Rev. E 79 (2009) 031402. `doi:10.1103/PhysRevE.79.031402`.

[109] J. Mo, A. Simha, M. G. Raizen, Broadband boundary effects on brownian motion, Phys. Rev. E 92 (2015) 062106. `doi:10.1103/PhysRevE.92.062106`.

[110] J. Mo, M. G. Raizen, Highly resolved brownian motion in space and in time, Annual Review of Fluid Mechanics 51 (1) (2019) 403–428. `doi:10.1146/annurev-fluid-010518-040527`.

[111] S. Ingelsten, A. Mark, F. Edelvik, A lagrangian-eulerian framework for simulation of transient viscoelastic fluid flow, Journal of Non-Newtonian Fluid Mechanics 266 (2019) 20 – 32. `doi:10.1016/j.jnnfm.2019.02.005`.

[112] S. Ingelsten, A. Mark, K. Jareteg, R. Kádár, F. Edelvik, Computationally efficient viscoelastic flow simulation using a lagrangian-eulerian method and gpu-acceleration, Journal of Non-Newtonian Fluid Mechanics 279 (2020) 104264. `doi:10.1016/j.jnnfm.2020.104264`.

Paper E

The Knudsen paradox in micro-channel Poiseuille flows with a symmetric particle

A. S. Kannan, T. S. B. Narahari, Y. Bharadhwaj, A. Mark, D. Maggiolo, G. Sardina, S. Sasic, and H. Ström. The Knudsen paradox in micro-channel Poiseuille flows with a symmetric particle. *Applied sciences* (Submitted November 2020)

Article

The Knudsen paradox in micro-channel Poiseuille flows with a symmetric particle

Ananda Subramani Kannan [1] ***, Tejas Sharma Bangalore Narahari** [1]**, Yashas Bharadhwaj** [1]**, Andreas Mark** [2]**, Gaetano Sardina** [1]**, Dario Maggiolo** [1]**, Srdjan Sasic** [1]**and Henrik Ström** [1]

[1] Department of Mechanics and Maritime Sciences, Division of Fluid Dynamics, Chalmers University of Technology, Göteborg, 412 96, Sweden; ananda@chalmers.se

[2] Fraunhofer-Chalmers Research Centre, Göteborg, 412 88, Sweden.

* Correspondence: ananda@chalmers.se

Featured Application: The present work addresses a perceived knowledge gap in rarefied flows, along with a relevant challenge while modeling gas-solid flows in confined geometries at the nano-scale, where simultaneous handling of local and non-local transport mechanisms over the particle surfaces must be realized. These phenomena are also of interest to several micro-fluidic applications including (but not limited to) lab-on-a-chip devices, micro-total analytic systems (μTAS) and point-of-care diagnostics (POC).

Abstract: The Knudsen paradox – the non-monotonous variation of mass-flow rate with the Knudsen number – is a unique and well-established signature of micro-channel rarefied flows. A particle which is not of insignificant size in relation to the duct geometry can significantly alter the flow behavior when introduced in such a system. In this work we investigate the effects of a stationary particle on a micro-channel Poiseuille flow, from continuum to free-molecular conditions, using the direct simulation Monte-Carlo (DSMC) method. We establish a hydrodynamic basis for such an investigation by evaluating the flow around the particle and study the blockage effect on the Knudsen paradox. Our results show that with the presence of a particle this paradoxical behavior is altered. The effect is more significant as the particle becomes large and results from a shift towards relatively more ballistic molecular motion at shorter geometrical distances. The need to account for combinations of local and non-local transport effects in modeling of reactive gas-solid flows in confined geometries at the nano-scale and in nanofabrication of model pore systems are discussed in relation to these results.

1. Introduction

A sub-micron sized particle when transported in a micro-channel can significantly alter the rarefied behavior of the carrier gas. These effects emerge partly because the dispersed particle serves as an extra momentum source or sink in the system, and partly due to the blockage induced by the particle, which further affects the effective hydrodynamic length of the bounding duct. These phenomena are of particular significance from a theoretical view-point due to the complex molecular interactions that prevail at the aforementioned spatial scales, necessitating novel approaches to understand the same. Moreover, these challenging systems are also of interest to several micro-fluidic applications including (but not limited to) lab-on-a-chip devices, micro-total analytic systems (μTAS) and point-of-care

diagnostics (POC) [1,2].

The Knudsen paradox [3–5] is a unique signature of micro-channel rarefied flows. Usually, such flows are characterized by the Knudsen number, $Kn = \lambda/a$, where λ is the mean-free-path of the gas and a is a suitable system length scale (for instance the channel height). Consequently, these flows can be classified into four regimes: continuum flows ($Kn < 0.001$), slip flows ($0.001 \leq Kn < 0.1$), transition flows ($0.1 \leq Kn < 10$), and free-molecular flows ($Kn \geq 10$) [6,7]. The Knudsen paradox is characterized by the variation in the mass-flow rate (Q) of a molecular gas in micro-channels, across these aforementioned regimes, where the ratio between the length and hydraulic diameter is large. In such systems, Q decreases with increasing Kn, reaches a minimum at $Kn \approx O(1)$ (in the transition regime) and further increases with an increase in Kn (towards the free-molecular regime). For this reason, the Knudsen paradox is also referred to in literature as the Knudsen minimum. The paradox was first studied experimentally and theoretically by Knudsen [3] in experiments of Poiseuille flow driven by the identical pressure drop in channels with varying widths. The observation of this minimum was attributed, by Pollard and Present [4], to the imbalance between two counteracting molecular effects: the obstruction of long diffusion paths due to molecular collisions, leading to a net decrease in Q, on the one hand and the development of drift transport leading to an increase in Q, on the other. Thus, it follows that, Q in a long tube must initially decrease with increasing pressure (when $L > \lambda \gg a$, where L is the channel length) and pass through a minimum value due to the obstruction to molecular diffusion. As the pressure crosses this threshold ($\lambda < a$), drift transport increases (towards the Poiseuille form) leading to an increase in Q.

The Knudsen paradox has also been confirmed through numerical assessments, first by Cercignani and co-workers [5,8,9] and later by others [10–12], to name a few. These authors solved the steady Boltzmann equation with a BGK (Bhatnagar–Gross–Krook) [13] collision term. For a detailed review of these approaches, the reader is referred to the book by Cercignani [14]. More recently, these numerical methods have been further extended and validated to handle a wide range of rarefied flows in a variety of geometries as described in the reviews by Sharipov [15], Beskok [16] , Karniadakis [17] and Colin [18]. In general, the reported methods are at the following levels of abstraction: i) micro-scale resolved techniques that directly model molecular scale effects (such as inter-molecular and molecule-wall interactions), ii) meso-scale resolved techniques (using the Boltzmann equation) that solve the molecular distribution function and iii) macro-scale (continuum) resolved techniques that incorporate velocity slip and temperature jump boundary conditions into the Navier–Stokes equations to model molecular phenomena. The continuum based methods are valid up to the transition regime [19], while the meso-and micro scale methods can in principle be applied across the entire Kn range [6]. Thus, these two alternatives are preferred while evaluating the Knudsen paradox. Consequently, the Lattice Boltzmann method (LBM) [20,21] and the direct simulation Monte-Carlo (DSMC) method [22,23] have gained prominence in rarefied micro-channel flow studies.

In general, research on single-phase rarefied Poiseuille flows are extensive (cf. [16–18]). However, related work on their multiphase counterparts (where a solid particle and a rarefied gas co-exist in the micro-channel) are relatively scarce. Currently, these reported multiphase studies are mostly limited to assessing stationary flow past a particle, for instance the studies by [24–27], to name a few, indicative of a knowledge gap. In fact, investigations on the effect of an additional particulate phase, on the Knudsen paradox noted in micro-channel Poiseuille flows (in the transition regime), have not been previously reported. An additional motive to study such rarefied particulate Poiseuille flows stems from the recent advancements in nanofabrication techniques. Novel nanofabricated reactor systems are increasingly used to study nanoscale reactive flows [28]. Such systems are often designed to mimic naturally occurring reactor geometries, such as individual pores inside a porous medium. Particles can either be dispersed (as in a gas-solid flow) or stationary (as in typical heterogeneous catalysis

applications). A requirement for the existence of a Knudsen minimum is that the duct exhibits free paths for molecular motion that are much longer than the mean radius, a configuration which is typically not readily encountered in natural porous media [4]. However, due to restrictions imposed by nanofabrication as well as increasing demand for advanced experimental equipment, artificial model pores may well fulfill these requirements and thus exhibit Knudsen minima effects. Furthermore, the spatial variability in the heterogeneous topology of natural porous media has been shown to reduce the relevance of rarefaction effects on the total flow rate in the slip flow regime [29], which could imply that effects observed in systems with regular pore patterns may differ from the systems they are meant to represent. As model pore manufacturing methods are swiftly advancing, possibilities to experimentally investigate reactive rarefied gas-solid flows in model pores will soon become available. It is then of great interest to understand the differences in flow and transport characteristics of artificially designed systems to their intended natural counterparts. Such studies are particularly relevant for understanding pressure-driven transport of nanoparticles through micro-channels as encountered during reactive particulate matter flows in catalytic automobile exhaust after-treatment devices [27]. This paper aims to address these open questions in rarefied Poiseuille flows with the simultaneous presence of a particulate phase. Consequently, we investigate the Knudsen paradox in a regular micro-channel Poiseuille flow with a stationary obstacle placed at its center and discuss the implications of our observations for reactive particulate flows.

The obstacle is intended to represent a particle which is not small in relation to the duct geometry. For simplicity, the particle is assumed to be square shaped, occupying the entire depth of the micro-channel and immobile. We use the DSMC method developed by Bird [22,23] for the respective assessments. This is an efficient particle based (micro-scale) method that simulates interactions between molecular parcels, which represents groups of molecules having the same properties such as velocity and temperature. The relevant macroscopic quantities of the flow are extracted by statistically averaging over these microscopic quantities. Consequently, we employ the thoroughly validated open source DSMC solver *dsmcFoam+* (implemented within the *OpenFOAM* software framework [30]), developed by White and co-workers [31], for the simulations presented in this paper. We evaluate the variation of a normalized form of Q (referred to as Q_{norm}) across the entire Kn range in micro-channel Poiseuille flows with a particle. We investigate the effect of the particle size, in terms of a blockage ratio given as H/h, where H and h are the channel and particle heights respectively, on the obtained Knudsen minimum. Additionally, the velocity along with the Mach number developed across the channel, are estimated to establish a hydrodynamic basis for the noted variation in Q_{norm}.

2. Problem description

In this paper we evaluate the pressure driven flow of rarefied nitrogen gas in a micro-channel. This is a Cartesian 2D planar setup with the flow along the x-direction. A stationary square-shaped particle is placed at the center of the micro-channel. We consider three different configurations, given by particle blockage ratios (or H/h where H and h are the micro-channel and particle heights respectively): 8, 4 and 2, which represent progressively increasing degree of channel obstruction (see Fig. 1). The channel length (L) is 5 times its height (H), which is is $0.4 \mu m$, to ensure that a fully developed flow with minimal entrance effects can be realized. The pressure drop (ΔP) across the channel is varied so as to reasonably span over the entire Kn range. Such a fundamental setup is chosen since it perfectly mimics the flow configuration studied in [5,32,33] and is well suited to describe the Knudsen paradox in micro-channels.

3. DSMC framework: *dsmcFoam+*

The direct simulation Monte-Carlo (DSMC), developed by Bird [23], is a stochastic particle-based technique for modeling real gases in which the molecular diameter is much smaller than the mean free path (λ). The primary objective of this method is to decouple molecular motion (modeled
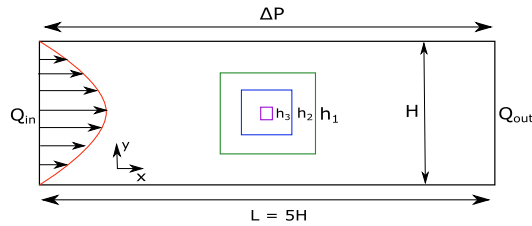
Figure 1. Schematic of the problem: 2D Planar Poiseuille flow in a micro-channel with a stationary obstacle in the middle. Note that the particle is square shaped with sides h1, h2 or h3 (decreasing in size), giving blockage ratios (H/h) 2, 4 and 8 respectively. The flow is along the *x*-direction.

deterministically) and inter-molecular collision (modeled probabilistically) over small time intervals. The time interval over which the solution is sought is subdivided into smaller sub-intervals over which the particle motion and collisions are decoupled. Consequently, the trajectories are computed over a time interval which is lesser than the mean collision time. Further, DSMC relies on discrete parcels, which each contain a collection of molecules, to represent the total molecular number density (N) of the real gas. Thus, this method is computationally cheaper than a fully deterministic method like molecular dynamics (MD), and is ideally suited for studying rarefied gas dynamics [23].

We use the open-source solver *dsmcFoam+* [31,33,34] for carrying out the assessments presented in this paper. This code-base is licensed under the GNU general public license with a publicly available software repository [35]. Further, it has been extensively validated against experimental and theoretical data across a wide variety of rarefied flows [31–33]. The algorithm employed in this solver can be summarized as follows. The flow domain is divided into cells (a Cartesian grid) which are in-turn populated with the DSMC parcels. Each of these parcels is assigned a position and a Maxwellian-distributed velocity based on the inlet conditions. Consequently, a Dirichlet type implicit boundary condition is used to assign the quantities associated with the molecules entering the computational domain (cf. [23,36]). The parcels are indexed into cells and arranged in an array to facilitate collisions. These parcels are then moved based on the type of interaction. Inter-molecular collisions are carried out probabilistically using the no-time counter (NTC) scheme proposed by Bird [23], while parcel-boundary interactions are simulated using a diffuse reflection model. The variable hard sphere (VHS) model [23] is used here to model the pair-wise collisions. The overall flow of molecules in the domain are driven by a downstream pressure outlet (Dirichlet type boundary condition for pressure cf. [23,37]). These steps are repeated to increase the sample size until the statistical errors are small enough. Finally, the desired macroscopic flow properties are calculated by spatially and temporally averaging the sampled data. Note that, for the mono-atomic gases like those considered in this study, the molecular collisions are considered elastic and they conserve both momentum and linear kinetic energy of collision. For a more detailed account of the DSMC method and the *dsmcFoam+* solver along with a detailed validation of the code, the reader is referred to [31,33,34].

4. Numerical setup

The channel, considered in the DSMC simulations, has dimensions as shown in Fig. 1 and is spatially discretized into *100 X 60 X 1* computational cells along the *x, y* and *z* directions respectively. Note that this is a pseudo-3D setup where the *z* direction is not solved for (i.e. a 2D planar simulation). This is done so as to mimic the setups of Cercignani et al. [5,8] and other similar studies [31–33]. A stationary obstacle (as shown in Fig. 1) is introduced in the center of the channel to obstruct the rarefied flow at varying degrees. This is given by particle blockage ratios (or H/h): 8, 4 and 2, which represent progressively increasing degree of channel obstruction. The surface and inlet temperatures are set to

300 K, while the inlet pressure is fixed based on the desired *Kn* (in our study this varies from 5000 pa to 255000 Pa). Further, the inlet to outlet pressure ratio is maintained at 3.0 for all the cases run (synonymous with the range prescribed in similar studies cf. [31,32,34,38]). The time step size used in computing the DSMC parcel motion was determined smaller than the local mean collision time. The values of mass flow rate at the inlet and outlet are monitored until these are equivalent. The relevant macroscopic properties (e.g., temperature, density, and velocity) are sampled after this steady state has been attained. The sampling is performed within each computational cell over a sufficiently large time step and over multiple realizations (to minimize statistical scattering) using relationships given by Hadjiconstantinou et al. [39]. These simulation conditions are summarized in Table 1.

Table 1. DSMC simulation conditions for a 2D planar micro-channel Poiseuille flow.

Property	value
Gas	N_2
Mass (in *Kg*)	$46.5 \times 10^{*27}$
Diameter (in *m*)	$4.17 \times 10^{*10}$
Particle blockage ratios (H/h)	8, 4 and 2
Micro-channel Aspect ratio (L/H)	5
Temperature (in *K*)	300
Inlet Pressure:P_{in} (in *Pa*)	varies from 5000 pa to 255000 Pa (based on the desired *Kn*)
Inlet/Outlet Pressure ratio	3
Time step (in *s*)	$1.72 \times 10^{*12}$
Parcels per cell	33

All gas properties have been obtained from Bird's monograph [23]

A typical DSMC simulation is usually constrained by the following discretization criteria: (i) the computational cell size must be smaller than the local mean free path (if possible collision partners are restricted to a parcel's current cell), (ii) the number of parcels per cell must be large enough to preserve collision statistics and (iii) the simulation time step must be chosen so that the parcels only cross a fraction of the average cell length during each time step. Condition's (ii) and (iii) are satisfied by employing a time-step much smaller than the mean collision time, while (i) is met by utilizing a spatial discretization that has already been validated exhaustively for the current setup (cf. [31–33]). All the simulations were carried out serially on a single node with 20 cores using an Intel® Xeon® (E5-2650) processor (up to 3.0 GHz). The simulations contained around 200,000 DSMC parcels in the case at a pressure of 255000 Pa (each parcel has a weighting factor of 10). Note that the parcel count reduces as the pressure (and consequently the mass flow of the gas) in the micro-channel reduces. Hence, in order to minimize the statistical scatter in the collected data, 2 realizations of each DSMC simulation were run for a total of 100,000 sampling intervals. The results presented in this paper are ensemble averaged over these 2 realizations (the scatter was noticeably reduced). Furthermore, the velocity extracted from the simulation (shown in Fig. 2) is displayed both using the scattered raw data as well as a polynomial fitted using a weighted least squares estimate [40], so as to facilitate a simplified visualization of the data. Each DSMC simulation needed a physical time of 100 h.

5. Results and discussion

We assess the Knudsen paradox, in the numerical setup described above, by varying the inlet pressure (P_{in}) and maintaining the inlet to outlet pressure ratio as 3. In order to compare our DSMC results to the results from Cercignani et al. [5,8], the mass flow rate Q (obtained from the simulations) is represented in a non-dimensional form. The dimensionless flow rate Q_{norm} used is [31,38]:

$$Q_{norm} = \frac{\dot{m}L\sqrt{2RT}}{H^2 w(P_{in} * P_o)} \tag{1}$$

where L, H and w are the length, height and width of the micro-channel respectively, and R and T are the specific gas constant and iso-thermal temperature of the gas. $\dot{m}$ is the mass flux extracted by the *dsmcFoam+* solver (cf. [31]), and P_{in} and P_o are the inlet and outlet pressures. Note that, Q_{norm} is independent of the local pressure gradient (depends only on its mean value), but depends mainly on a rarefaction parameter δ_m (i.e. on an inverse Knudsen number) given by:

$$\delta_m = \frac{\sqrt{\pi}}{2Kn} \tag{2}$$

The Eqs. 1 and 2 can be used to describe the rarefied flow with the particle as well under the same constraints i.e. the local pressure gradient (defined as $\frac{H}{P}\frac{dP}{dx}$) is small (or $\ll 1$). Correspondingly, we show the comparisons between *dsmcFoam+* and the data of Cercignani et al. [5,8], along with the effect of particle blockage on the Knudsen paradox. Prior to this discussion, we first establish a hydrodynamic basis for the effect of the stationary particle in the channel. This is done by comparing the corresponding velocity profiles across the micro-channel setups with and without the particle in the transition regime (at *Kn = 0.1*). We also briefly evaluate the compressibility effects of the particle on the flow system by examining the Mach number developed in in this flow regime.

5.1. Hydrodynamics of a stationary particle in the transition regime

The presence of a stationary and inert particle in a 2D planar micro-channel Poiseuille flow of a rarefied gas, in the transition regime, alters the inherent response of the system. This is because of the additional momentum sink in the flow due to the particle. We investigate the hydrodynamic consequences of such a flow obstruction by comparing the velocity in the micro-channel with a benchmark case without the particle. Such an assessment has a two-fold objective: (i) deviations from the ideal micro-channel Poiseuille flow due to the presence of the particle can be identified and (ii) the hydrodynamic basis for the observed Knudsen paradox can be deduced. We first discuss the impacts on the channel velocity profile (along the height), and follow this with a brief discussion on the compressibility of such particulate flows. Note that, all these hydrodynamic assessments are done under the conditions defined in Table 1 and at an outlet pressure P_o of 1 bar (*Kn = 0.1*). This *Kn* is chosen as it represents the unique hydrodynamics in the transition regime, where the Knudsen minimum has been observed in micro-channel Poiseuille flows [5,38].

The 2D planar micro-channel Poiseuille flow benchmark case without the particle is characterized by a parabolic velocity profile. Consequently, when the flow encounters a stationary particle at the center of the channel, its response is markedly altered. Fig. 2 shows the variation of the co-axial velocity along the y-direction ($U_x(y)$). As expected, the presence of the particle decelerates the overall flow, with the maximum velocity reduced due to the blockage. It follows that, at the center of the channel, the particle partitions the flow into two narrower channels, each developing its own parabolic velocity profile for $U_x(y)$, with a maximum velocity lower than the benchmark case. Note that, velocities at the wall boundaries are always nonzero due to a net slip-effect in the transition regime. The non-uniformities noted in the reported velocity profiles are attributed to the statistical scatter from the DSMC data. This scatter is more visible at the lowest blockage ratios, as the largest particle drastically alters the local length scale of the system, thereby decreasing the probability of molecular collisions in this region, which in turn increases the need for sampling to converge the statistics. Nevertheless, the results obtained for the lowest blockage ratio are deemed reasonable enough, as they follow the expected trend despite the scatter. These observations are further confirmed by the streamlines of the velocity along a $x * y$ plane, shown in terms of the Mach number ($Ma = u/c$, where u is the local fluid velocity and c is the speed of sound), in Fig. 3. The flow accelerates as it passes the particle, partly due to the pressure decrease but mostly due to continuity. Further, a symmetric low-velocity region is developed before and after the particle. The channeling effect created by
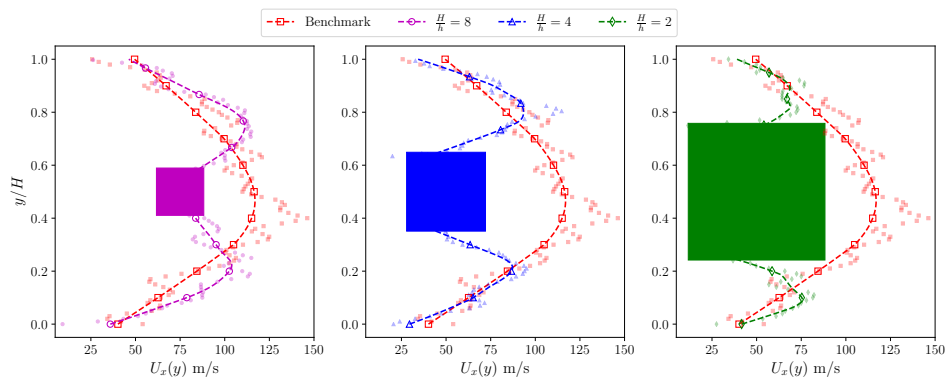
Figure 2. Comparison of the variations in co-axial velocity in the transition regime (*Kn = 0.1*) along channel height *H* at the center of the channel $x/L = 0.5$ across the chosen blockage ratios H/h of 8, 4 and 2 respectively with the benchmark case without a particle (represented by the dashed line with squares). In this figure, the square particle is used as an illustrative tool to mask the discontinuities in the region occupied by the particle. The open symbols represent the DSMC data, while the dashed lines represent the weighted least squares fit.

the presence of the particle has a consequent impact on the Knudsen paradox, as will be explained later.

Furthermore, the mach number (*Ma*) is used to assess compressibility effects in a flow system [41], where such effects are generally deemed negligible for *Ma* < 0.3. This criterion may however be violated in micro-channel Poiseuille flows. Fig. 3 shows *Ma* in the micro-channel for all cases with and without the particle at the conditions reported in Table 1. The benchmark case shows that such Poiseuille flows are sub-sonic in nature with *Ma* < 0.8. The highest *Ma* is observed at the flow outlet as expected. The additional momentum sink, due to the particle, leads to a lower flow velocity of the rarefied gas at the outlet and as the particle size increases, there is a corresponding decrease in the developed *Ma*. Thus, compressibility effects can be disregarded while assessing micro-channel Poiseuille flows with a stationary particle with an innegligible size in relation to the duct geometry (at the same driving pressure difference). This is an important observation for numerically representing such systems, as a constant density can be assumed while setting up the study.
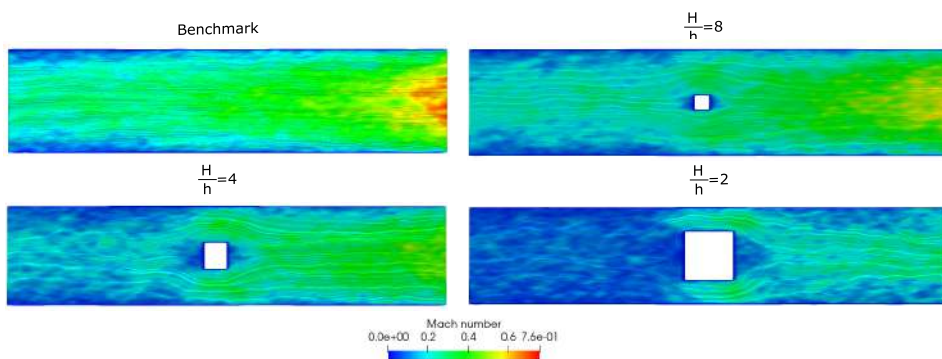

Figure 3. Contours of Mach number (*Ma*), overlaid with velocity streamlines (colored by *Ma*), along an $x * y$ plane for the benchmark case (see Table 1) and the DSMC simulations at blockage ratios H/h of 8, 4 and 2 respectively.

5.2. Effect of the particle on the Knudsen paradox

We assess the Knudsen paradox in the 2D setup (described in Fig. 1) by varying the inlet pressure (P_{in}) and maintaining the inlet to outlet pressure ratio as 3. As detailed earlier, the normalized mass flow rate in the channel Q_{norm} (see Eq. 1) is extracted from the DSMC simulations across the entire Kn range, i.e. at different δ_m (which is in turn related to Kn as shown in Eq. 2). Fig. 4 shows the Knudsen minima estimated from the DSMC simulations along with inherent uncertainties in the sampled data (through error bars). In this figure, the solid lines represent cases without a particle, while the dashed lines represent the cases with one. The comparisons between the benchmark case (without a particle) and the results given by Cercignani et al. [5,8] are reasonable, given the statistical spread of the sampled data. The agreement is good at high δ_m (or low Kn) values, with a deviation noted at the lower ones. The result in this region is more sensitive to the scatter in the DSMC data (indicated by the wider error bars in this region) and is also known to be affected by the lateral boundary condition in pseudo-3D systems [42]. However, these obtained results clearly depict the Knudsen paradox and are synonymous with those reported by White et al. [31] using the same solver. Moreover, the minima is noted at $\delta_m = 0.97$ (which is at around $Kn \approx 1$, i.e in the transition regime), as reported by others (cf. [5,8,38]). The predicted Knudsen minima for all the cases simulated are summarized in Table 2.
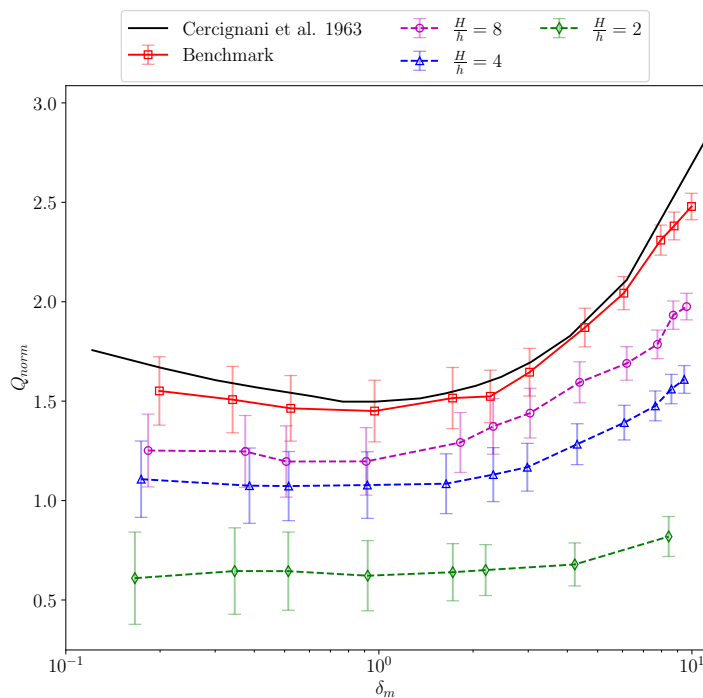

Figure 4. Knudsen paradox in 2D planar micro-channel Poiseuille flows with a stationary particle in the middle. The solid line (——) represents the results obtained by Cercignani et al. [5,8], while the red line (——) with open squares represents the benchmark results (without a particle). The dashed lines represent the results obtained from the DSMC simulations of a micro-channel at blockage ratios H/h of 8, 4 and 2 respectively. The error bars indicate the statistical spread (± 1 standard deviation) in the sampled data. Note that the error bars increase as H/h decreases (or the particle size increases) since the local Knudsen number in the restrictions created by the particle is higher.

When a particle is introduced in the channel, it serves as an additional momentum sink in the system and sections of high fluid velocity are created in the regions between the particle and wall (see Fig. 3). The Knudsen minimum may have shifted towards higher Knudsen numbers (see Table 2), although our data does not provide enough statistical confidence to confirm this. Nevertheless, the noted trends could be due to a shift towards relatively more ballistic molecules (that do not collide with each other) at shorter geometrical distances – a trend similar to that observed when going from a channel flow to a duct flow [42] or with flows in a bent channel [43]. In other words, the presence of the particle reduces the governing local length scales of the system, with a decreased probability of molecular interactions along the diffusion paths of the gas molecules. Moreover, the momentum sink effect causes the total mass flow rate in the channel to be reduced. Such a reduction in Q_{norm} is noticeable in Fig. 4, with lower mass flows noted as the particle size increases, thereby effectively blocking the channel to a higher degree. It can also be noted that the relative changes in Q_{norm} with increasing particle size in the transition regime diminishes, with the curve tending to flatten out. This occurs, as beyond the continuum regime, the frictional losses become relatively less important due to velocity slip. Moreover, as the particle becomes larger, there is an increased chance that the Knudsen paradox totally disappears, which means that Q_{norm} monotonically decreases without any increase at higher Kn (or lower δ_m), similar to observations made in bent channels by Liu et al. [43]. Synonymous with the inferences drawn from this study, we also attribute the observed behavior to the apparent increase in the local hydrodynamic resistances due to the particle. Thus, the global mass flow rate is now determined by the momentum loss imposed by the stationary particle and in this region the free paths for molecular motion are not longer than the mean channel height anymore.

Table 2. Knudsen minimum in 2D planar micro-channel Poiseuille flows with a stationary particle in the middle. Note that the reported minima is subject to the variations in the sampled data shown in Fig. 4.

Case	δ_m	Kn
Cercignani et al. [5,8,9]	0.77	1.16
Benchmark (without particle)	0.97	0.92
$H/h = 8$	0.38	2.32
$H/h = 4$	0.36	2.46
$H/h = 2$	0.17	5.34

5.3. Implications for reactive particulate flows

These assessments are particularly relevant when studying local mass diffusivities in the transition regime. In such studies, the local mass diffusivity becomes influenced by the particle-to-wall distance and the determination of a local diffusivity (for example in the region between the particle and the wall) requires a local Kn [44]. Both the continuum approximation and the assumption of thermodynamic quasi-equilibrium break down at finite Kn [15,45], implying that completely different mechanisms may govern mass transfer on different sides of an asymmetrically positioned particle.

It has also been shown that the mass transfer coefficient in pressure-driven channel flows at varying degrees of rarefaction is essentially constant with Kn, whereas the heat transfer coefficient is strongly dependent on Kn, leading to a breakdown of the well-known heat and mass transfer analogies [46]. This difference in behavior originates from the non-local transfer phenomena: whereas a molecule coming from a distant region with a significantly different temperature is able to transfer a significantly different energy load (to the molecules in the near-particle region), the mass transfer capability of any given molecule is always the same, independent of the region from which the molecule originates [46]. Moreover, for nano-fabricated systems with parallel channels, the existence of Knudsen minima implies that the mass-flow rate through a given channel may vary non-monotonously with the degree

of rarefaction in the transition regime. As the local rarefaction will depend on the local blockage and particle-wall distances for a gas-solid flow, and as these may exhibit highly dynamic characteristics, oscillations in flow rate (and thus in retention time) may be expected to arise spontaneously under certain conditions. For reactive systems, where particle sizes change continuously due to chemical reactions, and which may be controlled by either mass or heat transfer or chemical kinetics, controlling the non-local transport characteristics may thus require accounting for highly complex Knudsen minima effects.

The local mass diffusivity in a reactive nano-scale system will thus depend on the local flow configuration. The present work implies that, for an immobile particle, the Knudsen paradox may offer a possibility to indirectly assess or characterize these phenomena from the response of the global mass-flow rate to variations in the absolute pressure. Finally, for a suspended particle that is moving with the average gas flow velocity, the momentum sink effect may become insignificant, but the effects of the local length-scale reduction will remain in full. The latter effects are also the most relevant for nano-scale reactive flows.

6. Conclusions

In this paper, we present a DSMC investigation of the effect of a stationary particle on the Knudsen paradox observed in micro-channel Poiseuille flows. Such an investigation has previously not been reported in literature. The objective with this study was to assess the effects from representing natural porous media through nanofabricated model pores in rarefied gas-solid systems and heterogeneous catalysis applications. The open source solver *dsmcFoam+* is used to carry out the relevant studies. We show that the presence of a particle markedly alters the response of the rarefied flow system as it serves as an additional momentum sink in the flow. Further, as it becomes larger and subsequently blocks a larger portion of the duct (represented as the blockage ratios H/h), the mass-flow rate at the same nominal pressure difference decreases. Despite the noticeable scatter in the reported data, the general trends (in Q_{norm}) observed agree with conventional rarefied flow dynamics in micro-channels and parallelisms can be drawn from our study and that of Liu et al. [43] on micro-channels with bends. In both assessments, an increase in the local hydrodynamic resistances in the flow, leads to noticeable deviations from the behavior derived for straight micro-channel Poiseuille flows by Cercignani et al. [5]. Consequently, with the presence of a particle, the Knudsen minimum is shifted towards higher Knudsen numbers with the curve flattening out towards the free-molecular flow regime. This effect is more pronounced as the particle becomes large, and results from a shift towards relatively more ballistic molecular motion at shorter geometrical distances. These observations have significant implications for the design of model pore systems for reactive rarefied gas-solid flows, as well as investigations of heterogeneous catalysis using stationary catalyst particles. Most notably, the local mass diffusivity, which determines the overall reaction rate at mass-transfer limited conditions, will depend on the local flow configuration, which may thus be indirectly assessed from the response of the global mass-flow rate as a function of absolute pressure. Moreover, attention should be paid to the possibility for flow oscillations to manifest in nano-scale reactor systems with rarefied reactive gas-solid flow.

In conclusion, the present work addresses a perceived knowledge gap in rarefied flows, along with a relevant challenge while modeling reactive gas-solid flows in confined geometries at the nano-scale, where simultaneous handling of local and non-local transport mechanisms over the particle surfaces must be realized. The observed trends can be extended towards asymmetric particles as well, since the presence of any particle in the flow increases the overall hydrodynamic resistances in it. Thus, we underline the need to account for these complex transition regime effects while assessing such rarefied gas-particle systems particularly in the relevant micro-fluidic applications.

Abbreviations

The following abbreviations are used in this manuscript:

BGK	Bhatnagar–Gross–Krook
DSMC	Direct simulation Monte-Carlo
GNU	General Public License
MD	Molecular dynamics
μTAS	Micro-total analytic systems
NTC	No-time counter
OpenFOAM	Open-source Field Operation And Manipulation
POC	Point-of-care diagnostics
VHS	Variable hard sphere

References

1. Sajeesh, P.; Sen, A.K. Particle separation and sorting in microfluidic devices: a review. *Microfluidics and Nanofluidics* **2014**, *17*, 1–52. doi:10.1007/s10404-013-1291-9.

2. Bayareh, M. An updated review on particle separation in passive microfluidic devices. *Chemical Engineering and Processing - Process Intensification* **2020**, *153*, 107984. doi:10.1016/j.cep.2020.107984.

3. Knudsen, M. Die Gesetze der Molekularströmung und der inneren Reibungsströmung der Gase durch Röhren. *Annalen der Physik* **1909**, *333*, 75–130. doi:10.1002/andp.19093330106.

4. Pollard, W.G.; Present, R.D. On Gaseous Self-Diffusion in Long Capillary Tubes. *Phys. Rev.* **1948**, *73*, 762–774. doi:10.1103/PhysRev.73.762.

5. Cercignani, C.; Daneri, A. Flow of a Rarefied Gas between Two Parallel Plates. *Journal of Applied Physics* **1963**, *34*, 3509–3513. doi:10.1063/1.1729249.

6. Barber, R.W.; Emerson, D.R. Challenges in Modeling Gas-Phase Flow in Microchannels: From Slip to Transition. *Heat Transfer Engineering* **2006**, *27*, 3–12. doi:10.1080/01457630500522271.

7. Agrawal, A. A Comprehensive Review on Gas Flow in Microchannels. *International Journal of Micro-Nano Scale Transport* **2007**, *2*, 3411 – 3421. doi:10.1260/1759-3093.2.1.1.

8. Cercignani, C. *Plane Poiseuille flow and Knudsen minimum effect*; Vol. 2, Academic Press, New York, 1963; pp. 92–101.

9. Cercignani, C.; Sernagiotto, F. Cylindrical Poiseuille Flow of a Rarefied Gas. *The Physics of Fluids* **1966**, *9*, 40–44. doi:10.1063/1.1761530.

10. Huang, A.B.; Stoy, R.L. Rarefied Gas Channel Flows for Three Molecular Models. *The Physics of Fluids* **1966**, *9*, 2327–2336. doi:10.1063/1.1761622.

11. Loyalka, S.K.; Ferziger, J.H. Model Dependence of the Slip Coefficient. *The Physics of Fluids* **1967**, *10*, 1833–1839. doi:10.1063/1.1762366.

12. Ferziger, J.H. Flow of a Rarefied Gas through a Cylindrical Tube. *The Physics of Fluids* **1967**, *10*, 1448–1453. doi:10.1063/1.1762304.

13.   Bhatnagar, P.L.; Gross, E.P.; Krook, M. A Model for Collision Processes in Gases. I. Small Amplitude Processes in Charged and Neutral One-Component Systems. *Phys. Rev.* **1954**, *94*, 511–525. doi:10.1103/PhysRev.94.511.

14.   Cercignani, C. *The Boltzmann equation and its applications*; Vol. 67, *Applied Mathematical Sciences book series (AMS)*, Springer-Verlag New York Inc., 1988. doi:10.1007/978-1-4612-1039-9.

15.   Sharipov, F.; Seleznev, V. Data on Internal Rarefied Gas Flows. *Journal of Physical and Chemical Reference Data* **1998**, *27*, 657–706. doi:10.1063/1.556019.

16.   Ali Beskok, G.E.K. Report: A model for flows in channels, pipes, and ducts at micro and nano scales. *Microscale Thermophysical Engineering* **1999**, *3*, 43–77. doi:10.1080/108939599199864.

17.   Karniadakis, GEM, A.; Beskok, A, A.; Gad-el Hak, M, R. Micro Flows: Fundamentals and Simulation. *Applied Mechanics Reviews* **2002**, *55*, B76–B76. doi:10.1115/1.1483361.

18.   Colin, S. Rarefaction and compressibility effects on steady and transient gas flows in microchannels. *Microfluidics and Nanofluidics* **2005**, *1*, 268–279. doi:10.1007/s10404-004-0002-y.

19.   Arkilic, E.B.; Schmidt, M.A.; Breuer, K.S. Gaseous slip flow in long microchannels. *Journal of Microelectromechanical Systems* **1997**, *6*, 167–178. doi:10.1109/84.585795.

20.   Chen, S.; Doolen, G.D. LATTICE BOLTZMANN METHOD FOR FLUID FLOWS. *Annual Review of Fluid Mechanics* **1998**, *30*, 329–364. doi:10.1146/annurev.fluid.30.1.329.

21.   Agrawal, A.; Djenidi, L.; Antonia, R.A. Simulation of gas flow in microchannels with a sudden expansion or contraction. *Journal of Fluid Mechanics* **2005**, *530*, 135–144. doi:10.1017/S0022112005003691.

22.   Bird, G.A. Monte Carlo Simulation of Gas Flows. *Annual Review of Fluid Mechanics* **1978**, *10*, 11–31. doi:10.1146/annurev.fl.10.010178.000303.

23.   Bird, G.A. *The DSMC method*; CreateSpace Independent Publishing Platform, 2013.

24.   Beresnev, S.A.; Chernyak, V.G.; Suetin, P.E. Motion of a spherical particle in a rarefied gas. Part 1. A liquid particle in its saturated vapour. *Journal of Fluid Mechanics* **1987**, *176*, 295–310. doi:10.1017/S0022112087000685.

25.   Ström, H.; Sasic, S.; Andersson, B. A novel multiphase DNS approach for handling solid particles in a rarefied gas. *International Journal of Multiphase Flow* **2011**, *37*, 906–918. doi:10.1016/j.ijmultiphaseflow.2011.03.011.

26.   Corson, J.; Mulholland, G.; Zachariah, M. Hydrodynamic interactions between aerosol particles in the transition regime. *Journal of Fluid Mechanics* **2018**, *855*, 535–553.

27.   Kannan, A.S.; Naserentin, V.; Mark, A.; Maggiolo, D.; Sardina, G.; Sasic, S.; Ström, H. A continuum-based multiphase DNS method for studying the Brownian dynamics of soot particles in a rarefied gas. *Chemical Engineering Science* **2019**, *210*, 115229. doi:10.1016/j.ces.2019.115229.

28.   Albinsson, D.e.a. Operando detection of single nanoparticle activity dynamics inside a model pore catalyst material. *Science Advances* **2020**, *6*, 1–9. doi:10.1126/sciadv.aba7678.

29.   Pérez-Ràfols, F.; Forsberg, F.; Hellström, G.; Almqvist, A. A Stochastic Two-Scale Model for Rarefied Gas Flow in Highly Heterogeneous Porous Media. *Transport in Porous Media* **2020**. doi:10.1007/s11242-020-01476-z.

30.   Weller, H.G.; Tabor, G.; Jasak, H.; Fureby, C. A tensorial approach to computational continuum mechanics using object-oriented techniques. *Computers in Physics* **1998**, *12*, 620–631. doi:10.1063/1.168744.

31.   White, C.; Borg, M.; Scanlon, T.; Longshaw, S.; John, B.; Emerson, D.; Reese, J. dsmcFoam+: An OpenFOAM based direct simulation Monte Carlo solver. *Computer Physics Communications* **2018**, *224*, 22 – 43. doi:10.1016/j.cpc.2017.09.030.

32.   Roohi, E.; Darbandi, M.; Mirjalili, V. Direct Simulation Monte Carlo Solution of Subsonic Flow Through Micro/Nanoscale Channels. *Journal of Heat Transfer* **2009**, *131*. doi:10.1115/1.3139105.

33.   White, C.; Borg, M.K.; Scanlon, T.J.; Reese, J.M. A DSMC investigation of gas flows in micro-channels with bends. *Computers and Fluids* **2013**, *71*, 261 – 271. doi:10.1016/j.compfluid.2012.10.023.

34.   Scanlon, T.J.; Roohi, E.; White, C.; Darbandi, M.; Reese, J.M. An open source, parallel DSMC code for rarefied gas flows in arbitrary geometries. *Computers and Fluids* **2010**, *39*, 2078–2089. doi:10.1016/j.compfluid.2010.07.014.

35.   White, C.; Borg, M.; Longshaw, S. MicroNanoFlows: OpenFOAM-2.4.0-MNF. https://github.com/MicroNanoFlows/OpenFOAM-2.4.0-MNF, 2018.

36.   Wang, M.; Li, Z.   Simulations for gas flows in microgeometries using the direct simulation Monte Carlo method.   *International Journal of Heat and Fluid Flow* **2004**, *25*, 975 – 985. doi:10.1016/j.ijheatfluidflow.2004.02.024.

37.   W.W. Liou, Y.F. Implicit Boundary Conditions for Direct Simulation Monte Carlo Method in MEMS Flow Predictions. *Computer Modeling in Engineering Sciences* **2000**, *1*, 119–128. doi:10.3970/cmes.2000.001.571.

38.   Ewart, T.; Perrier, P.; Graur, I.A.; Meolans, J.G.   Mass flow rate measurements in a microchannel, from hydrodynamic to near free molecular regimes.   *Journal of Fluid Mechanics* **2007**, *584*, 337–356. doi:10.1017/S0022112007006374.

39.   Hadjiconstantinou, N.G.; Garcia, A.L.; Bazant, M.Z.; He, G.   Statistical error in particle simulations of hydrodynamic phenomena.   *Journal of Computational Physics* **2003**, *187*, 274 – 297. doi:10.1016/S0021-9991(03)00099-8.

40.   Cleveland, W.S. Robust Locally Weighted Regression and Smoothing Scatterplots. *Journal of the American Statistical Association* **1979**, *74*, 829–836. doi:10.2307/2286407.

41.   White, F. *Fluid Mechanics*; McGraw-Hill series in mechanical engineering, McGraw Hill, 2011.

42.   Tatsios, G.; Stefanov, S.K.; Valougeorgis, D.   Predicting the Knudsen paradox in long capillaries by decomposing the flow into ballistic and collision parts.   *Phys. Rev. E* **2015**, *91*, 061001. doi:10.1103/PhysRevE.91.061001.

43.   Liu, W.; Tang, G.; Su, W.; Wu, L.; Zhang, Y.   Rarefaction throttling effect: Influence of the bend in micro-channel gaseous flow. *Physics of Fluids* **2018**, *30*, 082002. doi:10.1063/1.5037430.

44.   Yang, G.; Weigand, B. Investigation of the Klinkenberg effect in a micro/nanoporous medium by direct simulation Monte Carlo method. *Phys. Rev. Fluids* **2018**, *3*, 044201. doi:10.1103/PhysRevFluids.3.044201.

45.   Gad-El-Hak, M. Gas and Liquid Transport at the Microscale.   *Heat Transfer Engineering* **2006**, *27*, 13–29. doi:10.1080/01457630500522305.

46.   Bond, D.; Goldsworthy, M.; Wheatley, V.   Numerical investigation of the heat and mass transfer analogy in rarefied gas flows.   *International Journal of Heat and Mass Transfer* **2015**, *85*, 971 – 986. doi:10.1016/j.ijheatmasstransfer.2015.02.051.